UNIVERSITY
of
GLASGOW

Investigation of factors affecting the sodium/calcium exchanger in a rabbit model of left ventricular dysfunction

Elspeth BA Elliott BSc (Hons)

Submitted September 2006 in fulfilment of the degree Doctor of Philosophy to the Faculty of Biomedical & Life Sciences, University of Glasgow, U.K.

Research carried out within the Faculty of Biomedical & Life Sciences, University of Glasgow, U.K.

ABSTRACT

The sodium-calcium exchanger (NCX) is the major calcium efflux pathway in the cardiomyocyte and thus is intrinsically involved in intracellular Ca^{2+} ($[Ca^{2+}]_i$) homeostasis. Previous work has identified that in a rabbit infarct model of left ventricular dysfunction (LVD), NCX protein is increased whilst NCX activity is decreased. This thesis examines the sub-cellular basis for this dichotomy. Investigation of the factors regulating NCX including the transverse-tubule (t-tubule) network, the proteins sorcin and phospholemman and NCX phosphorylation was performed and levels were quantified in LVD and control (sham) hearts using various techniques.

The fluorophore di-8-ANNEPS and confocal microscopy were used in isolated rabbit cardiomyocytes to label the t-tubule network. Quantification of the mean t-tubule density revealed a 25% reduction in LVD compared to control. On permeabilisation, this difference was not apparent indicating that this percentage of t-tubules in LVD was uncoupled from the surface sarcolemma and disconnected from the extracellular space. NCX protein is reported to be concentrated in the t-tubule network; therefore, NCX protein contained in the internalised tubules would be isolated rendering it non-functional.

Sorcin over-expression has been shown to stimulate NCX activity in the rabbit. Quantitative Western blotting of whole left ventricular homogenates showed that sorcin dimer expression was reduced by 33% in LVD *vs.* sham. This was independently confirmed using monoclonal and polyclonal primary antibodies.

Biochemical analysis of the phosphorylation status of the membrane protein phospholemman (PLM) showed no significant difference at either of the two major phosphorylation sites. *In vitro* back-phosphorylation assessed endogenous levels of phosphorylation of NCX itself and revealed a 3-fold hyperphosphorylation in LVD. Problems associated with this technique and interpretation of these data are discussed in detail.

In order to measure the functional effects of sorcin, single cell electrophysiology was carried out. Attempts to use recombinant sorcin (3 μmol/L) were

unsuccessful as the low $[Ca^{2+}]_i$ buffering required to measure cellular properties made the membranes' mechanical properties unstable. Finally, phosphorylation of sorcin as a modulator of NCX was investigated using constitutively phosphorylated and de-phosphorylated sorcin mutants. These were both ineffective indicating that the tertiary conformation of sorcin is critical for its effect on NCX function.

In summary, the results showed that t-tubule density, sorcin dimer expression and NCX phosphorylation status all contributed to the modulation of NCX in LVD whilst phospholemman and phosphorylation of sorcin were eliminated. Simplified estimates and previously published values were used to relate the quantitative change in each of the three factors modulating NCX to the dichotomy and assess their relative contributions in the model. In doing so, it was determined (using previously published data) that the reduced t-tubule network would account for a 16% loss of functioning NCX protein in contact with the extracellular space. Sorcin down-regulation was calculated to result in an 8% reduction in NCX activity. The NCX hyperphosphorylation result requires further confirmation. Combining the effects on NCX activity of t-tubule and sorcin reduction, a 23% reduction in NCX activity was accounted for. As NCX activity was reduced by approximately 57% in the model of LVD additional factors must account for the remaining 20%.

AIMS OF THESIS

In some animal models of heart failure, including that of the rabbit, sodium-calcium exchanger activity is depressed despite an increase in protein expression. The general aim of this thesis was to investigate the sub-cellular basis for the observed dichotomy between NCX activity and protein level in a rabbit model of LVD.

The following potential modulatory factors of NCX were examined:

(1) Transverse-tubule (t-tubule) density.

(2) The regulatory proteins sorcin and phospholemman.

(3) The phosphorylation status of NCX.

The comparative change in these factors was quantified and the relative contribution of each to the NCX dichotomy in LVD was assessed.

TABLE OF CONTENTS

LIST OF FIGURES

LIST OF TABLES

ABBREVIATIONS

ADJ	adjacent area
AM	acetoxymethyl ester
ATP	adenosine 5' triphosphate
ATPase	adenosine triphosphatase
BAPTA	1,2-bis(2-aminophenoxy)ethane N,N,N'N'-tetraacetic acid
BDM	2,3-butanedione monoxime
BSA	bovine serum albumin
β-escin	beta escin
β-ME	beta mercaptoethanol
Ca^{2+}	calcium ion
Ca^{2+}-ATPase	calcium pump
$[Ca^{2+}]$	calcium ion concentration
$[Ca^{2+}]_i$	intracellular calcium ion concentration
$[Ca^{2+}]_o$	extracellular calcium ion concentration
cAMP	adenosine 3':5'-cyclicmonophosphate
CaMK	calcium/calmodulin-dependent protein kinase
CICR	calcium-induced calcium release
Cl^-	chloride ion
Co-IP	co-immunoprecipitation
CLT	chelerythrine, PKC inhibitor
Cs^+	caesium ion
CSQ	calsequestrin
DAD	delayed afterdepolarisation
DCM	dilated cardiomyopathy
DHPR	dihydropyridine receptor
di-8-ANNEPS	di-8-AminoNaphthylEthenylPyridinium
DTT	dithiothreitol
EAD	early afterdepolarisation
EC	excitation-contraction
ECC	excitation-contraction coupling
ECL	ehanced chemiluminescence
EDTA	ethylenediaminetetraacetic acid
EF(%)	ejection fraction
EF-	elongation factor
EGTA	ethylene glycol bis(β-aminoethyl ether)-N,N,N',N'-tetraacetic acid
E_m	membrane potential
E_{NCX}	reversal potential for sodium calcium exchanger
Fura-2	fluorescent indicator (calcium sensitive)

Fura-FF	fluorescent indicator (calcium sensitive)
g	gram, weight
g	acceleration due to gravity
GAPDH	glyceraldehyde-3-phosphate dehydrogenase
HF	heart failure
HCl	hydrochloric acid
HEK	human embryonic kidney
HEPES	N-2-hydroxyethylpiperazine-N'-2-ethanesulphonic acid
Hz	hertz, frequency
I_{Ca}	calcium current
$I_{(Cl)Ca}$	calcium activated chloride current
I_{NCX}	sodium calcium exchange current
$I_{NS(Ca)}$	non-selective cation current
I_{ti}	calcium induced transient inward current
ICM	ischaemic cardiomyopathy
Ins(1,4,5)P_3	inositol (1,4,5)-triphosphate
I-V	current-voltage
K^+	potassium ion
K_d	dissociation constant
KOH	potassium hydroxide
L	litre, volume
LacZ	β-galactosidase
LAD	left atrial dimension
LASER	light amplification by stimulated emission of radiation
LTCC	L-type calcium channel
LVD	left ventricular dysfunction
LVEDD	left ventricular end diastolic dimension
LSCM	laser-scanning confocal microscopy
mAKAP	A kinase anchoring protein
MAPK	mitogen-activated protein kinase
mol/L	molar, concentration
Mg^{2+}	magnesium ion
mg	milligram, weight
$MgCl_2$	magnesium chloride
MI	myocardial infarction
min	minute, time
mL	millilitre, volume
mm	millimeter, length
mmol/L	millimolar, concentration
mol	mole, quantity
mRNA	messenger ribose nucleic acid

ms	millisecond, time
mV	millivolt, electrical voltage
n	sample size
Na^+	sodium ion
NaH_2PO_4	sodium dihydrogen orthophosphate
NaOH	sodium hydroxide
Na^+/K^+-ATPase	sodium potassium pump
NCX	sodium calcium
nm	nanometer, length
nmol/L	nanomolar, concentration
p	probability
PCr	phosphocreatine
PEF	penta elongation factor
pF	pico Farads, capacitance
PIP_2	phosphatidylinositol-4,5-bisphosphate
PKA	protein kinase A
PKC	protein kinase C
PMA	phorbol 12-myristate 13-acetate, PKC agonist
PLB	phospholamban
PLM	phospholemman
PMT	photomultiplier tube
PP	protein phosphatase
R_{max}	fluorescence measured at saturatingly high calcium
R_{min}	fluorescence measured at very low calcium
REM	remote area
RyR	ryanodine receptor
RyR2	ryanodine receptor type 2
s	second, time
SA/V	surface area / volume
SCBD	sorcin calcium binding domain
SDS-PAGE	sodium dodecyl sulphate gel electrophoresis
SEM	standard error of the mean
SERCA	sarco(endo)plasmic reticulum calcium ATPase
SLV	sarcolemmal vesicle uptake
SR	sarcoplasmic reticulum
TM	transmembrane domain
t-tubule	transverse tubule
τ	tau, time constant
µg	microgram, weight
µl	microlitre, volume

µmol/L	micromolar, concentration
V	volt, potential difference
VGSC	voltage-gated sodium channel
XIP	exchanger inhibitory peptide
°C	degrees Celsius, temperature

ACKNOWLEDGEMENTS

My sincere thanks go to my supervisor, Professor Godfrey Smith, for providing me with the opportunity to work in his lab. His willingness to help, continual enthusiasm and advice have been very much appreciated.

I am extremely grateful to Dr Susan Currie for her initial teaching and advice with the work on sorcin; without her expertise this section of the project would not have been possible.

Thanks also go to Aileen Rankin and Anne Ward for technical assistance with cell dissociation and to the people who have collaborated on work throughout this PhD.

I would like to extend my thanks to all the members of Godfrey's group for their help and for making the lab a fun place to work. A special mention to Debbie Reynolds for her advice and for making me laugh when things were difficult. I am indebted to Chris Loughrey for everything he has done for me throughout the time I have known him. His encouragement and support have, at times, seemed endless!

Finally, I thank my family for their love and support which has provided me with the foundation to achieve everything I have done.

Financial support from the British Heart Foundation is gratefully acknowledged.

AUTHOR'S DECLARATION

The material contained in this thesis is my own work, except where stated. This material has not been submitted in fulfilment of any other degree.

Some of the results obtained have been published in paper and abstract form and are detailed below:

Papers:

Excessive sarcoplasmic/endoplasmic reticulum Ca^{2+}-ATPase expression causes increased sarcoplasmic reticulum Ca^{2+} uptake but decreases myocyte shortening. Teucher N.; Prestle J.; Seidler T.; Currie S.; **Elliott E.B.**; Reynolds D.F.; Schott P.; Wagner S.; Kogler H.; Inesi G.; Bers D.M.; Hasenfuss G.; Smith G.L. Circulation (2004), 110(23):3553-9.

Na(+)/Ca(2+) exchanger expression and function in a rabbit model of myocardial infarction. Smith G.L.; **Elliott E.**; Kettlewell S.; Currie S.; Quinn F.R. (2006) J Cardiovasc Electrophysiol. May;17 Suppl 1:S57-S63.

Abstracts:

Decreased sorcin expression in a rabbit model of left ventricular dysfunction. **E.B. Elliott**, S. Currie and G.L. Smith *J Physiol* (2004) 557P C2, oral communication.

Decreased sorcin dimer but not monomer levels in a rabbit model of heart failure. **E.B. Elliott**, S. Currie and G.L. Smith *J Biophys* (2005) 2360-Pos/B471, poster.

CHAPTER 1
GENERAL INTRODUCTION

1.1 Excitation-contraction coupling

During the cardiac cycle, the ventricular myocytes contract and relax in order that the heart can function to pump blood round the body. This process, as with other muscle types, is brought about by a transient increase in intracellular calcium concentration ($[Ca^{2+}]_i$) of the cardiomyocytes. Electrical activation is converted into contraction by a signal transduction mechanism known as cardiac Excitation-Contraction Coupling (ECC) and, within this tightly regulated system, the dynamic control of Ca^{2+} plays a pivotal role. The theory of Calcium-Induced Calcium-Release (CICR) is now widely accepted as the most probable link underlying this process. CICR in the heart was first demonstrated using skinned cardiac cells from the dog. This work showed that injection of increasing concentrations of Ca^{2+} into the cell led to the release of Ca^{2+} in a dose-dependent manner (Fabiato, 1985). The precise control of Ca^{2+} movement between the intracellular environment, organelles and extracellular space is fundamental to CICR as is its loss to the contractile dysfunction during pathological conditions such as heart failure (HF).

The aim of the present chapter is to provide an overview of EC coupling in the mammalian cardiomyocyte. Particular reference will be made to extrusion pathways and the consequences of their disruption during heart failure.

1.2 Ca^{2+}-induced Ca^{2+}-release

Research conducted over the past 20 years has greatly enhanced our understanding of CICR both functionally and biochemically. This has defined Ca^{2+} release and extrusion and identified the major Ca^{2+}-handling proteins involved, their cellular locations and protein-protein interactions. The diagram on the next page summarises the main route for Ca^{2+} movement during CICR (Figure 1.1).

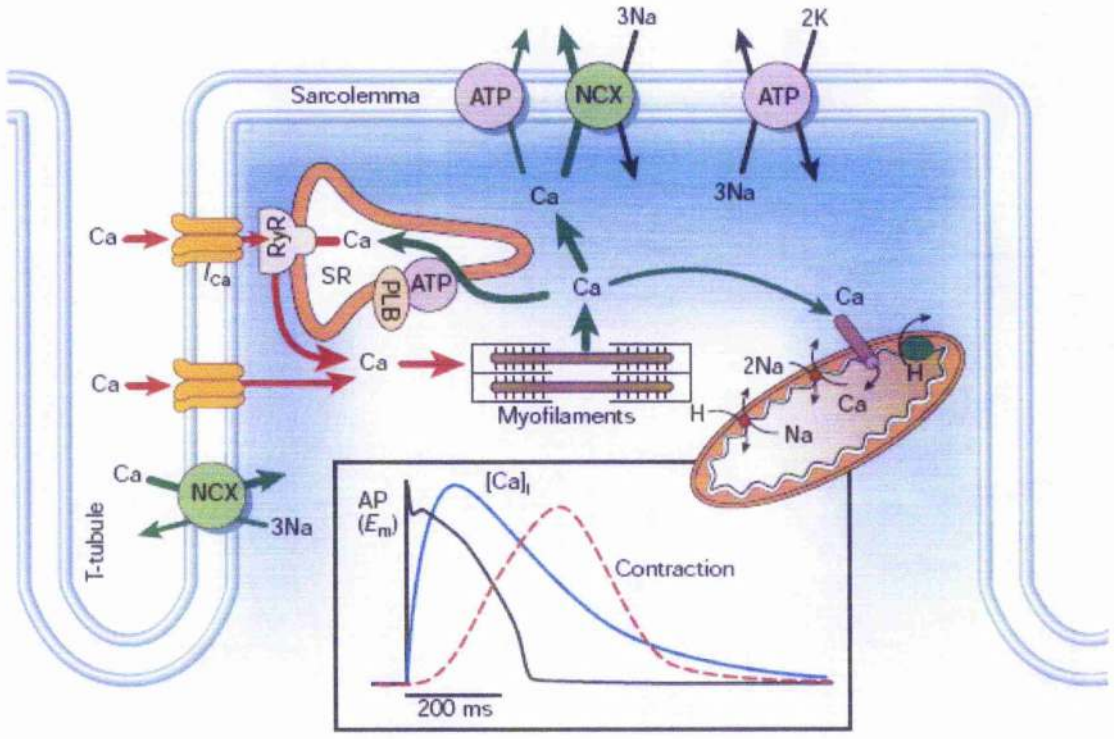

Figure 1.1 Ca^{2+}-cycling in the ventricular cardiomyocyte.

Schematic representation of the ventricular myocyte and the major Ca^{2+}-handling proteins. Inset shows the time-course of the relationship between the cardiac action potential, change in $[Ca^{2+}]_i$ and contraction. Diagram taken from Bers (2002).

1.2.1 Ca^{2+} influx via I_{Ca}

The cardiac ventricular action potential propagates as a wave of depolarisation along the sarcolemma and into the transverse tubules. These invaginations of the surface membrane rapidly transmit the electrical signal throughout the entire cell ensuring near synchronous activation. In doing so, the triggering event in CICR is initiated in which an influx of Ca^{2+} ions (I_{Ca}) occurs mainly via the opening of the voltage-dependent L-type Ca^{2+} channel (LTCC). LTCCs are situated predominantly on the t-tubule membrane (Carl *et al.*, 1995; Shepherd & McDonough, 1998; Kawai *et al.*, 1999) where they lie in close apposition to the terminal cisternae of the intracellular Ca^{2+} store called the sarcoplasmic reticulum (SR). These components collectively make up the spatial microdomain known as the dyadic cleft.

The cardiac LTCC is a multi-subunit transmembrane ion channel (α_{1C}, α_2, β_2, and δ). A diagram of the structure of the L-type Ca^{2+} channel is presented below (Figure 1.2). The α_{1C} subunit of the cardiac LTCC forms the pore of the channel and is considered responsible for its functional properties such as voltage-sensing during activation and inactivation (Perez-Reyes *et al.*, 1989). It comprises four homologous domains (I-IV) which themselves contain 6 membrane spanning domains (S1-S6); this is the site at which the three main classes of LTCC blockers (dihydropyridines, phenylalkylamines and benzothiazapines) bind. Potential phosphorylation sites (PO_4) are also indicated.

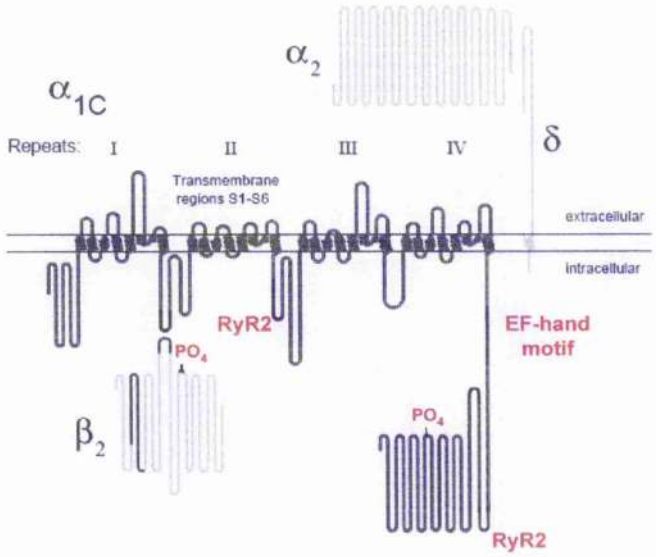

Figure 1.2 Structure of the cardiac voltage-gated LTCC.

Schematic diagram showing the subunits of the LTCC and their relative associations (α_{1C}, α_2, β_2, and δ). Potential phosphorylation sites (PO_4) for c-AMP dependent protein kinase (PKA) and possible interaction sites for RyR2 are labelled in red. Adapted from Bers & Perez-Reyes, (1999).

The LTCC is rapidly activated at a threshold voltage of -40 mV. Conductance through the channel increases to its maximum at +10 mV and decreases thereafter. Inactivation of the LTCC is long (60-200 ms), is dependent on both $[Ca^{2+}]_i$ and voltage and is mediated by calmodulin (Peterson *et al.*, 1999). In the

rabbit, the total Ca^{2+} entry during an action potential is approximately 12 μmol/L whilst inactivation of the channel may reduce this value by 50% (Puglisi *et al.*, 1999). It is estimated that I_{Ca} contributes just 23% of the total rise in cytosolic $[Ca^{2+}]$ in a steady state twitch (Delbridge *et al.*, 1996). The I-V relationship for the current through the LTCC (I_{Ca}) over the range of voltages during the action potential gives rise to a bell-shaped curve (Figure 1.3).

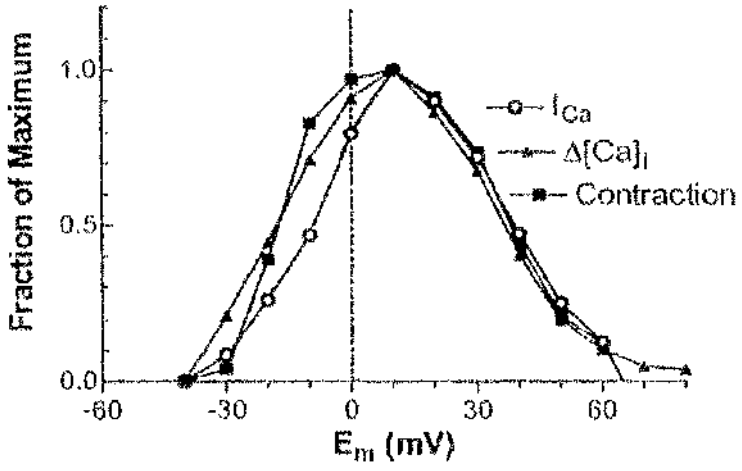

Figure 1.3 Voltage dependence of I_{Ca}, Ca transient and contraction.

Normalised I-V relationships for I_{Ca}, change in $[Ca^{2+}]_i$ and contraction in voltage-clamped guinea-pig ventricular myocytes. Adapted from Beuckelmann & Wier (1988).

When superimposed with the voltage-dependencies of the change in $[Ca^{2+}]_i$ and contraction over the same range the relationships are almost identical indicating that I_{Ca} is the major trigger for SR release (Beuckelmann & Wier, 1988).

1.2.2 Ca^{2+} release from the SR

The sarcoplasmic reticulum (SR) is the intracellular Ca^{2+} storage organelle in the cardiomyocyte. The SR forms an intricate network surrounding the myofilaments, the ends of which lie juxtaposed to the t-tubules at the dyadic cleft. In response to I_{Ca} influx following depolarisation, the raise in $[Ca^{2+}]_i$ in the dyadic cleft increases the open probability of the SR Ca^{2+} release channels or ryanodine receptors (RyR2s) causing them to open and release a greater quantity of Ca^{2+} from the SR. The initial I_{Ca} trigger $[Ca^{2+}]$ is therefore greatly amplified by

the Ca^{2+} released from the SR. In addition, SR Ca^{2+} serves to feed back and inactivate I_{Ca} to limit further I_{Ca} triggered release.

1.2.2.1 The ryanodine receptor

RYR2s are homotetramers (560 kDa per monomer) which reside in clusters on the terminal cisternae of the SR (Takeshima *et al.*, 1989). Current estimates of the number of RyR2s per cluster have yielded results between 4-20 (Wang *et al.*, 2001a) yet this value could be as high as 100 (Sobie *et al.*, 2002). Ca^{2+} "sparks" are local Ca^{2+} release events (approximately 200 nmol/L free Ca^{2+}) arising from an individual RyR2 cluster (Cheng *et al.*, 1993). During depolarisation, I_{Ca} simultaneously activates sparks throughout the myocyte. These spatially and temporally summate to form a homogeneous increase in Ca^{2+} across the myocyte - the Ca^{2+} transient (Cheng *et al.*, 1993). This global rise in $[Ca^{2+}]_i$ binds to and activates the myofilaments, causing contraction of the cardiomyocyte. Half maximal activation of contraction requires an $[Ca^{2+}]_i$ in the range of approximately 600 nmol/L free Ca^{2+} (Bers, 2002).

1.3 Mechanisms of Ca^{2+} efflux

In order for the heart to relax during diastole, Ca^{2+} must dissociate from the myofilaments and cytosolic $[Ca^{2+}]_i$ must be reduced 10-fold to resting levels (approximately 100-150 nmol/L free Ca^{2+}). This is achieved by transporting Ca^{2+} out of the cytosol via four extrusion pathways which act in competition with each other for cytosolic Ca^{2+}.

(i) **Sodium-calcium exchanger (NCX1).** NCX1 is the main route by which Ca^{2+} is extruded to the extracellular space through the transfer of 1 Ca^{2+} ion out of the cell in turn for 3 Na^+ ions into the cell. This is a passive process which transports Ca^{2+} due to the Na^+ concentration gradient set by the activity of the sarcolemmal Na^+/K^+-ATPase pump (i.e. the maintenance of a low intracellular Na^+ concentration ($[Na^+]_i$)). As a result of this, NCX1 is sometimes referred to as a secondary active transporter (Philipson & Nicoll, 2000). The exchanger function is modified by changes in $[Ca^{2+}]$ and $[Na^+]$ and by the membrane potential (E_m) (Bers, 2002). NCX1 is the cardiac isoform of the exchanger (NCX2 and NCX3 are

present in brain and skeletal muscle respectively); hereafter NCX1 will be referred to as NCX. NCX is located mainly on the t-tubule membrane (Yang *et al.*, 2002) and is proposed to be part of a macromolecular complex (Schulze *et al.*, 2003). The structure of NCX and the factors regulating its function are the focus of this thesis and more detail is presented in the remainder of this introduction (see 1.4.1) and in Chapter 6.

(ii) **SR Ca^{2+}-ATPase isoform 2a (SERCA2a).** SERCA2a is the cardiac form of the pump responsible for re-sequestering Ca^{2+} to the SR lumen in preparation for the next depolarisation-induced Ca^{2+} release. SERCA2a removal of Ca^{2+} is an active process which consumes 1 molecule of ATP for every 2 Ca^{2+} removed from cytosol. The activity of SERCA2a is determined by the small regulatory phosphoprotein - phospholamban (PLB) (Tada & Katz, 1982). In the dephosphorylated state PLB is inhibitory on SERCA2a Ca^{2+} uptake function; on phosphorylation (by protein kinase A (PKA) or Ca^{2+}/calmodulin-dependent protein kinase (CaMK)) the inhibition is relieved and SERCA2a activity increases SR Ca^{2+} uptake (Currie & Smith, 1999). More detail on PLB phosphorylation is presented in Chapter 5

(iii) **Plasma membrane Ca^{2+}-ATPase (PMCA).** This active transporter is present on the sarcolemma of the cardiomyocyte and contributes to Ca^{2+} efflux into the extracellular space. The transport of 1 Ca^{2+} ion requires the energy available for release by 1 molecule of ATP. The function of the pump is regulated both by calmodulin, phosphorylation by PKA and protein kinase C (PKC). Although the PMCA has a high affinity for Ca^{2+}, it has a slow turnover rate and an extremely low abundance compared to other membrane proteins (Carafoli, 1994).

(iv) **Mitochondrial Ca^{2+} influx.** Two modes of mitochondrial mediated influx exist, the Ca^{2+} uniporter and the rapid influx pathway. Ca^{2+} enters via the uniporter down an electrochemical gradient produced by the extrusion of protons by the respiratory chain. The K_m for Ca^{2+} influx on the uniporter is estimated to be above 30 μmol/L, hence the amount of Ca^{2+} entering the mitochondria during normal Ca^{2+} cycling and its contribution to the decay of the Ca^{2+} transient is negligible (Bassani *et al.*, 1992; Bers, 2001). The rapid influx mode of Ca^{2+} entry also relies on the large electrochemical gradient across the

mitochondrial membrane and may simply exist as an alternative conformation of the uniporter rather than a distinct transport mechanism (Gunter *et al.*, 2000).

The first two of these four efflux pathways are of major physiological relevance, with the latter two being referred to as the "slow systems" (Bassani *et al.*, 1992). The relative contribution of each efflux system was assessed in response to a caffeine-induced contraction in rabbit ventricular myocytes (Bassani *et al.*, 1992; Bassani *et al.*, 1994). Typical results are shown in Figure 1.4.

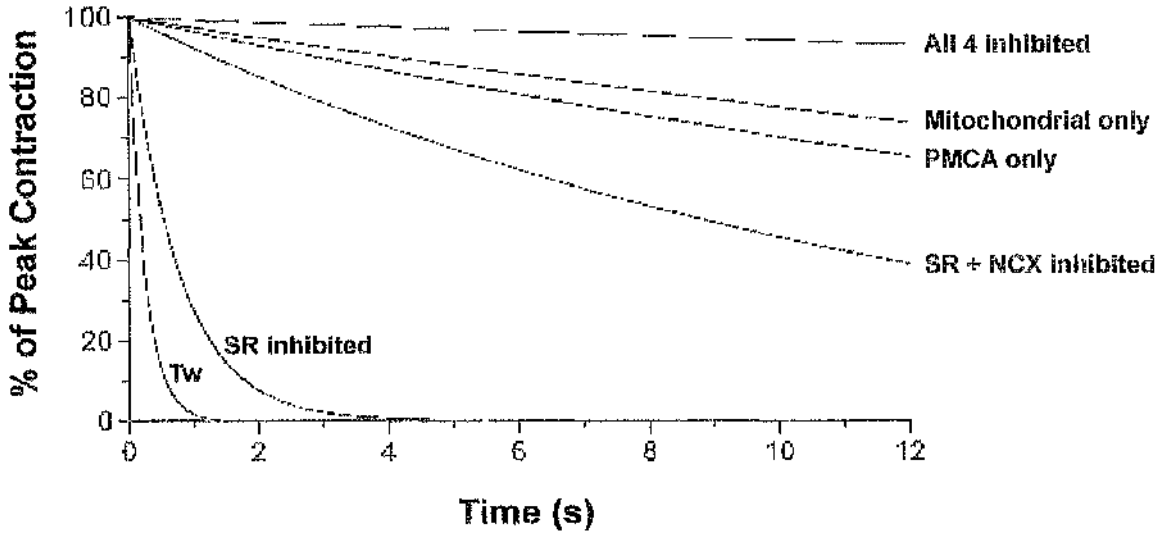

Figure 1.4 Relative contribution of Ca^{2+} efflux pathways to relaxation in the rabbit.

Diagram showing the time-course of decline from a normalised twitch in the rabbit ventricular myocyte when (i) all efflux pathways are operating (Tw; no inhibitors) and then in the presence of (i) SERCA2a inhibition (10 mmol/L caffeine), (ii) SERCA2a and NCX inhibition (10 mmol/L caffeine, Na^+/Ca^{2+} free medium), (iii) PMCA only (PMCA alone; 10 mmol/L caffeine, Na^+/Ca^{2+} free medium, 1 µmol/L carbonyl cyanide p-(tri-fluoremethoxy)phenylhydrazone (FCCP)) and (iv) mitochondrial Ca^{2+} uniporter alone (10 mmol/L caffeine, Na+ free medium, 10 mmol/L Ca^{2+}). Adapted from Bers (2001), based on data from Bassani *et al.*, (1992).

From these data, it was determined that, in the rabbit, SERCA2a and NCX contribute approximately 70 and 28% respectively to relaxation of the caffeine-induced contracture whilst the remaining two contribute less than 1% each (Bassani *et al.*, 1992; Bassani *et al.*, 1994).

1.3.1 Importance of NCX as an efflux mechanism

The extrusion process is critical to the maintenance of Ca^{2+} homeostasis in the ventricular myocyte, both with respect to the strict control of Ca^{2+} fluxes during the contraction-relaxation cycle and also in maintaining the Ca^{2+} gradient between the SR and cytosolic and the intracellular and extracellular milieu.

In cardiomyocytes at rest, because the $[Ca^{2+}]$ within the SR is magnitudes higher than the cytosolic $[Ca^{2+}]$, there is a leak of Ca^{2+} into cytosol which must be accounted for by these extrusion mechanisms in order to maintain Ca^{2+} homeostasis. The balance between the amount of Ca^{2+} re-sequestered to the SR (by SERCA2a) or extruded to the extracellular space (by NCX) will determine the resting SR $[Ca^{2+}]$ content.

NCX is the membrane spanning ion transporter which provides the major route of Ca^{2+} efflux from the cardiomyocyte to the extracellular space. The main role of NCX during the Ca^{2+} transient is to return the Ca^{2+} which entered on I_{Ca} thus maintaining flux balance and promoting relaxation of the ventricular myocyte. In the ventricular cardiomyocyte, Ca^{2+} influx must balance Ca^{2+} efflux such that the SR does not lose or gain Ca^{2+} (Eisner *et al.*, 2000). In mammalian species, SR-mediated Ca^{2+} uptake is main route by which Ca^{2+} is removed from the cytosol although the relative contribution of this and NCX extrusion varies from species to species. As mentioned on the previous page (Figure 1.4), SERCA2a and NCX account for 70 and 28% of extrusion respectively in the rabbit (Bassani *et al.*, 1994). In the rat, however, 92% of the cytosolic Ca^{2+} is re-sequestered into the SR by SERCA2a and only 7% is removed by NCX emphasising the dominance of SR Ca^{2+} at rest in rat in comparison to rabbit (Bassani *et al.*, 1994). Interestingly, the total Ca^{2+} flux during the transient and peak I_{Ca} in rabbit and rat are comparable (Bean & Rios, 1989; Bassani *et al.*, 1994) despite a higher extrusion via NCX in the rabbit. In light of this, it is hard to reconcile the disparity between fluxes in rabbit and rat (i.e. 4 times greater NCX-mediated efflux in the rabbit) in the face of comparable total Ca^{2+} fluxes and peak I_{Ca}. Examination of the integral of Ca^{2+} flux during I_{Ca} in the rat, however, reveals that I_{Ca} inactivates faster and recovers more slowly from the inactivation than in rabbit (Bassani *et al.*, 1994). Consequently, there is a larger I_{Ca}-mediated Ca^{2+}

influx in rabbit versus rat (21 *vs.* 14 μmol/L) (Yuan *et al.*, 1996). With respect to contribution of Ca^{2+} efflux pathways to relaxation in other species, mouse appears similar to rat whilst ferret, cat, dog, guinea-pig and human exhibit values close to those in rabbit (Bers, 2002).

This therefore demonstrates the importance of NCX-mediated Ca^{2+} efflux in the maintenance of SR Ca^{2+} content and Ca^{2+} homeostasis.

1.4 NCX

NCX is preferentially expressed in the sarcolemma of the cardiomyocyte thereby ensuring a uniform removal of Ca^{2+} on NCX throughout the cell and a rapid, controlled relaxation. The study of the precise cellular localisation of NCX protein in the different regions of cardiac sarcolemma (surface sarcolemma, t-tubule membrane and intercalated disc) has yielded differing results. These will be discussed in detail in Chapter 3 (3.1.5.2). NCX abundance varies with developmental stage and protein levels are higher in the embryo and neonate. Investigation in the rat has shown 2.5 times more exchanger in the foetal and neonate compared to the adult (Seki *et al.*, 2003). This reflects the reliance of the immature mammalian cardiomyocyte on trans-sarcolemmal Ca^{2+} fluxes via NCX for EC coupling (Balaguru *et al.*, 1997; Haddock *et al.*, 1999; Sedarat *et al.*, 2000; Bers, 2001). The levels of NCX protein are also altered in pathological conditions such as hypertrophy and heart failure (see 1.5.1 and 1.5.2).

1.4.1 Structure of NCX

The gene encoding for the cardiac NCX (NCX1) was cloned in 1990 and shown to consist of 938 residues (Nicoll *et al.*, 1990). Building on this significant advance, the detailed structure of NCX has been elucidated and is shown on the following page in Figure 1.5. NCX is composed of nine transmembrane domains (TM1-TM9) that lie in a circle within the membrane. This arrangement includes the exchange pore, consisting of pore-forming regions between TM's 2 and 3 and TM's 7 and 8, and an extensive intracellular loop, encompassing 550 amino acids between TM's 5 and 6 (Nicoll *et al.*, 1999; Schulze *et al.*, 2003).

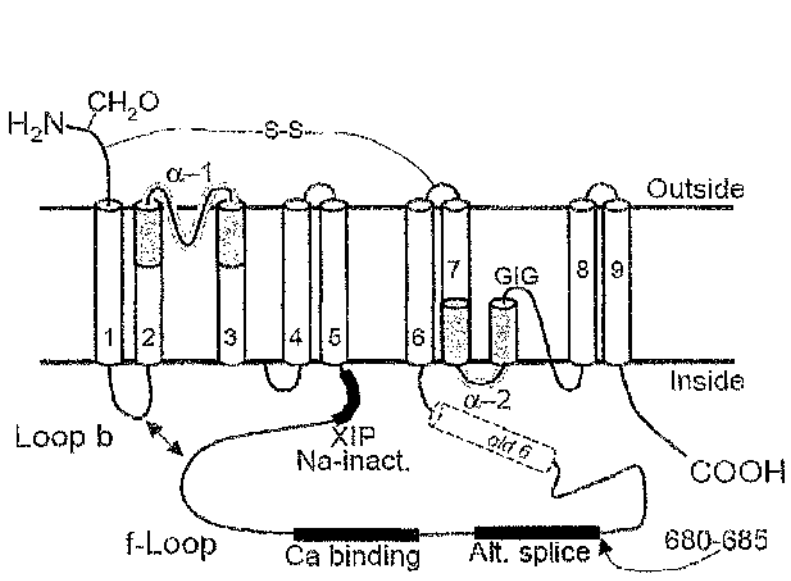

Figure 1.5 Structure of NCX1.

Schematic representation of the structure of NCX1 in the cardiac sarcolemma. The 9 transmembrane domains are labelled (1-9); intracellular C- and extracellular N-terminals are shown. The position of the XIP region, Ca^{2+} binding site and alternative splicing sequence are indicated in the large intracellular loop. Diagram adapted from Bers, (2001).

The loop region contains a high-affinity binding site for Ca^{2+}, an alternative splicing sequence and the endogenous "XIP" sequence (Nicoll *et al.*, 1999). The XIP region is a 20 amino acid long sequence (named due to the binding of exchanger inhibitory peptide here) and is involved in inactivation due to high $[Na^+]$ (Na^+-dependent inactivation) (Matsuoka *et al.*, 1997).

Schulze and colleagues (2003) recently suggested that NCX is part of a macromolecular signalling complex as has previously been shown for both the cardiac LTCC and RyR2. Within the complex there is a co-localisation of PKA and PKC, protein phosphatases 1 and 2 (PP1 and PP2A) and an A Kinase Anchoring Protein (mAKAP). The intracellular loop is the critical site at which the elements of the complex are anchored onto NCX. Leucine/isoleucine zipper regions contained here may connect mAKAP and PP1/PP2 to the NCX protein. In addition, it has been speculated that the adapter protein, ankyrin, links the intracellular loop with the cytoskeletal network and may account for the targeting of the NCX complex to the t-tubule membrane (Schulze *et al.*, 2003). A diagram of the proposed NCX complex is presented in Figure 1.6.

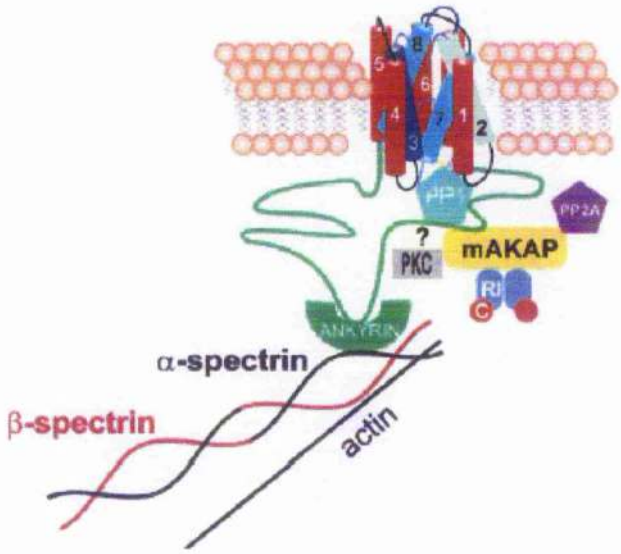

Figure 1.6 The NCX macromolecular complex.

Schematic representation of the spatial organisation of the NCX macromolecular complex. The transmembrane domains are numbered and the intracellular loop is shown in green. Proteins associating with the loop are defined in the text above. Adapted from Schulze *et al.*, (2003).

1.4.2 Electrochemical dependence of NCX function

The existence of a Na^+/Ca^{2+} countertransport system in cardiac muscle was first demonstrated by Reuter & Seitz (1968) who showed that the rate of Ca^{2+} efflux was dependent on $[Na^+]_o$ and $[Ca^{2+}]_o$. The stoichiometry of NCX has since been determined as $3Na^+:1Ca^{2+}$ (Reeves & Hale, 1984). This relationship dictates that transport via NCX is electrogenic (net difference of 1 positive charge for every Ca^{2+} ion transported) and therefore produces an ionic current (I_{NCX}) during its functioning. Ion transport via the exchanger is bidirectional and can work in "forward mode" extruding Ca^{2+} from the cardiomyocyte or "reverse mode" causing Ca^{2+} influx into the cardiomyocyte. The mode of operation of the exchanger is dependent on thermodynamic conditions. These can be used to define the equilibrium potential of NCX (E_{NCX}) which is the E_m where I_{NCX} equals zero. The following equation can be used to calculate E_{NCX}:

$$E_{NCX} = 3E_{Na} - 2E_{Ca}$$

Where E_{Na} and E_{Ca} are the equilibrium potentials for Na and Ca respectively defined using the Nernst equation.

The thermodynamic driving force for NCX activity is therefore defined as:

$$E_m - E_{NCX}$$

Thus when $E_m < E_{NCX}$, forward mode is favoured; Ca^{2+} leaves the cell and I_{NCX} is inward. When $E_m > E_{NCX}$, reverse mode is favoured; Ca^{2+} enters the cell and I_{NCX} is outward.

At rest (E_m = -80 mV), E_{NCX} will be approximately -33 mV and so I_{NCX} will be inward and the exchanger will be operating to extrude Ca^{2+} (Bers, 2001).

1.4.2.1 NCX function during the action potential

The electrochemical parameters which dictate NCX function are altered during the action potential and Ca^{2+} transient. As a consequence of this, the profile of NCX activity also varies during these events and in doing so contributes to the shaping of the action potential itself. This relationship is shown in Figure 1.7.

As previously stated, Ca^{2+} extrusion on NCX is favoured at rest because E_{NCX} is positive to E_m. The amount of Ca^{2+} transported is modest though due to substrate limitation ($[Ca^{2+}]_i$ is low at rest; approximately 100-150 nmol/L).

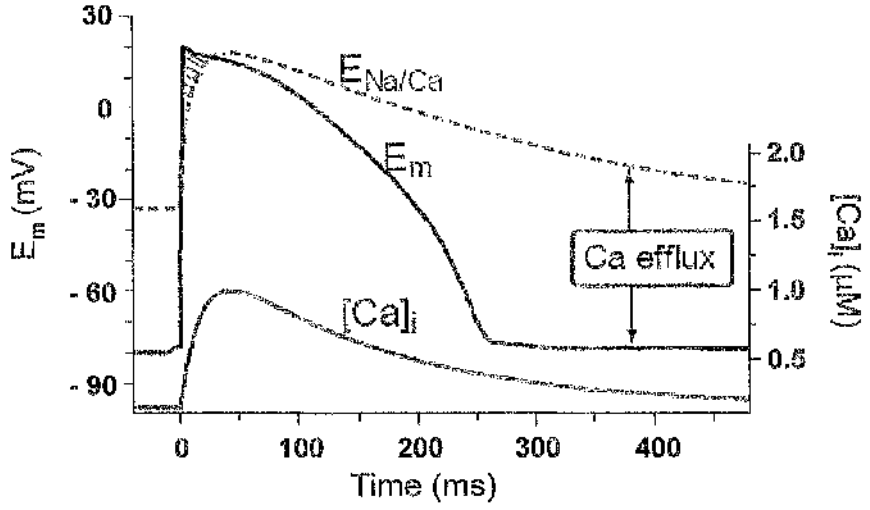

Figure 1.7 Changes in E_{NCX} during the action potential in rabbit ventricle.

Plot showing the change in E_{NCX} (dashed red line) in response to altered E_m (black) and $[Ca^{2+}]_i$ of the transient (blue) during the course of the action potential. The shaded area at the peak E_m represents the brief period of Ca^{2+} influx on NCX. Based on $[Na^+]_i$=8.9 mmol/L and peak $[Ca^{2+}]_i$=1 μmol/L. Adapted from Bers, (2001).

Upon depolarisation, Na^+ channels open and this large inward current rapidly brings E_m up to threshold for LTCC opening. These events cause $[Ca^{2+}]_i$ to rise and both E_m and E_{NCX} become more positive. E_m however, increases on a much faster timescale than E_{NCX} and it is this lag-time, between E_{NCX} increasing in line with E_m, that causes there to be a brief period in which E_m is positive to E_{NCX} and Ca^{2+} entry on NCX occurs (shaded area at the E_m peak in Figure 1.7). During this time, however, SR Ca^{2+} release is triggered (CICR) producing the peak of the $[Ca^{2+}]_i$ transient which moves E_{NCX} more positive to E_m. Additionally, E_m starts to become more negative with respect to E_{NCX} due to inactivation of LTCCs. Inward I_{NCX} is favoured once again and this large depolarising current (due to increasing driving force on I_{NCX}) maintains the late plateau phase of the cardiac action potential.

During the subsequent repolarisation phase of the action potential, $[Ca^{2+}]_i$ remains high, I_{NCX} is strongly inward and Ca^{2+} extrusion continues. $[Ca^{2+}]_i$ declines via I_{NCX} (although mainly through SERCA2a) and the resting state is re-established. Forward mode NCX function, in which Ca^{2+} is extruded from the cardiomyocyte, is therefore the principal mode of operation of the exchanger.

It must be noted, however, that this is a generalised overview of NCX activity during the action potential as sub-sarcolemmal ion concentrations may differ from those in the bulk cytoplasm due to spatial ionic gradients (Trafford *et al.*, 1995).

1.4.3 NCX and arrhythmogenesis

The role of NCX in the generation of triggered arrhythmias is well established and is due to two features of NCX functioning:

(i) NCX can generate an inward, depolarising current which, if large enough, can bring E_m up to threshold for an action potential to fire.

(ii) NCX activity can modulate SR Ca^{2+} content and contribute towards SR Ca^{2+} overload.

NCX has been implicated in the production of aberrant depolarisations called afterdepolarisations. These are oscillations of the E_m which depend on prior stimulation from the preceding action potential and can lead to the triggering of an arrhythmic action potential (Volders *et al.*, 2000). There are two types of afterdepolarisations; early and delayed (Figure 1.8).

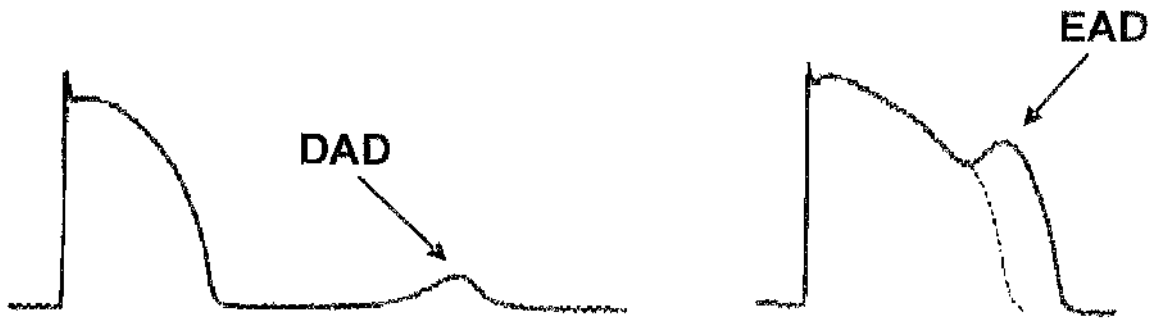

Figure 1.8 Delayed and early afterdepolarisations.

Schematic diagram showing the occurrence of a delayed afterdepolarisation (DAD) and an early afterdepolarisation (EAD) with respect to the action potential. Adapted from Volders *et al.*, (2000).

Delayed afterdepolarisations (DADs) occur when the action potential has fully repolarised to the resting E_m and are associated with SR Ca^{2+} overload. Early afterdepolarisations (EADs) occur during the plateau or late repolarisation phase and are associated with increased action potential duration.

The cellular event that initiates DADs is SR Ca^{2+} release as they can be blocked in the presence of ryanodine (Marban *et al.*, 1986). When the SR becomes overloaded, it releases Ca^{2+} spontaneously. Occasionally, localised spontaneous release events accumulate to produce global propagating Ca^{2+} release called Ca^{2+} waves. This then activates an arrhythmogenic Ca^{2+}-induced transient inward current (I_{ti}) (Kass *et al.*, 1978). I_{ti} may be due to any of the three following Ca^{2+} activated currents: (i) I_{NCX}, (ii) Ca^{2+} activated Cl^- current ($I_{Cl(Ca)}$) or (iii) a non-selective cationic current ($I_{NS(Ca)}$). This current depolarises E_m towards threshold and, if sufficiently large, can trigger an action potential. $I_{NS(Ca)}$ is not considered to contribute significantly to I_{ti} and the relative proportion made up of I_{NCX} and $I_{Cl(Ca)}$ varies with the species and cardiomyocyte cell type. In rabbit ventricular myocytes, over 90% of I_{ti} has been attributed to I_{NCX} (Schlotthauer & Bers, 2000) thus highlighting the fundamental contribution of NCX activity in the development of DADs.

EADs occurring either in the plateau or in the early phases of repolarisation are considered to be due to a voltage "window" which allows reactivation of I_{Na} and I_{Ca} and act to reverse repolarisation. EADs are associated with long duration action potentials and it is this prolongation which provides sufficient time for voltage-gated sodium channels (VGSCs) and LTCCs to recover from inactivation and hence be reactivated by the falling E_m during repolarisation (Marban *et al.*, 1986; Volders *et al.*, 2000). EADs which occur in the later stages of repolarisation (below -40 mV) are considered to be due to a mechanism similar to DADs as described above.

1.4.4 Regulation of NCX function

NCX function in the ventricular myocyte is regulated by a great range of intracellular proteins and messengers, the list of which continues to grow. The major regulators of NCX and those which are covered in the current thesis are briefly described below.

(i) **Ca^{2+}** - Regulation of NCX by Ca^{2+} occurs through the intracellular loop. When Ca^{2+} binds to the high-affinity site here, it causes a conformational change which activates the exchanger (Philipson & Nicoll, 2000).

(ii) **Na^+** - Application of Na^+ to the intracellular side of NCX has been shown to produce Na^+-dependent inactivation (Hilgemann, 1990). This is suggested to involve the XIP region on the intracellular loop (Matsuoka *et al.*, 1997).

(iii) **Phosphatidylinositol-4,5-bisphosphate (PIP_2)** - the intracellular messenger PIP_2 has been postulated to increase NCX activity through attenuation of Na^+-dependent inactivation at the XIP region (Hilgemann & Ball, 1996; He *et al.*, 2000; Philipson & Nicoll, 2000).

(iv) **Phosphorylation** - The phosphorylation and subsequent regulation of cardiac NCX function via PKC or PKA remains controversial (Ruknudin *et al.*, 2000; Ginsburg & Bers, 2005).

(v) **Sorcin** - Sorcin is a small protein (22 kDa) which is highly expressed in cardiac muscle. Previous work in rabbit cardiomyocytes has shown that sorcin interacts with and inhibits NCX activity (Seidler *et al.*, 2003; Smith *et al.*, 2005b).

(vi) **Phospholemman (PLM)** - PLM is a membrane phosphoprotein which has been shown to inhibit NCX function (Zhang *et al.*, 2003). This is mediated by phosphorylation of PLM.

Of these, regulation of NCX by sorcin, PLM, and phosphorylation will be focussed on in Chapters 4, 5 and 6 of this thesis respectively. An additional "structural regulator", the t-tubule network, has also been investigated in Chapter 3.

1.5 Heart failure

In its most basic terms, heart failure describes the inability of the heart to provide sufficient cardiac output to meet the metabolic demands of the organs. It is a clinical syndrome of symptoms and signs, usually chronic and involving both local and systemic alterations.

Heart failure is a major health problem facing the Western world. Indeed, it is the only cardiovascular disease which is increasing both in incidence and prevalence. The prognosis of patients with advanced heart failure (NYHA Class III or IV) is poor, with five year mortality rates around 50% (Narang *et al.*, 1996). In order to better design drug therapy towards the treatment of this growing health burden, a better understanding of the factors contributing towards the development of heart failure must be sought. Determination of the mechanisms behind the dysfunction both in single cells and in the whole heart will enable therapeutic targets to be identified.

At the whole heart level, the contractile performance of the failing heart is substantially reduced and mortality arises by one of two main routes (i) progressive decline of cardiac function or (ii) sudden cardiac death due to arrhythmia. The most common cause of heart failure is left ventricular dysfunction (LVD) as a consequence of myocardial infarction (MI). Systemic effects arise due to back pressure and congestion; these manifest as pulmonary and peripheral oedema.

At a cellular level in failing hearts, both contraction and relaxation are depressed due to altered Ca^{2+} handling. Most studies agree that this is due to altered function, expression and/or regulation of the major Ca^{2+} handling proteins and ion currents. This has been demonstrated for LTCC, RyR2, SERCA2a, PLB, NCX in both animal models of heart failure and in the human failing heart (Hasenfuss *et al.*, 1996; Hasenfuss *et al.*, 1999; Sipido *et al.*, 2002). The alterations in NCX activity and protein/mRNA will be expanded upon in the following sections.

1.5.1 Changes in NCX in human heart failure

As with all studies at the single cell level in humans, the major set-back to defining alterations in NCX function and protein expression is accessibility to tissue. The majority of human studies use tissue obtained from explanted hearts at the time of transplant. It is, however, almost impossible to account for variation within this group attributable to their backgrounds (underlying pathology of heart failure and other complicating diseases, medication, genetic make-up and lifestyle). Normal healthy tissue samples are extremely scarce.

Studies on the alterations in NCX activity and expression in human heart failure tissue have produced conflicting results. In addition, there is a lack of functional measurements of NCX activity with most studies concentrating on protein levels. In general, the data obtained have either shown an increase (Reinecke *et al.*, 1996; Hasenfuss *et al.*, 1999) or no change (Prestle *et al.*, 1999; Schwinger *et al.*, 1999). The variation in protein levels may have been attributable to the underlying cause of heart failure in these patients. With this in mind, Hasenfuss and colleagues divided their patient population according to their diastolic function. In doing so, it was determined that the group with disturbed diastolic function had unchanged NCX expression accompanied by a decrease in SERCA2a, whilst the group with preserved diastolic function had increased NCX expression in combination with unchanged SERCA2a expression (Hasenfuss *et al.*, 1999).

1.5.2 Animal models of heart failure

Due to the difficulties associated with human studies, animal models are essential in our understanding of the mechanisms leading to heart failure. Many animal models of hypertrophy and heart failure have been produced in order to mimic the situation in humans. Modes of induction which have been used include myocardial infarction(Pye & Cobbe, 1996; Litwin & Bridge, 1997), combined pressure and volume overload (Pogwizd *et al.*, 1999), pressure overload (Wang *et al.*, 2001b) and rapid pacing (Yao *et al.*, 1998).

The overall aim of animal models is to identify potential therapeutic targets for the treatment of human heart failure. It is therefore important to use a species and induction mode which mimics the human pathophysiology as closely as possible. The model used in the present thesis was a rabbit infarct model of LVD. The rabbit is a pertinent choice for a model species in which to study alterations in Ca^{2+} homeostasis because the profile of Ca^{2+} handling (Ca^{2+} extrusion and SR dependence) in the rabbit is more similar to that of human than those of rat or mouse. The anatomy of the coronary vasculature in the rabbit is also similar to the human heart in that there is minimal collateral circulation present (Neary *et al.*, 1998).

The rabbit infarct model has been well characterised in terms of its haemodynamic function, shown to develop LVD as a result of the infarct and to exhibit many of the parameters associated with heart failure in the human (Pye & Cobbe, 1996). The production of the model is described in detail in Chapter 2 (2.1.1). Ligation of the left coronary artery leads to an abrupt loss of blood supply to the apical region of the heart and subsequently a defined transmural infarct. The procedure is associated with an incidence of sudden death post-operatively which may be linked to arrhythmia. Following recovery, LVD animals exhibit significantly reduced left ventricular mean ejection fractions and significantly increased left ventricular end-diastolic dimensions (LVEDD) and left atrial dimensions (LAD) *vs.* sham-operated rabbits. In addition, they show evidence of systemic congestion in significantly increased heart, liver and lung weights (Ng *et al.*, 1998; McIntosh *et al.*, 2000)

1.5.2.1 Changes in NCX in animal models of heart failure

Studies of NCX activity and protein levels in animal models of hypertrophy and heart failure have also yielded vastly conflicting results. In a recent review of NCX activity and/or protein expression in animal models by Sipido *et al.*, there were three general subsets; those which exhibited an increase, those which exhibited a decrease and those in which no difference was apparent (Sipido *et al.*, 2002). The discrepancies may be partly due to (i) species differences, (ii) mode of induction of hypertrophy/failure, (iii) severity of hypertrophy/failure and (iv) in the case of infarct models, the distance from the infarct of the cells

under study. Another important point raised by this review is that activity and protein expression are not positively correlated and that it is imperative to assess both in order to determine the net physiological effect. It is therefore unclear as to the general effect which cardiac remodelling has on NCX function and expression and thus its role in heart failure.

Of the large number of animal models in which NCX has been studied five have been performed in the rabbit whilst eight have been induced by MI. In order to demonstrate the diversity of the results obtained in these studies, summary tables are presented on the following pages highlighting the main results of NCX protein/mRNA and NCX function (I_{NCX} or sarcolemmal vesicle uptake (SLV) as indicated) detected in rabbit models (Table 1.1) and in MI-induced models (Table 1.2).

Table 1.1 NCX in rabbit models of hypertrophy and heart failure.

Summary of the main results obtained in each rabbit model of hypertrophy/heart failure. Abbreviations: SLV - sarcolemmal vesicle. Data taken from Sipido *et al.*, (2002) and are expressed as % change *vs.* control.

First Author & Year	Rabbit Model	NCX protein/mRNA	NCX Function
Heyliger *et al.* (1995)	Aortic banding	Not assessed	No change (SLV uptake)
Yao *et al.* (1998)	Pacing-induced tachycardiac	↓ by 34 % (mRNA)	↓ outward current (by 24 %)
Pogwizd *et al.* (1999)	Aortic banding & aortic regurgitation	↑ by 200 % (mRNA) ↑ by 250 % (protein)	↑ outward current (by 200 %) & ↑ inward current
Litwin & Bridge (1997)	Ligation	Not assessed	↑ outward current
Quinn *et al.*, (2003)	Ligation	↑ by 26% (mRNA) ↑ by 32 % (protein)	↓ I_{NCX} (by 25 %)

Table 1.2 NCX in ligation models of hypertrophy and heart failure.

Summary of the main results obtained in each MI model of hypertrophy/heart failure. Abbreviations: SLV - sarcolemmal vesicle, REM - remote area and ADJ - adjacent area. Data taken from Sipido *et al.*, (2002) and are expressed as % change *vs.* control.

First author & year	Species	Age	Model	NCX mRNA	NCX Protein	NCX Function
Dixon/Sethi *et al.*, (1992/9)	Rat	4-16 weeks	Ligation (LCA)	Not assessed	Not assessed	↓ by 23-50 % (SLV uptake)
Makino *et al.*, (1996)	Rat	8-12 weeks	Ligation (LCA)	Not assessed	Not assessed	↓ by 40 % (SLV uptake)
Zhang *et al.*, (1996/8/9)	Rat	3 weeks	Ligation (LCA)	Not assessed	No change	↓ outward current
Wasserstrom *et al.*, (2000)	Rat	6 weeks	Ligation (LCA)	↑ by 130-140 %	↑ by 137 %	↑ outward current
Yoshiyama *et al.*, (1997)	Rat	1 week 3 weeks 3 month	Ligation (LAD)	↑ by 160 % ↑ by 160 % ↑ by 160 % (REM)	↑ by 210 % ↑ by 150 % ↑ by 90 % (ADJ)	Not assessed
Litwin & Bridge (1997)	Rabbit	8 weeks	Ligation (RCX)	Not assessed	Not assessed	↑ outward current
Pu *et al.*, (2000)	Dog	5 days	Epicardial border zone	Not assessed	Not assessed	No change
Quinn *et al.*, (2003)	Rabbit	8 weeks	Ligation (RCX)	↑ by 26 %	↑ by 32 %	↓ inward current (by 30 %)

It is evident from Tables 1.1 and 1.2 that no consistent pattern of NCX alteration existed between models either in the same species or by the same mode of induction.

Of the studies of NCX in animal models, there are many which show that protein and activity are either both increased (Pogwizd *et al.*, 1999; Gomez *et al.*, 2002) or both decreased (Yao *et al.*, 1998; Qin *et al.*, 1996). Previous work in the rabbit model of LVD featured in this thesis identified a paradoxical change in NCX activity and protein/mRNA expression (Quinn *et al.*, 2003). NCX protein levels and mRNA were increased by 32 and 26% respectively. In contrast, assessment of I_{NCX} using voltage-clamped single cells revealed that I_{NCX} was reduced to 75% of the sham current. The dichotomy detected in our model is in agreement with findings in a mouse aortic banding model (Wang *et al.*, 2001b). Here NCX mRNA and protein were increased by 26 and 71% respectively compared to controls. I_{NCX} was, however, significantly decreased both in forward and reverse modes.

In summary, the investigation of NCX in both human and animal models of hypertrophy or heart failure has not yet come to a clear consensus as to the altered profile of NCX compared with that in healthy myocardium. It is also evident that the full profile of NCX in the cardiomyocyte (activity, protein and mRNA expression) must be studied in order to characterise the mechanisms at play in hypertrophy and heart failure. The conflicting protein and activity measurements in our model and that of Wang *et al.*, suggest that the profile of NCX in hypertrophy and failure may be more complex than the literature would suggest and that abnormal regulation of NCX may also be contributing to the contractile abnormalities in the failing heart. An investigation of a number of factors involved in the regulation of NCX was therefore undertaken in the present thesis.

CHAPTER 2
GENERAL METHODS

2.1 Rabbit model of Left Ventricular Dysfunction

The investigation utilised a rabbit infarct model of left ventricular dysfunction produced by ligation of the circumflex branch of the left coronary artery followed by an eight-week recovery period. This model has previously been characterised by Pye *et al* (1996).

All procedures were carried in accordance with The Animals (Scientific Procedures) Act 1986 and had been approved by the University of Glasgow's ethics committee.

All surgical and post-operative procedures were undertaken by staff at Glasgow Royal Infirmary.

2.1.1 Coronary artery ligation protocol

Adult New Zealand white rabbits (male, approximately 12 weeks old and 2.5-3 kg in weight) were pre-medicated with intramuscular fentanyl/fluanizone 0.4 mL/kg (Hypnorm™, Jansen Pharmaceuticals). Anaesthesia was induced via a cannula in the marginal ear vein using midazolam (1-2 mg/kg). The rabbit was intubated, ventilated and anaesthesia was maintained via a 1:1:1 mixture of nitrous oxide, oxygen and halothane. A left thoracotomy was performed and a ligation was made at the mid point between the origin of the major left ventricular (LV) branch of the left coronary artery (circumflex coronary artery) and the apex of the heart. This quickly resulted in an apical infarct. Once the animal had stabilised, the wound was closed and saline was administered to replace fluids lost during the procedure. Postoperatively, rabbits were given antibiotics and analgesia (buprenorphine, 0.03 mg/kg/8 hr for 3-4 days). Good animal husbandry was employed throughout the animals' recovery. The infarct accounted for approximately 30-40% of the LV following the eight week recovery period as is shown diagrammatically in Figure 2.1.

Figure 2.1 Apical infarct produced in rabbit model of LVD.

Diagram showing a typical apical infarct (right in grey) produced by ligation of the circumflex artery (left) following an eight week recovery period. Diagram taken from Burton *et al.*, (2000).

A second population of sham-operated animals was created which underwent the same surgical intervention with exception of the ligation; recovery period and post-operative care were as before.

Eight weeks following the procedure the left ventricular function and dimensions were assessed by echocardiography and haemodynamic assessment. This was performed using a Toshiba 5 MHz short focus, wide-angle phased array ultrasound system and a Toshiba SSH160A echocardiograph whilst the animal was lightly sedated. Measurement of the left ventricular end-diastolic internal diameter gave an estimation of left ventricular size. End-diastolic and end-systolic images allowed ejection fraction (EF) to be calculated as (end-diastolic area - end-systolic area/end-diastolic area)

2.2 Single cell studies

2.2.1 Isolation of single cardiomyocytes

Following the eight-week recovery period, animals were sacrificed for in vitro studies. In addition to the heart, the lungs and liver were removed and weighed from animals with LVD as an indication of severity of the ventricular impairment.

Isolated single cardiomyocytes were obtained through enzymatic digestion of the extracellular matrix and connective tissue which interlink cells in the whole heart.

2.2.1.1 Solutions

Solutions were freshly prepared for each experimental run. All concentrations are in (mmol/L) except where stated otherwise; pH correction was performed at room temperature (20-21 °C).

Base Krebs' - NaCl (120), KCl (5.4), NaH_2PO_4 (0.52), $MgCl_2.6H_2O$ (3.5), HEPES (20), Taurine (20), Creatine (10), Glucose (11.1); pH 7.4 with NaOH.

Enzyme solution - as for base Krebs' with 0.67 mg/mL collagenase and 0.04 mg/mL protease added.

Bovine serum albumin (BSA) solution - as for base Krebs' with 1% BSA added. Successive [Ca^{2+}] of this solution were produced (0.062, 0.125, 0.25, 0.5, 1.0).

2.2.1.2 Isolation protocol

Prior to experiments, rabbits with or without LVD were euthanased via overdose with Euthatal (sodium pentobarbitone, 100 mg/kg, i.v. with 500 i.u. heparin). The heart was quickly excised and placed into ice-cold Krebs' solution. This was then gently agitated in two washings of Krebs' to ensure removal of excess blood. The excised heart was mounted via the aorta onto the outflow of a Langendorff retrograde perfusion system and secured using thread. Perfusion was commenced with nominally Ca^{2+}-free Krebs' (37 °C at 25 mL/min) in order to

wash out any residual blood and Ca^{2+}. The pulmonary artery was cut to provide an outflow for the perfusate and excess fat/connective tissue was trimmed away. The heart was then perfused with enzyme solution which was collected as it flowed out and, once the initial volume had passed, was re-circulated through the system with the addition of 0.05 mmol/L Ca^{2+}. This digestion phase continued for approximately 5-7 min until the heart became soft. After this time had elapsed the heart was washed free of the enzyme with BSA solution (0.062 mmol/L Ca^{2+}) and cut down once it felt soft to the touch. The heart was placed into a petri dish containing BSA solution (0.125 mmol/L Ca^{2+}). The basal LV was removed - care was taken to ensure that this section did not include either infarcted or peri-infarcted tissue from animals with LVD while a corresponding area was taken from sham animals. This was chopped up using scissors. The tissue pieces and solution were placed into a flask and left to shake for 1 hr at room temperature. Following this, the suspension was removed and dissociated cells were allowed to sediment by gravity. The supernatant was aspirated and cells were re-suspended in BSA solution with 0.25 mmol/L Ca^{2+}. The cells were subsequently transferred using the same steps to BSA solution containing 0.5 then finally 1.0 mmol/L Ca^{2+}.

Isolated cardiomyocytes used for the various investigations in this thesis were obtained either in BSA solution with 0.125 (T-tubule staining) or 1.0 mmol/L Ca^{2+} (electrophysiological measurement).

Cells were stored for up to 4 hours in respective BSA solutions at room temperature until required.

2.2.2 Permeabilisation of isolated cardiomyocytes using β-escin

The permeabilising agent β-escin was used in the present thesis to permeabilise isolated cardiomyocytes in order to allow examination of intracellular structure (t-tubules) and protein distribution (NCX). The mechanism of action of β-escin involves complexing with membrane-bound cholesterol to form aqueous pores of approximately 8 nm in diameter. Previous work quantitatively assessed permeabilisation over a range of concentrations in isolated rabbit cardiomyocytes. The protocol was centred on the feature of Ca^{2+}-mediated

contraction in which relaxed, rod-shaped cells with permeable membranes would contract when exposed to high [Ca^{2+}]. Two HEPES-buffered Krebs'-based bathing solutions were produced, one with high Ca^{2+} (Ca^{2+}EGTA), the other with low Ca^{2+} (EGTA). These had the following composition (mmol/L): KCl (100), MgCl (5.5), HEPES (25), K_2ATP (5), Na_2PCr (10) with either EGTA or Ca^{2+}EGTA (both 5) added. The Ca^{2+} concentrations of 5 mmol/L EGTA and 5 mmol/L Ca^{2+}EGTA solutions were calculated at <1 nmol/L and 20 μmol/L respectively. Cells were exposed to varying concentrations of β-escin in each solution. The haemocytometer method of cell counting was then employed to quantify the number of rods. This rod count was expressed relative to the control rod count (no permeabilising agent) in order to relate the decrease in rod count to the degree of permeabilisation. From this study, a permeabilisation protocol was constructed which defined a minimum effective concentration of β-escin - the concentration which selectively permeabilises the sarcolemma of more than 95% of a population of isolated cardiac myocytes (results shown in Figure 2.2).

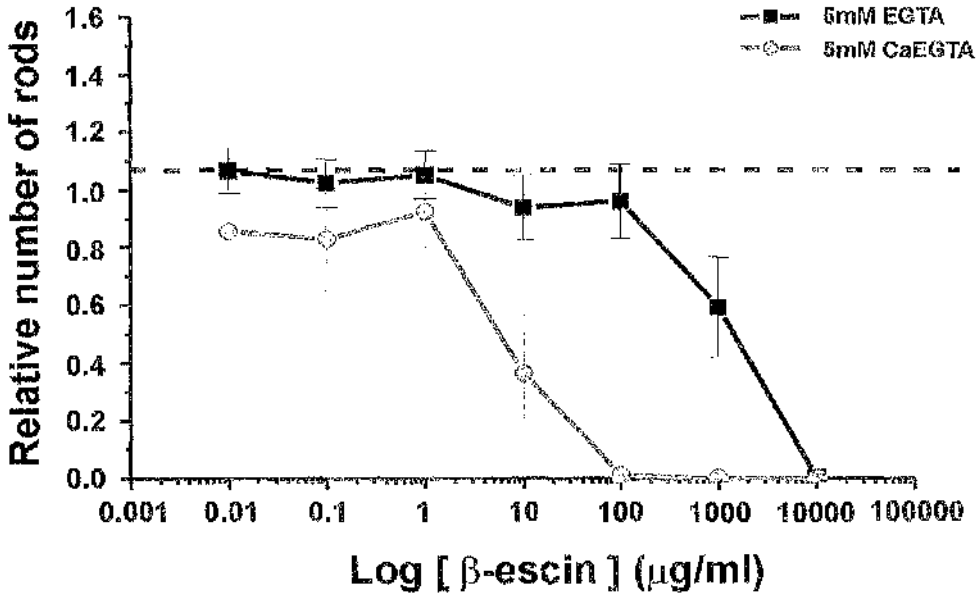

Figure 2.2 Permeabilising effect of β-escin on isolated cardiomyocytes.

Concentration-response curve showing the permeabilising effect of β-escin (0.01-10000 μg/mL, 2 min exposure) on isolated cardiomyocytes in 5 mmol/L EGTA (< 1 nmol/L [Ca^{2+}]) and 5 mmol/L Ca^{2+}EGTA (20 μmol/ [Ca^{2+}]); results normalised against the control count. 100 μg/mL was determined as the minimum effective concentration. Declining rod numbers after this point were attributed to cellular damage by β-escin.

The protocol recommended a β-escin concentration of 100 μg/mL to successfully permeabilise isolated rabbit cardiomyocytes and was employed throughout the t-tubule studies in this thesis.

2.2.3 Laser Scanning Confocal Microscopy

The confocal microscope is a very powerful experimental tool capable of producing high quality, optically sectioned images of biological specimens. It brings together the properties of conventional microscopy in combination with lasers, fluorescent probes and technological innovations which eliminate the interference from out-of-focus light.

2.2.3.1 Principles of fluorescence

The process of fluorescence involves the excitation of an outer electron from an atom into a higher energy state which then decays releasing a light photon (Figure 2.3).

The energy contained in an incident photon from an external source is absorbed by an outer electron in the ground state (G_0) thereby exciting it and promoting it into a higher excited energy state (S_1'). This state is unstable (typical lifetime 1-10 ns) and the electron spontaneously decays to the metastable state (S_1) releasing a small amount of its energy as heat which is dissipated to the surroundings (a non-radiative transition). It then remains here for a short time before returning to the ground state and emitting its energy in the form of a photon.

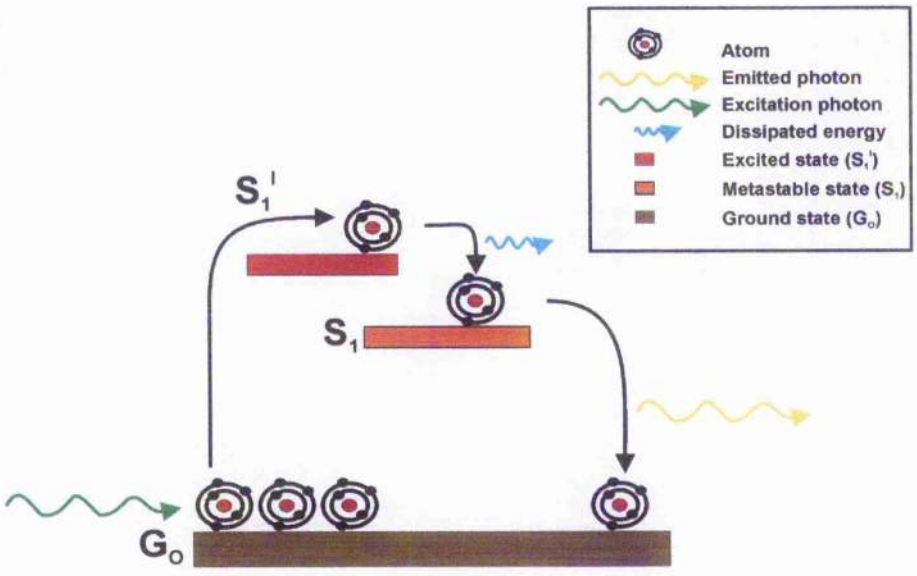

Figure 2.3 Schematic diagram of fluorescence

An outer electron from an atom is excited from the ground state (G_0) into a higher energy level (S_1') via absorption of an incident photon. This then decays spontaneously (to S_1) before returning to the ground state and releasing its energy in the form of a photon. Released photons form the basis of fluorescence.

The process of fluorescence is applicable to many aspects contained within this thesis which utilise fluorescent probes/markers as reporters of cellular function/structure.

2.2.3.2 Principles of laser scanning confocal microscopy

Laser Scanning Confocal Microscopy (LSCM) is a specialised form of fluorescence microscopy which images only from the plane of focus leading to the production of high resolution output. A highly intense beam of light provided by a laser (Light Amplification by Stimulated Emission of Radiation) is used to excite the fluorescence source known as a fluorophore. This is a molecule containing aromatic residues which can be targeted to a specific region of the specimen and excited at a distinct wavelength to report on various cellular processes. An extension of this is achieved by using two fluorophores with differing excitation wavelengths to label two areas of a cell.

The following diagram (Figure 2.4) and explanation highlight the features which make LSCM possible.

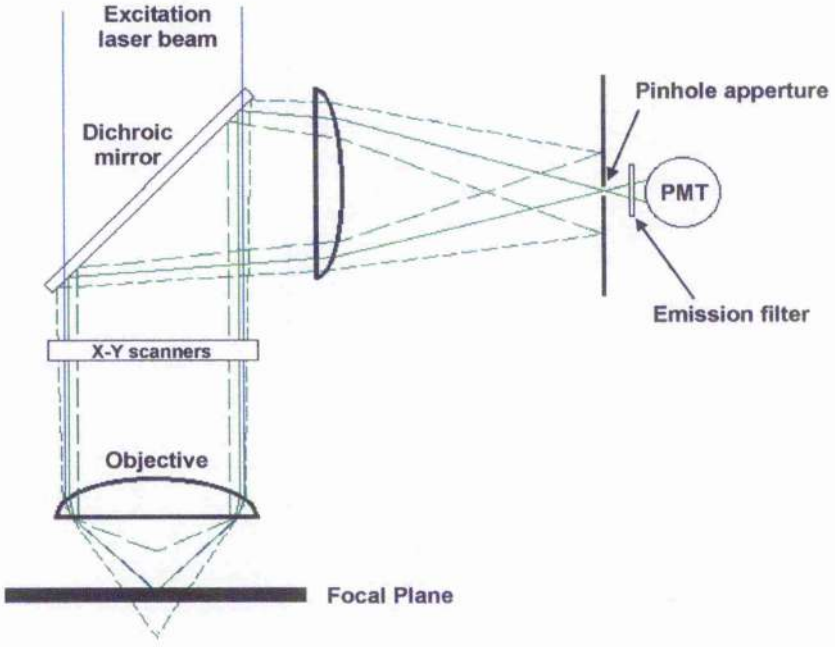

Figure 2.4 Features of a confocal microscope

Taken from "The confocal principle and microscope design", www.gonda.ucla.edu/bri_core/confocal.htm.

1. Very high intensity excitation light of a specific wavelength is provided by a laser.

2. The light passes to the scanning mirrors (controlled by a computer) which scan the laser beam over the focal point of the objective thus exciting the fluorophore within this highly restricted region. Minimal excitation occurs to the surroundings as the high level of collimation of the laser beam produces a single point of excitation which falls off rapidly outside the focal point.

3. Emitted light is then focussed back through the optics to the dichroic mirror. This is designed to reflect light shorter than a pre-defined wavelength and pass light longer than this pre-defined wavelength. Thus any contaminating excitation light will be reflected and only emitted light (which is of longer wavelength, see above) will pass through.

4. The light then passes through a pinhole aperture which is situated in front of the detector in a conjugate plane to the focal point of the objective. This serves to further limit emitted light from above and below the focal point.

5. Emitted photons are received and the signal amplified by a photomultiplier tube which is connected to a computer which builds up the image one pixel at a time.

2.3 Biochemical methods

2.3.1 Quantitative Western Blotting - Principles

The technique of Western blotting or protein immunoblotting allows the isolation of a protein of interest from a mixture of proteins. There are two main steps involved: (i) SDS-Poly Acrylamide Gel Electrophoresis (SDS-PAGE) and (ii) probing with immuno-specific antibodies directed against the antigen (protein of interest).

SDS-PAGE separates proteins in a mixture according to molecular weight over an electric field. Firstly the sample of protein is mixed with the anionic detergent sodium dodecyl sulphate (SDS). This breaks down all non-covalent linkages within each protein promoting unfolding of all tertiary and secondary structure. The concomitant heating of the sample (approximately 10 min at 70 °C) at this time serves to further denature the structure. The inclusion of a second reducing agent (most commonly dithiothreitol (DTT) or β-mercaptoethanol (β-ME)) ensures all disulphide bonds are broken, leaving proteins as single polypeptide chains. SDS then uniformly coats the linearised main chains of each protein in negative charge at a ratio of about one SDS to every two amino acid residues. This results in a polypeptide chain which is strongly negatively charged in proportion to its molecular mass.

The polyacrylamide gel exists as a cross-linked meshwork of acrylamide monomers forming a solid gel with small pores of different sizes/orientations. The protein mixture is applied to the gel and an electric current is applied from top to bottom. Proteins are then "sieved" by the gel matrix according to

molecular weight as smaller proteins migrate faster through the meshwork than larger ones and a banding pattern of proteins is produced. The gel system can be calibrated using proteins of known molecular weight (markers) such that proteins of unknown weight can be determined. Following gel electrophoresis the protein bands are transferred to a nitrocellulose membrane. This is achieved by applying an electric current over the gel and membrane with the positive electrode on the side of the membrane. The negatively charged proteins are then drawn over onto the membrane from the gel in exactly the same pattern of distribution. Alterations in the percentage of polyacrylamide can be used regulate pore size and hence migration rate such that the protein of interest runs in the middle of the gel; this ensures good separation of proteins and improves efficiency of transfer.

Detection of the protein of interest from the mixture imprinted on the membrane is achieved using highly specific antibodies. Two antibodies, primary and secondary, are used in Western blotting. The primary antibody recognises the protein of interest to which it binds forming a protein-antibody complex. The remaining sites on the membrane not occupied by protein-antibody complex must be blocked using a generic protein (BSA or non-fat milk powder) in order to limit non-specific binding of the antibody and artefactual staining. The secondary antibody is directed against the immunoglobulins of the species in which the primary antibody was raised. It binds specifically to all areas on the membrane where the primary antibody is present. The secondary is conjugated to a large reporter tag such as horseradish peroxidase, which upon contact with the relevant substrate solution, catalyses a chemiluminescent reaction leading to the production of light. Due to the specificity of the antibodies the light is only present at points where the protein of interest is located and the intensity of the signal is directly proportional to the amount of protein present. This can then be detected by autoradiography. Sources of variation in the quantitative Western blotting protocol include (i) inaccuracies in the preparation of the sample and the estimation of its total protein content, (ii) inaccuracies in pipetting volumes during gel loading, (iii) inefficiency of transfer of proteins from the gel to the membrane, (iv) incomplete antibody binding and (v) inaccuracies in the optical density measurement.

All quantitative Western blotting in this thesis was carried out as described by Laemmli (1970).

2.3.1.1 Internal standards

The inclusion of a probe for an internal standard is good practice to account for the inherent variation in quantitative Western blotting protocols. An internal standard is a protein which is present in the sample under investigation but which is at equal levels in both of the experimental groups. This protein is then additionally detected from the same gel that samples have been run on (using immunospecific antibodies raised against it) and quantified. Normalisation of the signals for the protein of interest to this internal standard allows the true endogenous protein levels to be obtained by reducing the interference attributable to the protocol itself.

Quantification of protein levels in the rabbit model of LVD previously used the SR Ca^{2+} binding protein calsequestrin (CSQ) as this had been considered to be unaltered in response to heart failure. Subsequent detailed quantification of CSQ determined that there was a significant increase in CSQ protein expression in LVD *vs.* sham (Alexis Duncan, doctoral thesis, 2002). This then led to the search for an alternative internal standard.

Glyceraldehyde-3-phosphate dehydrogenase (GAPDH) is a house-keeping protein which is highly expressed by cardiomyocytes. It is commonly used as an internal standard in protein quantification studies in heart failure and hypertrophy where it is considered to be unaltered compared to controls (Smith *et al.*, 1996; Lim & Molkentin, 1999). Investigation of GAPDH mRNA levels in the rabbit model of LVD used in this thesis confirmed that there was no significant difference in LV tissue between sham and LVD animals (Figure 2.5). GAPDH was used as an internal standard in the investigation of sorcin protein expression presented in this thesis (see Chapter 4).

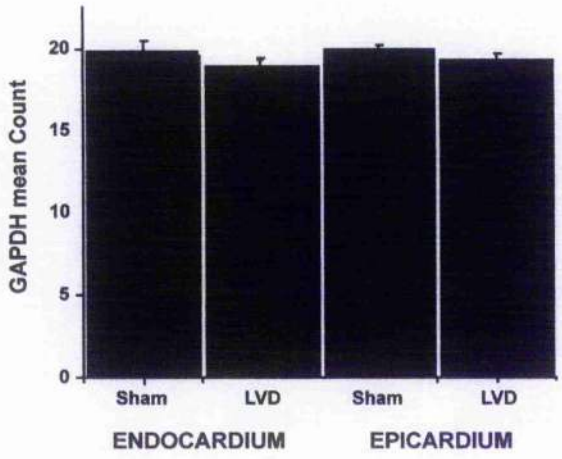

Figure 2.5 GAPDH mRNA expression in left ventricular tissue.

GAPDH mRNA expression in endocardium and epicardium from sham-operated (n=6) and LVD (n=10) rabbits. Data are expressed as the mean cycle time ± S.E.M. No significant difference existed between sham-operated and LVD. Adapted from Currie *et al.*, (2005).

2.3.2 Immunocytochemistry – Principles

Immunocytochemistry involves the localisation of a protein of interest in tissue sections or cells. In common with Western blotting, it involves the use of highly specific primary and secondary antibodies. Firstly the cells or tissue are fixed such that the micro-architecture of the cell is preserved. Cells are then permeabilised such that the intracellular contents can be accessed. The primary antibody is incubated with the sample and forms an antibody-antigen complex wherever the protein of interest is located. All sites of the cell not occupied by the antibody-antigen complex are blocked to limit non-specific binding. The secondary is conjugated with a reporter molecule such as an enzyme or a fluorescent tag and selectively binds to the primary antibody-antigen complexes within the sample. Visualisation of the secondary occurs via the addition of a substrate (in the case of enzyme tags) then autoradiography or fluorescence microscopy to determine the spatial distribution of the protein of interest.

2.3.3 Co-immunoprecipitation – Principles

Co-immunoprecipitation ascertains whether a physical association exists between two proteins and is usually performed after a functional link has been established. Samples of tissue extract are prepared and purified to remove non-specific contaminants. The extract is then incubated with an immunospecific antibody (usually polyclonal) directed against one of the two proteins of interest (the antigen); during this time, antibody-antigen complexes will form. Following this, the extract is run over sepharose beads which have previously had protein G adhered to them. As the extract flows, the antigen-antibody complex will interact with the protein G thus sticking it onto the bead and separating it from other proteins in the extract. If the second protein of interest is physically associated to the antigen then it too will stick on to the beads. The remaining proteins contained in the extract are then washed off and the precipitated protein (that which is stuck to the protein G-sepharose conjugate) is eluted using high-stringency washes and heat. In order to confirm the identity of the proteins contained within the immunoprecipitate, SDS-PAGE and immunoblotting are performed. If this is positive for both proteins then a physical association exists between the two. A schematic representation of the general method of co-immunoprecipitation is illustrated in Figure 2.6.

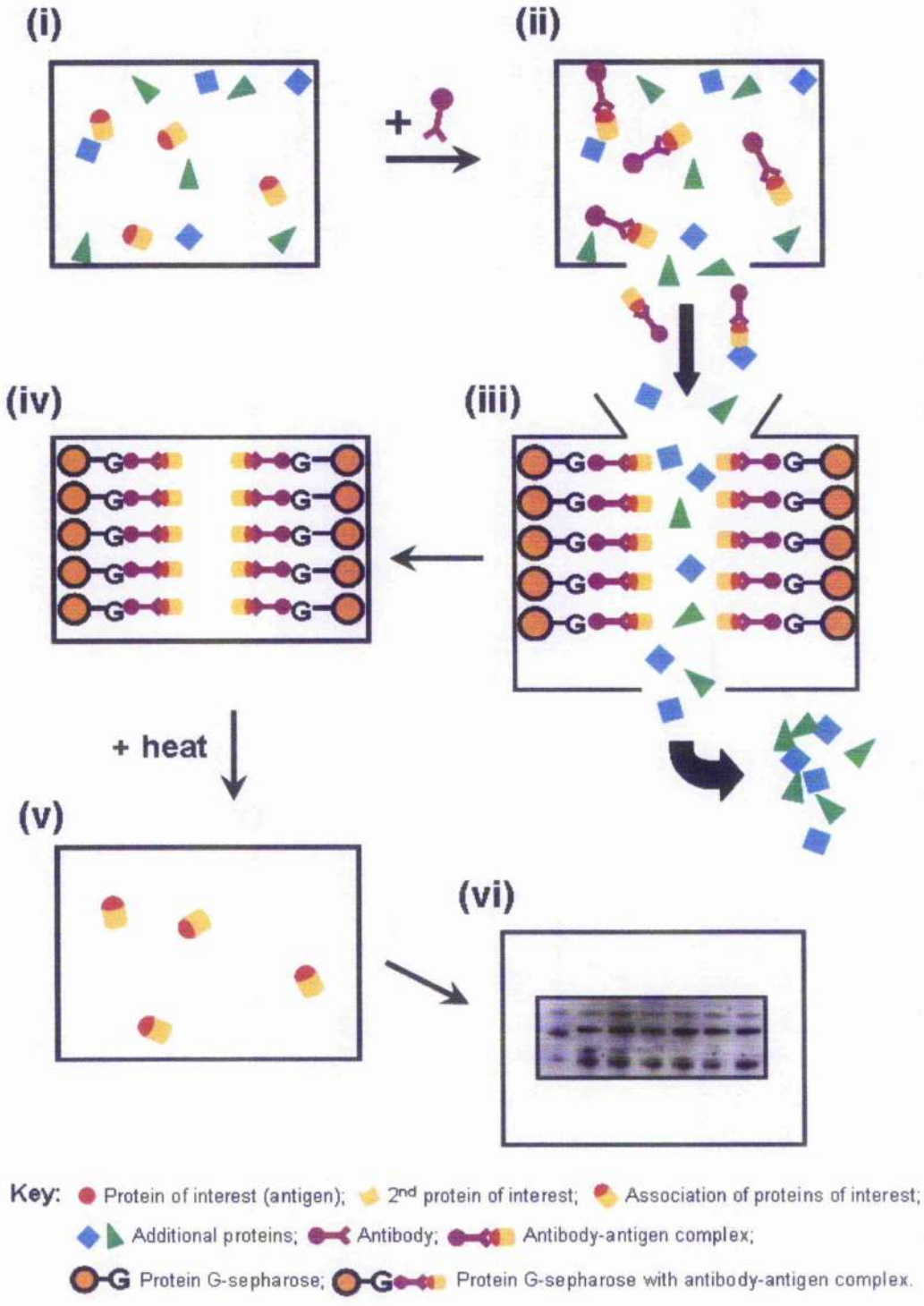

Figure 2.6 Schematic representation of co-immunoprecipitation.

(i) A left ventricular homogenate extract is produced which consists of a mixture of different proteins. **(ii)** incubation of the extract with an immunospecific antibody directed against the protein of interest. **(iii)** addition of extract into a protein G-sepharose column to which antibody-antigen complexes stick (captured immunoprecipitate). **(iv)** additional proteins are washed off. **(v)** immunoprecipitate is eluted from the column. **(vi)** Western blots to both proteins of interest are performed on the immunoprecipitate.

The major drawback of this technique is that it does not determine the nature of the interaction, that is, whether it occurs directly or indirectly via another protein or anchoring protein.

2.3.4 *In vitro* back-phosphorylation – Principles

In vitro back-phosphorylation determines the endogenous phosphorylation status of a protein using radiolabelled substrates (usually ^{32}P) and autoradiography techniques. The tissue sample is converted into a lysate preparation through the addition of detergent to break down membranes. The protein of interest is then immunoprecipitated from this and incubated with radiolabelled phosphate before separation by SDS-PAGE to isolate the protein of interest. Following this, autoradiography is used to assess the incorporation of the radioligand into the protein of interest. The levels of incorporation are inversely related to the level of endogenous phosphorylation.

2.3.5 Biochemical solutions

Solutions were freshly prepared for each experimental run. All concentrations are in (mmol/L) except where stated otherwise; pH correction was performed at room temperature (20-21 °C).

2.3.5.1 Solutions for homogenate preparation

Sorcin homogenisation buffer - TRIS (20), dithiothreitol (DTT, 1), EGTA (2) and 100 µl protease inhibitors (complete EDTA-free protease inhibitor mix, Roche); pH 7.4 with NaOH.

PLM homogenisation buffer - TRIS (20), DTT (1), 100 µl protease inhibitors (as above), 100 µl phosphatase inhibitors (sodium vanadate (1), sodium fluoride (5)); pH 7.4 with NaOH.

NCX homogenisation buffer - HEPES (50), NaCl (150), KCl (3), sodium pyrophosphate (25), ATP (10), EDTA (5), 100 µl protease inhibitors; pH 7.4 with NaOH.

2.3.5.2 Solutions for gel electrophoresis and immunoblotting

Sample buffer - ready-made at 4X (Invitrogen Ltd., U.K.) Composition: Glycerol 10% (w/v), Tris base (564), Tris HCl (424), LDS 2% (w/v), EDTA (2.04), SERVA Blue G250 (0.88), Phenol Red (0.7); pH 8.5.

β-ME sample buffer - as for sample buffer but with addition of 5% β-ME.

Running buffer - ready-made at 20X (Invitrogen Ltd., U.K.) Composition: 2-(N-morpholino) ethane sulphonic acid (MES) (1M), Tris base (1M), SDS (69.3), EDTA (20.5) diluted to 1X in double distilled water; final pH 7.3.

Transfer buffer - ready-made at 20X (Invitrogen Ltd., U.K.) Composition: bicine (500), Bis-Tris (500), EDTA (20.5) diluted to 1X in 20% methanol and double distilled water to final pH of 7.2.

Antibody incubation buffer - $MgCl_2$ (100), 0.5% Tween 20, 1% Triton X-100, 1% BSA, 5% Foetal calf serum, Tris-HCl (100), pH 7.4 with NaOH.

Blocking buffer - antibody incubation buffer with 3% BSA added.

Rinse buffer - NaCl (150), EDTA (1), 0.1% Triton X-100, Tris-HCl (10), pH 7.4 with NaOH.

High-salt rinse buffer - as for rinse buffer but with NaCl (600).

2.3.6 Preparation of tissue homogenates for Western blotting

Tissue homogenates were prepared from rabbits with and without LVD. Animals were sacrificed (as in 2.1.1); the heart was excised and washed thoroughly before preparation of homogenates commenced. In each case, approximately 0.25 g of isolated free left ventricular wall was cut from the basal region of the heart; any excess fatty tissue was removed. In addition, the lungs and liver of animals with LVD were removed and weighed for reference.

All samples were kept on ice throughout the procedure to limit degradation of proteins; these were aliquoted and stored at -80 °C until required for biochemical analysis.

2.3.6.1 Sorcin and PLM

Ten times volume of the relevant ice-cold homogenisation buffer was added to the section of ventricle. The tissue was finely chopped using scissors then homogenised using an Ultraturrax T8 (Labortechnik) until no solid tissue pieces remained.

2.3.6.2 NCX

The section of ventricle was immediately frozen in liquid nitrogen. Tissue was roughly chopped using a clean scalpel blade and chunks were then pulverised in a mortar and pestle. Five times volume of ice-cold homogenisation buffer was added gradually during this time. The pulp was homogenised in a glass homogeniser for 20 min until a homogeneous mixture was obtained. This was then centrifuged at 2000 rpm at 4 °C for 15 min, the supernatant was drawn off and homogenised over ice once more for 2-3 min. The homogenate was centrifuged at 5000 rpm at 4 °C for 5 min. The supernatant was removed and stored at -80 °C. This constituted the extract used for in vitro phosphorylation studies

2.3.6.3 Protein assay of tissue homogenates

Assessment of total protein content was performed using the Bradford Assay and CoomassiePlus™ protein assay reagent with BSA (0.1 - 1 mg/mL) as a standard. This assay was chosen as it was fast, accurate and was known to be capable of resolving the protein levels present in rabbit left ventricular homogenates.

When unbound to protein, Coomassie exhibits an absorbance maximum of 465 nm; this shifts to 595 nm on binding of protein. Measurement of absorbance at 595 nm from the Coomassie/homogenate mixture is therefore a reflection of the amount of protein in the homogenate sample. The inclusion of BSA standards

provides calibration points on a standard curve for the conversion of absorbance into μg of protein.

Each BSA standard was pipetted in triplicate into separate wells of a 96-well plate. Aliquots of each ventricular homogenate were defrosted, vortexed and prepared at 1:20, 1:30 and 1:40 dilutions in double distilled water and kept on ice. These were vortexed to ensure even dispersal of the homogenate and pipetted in triplicate to vacant wells of the plate. CoomassiePlus™ reagent was then added to each and all air bubbles were removed. The plate was read using a Dias Microwell Plate Reader (Dynatech Medical Products Ltd, St Peter Port, U.K.) at an optical density of 595 nm. Optical density data were calculated and displayed using Data Reduction version 1.4 software (Dynatech Laboratories, U.K.) on a computer. The mean optical density and corresponding standard deviation for each sample was calculated for each triplicate. Samples that had an error of greater than 0.05 were discarded and the assay was repeated. The product of the concentration output by the reader and the dilution factor gave the total protein concentration (mg/mL) for each dilution. A standard curve of optical density (arbitrary units; linear scale) versus concentration of total protein (mg/mL; logarithmic scale) was produced in Data Reduction by fitting a sigmoidal curve through the points of optical density of the BSA standards (Figure 2.7); R^2 was commonly 0.99. Protein concentrations which lay on the linear aspect of this curve (i.e. within the range of detection) were then averaged and a mean total protein concentration (mg/mL) for the homogenate was produced.

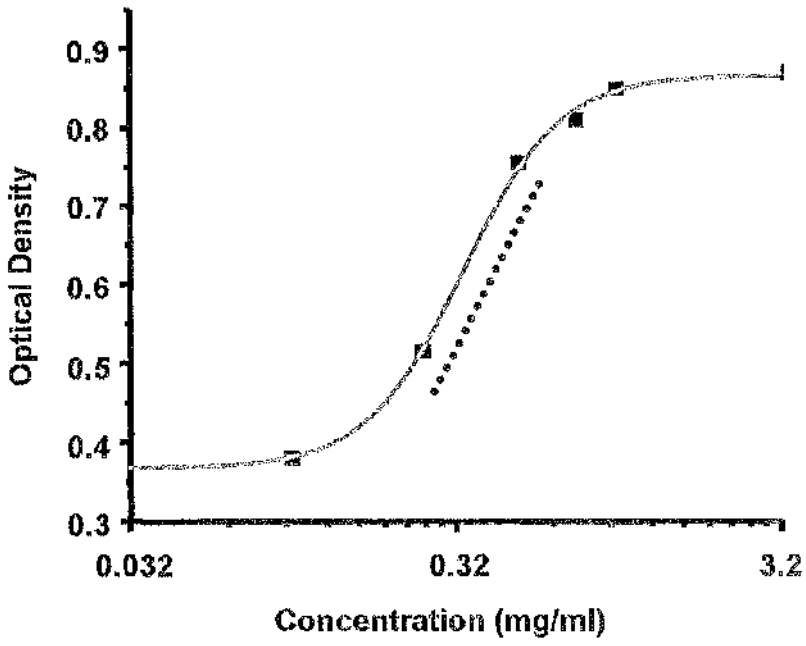

Figure 2.7 Standard curve of concentration *vs.* optical density.

Optical densities (arbitrary units) of BSA standards (0.1-1.0 mg/mL) were plotted (■) and a sigmoidal curve was fitted through the points. Concentrations of sample which lay on the linear aspect of the plot (dotted line) were selected and averaged to determine total protein content of the homogenate.

2.4 Technical difficulties

Much of the work contained within the present thesis was associated with extensive technical problems which, in many cases, hindered the progression of investigation of factors affecting NCX up to a functional level. This section aims to provide a brief summary of the problems relating to the studies described in Chapters 3, 4, 6 and 7.

2.4.1 Chapter 3 - The transverse tubular network

The detubulation of single rabbit cardiomyocytes was the main area of this chapter in which technical difficulties were experienced. As mentioned in Chapter 3 (3.3.5), it was first anticipated that the protocol described by Kawai *et al.* (1999) would be transferable to the rabbit (1.5 mol/L formamide for 15 min). This was, however, not the case as more than 90% of the cell population (assessed by haemocytometer counting) hypercontracted in response to this

method. The failure of this protocol in rabbit cardiomyocytes was assessed for its dependence on a number of factors which were then altered in an attempt to improve the cell survival rates; these are summarised below.

(i) **pH** - (a) the shift in pH of the mock extracellular solution on addition of 1.5 mol/L formamide was assessed. This was shown not to vary significantly (from pH 7.4 to 7.49) and (b) increase of the HEPES concentration from 5 to 10 mmol/L; this did not improve survival rates on exposure to 1.5 mol/L formamide.

(ii) **[Ca^{2+}]** - (a) cells were obtained in either 0.125 or 1 mmol/L added $CaCl_2$ following dissociation and (b) cells were obtained in 1 mmol/L [Ca^{2+}] and re-suspended *in* either 0 or 5 mmol/L added EGTA. Neither alteration in [Ca^{2+}] *in* (a) or (b) showed any difference in the survival numbers following exposure to 1.5 mol/L formamide.

(iii) **Time** - (a) the timescale of hypercontraction in response to 1.5 mol/L formamide (1, 5 and 10 mins following addition) was assessed. This revealed that cell hypercontraction was complete by 1 min. (b) the incubation time in 1.5 mol/L formamide was reduced from 15 to 10 and 5 min; this did not improve the success of the protocol.

(iv) **Concentration** - reduction of formamide concentration from 1.5 to 0.75 mol/L; this did not prevent hypercontraction of cells. Further reduction of formamide concentration (below 0.75 mol/L) was not investigated as this was considered to be below the concentration required to maintain a sufficient osmolarity gradient needed to induce detubulation.

Following this, the protocol utilising mannitol was attempted (3.3.5.1). As this was also unsuccessful, the protocol of Kawai *et al.* (1999) was revisited and adapted to include the addition of (i) 10 mmol/L caffeine (to empty the SR of Ca^{2+} and prevent oscillations/hypercontracture developing) and (ii) 10 mmol/L BDM (to inhibit myofilament contraction and hypercontraction developing). The inclusion of caffeine did not prevent cardiomyocytes hypercontracting when exposed to 1.5 mol/L formamide whilst 10 mmol/L BDM did. As a result, the detubulation study was successfully carried out with a modified form of the

protocol of Kawai *et al.* (1999) in order to provide a proof of principle for the detection of internalised t-tubules. In light of these difficulties with the detubulation protocol, it was not possible to assess functional parameters such as synchrony of Ca^{2+} release in detubulated rabbit cardiomyocytes as originally planned.

2.4.2 Chapter 4 – Quantification of sorcin

The majority of the technical difficulties associated with the work contained in this thesis were experienced with the detection and quantification of endogenous sorcin protein expression in rabbit whole LV homogenates (Chapter 4). As a result, this project became extremely time-consuming. Many of these problems are presented in detail in Chapter 4 itself; the list below summarises these and additional points not mentioned in the text in chronological order.

(i) **Breakdown of spectrophotometer for reading protein assay plates.** An alternative machine was sourced from a neighbouring department whilst servicing was performed. On duplication of sample readings in order to verify accuracy between these two machines, it became evident that the original machine was more accurate. Many samples therefore had to have protein content re-measured in order to reduce variation attributable to this feature.

(ii) **Anti-mouse HRP-conjugated secondary changed.** Initially the monoclonal study was begun using a commercially available anti-mouse HRP-conjugated secondary from BDH laboratory supplies. This began to produce blots with patchy backgrounds rendering these experiments useless and so an alternative secondary (Amersham) was sourced. The latter was tested with a known reliable primary (anti-RyR) yielding a positive result (not shown) and so the Amersham secondary was optimised for dilution and employed in all subsequent sorcin blots using the monoclonal primary.

(iii) **Only sorcin dimer detectable with the monoclonal primary** - additional denaturing conditions were investigated in an attempt to detect the monomer; see "Verification of denaturing conditions" (4.4.2) and Figure 4.5.

(iv) **Degradation of the monoclonal primary** - the primary used in the monoclonal study deteriorated (see Figure 4.6). The protocol was repeated several times to rule out errors associated with the procedure and/or equipment. Following communications over several months with the manufacturer, who insisted initially that there was no problem, a replacement batch was obtained after all available data were forwarded to them. This also proved unsuccessful despite extensive re-optimisation of dilutions for both this and the accompanying Amersham secondary.

(v) **Obtainment of alternative primary** - the polyclonal rabbit anti-sorcin primary (see 4.4.5) was optimised and detected both sorcin monomer and dimer. This was used to (a) produce additional blots to rule out sample degradation due to storage at -80 °C (see Figure 4.7) as a cause for the monoclonal failure and (b) repeat the quantification of sorcin from samples used in the monoclonal study (plus 7 additional samples). By this point, only 1 load could be performed in the latter due to time-constraints.

2.4.3 Chapter 6 – NCX phosphorylation

The work contained within Chapter 6 was performed in collaboration with Dr Dan Schulze's group, University of Maryland, Baltimore. This was known to be the only group in the world competent at performing a biochemical assay for PKA-mediated phosphorylation of cardiac NCX (Ruknudin *et al.*, 2000; Wei *et al.*, 2003). Samples were prepared in Glasgow according to the precise methods of Ruknudin *et al.* (2000) which necessitated the entire heart to be used due to the high concentrations of NCX protein required for the assay. As a result it took many months to acquire samples and so these were couriered on a batch basis. Disappointingly, the individual performing the assay left the Baltimore group before all couriered samples were assayed. This prevented a robust determination of the NCX phosphorylation status in the LVD rabbit model since only 3 of 9 pairs of samples were analysed. Further functional development of this potential modulator of NCX activity in LVD was therefore prevented.

2.4.4 Chapter 7 –Electrophysiological studies of sorcin

Both electrophysiological approaches in Chapter 7 were associated with problems as discussed below. At the time these studies were carried out, there was a change in the enzyme batch used for cell isolation which hindered all group members utilising single cells. This may have additionally contributed to technical difficulties in this chapter.

2.4.4.1 EC coupling studies using recombinant sorcin

The difficulties associated with measuring NCX-mediated extrusion when recombinant sorcin was included in the patch pipette are detailed in section 7.4.1 and were centred on the inability to maintain a gigaohm seal. Several interventions (detailed in section 7.4.1) were investigated to aid pipette sealing yet none proved successful. The project had to be abandoned due to time constraints.

2.4.4.2 Effect of sorcin phospho-mutants on NCX activity

The study of the NCX I-V relationship in cells over-expressing constitutively phosphorylated and de-phosphorylated mutants showed no significant difference. This was the first time that these mutants had been tested functionally and it was concluded that the point mutation may be interfering with the conformation of sorcin.

CHAPTER 3
THE TRANSVERSE-TUBULAR NETWORK

3.1 Introduction

The transverse tubule network (t-tubule network) of the ventricular myocyte exists as a tortuous and highly branched set of membrane invaginations. These extend deep into the body of the cell and are critical to the precise functioning of the cardiomyocyte. The t-tubules are present at regularly spaced intervals of 1.8 to 2 μm and emanate from the Z-lines to form a highly branched set of interconnections extending both transversely and longitudinally. The ventricular myocyte is approximately 20 μm thick and the presence of a greatly developed, wide diameter t-tubule network provides it with an excitatory network through which the action potential can rapidly propagate through the entire cell. Many of the proteins and ion channels necessary for the coupling of electrical excitation to Ca^{2+} release are located either within or adjacent to the t-tubule membrane. In particular, the t-tubule network is the main site where junctional complexes exist in which LTCCs (residing in the sarcolemma) and RyR2s (residing in the junctional SR membrane) lie in close proximity. As a result of this, the t-tubule network is the predominant region where EC coupling initiates. This system also allows the extracellular fluid and the ions required for initiation of the action potential and EC coupling to be uniformly accessible to all areas of the heart muscle. Consequently, diffusion distances to the cell interior are reduced, ensuring spatially and temporally synchronous Ca^{2+} increases and simultaneous activation and relaxation throughout the volume of the cardiomyocyte (Haddock *et al.*, 1999; Kawai *et al.*, 1999; Brette & Orchard, 2003).

3.1.1 Structure of the transverse tubular network

The t-tubules form an extremely complex system within the cardiomyocyte and their abundance varies throughout the anatomical regions of the heart itself. In cardiac muscle, the t-tubules are found predominantly within the ventricular cardiomyocytes whilst atrial, pacemaking and conductive tissue possess little or no t-tubule network. Additionally, the density of t-tubule network within cardiac muscle varies with species. All mammalian ventricle studied has shown the presence of a t-tubule network, yet its absence has been confirmed in

reptile, amphibian and avian ventricular myocardium (Bers, 2001; Brette & Orchard, 2003). Estimates of the percentage of the sarcolemma contained within the t-tubule network of the ventricle have yielded variable results both between species and for the same species with estimates ranging from 21% to 64% (Bers, 2001; Brette *et al.*, 2006). More agreement has been reached on the percentage of cell volume contained within the t-tubule network; of studies conducted in the last 20 years, most report this to occupy approximately 3.5% of the cardiomyocyte (Forbes *et al.*, 1984; Tidball *et al.*, 1991; Soeller & Cannell, 1999).

The t-tubules were originally thought only to occur transversely. Subsequently it has been shown that although this is their predominant orientation they also run in the longitudinal, oblique and axial planes, forming an ordered yet complicated three-dimensional mesh throughout the ventricular myocyte (Forbes *et al.*, 1984; Soeller & Cannell, 1999; Bers, 2001; Brette & Orchard, 2003). As a result of this finding, it has been suggested that the former misnomer of transverse tubular network be replaced by terms more accurate such as sarcolemmal tubule network, sarcolemmal Z-rete (Soeller & Cannell, 1999) and transverse-axial tubular system (TATS) (Forbes *et al.*, 1984) however t-tubule network still remains the preferred term. Tubules are larger in cardiac muscle than in other muscle types such as skeletal, with diameters in the range of approximately 200 to 300 nm (Soeller & Cannell, 1999; Bers, 2001; Sobie *et al.*, 2002) although reports of an occasional t-tubule of approximately 70-80 nm exist (Ogata & Yamasaki, 1990). One of the most detailed studies of t-tubule structure was that of Soeller and Cannell (1999). They examined the t-tubule network in the rat by immersing the cardiomyocyte in dextran-linked fluorescein solution before imaging using two-photon microscopy. Deconvolution techniques were then applied to reduce distortion of the image by the point spread function in order to produce an approximate three dimensional model of the t-tubule network (Figure 3.1).

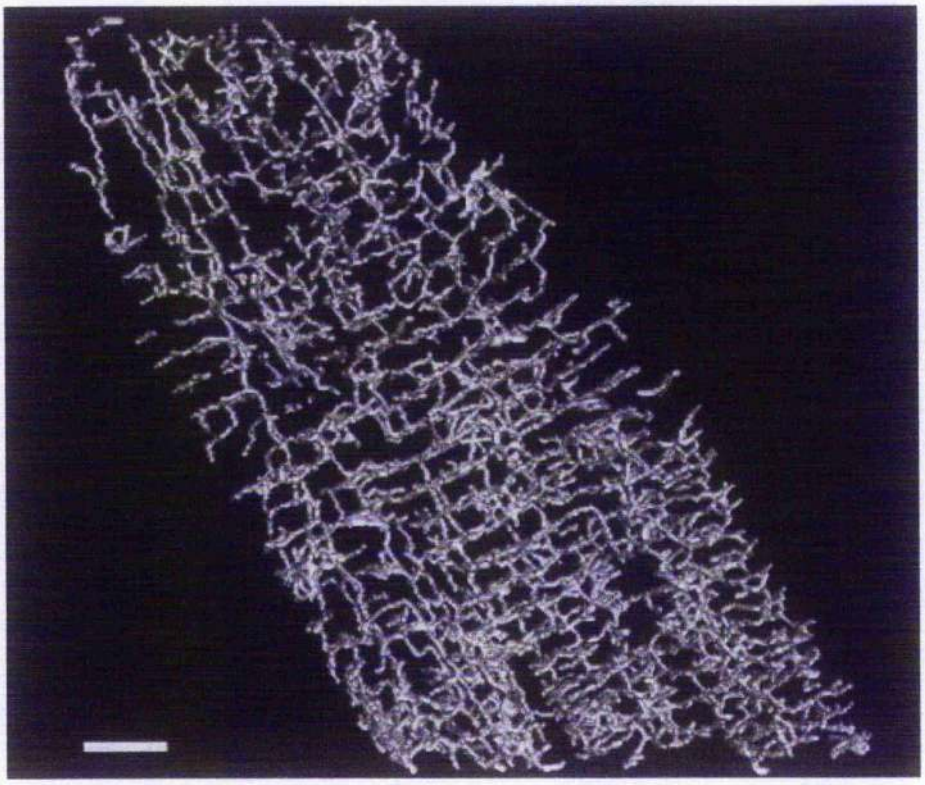

Figure 3.1 Structure of the transverse tubular network in a rat ventricular cardiomyocyte.

Scale bar = 5 μm. Diagram taken from Soeller and Cannell, (1999).

Using these images, it was determined that the majority of t-tubules (approximately 60%) penetrate the surface sarcolemma at the Z-lines of the myofibrils thus placing them at regular intervals of approximately 1.8 μm, in agreement with sarcomere length, with the remainder existing between neighbouring Z-lines, as shown by earlier studies (Page, 1978; Shacklock *et al.*, 1995). In addition they showed that t-tubules are absent from the nuclei and branch much more extensively than previously thought, the majority being short with the average length of t-tubule between branching points being 7 μm (Soeller & Cannell, 1999).

3.1.1.1 Structural specialisations of the t-tubule network

The t-tubule network is highly specialised for optimal contractile functioning. It is inherently subjected to a high level of mechanical stress during the cardiac contraction-relaxation cycle yet the tubules continue to retain their morphology and regular Z-line spacing. The presence of a highly developed "protein

scaffold" forming an association with the basement membrane has been shown to support the t-tubules (Kostin *et al.*, 1998). This includes cell matrix focal adhesion molecules such as vinculin, which serves as an anchor for actin, and the membrane-associated proteins dystrophin and spectrin. Together these confer structural support to the t-tubules, allowing them to withstand the forces exerted on them during the heartbeat and maintain an open lumen and regular position within the cardiomyocyte. In addition, they have also been implicated in the interconnection of adjacent myofibrils with the t-tubule membrane facilitating efficient Ca^{2+} exchange during contraction (Frank *et al.*, 1994; Kostin *et al.*, 1998).

Critically for efficient cardiac function, the t-tubule membrane is highly specialised for EC-coupling. LTCCs are concentrated in the t-tubule membrane which is itself coupled to the SR via its close apposition with the foot processes on the terminal cisternae of the junctional SR (Ogata & Yamasaki, 1990; Kawai *et al.*, 1999). Approximately 20-50% of the t-tubule membrane is associated with the SR in ventricular cardiomyocytes, highlighting the importance of this t-tubule-SR structural specialisation (Bers, 2001). This allows the functional coupling of the LTCC s and the RYR2s at the dyadic cleft (Carl *et al.*, 1995). As the t-tubule network penetrates through the cardiomyocyte and as a result of this coupling, Ca^{2+} sparks at the subsarcolemmal space and cell interior occur simultaneously throughout the cardiomyocyte. This gives rise to a synchronous elevation in $[Ca^{2+}]_i$ and the subsequent Ca^{2+} transient is produced simultaneously throughout the cell (Haddock *et al.*, 1999).

The t-tubules present a diffusional delay with the extracellular fluid as exchange of fluid only occurs at the mouth of the tubule. The t-tubules in cardiac muscle are of larger diameter than their relatives in skeletal muscle (30-40 nm) allowing more rapid exchange of Ca^{2+} and other ions (Bers, 2001). Examination of the rate of diffusion of Ca^{2+} ions in t-tubules in guinea pig ventricular cardiomyocytes has provided some insight into this phenomenon. On rapidly changing $[Ca^{2+}]_o$, the increment of I_{Ca} occurred in two distinct phases; 36% changed quickly (time constant (τ) of 20 ms) whilst 64% changed more slowly (τ=200 ms). This effect was absent in atrial cells lacking t-tubules, thus the slower time scale in ventricular cells represents the diffusional delay down the t-

tubules (Shepherd & McDonough, 1998). This feature alludes to the possibility of accumulation and/or depletion of ions within the t-tubules. Although this is not of particular relevance in normal myocardium, it may come into play in situations where the t-tubules become disrupted or distorted (see 3.1.7 and 3.5).

3.1.2 Development and plasticity of the t-tubule network

The t-tubule network of ventricular myocytes is not a fixed structure and exhibits plasticity during development, cell culture and pathological conditions.

3.1.2.1 T-tubule network in the embryo and neonate

It is well established that embryonic and neonatal cardiomyocytes are almost completely devoid of a t-tubule network, have a sparse SR, reduced LTCC abundance but enhanced NCX expression. With regards to EC coupling, SR Ca^{2+} release is reported to have a diminished functional role instead relying mainly on trans-sarcolemmal Ca^{2+} fluxes via reverse-mode NCX (Balaguru *et al.*, 1997; Haddock *et al.*, 1999; Sedarat *et al.*, 2000; Bers, 2001). Proteins present in t-tubule membranes have also been shown to be absent in neonatal cardiomyocytes but rapidly increase their abundance and co-localisation at later developmental stages (Frank *et al.*, 1994; Sedarat *et al.*, 2000).

The absence of a t-tubule network in the neonate has been confirmed in isolated ventricular myocytes from the rabbit (Haddock *et al.*, 1999). Field stimulation of neonatal cells produced biphasic Ca^{2+} transients that exhibited steep spatial Ca^{2+} gradients. $[Ca^{2+}]_i$ was shown to rise firstly in the subsarcolemmal space before spreading to the cell centre and Ca^{2+} sparks occurred predominantly at the cell periphery. In adult cells, $[Ca^{2+}]_i$ rose simultaneously throughout the cell during the transient and Ca^{2+} sparks were observed uniformly throughout the cell. Unlike adult cells, neonatal transients were not dependent on SR Ca^{2+} as thapsigargin application had no effect thereby supporting trans-sarcolemmal Ca^{2+} flux as their source of Ca^{2+} (Haddock *et al.*, 1999).

Rat foetal ventricular myocytes (12 day old) exhibit similar biphasic transients yet these have been shown to arise spontaneously (Seki *et al.*, 2003). Unlike

previous studies though, the transient could be completely inhibited by LTCC blockers indicating a reliance on I_{Ca}. The occurrence of Ca^{2+} sparks in foetal cells was extremely low while this situation reversed in the neonate where the frequency increased rapidly from 6 to 12-day old cells. Ca^{2+} sparks were observed mainly in the subsarcolemmal region in 6-day old cells whereas, in 12-days old cells, sparks were frequently apparent through the entire volume of the cardiomyocyte (cell periphery and centre). This shift in spark frequency coincided with the development of the t-tubule network throughout the cell interior and co-localisation of LTCCs and RyR2s in the t-tubule membrane (Seki *et al.*, 2003).

It is known that cytoplasmic arrays of RyR2s occur at the Z-lines of neonatal rabbit ventricular myocytes (Sedarat *et al.*, 2000) and that these release Ca^{2+} in response to agents such as caffeine indicating that the neonatal SR stores Ca^{2+} to a similar degree as adult cells (Balaguru *et al.*, 1997). Previous reports in rabbit immature ventricular myocytes have determined that SR Ca^{2+} does not participate in EC coupling (Balaguru *et al.*, 1997; Haddock *et al.*, 1999). It is controversial that Seki and co-workers suggest an involvement of SR release and I_{Ca} in producing foetal Ca^{2+} transients and they attribute their anomalous findings to developmental species differences between the rat and rabbit (Seki *et al.*, 2003). It has been suggested, at least in rabbit, that there is a spatial disconnection of the sarcolemma in the neonate from the RyR2s present in the SR membrane due to the absence of a t-tubule network (Haddock *et al.*, 1999).

Formation of the t-tubule network is known to start early after birth in the mammalian ventricular myocyte at approximately 8-10 days of age (Sedarat *et al.*, 2000). This time scale also coincides with the progression to the mature form of EC coupling (Haddock *et al.*, 1999). It is proposed that t-tubules form via a regeneration of caveolae-like elements, flask-shaped invaginations of the sarcolemma, which anastomose to form beaded t-tubule precursors. These then link up to produce the finished t-tubule within which the glycocalyx remains associated with the sarcolemma (Forbes *et al.*, 1984; Franzini-Armstrong, 1991; Yuan *et al.*, 1991; Carozzi *et al.*, 2000). In skeletal muscle it has been shown that prior to all this, LTCCs and RyRs form a complex in the developing myotube which becomes incorporated into the t-tubule once their production has been

initiated. Ultimately this leads to the formation of the junctional complex between the t-tubule and SR membrane known as the triad (Yuan *et al.*, 1991). A similar biogenesis path may occur for the cardiac dyad. In common with caveolae, t-tubules are high in cholesterol and display a distinct lipid composition (Rosemblatt *et al.*, 1981) and the developing t-tubules are highly susceptible to cholesterol-disrupting agents such as amphotericin B (Carozzi *et al.*, 2000). Beaded calveolae-like elements have been shown to remain present at the intersection of the t-tubule and surface membrane in the adult phenotype and previous work has implicated them in three functions:

(i) to convey a degree of flexibility and protection to the t-tubule during contraction (Forbes *et al.*, 1984).

(ii) to act as reservoirs of membrane capable of being recruited and stretched to form new areas of t-tubule during cellular hypertrophy ("membrane augmentation") (Prescott & Brightman, 1976; Forbes *et al.*, 1984). Although this function has been suggested, it probably does not occur in cardiac muscle as caveolin-3, the muscle-specific isoform of the major caveolae protein constituent, is absent from the t-tubules of adult cardiomyocytes (Parton *et al.*, 1997; Bers, 2001).

(iii) to act as a barrier preventing mixing of proteins of the t-tubule and sarcolemma thereby maintaining the unique protein composition of the t-tubule network (Flucher, 1992).

During t-tubule network formation it has therefore been proposed that caveolae and caveolin-3 contribute to the lipid organisation required for production of the t-tubules following which it is the cytoskeleton and protein scaffold, mentioned earlier in 3.1.1.1, which contribute to the maintenance of their ultrastructural morphology (Parton *et al.*, 1997; Kostin *et al.*, 1998).

3.1.2.2 T-tubule network during cell culture

A rapid depletion of the t-tubule network in mammalian ventricular cardiomyocytes occurs during short-term cell culture (Lipp *et al.*, 1996; Mitcheson *et al.*, 1996; Kostin *et al.*, 1998). This phenomenon has been termed

by one group as "redifferentiation" and is reported to be associated with a fusion of adjacent t-tubules with their subsequent clustering in the perinuclear region (Kostin *et al.*, 1998). Functional measurements in guinea-pig ventricular cardiomyocytes which were maintained in culture for 48 hr showed spatially inhomogeneous Ca^{2+} transients both when elicited by I_{Ca} alone and by additional SR-release (CICR). In contrast, freshly dissociated cells consistently displayed spatial uniformity in Ca^{2+} transients. On reduction of I_{Ca} duration to approximately 50 ms, Ca^{2+} waves were produced in cultured cells which either propagated throughout the cell or were spatially restricted to one end. In addition it was noted that they possessed significant subcellular $[Ca^{2+}]_i$ gradients during I_{Ca} induced transients which were of higher incidence at the ends of the cardiomyocyte. Cultured cells were devoid of a t-tubule network (via membrane staining using di-8-ANNEPS) and displayed a 65% decrease in membrane capacitance (*vs.* control), consistent with a loss of membrane area. The basis of the non-uniformity of Ca^{2+} transients in cultured cells was due to the deficiency in functional t-tubules which would reduce the number of functionally coupled LTCCs and RyR2s throughout the cell interior leading to spatially non-uniform Ca^{2+} entry on I_{Ca} (Lipp *et al.*, 1996). A similar loss of t-tubule network was verified in adult rabbit ventricular cardiomyocytes with additional information provided on the alteration of ion channel currents in response to differing durations of cell culture (Mitcheson *et al.*, 1996). Cell capacitance decreased by 42% following 24 hr culture; decreases were also detected in I_{Ca} and the inward rectifying K^+ current after this time, with the former showing recovery after 96 hr. In general there was no uniform or consistent change in ion channel currents with culture time. This may be attributable to changes in gene expression and/or preferential membrane loss from particular sites (Mitcheson *et al.*, 1996). The experimental conditions used in both of these studies did not supplement the culture with metabolic stabilisers (e.g. taurine, D,L-Carnitine, creatine, penicillin/streptomycin) in which the degree of stress and extent of morphological/ion channel disruption may be less. A 50% decrease in t-tubule density was however experienced by rat cardiomyocytes maintained in supplemented culture media for 96 hr (Leach *et al.*, 2005). In addition to the t-tubular remodelling which occurs in cell culture, there is also a redistribution of the proteins contained within the network. LTCCs and RyR2s, which both concentrate within the t-tubule network, were shown to alter their sub-cellular

locations from a typically transverse pattern of localisation in freshly dissociated cells to a more punctuate arrangement in response to culture (Leach *et al.*, 2005). The loss of t-tubules could be reduced significantly to just 16% following 96 hr culture through inclusion of the actin disruptor cytochalasin D which also prevented the redistribution of LTCCs and RyR2s. This agent affects the rate of actin polymerisation/de-polymerisation at the fast growing (barbed) end of the actin molecule (Goddette & Frieden, 1986). Thus, cytochalasin D appears to maintain the cardiomyocyte in a structurally stabilised and functional state in culture. Similar results were obtained using cycloheximide, a protein synthesis inhibitor (Leach *et al.*, 2005).

The t-tubule network is also known to exhibit plasticity in disease states such as hypertrophy and heart failure; these alterations will be discussed in section 3.1.7.

3.1.3 T-tubule network and species dependence

As mentioned previously, all mammalian ventricle studied has shown the presence of a t-tubule network yet the composition of the t-tubule network within each species of mammal varies. Satoh *et al.* (1996) showed significant differences between calculated capacitance:volume ratios for cardiomyocytes from the rat, rabbit and ferret. They found no significant differences between average maximal cell length (142.8, 138.0 and 141.9 μm in rabbit, ferret and rat respectively) and only a small but significant difference for rabbit cardiomyocyte thickness when compared to ferret and rat (12.2 *vs.* 14.0 and 13.3 μm respectively). They did however find significant species-dependence in cell capacitance (289 *vs.* 138 and 162 pF in rat *vs.* rabbit and ferret respectively) thus demonstrating variation in membrane surface area between different species. One possible explanation put forward by the authors is a varying number and/or size of t-tubules in each species studied. The higher capacitance:volume in rat may reflect an increased dependence in the rat for SR Ca^{2+} release during EC coupling.

3.1.4 Experimental manipulation of t-tubule network structure

Artificial disruption of the t-tubule network has been achieved through the introduction of agents which provide an "osmotic shock" to the myocyte. This approach has allowed for further elucidation of t-tubule network structure, function and protein composition.

The technique produces physical uncoupling of the surface sarcolemma and t-tubule membrane - a "detubulation" - thereby leading to functional consequences such as altered Ca^{2+} handling. Two main detubulation protocols have been developed; the first utilises glycerol with subsequent cooling steps whilst the second involves formamide. The latter protocol has been applied and characterised more thoroughly in cardiac muscle and is considered to produce a more substantial and consistent detubulation due to the higher membrane permeability of formamide (Putnam, 1996). Using either protocol to detubulate, the agent is applied extracellularly and partially taken up into the cytoplasm. On its removal, water enters the myocyte causing it to swell and pinch off the t-tubule mouth from the surface sarcolemma. As the agent leaves the cell it is accompanied by water and the cell size returns to normal. The surface membrane then reseals over where the t-tubule mouth existed in order to maintain a barrier between the intracellular and extracellular environments and the remnants of the t-tubule network form into intracellular vesicles (Putnam, 1996; Kawai *et al.*, 1999). This vesiculation serves to protect the myocyte as the high intratubular $[Ca^{2+}]$ (of the extracellular fluid) would be potentially fatal to the myocyte if released into the cytoplasm. The maintenance of a normal cell shape thus supports the formation and purpose of intracellular vesicles (Brette *et al.*, 2002).

3.1.4.1 Detubulation using glycerol

Detubulation was first pioneered in amphibian skeletal muscle using glycerol (Gage & Eisenberg, 1969). The classic electrophysiological criterion for successful detubulation in skeletal muscle is abolition of the afterdepolarisation. This is a notable feature of skeletal muscle action potentials attributable to propagation into the t-tubule network. More recently an optimised form of the

glycerol detubulation protocol was produced which utilised timed exposures to glycerol followed by a high $[Ca^{2+}]$-$[Mg^{2+}]$ solution and steady cooling (Koutsis *et al.*, 1995). This was applied to frog skeletal muscle preparations and shown to produce successful detubulation in a high number of viable myocytes (Sheikh *et al.*, 2001). Detubulation was demonstrated by reduced t-tubule staining (with di-8-ANNEPS) and abolition of the after depolarisation. The inclusion of dye during the osmotic shock step allowed access of dye into t-tubule lumens prior to their detachment. Subsequent confirmation of the presence of intracellular vacuoles verified previous reports of detubulation in skeletal muscle (Krolenko, 1969).

As mentioned above, an osmotic mechanism underlies the effects of glycerol treatment on the t-tubule network. This is supported by evidence suggesting that detubulation can be halted on replacement with glycerol or reversed addition of sucrose (as it is non-membrane permeant) to differing degrees dependent on the time of their introduction during the cooling period of the protocol (Gallagher & Huang, 1997). In addition, loop diuretics, which inhibit the Na-K-Cl co-transporter and hence membrane water fluxes, were shown to decrease detubulation (Khan *et al.*, 2000).

3.1.4.2 Detubulation using formamide

A similar protocol was developed using the membrane permeable agent formamide (Argiro, 1981). Formamide-induced detubulation was applied to isolated rat ventricular cardiomyocytes in order to determine the function of t-tubules in cardiac cells (Kawai *et al.*, 1999). Application of 1.5 mmol/L formamide induced a rapid decrease in cell volume which recovered after approximately 7 min. On washout of formamide a sudden increase in cell volume and subsequent detubulation occurred as reported for glycerol. Formamide treated cardiomyocytes stained with di-8-ANNEPS demonstrate a clear loss of striations particularly towards the cell centre and whole cell voltage-clamp experiments reveal a 26-32% decrease in membrane capacitance compared to controls (Kawai *et al.*, 1999; Despa *et al.*, 2003; Brette *et al.*, 2006). These results are consistent with a physical and electrical disconnection of t-tubules from the surface sarcolemma, thereby impairing access of di-8-

ANNEPS and indicating a loss of membrane area, both of which are attributable to detubulation.

3.1.4.3 Mechanism of formamide and absence of direct effects

The mechanism of action in formamide-induced detubulation is also osmotic as suggested by the changes in cell volume on application/removal of formamide (Kawai *et al.*, 1999). T-tubules become disrupted as the cell expands during removal of formamide which was demonstrated by the incorporation of FITC-labelled dextran into the subsequently formed intracellular vesicles only when included in the washout solution (Brette *et al.*, 2002).

Potential direct effects of formamide on the protein and cardiomyocyte function have been eliminated by multiple pieces of evidence. The alterations in t-tubule network structure and cardiomyocyte function are seen on washout of formamide and not on its addition, thereby ruling out an immediate effect. Direct structural effects were examined following formamide-induced detubulation by immunolabelling of β-tubulin (a component of the microtubular network) which demonstrated no change in the cellular cytoskeleton (Brette *et al.*, 2002) and no alteration in contractile protein integrity (Monterrubio *et al.*, 2002). The responses of I_{Ca} to BAY K 8644 (a Ca^{2+} channel agonist) and isoprenaline (a β receptor agonist) remain unaltered by formamide treatment (Kawai *et al.*, 1999). In atrial cardiomyocytes, which lack a t-tubule network to begin with, formamide treatment shows no change in cell capacitance, action potential characteristics or Ca^{2+} handling compared to control atrial cardiomyocytes indicating it had no direct effect on ion channels/transporters (Brette *et al.*, 2002). Finally, application of caffeine demonstrated similar SR Ca^{2+} contents in control and formamide-treated cells both in skeletal muscle preparations (Monterrubio *et al.*, 2002) and isolated rat ventricular cardiomyocytes (Kawai *et al.*, 1999).

3.1.5 Localisation of Ca^{2+} cycling proteins, transport mechanisms and ion channels in the t- tubule network

A further demonstration of the specialisation of the t-tubule network is its distinct protein composition from that of the surface sarcolemma. Many of the Ca^{2+} cycling proteins and transport mechanisms involved in EC coupling are preferentially located here. Five main approaches have made the study of membrane localisation and concentration of proteins possible; these are (i) immunocytochemistry, (ii) comparison with systems lacking t-tubule networks, (iii) detubulation (iv) diffusional delay studies and (v) high-resolution scanning or "smart" patch-clamping.

The detubulation technique has contributed to knowledge of protein localisation as it allows distinction to be made between proteins located at the surface sarcolemma and t-tubule network. Whole-cell voltage clamp measurement of membrane currents in detubulated and control cells has determined which currents, and hence protein channels, are preferentially located in the t-tubule network. High-resolution scanning or "smart" patch-clamping is a specialised form of patch clamping which allows for precise control of the patch pipette (approx. 100 nm tip radius) to a distinct sub-cellular membrane location. This then allows for specific recording of currents at these localities (Gu *et al.*, 2002). The advantage of detubulation or smart patch-clamping is that there is no need for fixation of the tissue (as is required with immunocytochemistry) and so they provide insight into the functional distribution of proteins.

A large proportion of localisation studies have employed immunocytochemistry, yet the technique is not without its drawbacks both in its methodology and interpretation; these are well summarised by Brette and Orchard (2003). Immunocytochemistry is subject to inaccuracies due to membrane folding, leading to areas of high artefactual staining, and access of the antibody conjugate to the protein of interest. In addition it does not definitively show that a protein has been inserted into the membrane although co-localisation with vinculin, a component of the cytoskeleton, has been performed in an attempt to show this (Kieval *et al.*, 1992; Brette & Orchard, 2003).

Discrepancies between each investigation may also be due to factors such as inter-species variation (Frank *et al.*, 1992).

The localisation and co-localisation of these proteins is fundamental to the spatial coupling of electrical and Ca^{2+} signalling required for precise control during the cardiac cycle. Evidence supporting location within or adjacent to the t-tubule membrane exists for the LTCC, RyR2, NCX, Na^+/K^+-ATPase, VGSCs and some K^+-channel isoforms; more debate exists as to whether these are concentrated in the t-tubules with respect to the surface sarcolemma. The evidence to support the presence/concentration within or close to the t-tubule network for LTCCs, RyR2s, NCX, VGSCs and the protein sorcin will be discussed in the following sections.

3.1.5.1 L-type Ca^{2+} channel and Ryanodine receptor

Immunolocalisation studies have shown there is a juxtapositioning of LTCCs and RyR2s contained within the t-tubule and SR membranes respectively at the dyadic junction (Carl *et al.*, 1995; Scriven *et al.*, 2000). The work of Scriven and colleagues demonstrated this well using dual-immunocytochemical staining, image deconvolution techniques and digital image analysis. They determined that 56.7% of LTCCs were co-localised with RyR2s, a value close to the 63% limit of co-localisation detection of the protocols employed. They did however detect only 36.7% of RyR2s co-localised with LTCCs which was due to the much higher level of RyR2 staining and that the discrepancy in percentage detection was due to RyR2 protein present on corbular SR. Insight into the mechanism of the co-localisation of LTCCs and RyR2s has been gained from work in skeletal muscle. This has shown that production of an LTCC-RyR1 complex precedes the onset of t-tubule formation. The complex then fuses with the developing t-tubule and may account for the localisation of LTCCs to the t-tubule membrane (Yuan *et al.*, 1991). In cardiac muscle, LTCCs are synthesised in the peri-nuclear area then trafficked to the t-tubule (Leach *et al.*, 2005) and following this, a similar mechanism to that shown in skeletal muscle may take place. This spatial association of LTCCs with RyR2s is known to increase steeply during development with a significantly higher degree of internal couplings leading to the adult SR-dependent mechanism of EC coupling (Sedarat *et al.*, 2000; Seki *et al.*, 2003).

The co-localisation of and close coupling of LTCCs with RyR2s in the network thereby strengthens the importance of the t-tubule membrane as the main site of EC coupling.

There is a large body of evidence to support a concentration of LTCCs within the t-tubule network of ventricular cardiomyocytes. Immunocytochemistry has shown this in rabbit (Carl *et al.*, 1995), rat (Scriven *et al.*, 2000; Leach *et al.*, 2005) and guinea-pig (Gathercole *et al.*, 2000). In rabbit cardiomyocytes kept in culture for 24 hr, I_{Ca} was decreased by 50% compared to control. Although this partially recovered following 6 days in culture, the accompanying loss of t-tubule density (57%) supports a predominantly t-tubular location for LTCCs (Mitcheson *et al.*, 1996). Detubulation of rat ventricular myocytes produced a 26% decrease in membrane capacitance accompanied by a 76% decrease in I_{Ca} density and decreased Ca^{2+} transient amplitude. This implied an 8.7 times greater I_{Ca} density in the t-tubule network than surface membrane (Kawai *et al.*, 1999). In keeping with this figure, further work from the same group and that of others has estimated that 75-80% of I_{Ca} is located in t-tubule network (Brette *et al.*, 2004; Louch *et al.*, 2004). The remaining 20-25% of LTCCs located at the surface sarcolemma have an equal coupling efficiency with RyR2s as that in the t-tubule network. The rapid rising phase of the Ca^{2+} transient remained in detubulated cells indicating that the link between Ca^{2+} entry and Ca^{2+} release is the same in the t-tubule network and surface sarcolemma (Kawai *et al.*, 1999).

Diffusional delay studies were carried out in guinea-pig ventricular and rabbit atrial myocytes. These examined the time-course of current change of I_{Ca} in response to fast solution exchange of $[Ca^{2+}]_o$. Comparison of ventricular cells with atrial cells indicated that whilst atrial cells exhibited a single time-course of current change, ventricular cells displayed slow and fast components of current change. This biphasic response was attributed to the presence of the highly tortuous t-tubule network in ventricular cells presenting a physical barrier to diffusion of Ca^{2+} ions down the lumen. The slow phase of I_{Ca} constituted 64% of the whole cell change in current suggesting a concentration of LTCCs in the t-tubule network (Shepherd & McDonough, 1998). Finally, high-resolution scanning or "smart" patch-clamping has determined that there are approximately 2 LTCCs per t-tubule opening in isolated rat cardiomyocytes (Gu

et al., 2002). Using this technique, LTCCs were found to be present only at the mouth of the t-tubules whilst the remaining surface membrane was devoid of any LTCCs. The technique is limited in this context by its inability to measure LTCCs within the t-tubule lumen yet smart patch-clamping has the advantage of allowing an understanding of the functional LTCC distribution. Studies which conclude that LTCCs are uniformly distributed between the t-tubule network and surface sarcolemma do exist (Shepherd & McDonough, 1998). The majority however agree, however, that LTCCs are concentrated within the t-tubule network of the ventricular myocyte. In addition, parallel biochemical and immunoelectron studies on skeletal muscle have confirmed that LTCCs are densely distributed in the t-tubule network (Fosset *et al.*, 1983; Jorgensen *et al.*, 1989).

3.1.5.2 Sodium-calcium exchanger

The location of NCX in the sarcolemma of ventricular myocytes is a subject of debate. Some researchers favour an equal distribution between t-tubule and surface membranes whilst others suggest a t-tubule network concentration with respect to the surface sarcolemma.

In an immunofluorescence study of rat and guinea-pig ventricular myocytes, NCX was shown to be distributed throughout all membrane in contact with the extracellular space. A classic pattern of t-tubule staining was obtained which appeared highly organised at 1.8 μm intervals (Kieval *et al.*, 1992). Detubulation, as a tool to investigate NCX distribution, was first used in rat ventricular myocytes (Kawai *et al.*, 1999). Following this, a comparable decrease in rate of decline of the caffeine-induced Ca^{2+} transient (representative of NCX activity) to the decrease in capacitance was observed. Thus a uniform distribution of NCX between the surface sarcolemma and t-tubule was suggested (Kawai *et al.*, 1999) yet was later brought into question due to contradicted by the same group as detailed below (Yang *et al.*, 2002).

Evidence to support an inhomogeneous distribution of NCX between the surface sarcolemma and t-tubule network in ventricular myocytes is extensive. One of the first studies utilising immunofluorescent labelling of guinea-pig and rat

ventricular myocytes employed both monoclonal and polyclonal antibodies directed against NCX (Frank *et al.*, 1992). The fluorescence was most intense in a regular striated pattern at the level of the Z-line with weaker more patchy fluorescence around the cell perimeter. This localisation was validated by electron microscopic examination of immunogold-labelled rat papillary muscle cryosections which showed a similar pattern. Results from this work demonstrated that NCX was localised and concentrated within the membrane of the t-tubule network. Further research from the same group corroborated this t-tubular concentration in adult rabbit ventricular myocytes. This also showed that NCX localisation in the t-tubules commenced in line with the development of the t-tubule network in ventricular cells from immature rabbits (Chen *et al.*, 1995). In detubulated rat ventricular myocytes (formamide-induced), application of caffeine revealed a significant prolongation in the decline of $[Ca^{2+}]_i$ and rise of $[Ca^{2+}]_o$ indicative of reduced Ca^{2+} efflux. Measurement of the NCX I-V relationship in detubulated cells showed no significant difference when Ni^{2+} was included in the perfusate thus I_{NCX} appeared to be almost completely abolished following formamide treatment. From this, it was concluded that NCX was almost exclusively present in the t-tubules (Yang *et al.*, 2002). More recent detubulation studies have also shown NCX effects. A continuation of the work by Yang and colleagues (2002), again in rat, showed an approximately 40% decrease in I_{NCX} density both in forwards and reverse modes accompanied by a 32% decrease in capacitance. This indicated that whilst approximately 37% of functional NCX transporters were present in the surface sarcolemma the remaining 63% of NCX resided in the t-tubule network; i.e. it was at a 3.6 times greater density in the t-tubule network compared to the surface sarcolemma (Despa *et al.*, 2003). The currents recorded in this study were approximately 20% larger than those of the previous study (Yang *et al.*, 2002) and so the remaining I_{NCX} in detubulated cells was capable of being resolved. Results from a different group have confirmed NCX is present on the surface sarcolemma, intercalated disc as well as t-tubule network in rat. This work additionally identified the presence of NCX only on the vertical elements of the network with its absence on longitudinal elements in contrast to earlier work (Scriven *et al.*, 2000). Detubulation produced an approximately 40% reduction in peak I_{NCX} accompanied by a 27% reduction in cell capacitance pointing towards a 16% reduction and localisation of I_{NCX} to the t-tubule network. Thus NCX appeared to

be concentrated only within the vertical t-tubules indicative of additional sub-regional localisation within the network (Thomas *et al.*, 2003).

If functional NCX molecules are indeed concentrated within the t-tubule network as growing evidence suggests, the overall functional outcome on Ca^{2+} fluxes in the cardiomyocyte will depend on their spatial location in relation to the dyad. Some studies report NCX to be within nanometers of RyR2 in the dyad (109 ± 8 nm on average) and of comparable distance with LTCCs from RyR2s (Thomas *et al.*, 2003) whilst others determine NCX to be located further from the dyad (Scriven *et al.*, 2000).

3.1.5.3 Voltage- gated Na^+ channel

Rapid and synchronous transmission of electrical activation throughout the sarcolemma relies on the activation of the VGSC. The diffusional delay work by Shepherd and McDonough (1998) suggested a uniform distribution of VGSCs between the surface sarcolemma and t-tubule network. An exact quantification of the time course the change in I_{Na} change was not possible due to the large size and fast kinetics of the current (Shepherd & McDonough, 1998).

It has been proposed that VGSCs are concentrated at the mouth of the t-tubule. The rapid depolarisation of the t-tubular membrane, as with all types of excitable membrane, relies on the local circuit current generated up-stream to discharge the membrane's capacitance thus bringing it up to threshold for action potential firing. Sheikh and co-workers (2001) used a cooled amphibian skeletal muscle preparation to determine the influence of the t-tubules on conduction velocity. They tested the hypothesis that the t-tubular membrane was acting as a current drain on the cell, thus delaying conduction velocities achievable in the surface membrane. The t-tubules were removed using a glycerol detubulation protocol in order that myocytes with and without t-tubules could be compared for conduction velocity. T-tubular detachment did not influence surface membrane action potential conduction. These findings suggested a mode of firing in the membrane of the t-tubules that was independent of the local circuit current generated in the surface membrane and that there was a functional separation of t-tubules from the surface sarcolemma. Through immunolabelling

techniques, they claimed this to be due to a clustering of voltage gated sodium channels at the mouth of each t-tubule. Once activated by the surface membrane potential, these VGSCs were capable of acting as a booster station bringing the membrane of the t-tubule up to threshold, exciting the length of the t-tubule and hence limiting the capacitative drain on the surface sarcolemma (Sheikh *et al.*, 2001).

3.1.5.4 Sorcin

Sorcin is a small (21.6 kDa), Ca^{2+}-binding protein highly abundant in the cardiomyocyte. Although not strictly a Ca^{2+}-cycling protein involved in EC coupling, sorcin is capable of binding Ca^{2+} at micromolar concentrations and translocating to membrane where it modulates the activity of the major cardiac Ca^{2+}-handling proteins. Sorcin has been shown to localise within the t-tubule network and co-localise with RyR2 at the dyadic junction (Meyers *et al.*, 1995a). It is of particular relevance to the work detailed in this thesis and an extensive review of the effects of sorcin in the cardiomyocyte is presented in Chapter 4.

3.1.6 Function of the t-tubule network

The t-tubule network is a highly specialised feature of the ventricular myocyte ultrastructure which ensures temporally and spatially synchronous coupling of electrical excitation to SR Ca^{2+} release throughout the body of the cardiomyocyte. The critical dependence on the t-tubule network for providing this synchronicity has been demonstrated by a number of studies some of which have been discussed previously in this introduction. The current section will provide an overview and summary of these and earlier studies undertaken to elucidate t-tubule function.

The t-tubules have been shown to be the predominant site at which Ca^{2+} sparks originate (Shacklock *et al.*, 1995; Tanaka *et al.*, 1998). In isolated intact rat ventricular myocytes stained with both fluo-3 and di-8-ANNEPS, 85% of Ca^{2+} sparks occurred within 0.5 μm of the t-tubule at the t-tubule-SR junction. Of these, 30% were shown to be 0.2 μm from the t-tubule - the limit of resolution of the methods employed. In addition, it was observed that in certain

cardiomyocytes under study, particular t-tubules exhibited an enhanced probability of being the sites of origin of Ca^{2+} sparks. It was proposed that this was due to either an uneven distribution of LTCCs or state of SR loading (Shacklock *et al.*, 1995). Similar work by different groups also in rat myocytes confirmed that the appearance of highly localised SR Ca^{2+} release, in the form of either Ca^{2+} sparks or spikes, coincided with the positioning of the t-tubules at the level of the Z-lines (Song *et al.*, 1998; Tanaka *et al.*, 1998). More recently, it has been shown that an increase in the incidence of Ca^{2+} sparks was directly related to formation of the t-tubule network (from rat foetal cardiomyocytes through neonatal to adult) thus demonstrating the dependence on t-tubules for spark production throughout the cell (Seki *et al.*, 2003). Reduction in t-tubule density was also associated with the loss of Ca^{2+} sparks (Seki *et al.*, 2003). It is unsurprising that the t-tubule should be the main site at which Ca^{2+} sparks originate due to the well demonstrated high t-tubule concentration of Ca^{2+} flux pathways (LTCC and NCX) and co-localisation of LTCCs and RyR2s enabling highly efficient CICR.

Comparison of functional data from systems which either lack or have a sparse t-tubule network has yielded critical information as to its function. A biphasic pattern of Ca^{2+} release has been demonstrated in formamide detubulated adult rat ventricular cardiomyocytes (Kawai *et al.*, 1999; Brette *et al.*, 2002), neonatal ventricular cardiomyocytes (Haddock *et al.*, 1999; Seki *et al.*, 2003), atrial cardiomyocytes (Huser *et al.*, 1996) Purkinje cells (Cordeiro *et al.*, 2001) and cultured ventricular myocytes (Lipp *et al.*, 1996). These are as the result of two phases of SR Ca^{2+} release (i) true CICR triggered by I_{Ca} (at the cell periphery) and (ii) propagated SR Ca^{2+} release (at the cell centre) (Kawai *et al.*, 1999; Brette *et al.*, 2002). The biphasic distribution of the transient and its change to a monophasic distribution (with postnatal t-tubule development) during maturation are highly supportive of a role for the t-tubule network in synchronising SR Ca^{2+} release throughout the entire cell in the ventricular myocyte. An additional role of the t-tubule network in shaping the action potential duration has also been suggested mainly due to the localisation of I_{Ca} in the t-tubule network (Brette *et al.*, 2006).

3.1.7 Pathological remodelling of the t-tubule network

Previously, a number of groups have suggested that hypertrophy of cardiomyocytes from failing hearts is associated with remodelling of the t-tubule network.

One of the earliest studies examining the t-tubule network showed that hypertrophy was associated with a proliferation of the network which was suggested to occur in an attempt to maintain surface area:volume ratios in the face of increasing cell size (Page & McCallister, 1973). Later, work in hypertrophied rat cardiomyocytes revealed that these cells exhibited a reduced ability of I_{Ca} to trigger SR release and an increase in the inactivation time for I_{Ca}. From this it was concluded that hypertrophy leads to a "change in the microarchitecture of the dyad" which comprised a widening of the t-tubule/SR junction (Gomez *et al.*, 1997).

An emerging theme from more recent work is that a general loss of the t-tubule network occurs in animal models of heart failure (He *et al.*, 2001; Balijepalli *et al.*, 2003; Quinn *et al.*, 2003). T-tubule density was assessed in a canine tachycardia pacing-induced model of cardiomyopathy using di-8-ANNEPS (He *et al.*, 2001). In control myocytes, t-tubules in the cell centre appeared as a highly regular pattern of punctuate dots at approximately 1.6 μm intervals representing t-tubules visualised in cross-section. By contrast, the distribution of the t-tubule network in failing cells exhibited a much more disorganised arrangement. Quantification of the average cell area occupied by the t-tubule network revealed an approximately 24% decrease compared to control myocytes ($8.7 \pm 0.4\%$ *vs.* $11.5 \pm 0.4\%$ respectively; $p<0.001$). Most commonly, this loss of t-tubule network was preferentially located towards the cell ends adjacent to the intercalated disc. The extent of depletion was variable within cells from the same hearts and among cells from different hearts and the level of depletion appeared to be correlated with the degree of failure. In hearts experiencing the highest degrees of failure there was sparse di-8-ANNEPS staining other than of the surface sarcolemma. As LTCC's are known to concentrate in the t-tubule network, whole cell patch clamp was used to quantify I_{Ca} and determine if the loss of t-tubules had a knock-on effect on the channel. No significant difference

existed in whole cell I_{Ca} between sham and failure but further investigation of intramembrane charge movement associated with the gating of LTCC's revealed a 50% decrease in LTCC density in failure cells. This decrease in the total number of sarcolemmal LTCC's would be expected to decrease whole cell I_{Ca} and so it was suggested that the functional properties of the remaining channels served to compensate for the reduction in channel numbers (He *et al.*, 2001). Building on this work, the same group later went on to examine the alterations in t-tubule protein distribution which accompanies the depletion of the t-tubule network in order to evaluate a potential mechanism for this loss (Balijepalli *et al.*, 2003). Left ventricular tissue (isolated myocytes and whole homogenates) from dogs with and without tachycardia-induced cardiomyopathy was studied using fluorescence microscopy and membrane fractionation techniques. Tissue and cells were labelled with fluorescent markers for surface membrane glycoproteins, Na^+/K^+-ATPase pump, LTCC subunit $Ca_v1.2$ and NCX. In intact and permeabilised (fixed) control cells, each membrane marker yielded a positive staining pattern at the surface membrane and formed a distinctly regular array of dots representing the t-tubule network (t-tubular staining for $Ca_v1.2$ in the latter was faint). Failing cells, however, showed a clear loss and irregular pattern of t-tubule network staining indicating that a disorganisation had occurred. As in the previous study, the level of loss/irregularity was found to be variable between cells. Using these techniques, the proportion of the cell area which stained positive for t-tubule network - "T-index" - was assessed using each marker (Balijepalli *et al.*, 2003). Failing cells exhibited a significant decrease in the T-index assessed with surface glycoprotein and Na^+/K^+-ATPase markers when compared to control ($5 \pm 2\%$ *vs.* $10 \pm 2\%$ respectively; $p<0.001$) and similar values were obtained when NCX was used to label the t-tubule network (T-index: failure $5 \pm 1\%$ *vs.* control $11 \pm 3\%$; $p<0.001$)(Balijepalli *et al.*, 2003).

A significant reduction in the t-tubule network has also been demonstrated in a rabbit model of heart failure (Quinn *et al.*, 2003). Di-8-ANNEPS staining of intact isolated ventricular myocytes revealed that on average there was a 40% depletion of t-tubules in failing cells compared to sham (Quinn *et al.*, 2003). In a mouse model of myocardial infarction, t-tubule network morphology was inspected at 1 and 3 weeks post-infarction (Louch *et al.*, 2006). At 1 week,

isolated ventricular myocytes from these animals exhibited a slight disorganisation in the t-tubule network which progressed to a profound rearrangement at 3 weeks characterised by irregular gaps between adjacent t-tubules. These gaps were shown to correlate with the positioning of SR delayed release sites (Louch *et al.*, 2006). The mechanism of dyssynchronised Ca^{2+} release in heart failure was carefully investigated in isolated ventricular myocytes from a spontaneously hypertensive rat model (Song *et al.*, 2006). Using Ca^{2+} spikes to define localised SR Ca^{2+} release events triggered only by LTCC fluxes, it was determined that failing cells frequently exhibited regions which did not produce Ca^{2+} release on depolarisation, so called "missed events". The lack of spikes later on in the depolarisation pulse indicated that late sparks which characterise heart failure cells are the result of secondary CICR; that is the primary sparks stimulate the later sparks and the transient proceeds in a regenerative manner. Examination of t-tubule network structure revealed a profound disorganisation in failing cells and a general movement of transverse elements away from the Z-lines. Dual-immunofluorescent labelling of LTCCs and RyR2s indicated that LTCCs followed the t-tubules away from the Z-line whereas RyR2s retained a regular striated pattern. Consequently, this structural remodelling establishes a population of uncoupled RyR2s or "orphaned" RyR2s which are physically isolated from their I_{Ca} trigger and are thus incapable of normal CICR and form the basis of the observed missed events. These orphaned RyR2s are however capable of releasing Ca^{2+} when activated as a consequence of secondary CICR (Song *et al.*, 2006).

Studies of the t-tubule network in human myocardium remain relatively rare and, to date, no comprehensive quantification has been made of t-tubule network density in human ventricular myocytes in response to cardiomyopathy or failure. In keeping with animal model findings, it is generally accepted that failing human cardiac tissue undergoes a remodelling of the t-tubule network. Isolated ventricular myocytes and tissue sections from explanted human hearts with chronic heart failure showed a generalised disorganisation of the myocyte ultrastructure (Schaper *et al.*, 1991). In particular, electron microscopy and immunofluorescence revealed a proliferation of dilated t-tubules in failing tissue. Further investigation of the t-tubule network in human cardiomyopathic hearts confirmed that tubules were dilated, as demonstrated by an increased

intermyofibrillar pattern in immmunohistochemical staining for the "protein scaffold" proteins (see 3.1.1.1). In addition, this re-examination determined that although the t-tubules present were dilated, the overall density of the network was reduced when compared to rat control myocytes (Kostin *et al.*, 1998). T-tubule dilation was also detected in failing human myocardium through distribution studies of the membrane cytoskeleton protein dystrophin using electron microscopy and immunospecific labelling techniques (Kaprielian *et al.*, 2000). Additionally, t-tubules were twisted and an increased proportion of tubules existed as longitudinally orientated elements compared to control tissue. Critically, this study determined that there was a generalised increase in the density of the t-tubule network in failing cells compared to controls although the increase was not quantified. More recent preliminary investigations in isolated human ventricular myocytes have yielded conflicting results, reporting that the t-tubule network is either unchanged (Ohler *et al.*, 2002) or decreased in response to heart failure (Wong *et al.*, 2002). A major set-back to human studies is the widespread inaccessibility to human control tissue and therefore controls such as pig (Schaper *et al.*, 1991; Louch *et al.*, 2004), rat and monkey (Kostin *et al.*, 1998) have been employed. Although human tissue was obtained in one study (Kaprielian *et al.*, 2000), a clear reference point for the t-tubule network in healthy human cardiomyocytes is required before an adequate quantification of the t-tubule network in response to conditions of failure or cardiomyopathy can be determined.

Table 3.1 summarises the experimental models and remodelling in the t-tubule network obtained from the major studies detailed above.

Table 3.1 Summary table of remodelling of the t-tubule network in heart failure/cardiomyopathy.

References: [1] (Gomez *et al.*, 1997); [2] (Song *et al.*, 2006); [3] (He *et al.*, 2001); [4] (Balijepalli *et al.*, 2003); [5] (Quinn *et al.*, 2003); [6] (Louch *et al.*, 2006); [7] (Schaper *et al.*, 1991); [8] (Kostin *et al.*, 1998); [9] (Kaprielian *et al.*, 2000); [10] (Wong *et al.*, 2002); [11] (Ohler *et al.*, 2002). Abbreviations: **DCM** dilated cardiomyopathy; **ICM** ischaemic cardiomyopathy; **TT** t-tubule; **SR** sarcoplasmic reticulum; **LTCC** L-type Ca^{2+} channel; **RyR2** ryanodine receptor; **?** indicates where morphological appearance was speculative and no evidence existed to support it from that study.

Species / Model	Morphological appearance of TT network	TT network % change (vs control)	Additional findings relating to TT network
Rat / Hypertrophy [1]	Widening of TT-SR junction ?	Not assessed	
Rat / SHR/HF [2]	TTs moved away from Z-line	Not assessed	LTCCs remain with TTs; some RyR2s are "orphaned"
Canine / Tachycardia [3]	Irregular and disorganised; loss of TTs at cell ends	↓ by 24 %	50 % ↓ in LTCC density
Canine / Tachycardia [4]	Irregular and disorganised; loss of TTs	Not assessed	50 % ↓ in surface glycoproteins, Na+/K+-ATPase and NCX
Rabbit / Infarct [5]	Many areas devoid of TTs	↓ by 40 %	
Mouse / Infarct [6]	Profound disorganisation; irregular gaps between adjacent TTs	Not assessed	Regions of delayed SR Ca^{2+} release at gaps
Huan / DCM [7]	Proliferation of dilated TTs	Not assessed	
Human / DCM [8]	Dilated TTs	↓ (not quantified)	
Human / DCM/ICM [9]	↑ tortuosity; dilated TTs; more longitudinal TTs	↑ (not quantified)	
Human / DCM/ICM [10]	Spatially more irregular	↓ (not quantified)	
Human / CM [11]		No change	

3.2 Aims

The aims of the present chapter were as follows:

1. To quantify the relative t-tubule area in isolated ventricular myocytes from rabbits with and without LVD.

2. To investigate protocols which would deplete the t-tubule network in isolated rabbit ventricular myocytes.

3. To establish a proof of principle for the technique in detecting internalised t-tubules.

4. To determine the pattern of NCX distribution in sham and LVD isolated ventricular myocytes.

3.3 Methods

3.3.1 T-tubule staining and determination of relative t-tubule area

The investigation of relative t-tubule area was performed in isolated ventricular cardiomyocytes from rabbits with and without LVD. T-tubules were visualised using the voltage-sensitive membrane specific fluorescent probe di-8-AminoNaphthylEthenylPyridinium (di-8-ANNEPS) and were imaged throughout the depth of the cell using the z-stack function of the confocal microscope. Relative t-tubule area was quantified in cardiomyocytes with intact membranes and also in permeable cardiomyocytes which had been treated with the agent β-escin.

The indicator di-8-ANNEPS becomes highly fluorescent on binding to membrane and, on its addition to the extracellular environment, selectively labels all membrane in contact with the extracellular fluid. Di-8-ANNEPS is well retained in the outer leaflet of the membrane, limiting labelling of intracellular membranes and therefore serving as an ideal marker for the sarcolemma and t-tubule membranes. When bound to phospholipid membrane, its absorption spectrum is in the range of 450 and 510 nm, whilst emission is above 570 nm. Di-8-ANNEPS is highly photostable and is well able to withstand repeated imaging as was required for the study.

Fura-FF pentapotassium salt (cell impermeant) was used as an extracellular marker to verify the integrity of the sarcolemma. Fura-FF was excited at 810 nm using two-photon excitation and emissions were collected between 500 and 700 nm. Exclusion of Fura-FF, and hence absence of fluorescence in the cell interior, clearly indicated cells with fully intact membranes whilst the inclusion of intracellular Fura-FF defined cells with permeable membranes.

Once established, this protocol was applied to a number of cells both intact and permeabilised from LVD and sham hearts. A quantitative evaluation of the relative cell area which stained positive with Di-8-ANNEPS was performed using the analysis method detailed in 3.3.7. Relative cell area which stained positive with Di-8-ANNEPS was then taken to represent the relative t-tubule area of the cell.

Two additional investigations were performed. Firstly, the t-tubule network was depleted using the agent formamide. The mechanism for this action has been described in 3.1.4.3. Secondly, the technique of chemistry was used to determine the distribution pattern of NCX within the isolated ventricular myocyte.

All isolated left ventricular myocytes were obtained as previously described in 2.2.1 General methods.

3.3.2 Solutions for t-tubule studies

The solutions given below were freshly prepared for each experimental run. All concentrations are in mmol/L except where stated otherwise; pH correction was performed at room temperature (20-21 °C).

Mock intracellular solution - KCl (100), NaCl (10), MgCl (5.5), HEPES (25), Na_2ATP (5), Na_2PCr (10) with EGTA (5) added to prevent contraction; pH 7.4 with KOH.

Mock extracellular solution - NaCl (140), KCl (4), MgCl (1), HEPES (5), glucose (11.1), $CaCl_2$ (1.8); pH 7.4 with NaOH.

10 mmol/L BDM mock extracellular solution - as for mock extracellular solution above but with BDM (10) added to prevent contraction.

3.3.3 Preparation of cells for t-tubule studies

Isolated left ventricular myocytes were obtained in BSA solution with 0.125 mmol/L Ca^{2+}. These were filtered, gently centrifuged for approximately 12 s at 5 *g* and re-suspended in mock intracellular solution. The solution was agitated to ensure even dispersion of cells and divided into equal volumes for (i) intact cells and (ii) permeable cells. "Intact" cells were dealt with first and cells for permeabilisation were stored at 4 °C until required.

Di-8-ANNEPS was added to the "intact" cell suspension to a final concentration of 20 μmol/L and incubated at room temperature for 5 min. 5 mmol/L EGTA solution was added in order to terminate incubation. A sample of the suspension

was pipetted into a home-made perspex bath (estimated volume 200 μl); this solution also contained 50 μmol/L Fura-FF free acid. Cells were allowed to settle onto the cover slip for approximately 2 min before imaging.

β-escin was added to the "permeable" cell suspension at a final concentration of 100 μg/mL and incubated for approximately 15 s in order to limit cellular degradation by β-escin, washed once and re-suspended in 1 mL of mock intracellular solution. Thereafter "permeable" cells were treated exactly as "intact" cells above.

The use of Fura-FF served as a "quality control" step for the experimental protocol. It accounted for cells in the "intact" group whose membranes had become permeable through some other process (i.e. mechanical disruption during centrifugation) and also for cells in the "permeable" group which had been incompletely permeabilised during β-escin treatment. These cells were not used for imaging.

3.3.4 Dimensions of isolated cardiomyocytes

Measurement of the dimensions of isolated ventricular myocytes from sham and LVD animals was performed by Mrs Aileen Rankin.

Isolated left ventricular myocytes were obtained in BSA solution with 1.0 mmol/L Ca^{2+}. This ensured that cells possessed intact membranes and were not contracted. Cells were placed on the stage of a light microscope and dimensions were assessed using an eye-piece graticule. Cells from each group were measured for length and width and results were averaged to obtain mean values.

3.3.5 Detubulation

It is known that t-tubules can become disrupted following an osmotic shock. In this study, detubulation of isolated rabbit ventricular cardiomyocytes was initially attempted using the protocol of Kawai *et al.* (1999) but this proved unsuccessful. An approach using mannitol, which has greater membrane permeability than formamide, was therefore investigated as an agent to provide

a larger osmotic shock (Allen & Smith, 1987). Once again, this method proved unsuccessful at detubulating rabbit cardiomyocytes. The agent formamide was re-examined and an adapted version of the protocol was successful in producing a substantial depletion of the t-tubule network. This was then applied to a number of cells and the relative t-tubule density was determined; a sub-population of these were then permeabilised and assessed for relative t-tubule density.

3.3.5.1 Detubulation using mannitol

Isolated rabbit left ventricular cardiomyocytes were obtained in base Krebs' solution with 1 mmol/L added $CaCl_2$. The suspension was spun down (approximately 12 s at 5 *g*) and re-suspended in mock extracellular solution. A sample of this was reserved in order to constitute a "control" group that did not undergo treatment with mannitol.

The remaining suspension was divided into two equal volumes and was incubated with either 300 or 400 mmol/L mannitol at room temperature for 5 min. Following this, cells were spun down (approximately 12 s at 5 g) and re-suspended in mock extracellular solution. All cells were stored at 4 °C until required for imaging.

3.3.5.2 Detubulation using formamide

Single left ventricular cardiomyocytes from either sham or LVD rabbits were obtained in base Krebs' with 1 mmol/L added $CaCl_2$. The suspension was spun down (approximately 12 s at 5 *g*) and re-suspended in 10 mmol/L BDM mock extracellular solution. A sample of this was reserved in order to constitute a "control" group that did not undergo treatment with formamide.

1.5 mol/L formamide was added to the remaining suspension and incubated at room temperature for 15 min. Following this, cells were spun down (approximately 12 s at 5 g) and re-suspended in 10 mmol/L BDM mock extracellular solution. The solution was agitated and divided into equal volumes for "intact" and "permeable" cells.

Permeabilisation with β-escin ("permeable" set) and cell staining with Di-8-ANNEPS ("control", "intact" and "permeable" sets) was performed for the appropriate groups according to the methods stated above but all re-suspension steps used 10 mmol/L BDM mock extracellular solution. All cells were stored at 4 °C until required for imaging.

3.3.6 Confocal microscopy for t-tubule detection

The principles behind confocal microscopy are described in General methods (2.2.3.2).

The cell suspension was contained within a home-made perspex bath situated above the objective of an inverted microscope (Nikon, Eclipse) and viewed using a X40 oil lens; images were recorded using a BioRad 2000 confocal microscope. A mira laser was used to excite Fura-FF at 810 nm and emissions were collected between 500 and 700 nm thus allowing determination of surface membrane integrity. In order to visualise membranes, a Kr/Ar laser excited Di-8-ANNEPS at 488 nm whilst emissions were collected at >518 nm; laser power was maintained at approximately 0.45 mW throughout scanning to avoid damaging cells and bleaching of the dye. Iris diameter was set at 1.8 providing an axial resolution of 0.9 μm (Loughrey *et al.*, 2002). Zoom was adjusted such that the cell length spanned the entire field of view. Data were acquired in image-scan mode at 2 ms per line (512 x 512) and each section was Kalman averaged (n=4). Z-stacks of images were produced from each cell by scanning every 0.5 μm from the top to the bottom of each cell.

3.3.7 Quantitative analysis of relative t-tubule area

All cells were randomised and analysis was blinded in order to ensure a reproducible and unbiased method. Images were analysed using a programme created by Prof. Godfrey Smith in IDL (Quinn *et al.*, 2003). In this, each confocal fluorescence X-Y image from the stack was converted into a binary image with white and black corresponding to positive and negative di-8-ANNEPS staining respectively. The binary image was produced by sampling the mean pixel intensity of the perimeter stain (sarcolemma) of each cell and calculating

an average value for reference purposes. The cell was then divided into ten equal portions along its length and all pixels greater than or equal to a threshold value (75%) of the perimeter mean pixel intensity were converted to white and considered representative of positive di-8-ANNEPS (membrane) staining. Those below the threshold value were assigned as black. The perimeter stain was eroded thus all remaining pixels were those contained within the cell interior i.e. t-tubules. The total number of white pixels (t-tubule pixels) in each of the ten sections was counted and reported by the programme. The analysis method also took into account the zoom value for each individual cell such that the t-tubule area was corrected for alterations in cell dimensions. A diagrammatic representation of the analysis method is shown in Figure 3.2.

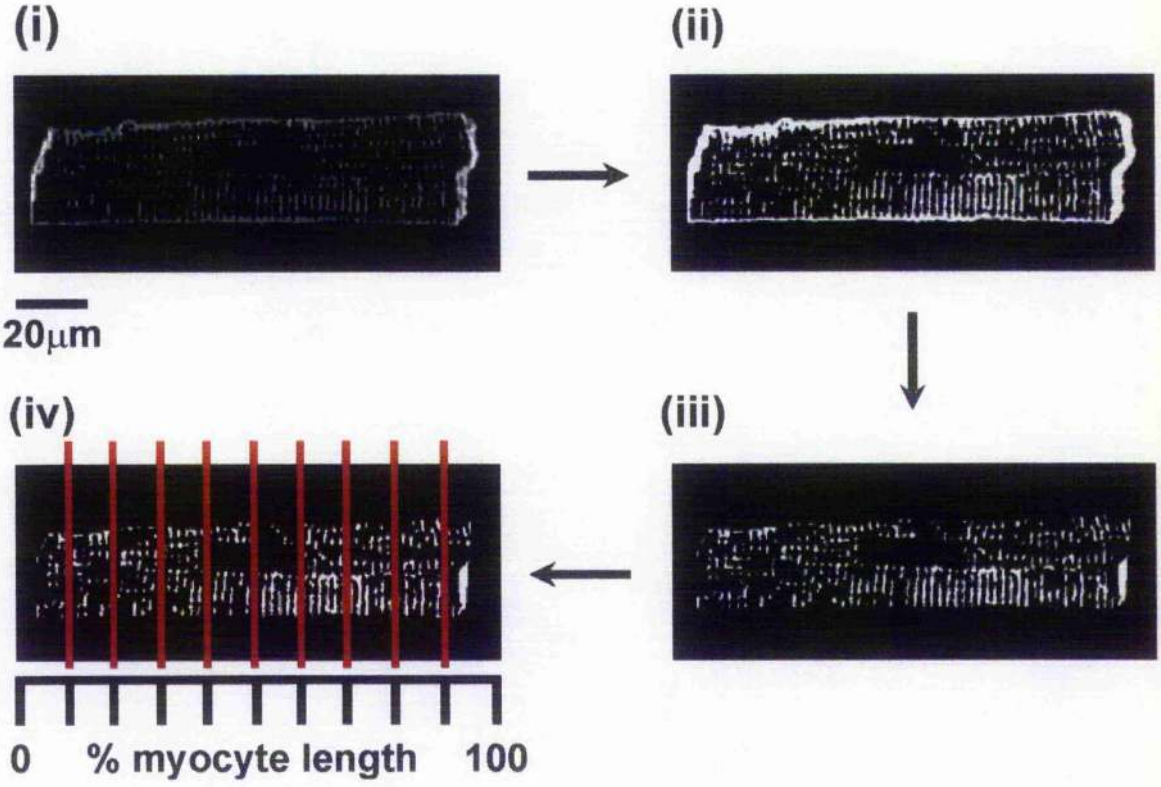

Figure 3.2 Analysis method for resolving relative t-tubule area.

(i) Confocal image of a single isolated left ventricular rabbit cardiac myocyte stained using Di-8-ANNEPS. **(ii)** Corresponding binary image produced from the same cell. White areas represent positive stain for Di-8-ANNEPS and therefore membrane area. **(iii)** As (ii) but with removal of the surface sarcolemma and intercalated discs leaving binary image attributable only to membrane comprising t-tubule. **(iv)** Division of the cell into ten equal sections along the length. The pixels staining positive (white) in each section were then counted and output as t-tubule area.

In each cell only the middle 10 - 15 sections of the stack, which clearly spanned the entire cell length, were analysed. This ensured that sections were of comparable dimensions and were free from the complicating influences of the surface sarcolemma above and below. The only regions of the section which were excluded from the counting procedure were the intercalated discs at either end of the cell as these were considered not to be part of the t-tubule network. The nucleus/nuclei were not excluded in the analysis step as these areas were assumed to be approximately uniform within each cell. A degree of nuclear staining was, however, apparent in the permeabilised groups. In order to assess the contribution of the area occupied by the nucleus to the total t-tubule area of the cell additional analysis was performed. A subset of LVD intact and permeable cells were selected at random and analysed either with or without exclusion of the nucleus which was most prominent in the middle sections. The analysis was performed on the four most central sections where the diameter of this nucleus was greatest.

As stated, the analysis programme output the total number of t-tubule pixels in each of ten sections along the cell length. The pixels from 0-50% of the cell length were then averaged with those from 100-51% (i.e. a symmetrical reflection around the cell centre) as it was assumed that there was no biological reason for the halves of the cell to be different. These pixels were then summed to produce the relative t-tubule area of the cell. This method was employed for the quantification of relative t-tubule area in sham and LVD cardiomyocytes and those subject to formamide-induced detubulation.

3.3.8 Statistical analysis

The relative t-tubule area for intact sham, intact failure, permeable sham and permeable failure and all groups in the detubulation studies was calculated by averaging the mean di-8-ANNEPS staining from a number of cells from each group. The relative cell area staining with di-8-ANNEPS was then taken to represent the relative t-tubule area of the cardiomyocytes.

A two-tailed unpaired Student's T-test was used to determine significant differences between groups ($p<0.05$) whilst a two-tailed paired Student's T-test was used to indicate statistical significance within groups ($p<0.05$).

ANOVA multiple comparison with Bonferroni post-test correction was used to determine significance between groups for confocal sections (Figure 3.8) and the relative t-tubule area along cell length in intact cells (Figure 3.14). Statistical significance was taken as $p<0.05$.

3.3.9 Immunocytochemistry of NCX

The principles behind the technique of immunocytochemistry are reviewed in General methods (2.3.2).

3.3.9.1 Solutions for immunocytochemistry

Solutions were freshly prepared for each experimental run. All concentrations are in (mmol/L) except where stated otherwise; pH correction was performed at room temperature (20-21 °C).

NaCl/Pi solution -NaCl (140), KCl (2.7), Na_2PO_4 (10), KH_2PO_4 (1.8); pH 7.3 with HCl.

High salt NaCl/Pi solution - as for NaCl/Pi solution but with NaCl (600).

3.3.9.2 Protocol for immunocytochemistry

Single cardiac myocytes were obtained in Krebs' and allowed to settle for 1 hour in the wells of 8-well, pre-flamed culture slides. Myocytes were then fixed for 30 min in NaCl/Pi solution containing 2% (w/v) paraformaldehyde. The solution was poured off each well and carefully washed three times in the order NaCl/Pi solution, high salt NaCl/Pi solution, NaCl/Pi solution. Cells were permeabilised for 10 min in NaCl/Pi solution containing 1% (w/v) Triton X-100 and blocked for 1-2 hr in NaCl/Pi solution containing 1% (w/v) BSA. The chambers were exposed to primary antibody (mouse monoclonal anti-NCX1, Novus Biologicals, 1:1000 in NaCl/Pi) overnight at 4 °C.

The following day, the antibody solution was poured off and each chamber was washed three times as before. The secondary antibody (donkey polyclonal (FITC-conjugated) anti-mouse IgG, Abcam Ltd., 1:500 in NaCl/Pi) was applied for 1 hr at room temperature with a foil covering to protect the fluorescent conjugate from degradation.

Cells were then washed three times and the plastic chamber divider was removed. Vectashield™ solution was flooded over the slide and a coverslip was applied such that no air bubbles were trapped beneath. This further minimised degradation of the fluorescent conjugate and helped to reduce photobleaching during imaging. Slides were sealed with lacquer and left to dry in the dark before imaging with the confocal microscope.

Slides were imaged as described in section 3.3.6 with the following alterations. A Kr/Ar laser excited the FITC-conjugate at 488 nm whilst emissions were collected at >518 nm. Zoom was adjusted such that the cell length spanned the entire field of view and the plane of focus was positioned through the centre of the cell. Data were acquired in image-scan mode at 2 ms per line (1024 x 1024) and the section was Kalman averaged (n=4).

3.4 Results

3.4.1 Dimensions of isolated cardiomyocytes

The mean lengths and widths of isolated left ventricular myocytes from sham and LVD rabbits are presented in Figure 3.3.

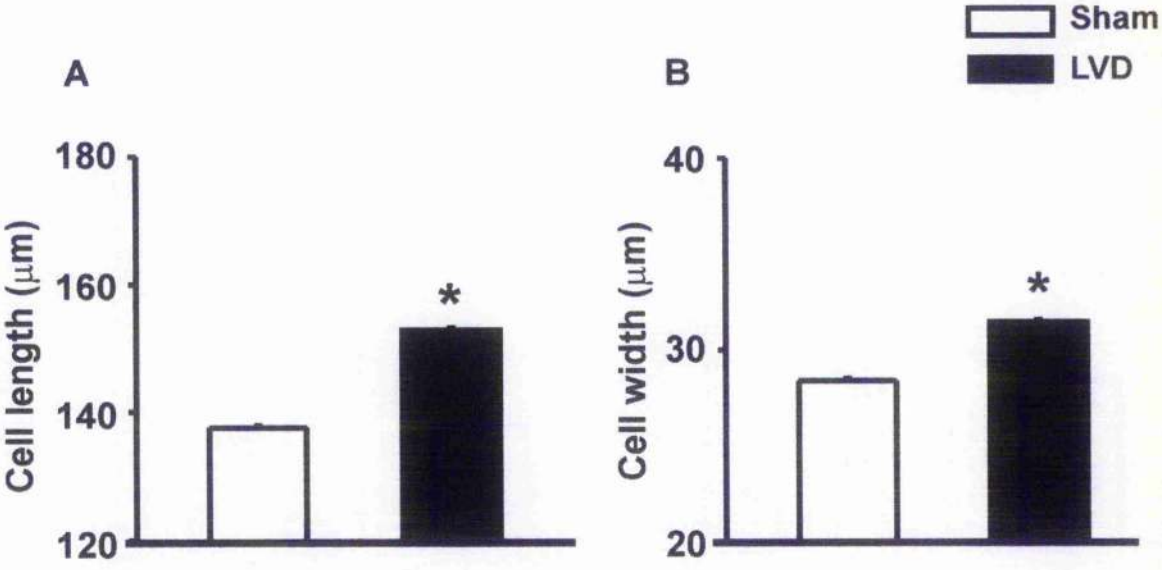

Figure 3.3 Dimensions of isolated sham and LVD cardiomyocytes.

A Average cell lengths of isolated sham and LVD rabbit ventricular myocytes. Mean data for sham and LVD myocytes were 137.6 ± 0.3 (n=702 cells) and 152.9 ± 0.4 (n=601 cells) respectively; * $p<0.001$.

B Average cell widths of isolated sham and LVD rabbit ventricular myocytes. Mean data for sham and LVD myocytes were 28.4 ± 0.1 and 31.4 ± 0.1 respectively; * $p<0.001$; n numbers as in A.

Evidence of cellular hypertrophy existed in the LVD group which manifested as increases in both cell length and width. LVD myocyte length was on average 111% that of the sham length whilst LVD myocyte width increased to 110% of sham width.

3.4.2 Staining of ventricular cardiomyocytes

The integrity of the sarcolemma was determined by applying the cell impermeant fluorophore Fura-FF. Figure 3.4 A(i) shows a transmission image of an isolated cardiomyocyte whilst Figure 3.4 A(ii) shows a confocal image of the same cell stained with Fura-FF. The black interior of the cell demonstrates that Fura-FF was excluded from the intracellular environment, indicating that it possessed an intact sarcolemma. Faint dots of Fura-FF represent t-tubule access of the dye. In permeable cardiomyocytes, the cell was indistinguishable from the background due to entry of Fura-FF into the intracellular space through the permeable sarcolemma.

Di-8-ANNEPS was used in order to visualise the t-tubule network within isolated cardiomyocytes. Figure 3.4 B(i) shows a confocal image of an isolated intact cardiomyocytes (central section) stained with di-8-ANNEPS with a magnified portion in Figure 3.4 B(ii). This enlarged image demonstrates that three main regions of the membrane are stained; these are the surface sarcolemma, the t-tubule network and the intercalated discs. Within the interior of this cell, the t-tubule network appears as a regular array of dots which correspond to t-tubules viewed in cross-section. In more superficial sections and towards the cell edges the t-tubules were visualised as lines perpendicular to the surface sarcolemma as well as dots.

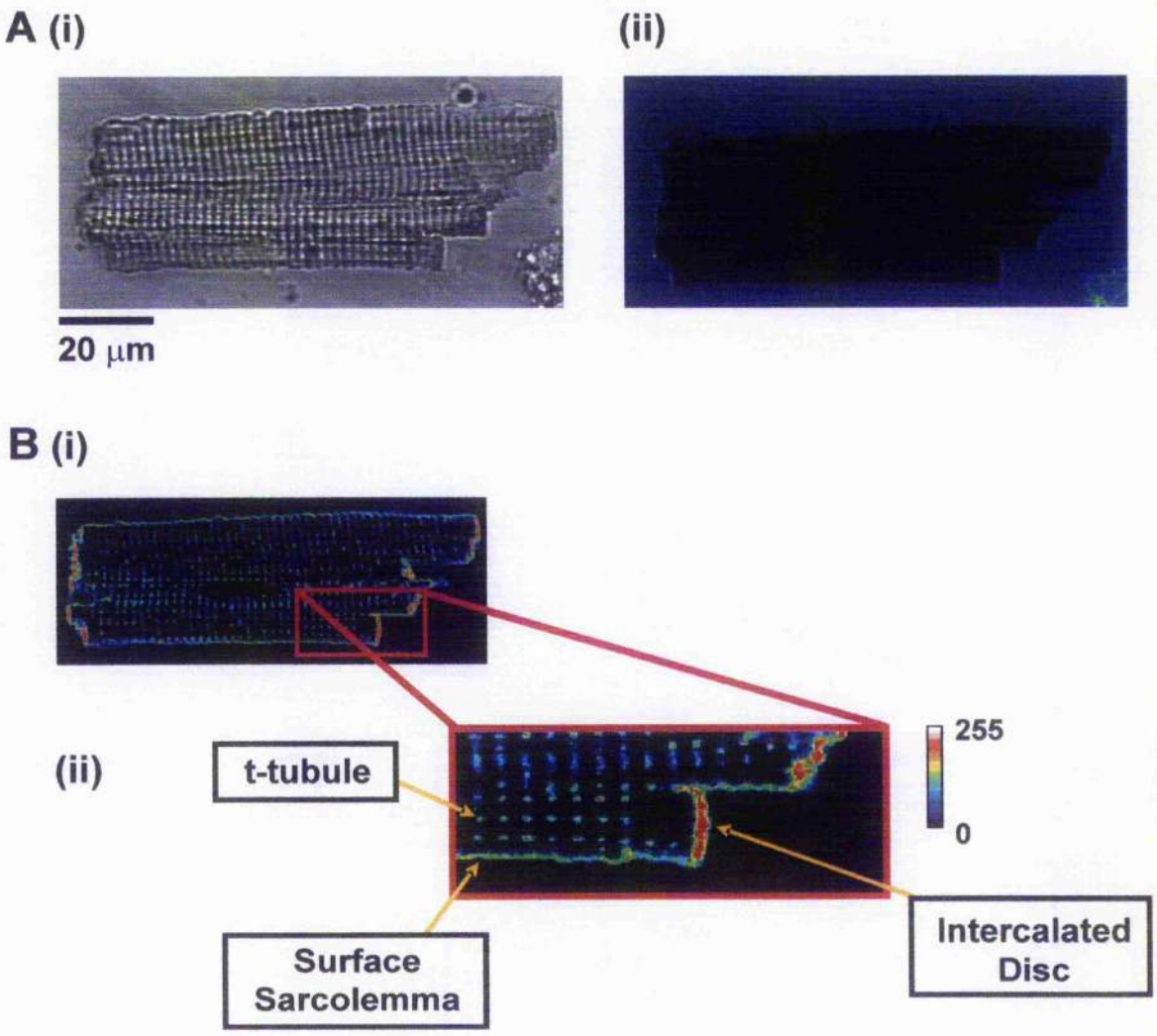

Figure 3.4 Assessment of membrane integrity in isolated cardiomyocytes and staining of membrane components using di-8-ANNEPS.

A (i) Transmission image of a single isolated left ventricular rabbit cardiomyocyte. **(ii)** Corresponding confocal image of the same cardiomyocyte stained with FURA FF; exclusion of dye (blue) from the cell interior indicates the membrane is intact.

B (i) Single isolated left ventricular rabbit cardiomyocyte stained using di-8-ANNEPS. **(ii)** Enlarged portion of (i) showing the individual membrane components stained as indicated by the labels; t-tubules appeared as punctate dots in deep sections (such as this) and lines perpendicular to the surface sarcolemma in more superficial sections.

3.4.3 Detubulation

3.4.3.1 Detubulation with mannitol

Figure 3.5 A(i) shows a confocal image of a control isolated cardiomyocyte stained with di-8-ANNEPS whilst Figure 3.5 A(ii) shows a myocyte which had undergone exposure to mannitol (300-400 mmol/L) prior to staining. The latter shows a high degree of intracellular staining of t-tubules remains. Quantification of the relative t-tubule area in control and mannitol-treated cells yielded results presented in Figure 3.5B.

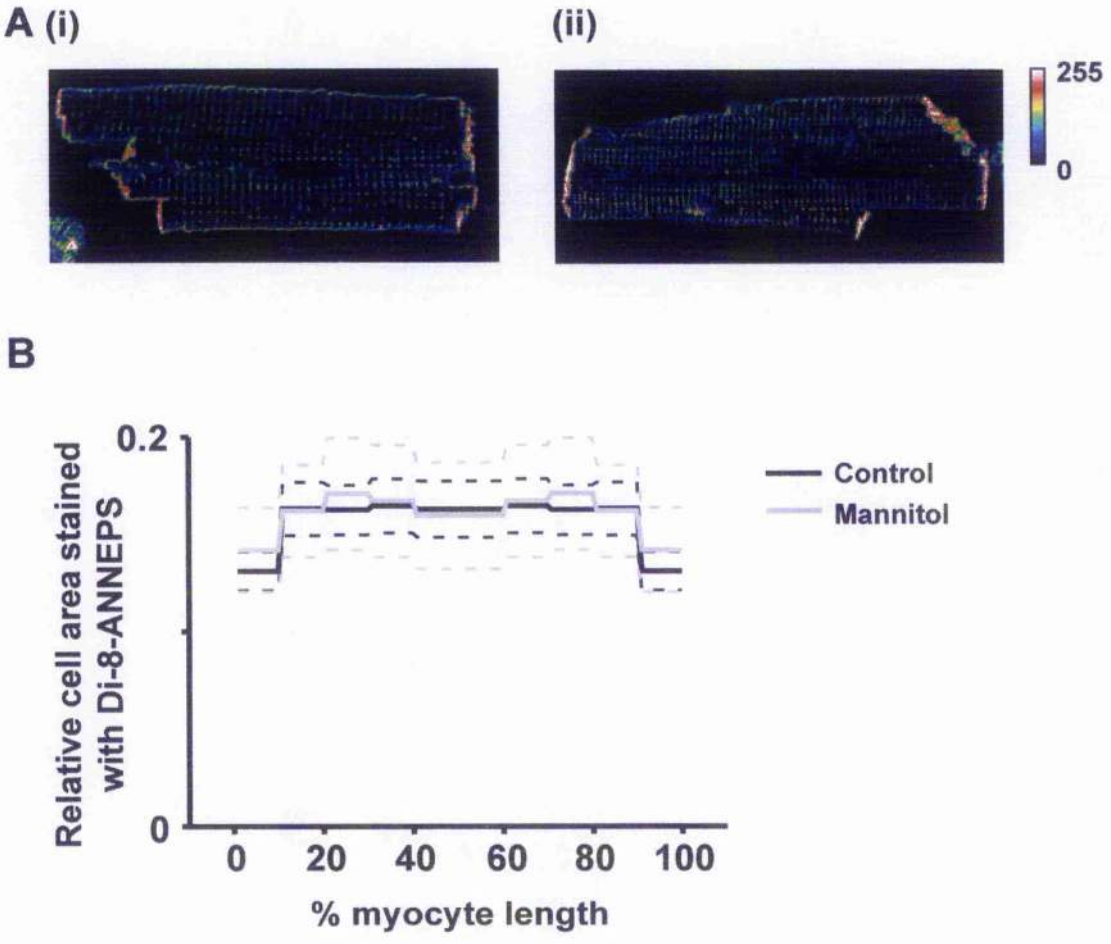

Figure 3.5 Detubulation using mannitol.

A (i) Confocal image of a control rabbit cardiomyocyte (intact) stained using di-8-ANNEPS. **(ii)** Cardiomyocyte previously exposed to an osmotic shock using mannitol (300-400 mmol/L) then stained as in (i).**B** Relative cell area stained with di-8-ANNEPS along the cell length of control (black; n=32 cells) and mannitol-treated cardiomyocytes (grey; n=8 cells). Dashed lines represent ± SEM values.

There was no significant difference in relative t-tubule area in sham cells *vs.* mannitol-treated cells (0.16 *vs.* 0.16), thereby demonstrating that mannitol was unsuccessful in detubulating isolated ventricular cardiomyocytes.

3.4.3.2 Detubulation with formamide

A well established protocol has been described for detubulation of rat cardiomyocytes using the agent formamide (Kawai *et al.*, 1999). This osmotic shock protocol was adapted in the present study and applied to isolated rabbit cardiomyocytes. Figure 3.6 A(i) on the next page shows a control cell stained with di-8-ANNEPS. An image of a cell previously treated with formamide is also presented in Figure 3.6 A(ii) with a magnified portion allowing the cell interior to be viewed in more detail. This image shows a clear absence of intracellular staining with di-8-ANNEPS following formamide exposure. The profile of relative t-tubule area for both control and formamide-treated cardiomyocytes, presented in Figure 3.6 B, shows there was a significant reduction in t-tubule area in formamide-treated cells compared to controls (0.04 *vs.* 0.157; $p<0.001$). Together, these results demonstrate that the formamide protocol used in this study produced a successful detubulation of isolated rabbit cardiomyocytes.

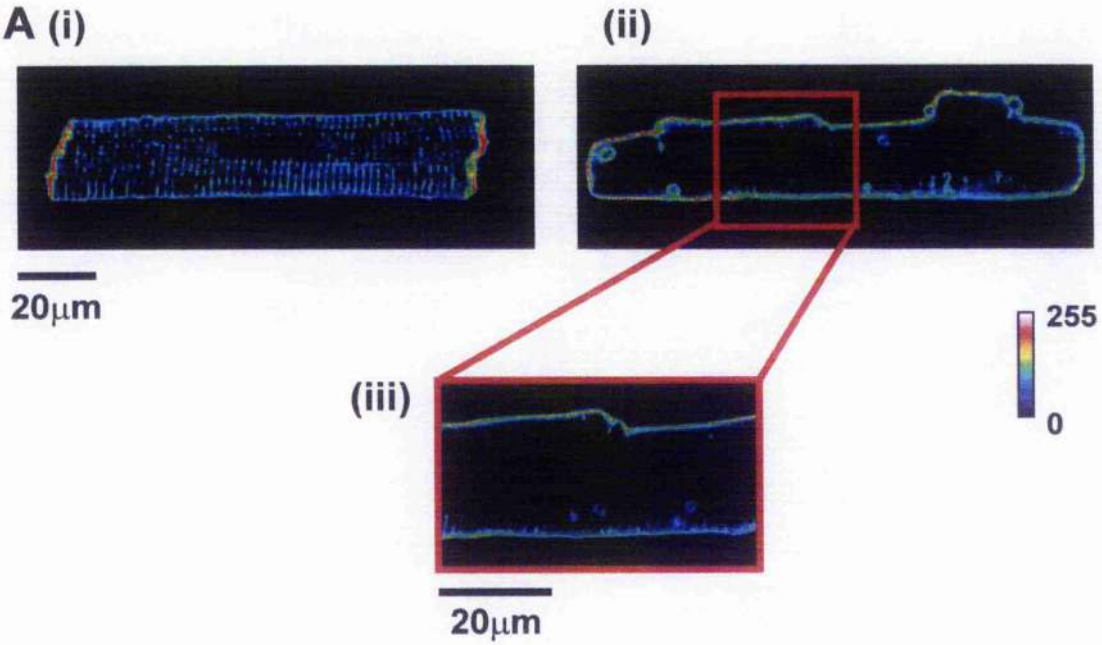

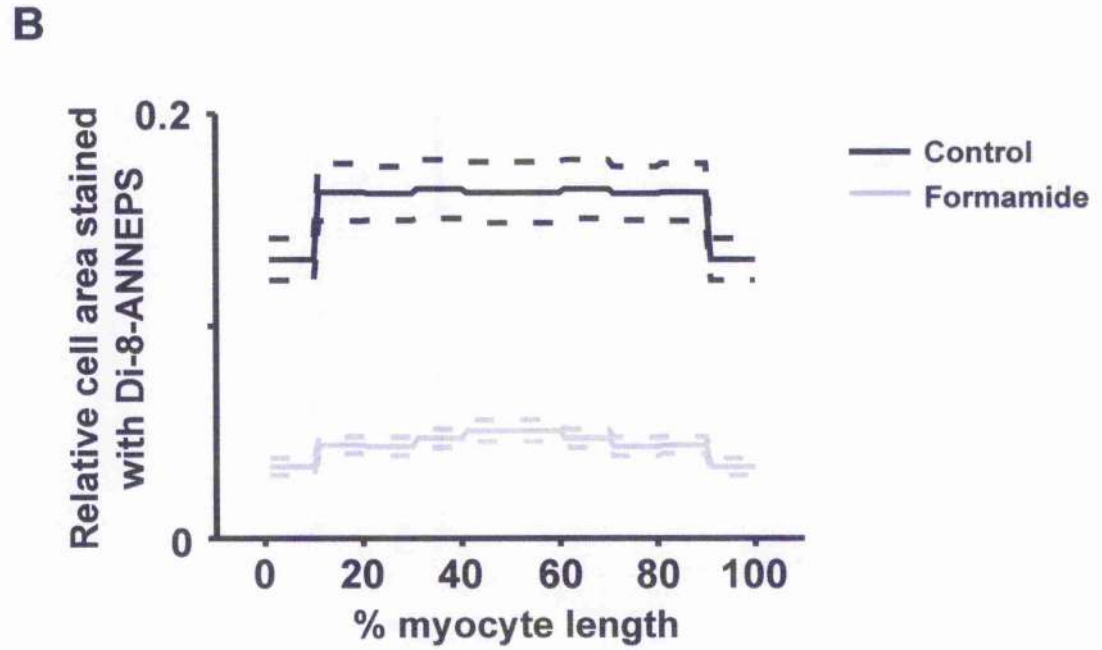

Figure 3.6 Detubulation using formamide.

A Confocal images of isolated intact cardiomyocytes stained with di-8-ANNEPS: **(i)** control and **(ii)** exposed to an osmotic shock using formamide (1.5 mol/L). **(iii)** Enlarged section of (ii) showing the extensive depletion of t-tubules following formamide treatment.

B Graph showing the relative cell area stained with di-8-ANNEPS along the cell length of intact left ventricular rabbit cardiomyocytes for control (black; n=32 cells) and formamide-treated cardiomyocytes (grey; n=16 cells). Dashed lines represent ± SEM values. Formamide-treated cells show a significant decrease in the relative t-tubule area *vs.* control indicating formamide produced a significant detubulation (0.04 *vs.* 0.157; $p<0.001$).

A level of variation in the degree of detubulation was seen in response to the formamide osmotic shock protocol. Figure 3.7 shows some of the patterns of detubulation obtained using this technique. A description of each pattern is provided in the figure legend.

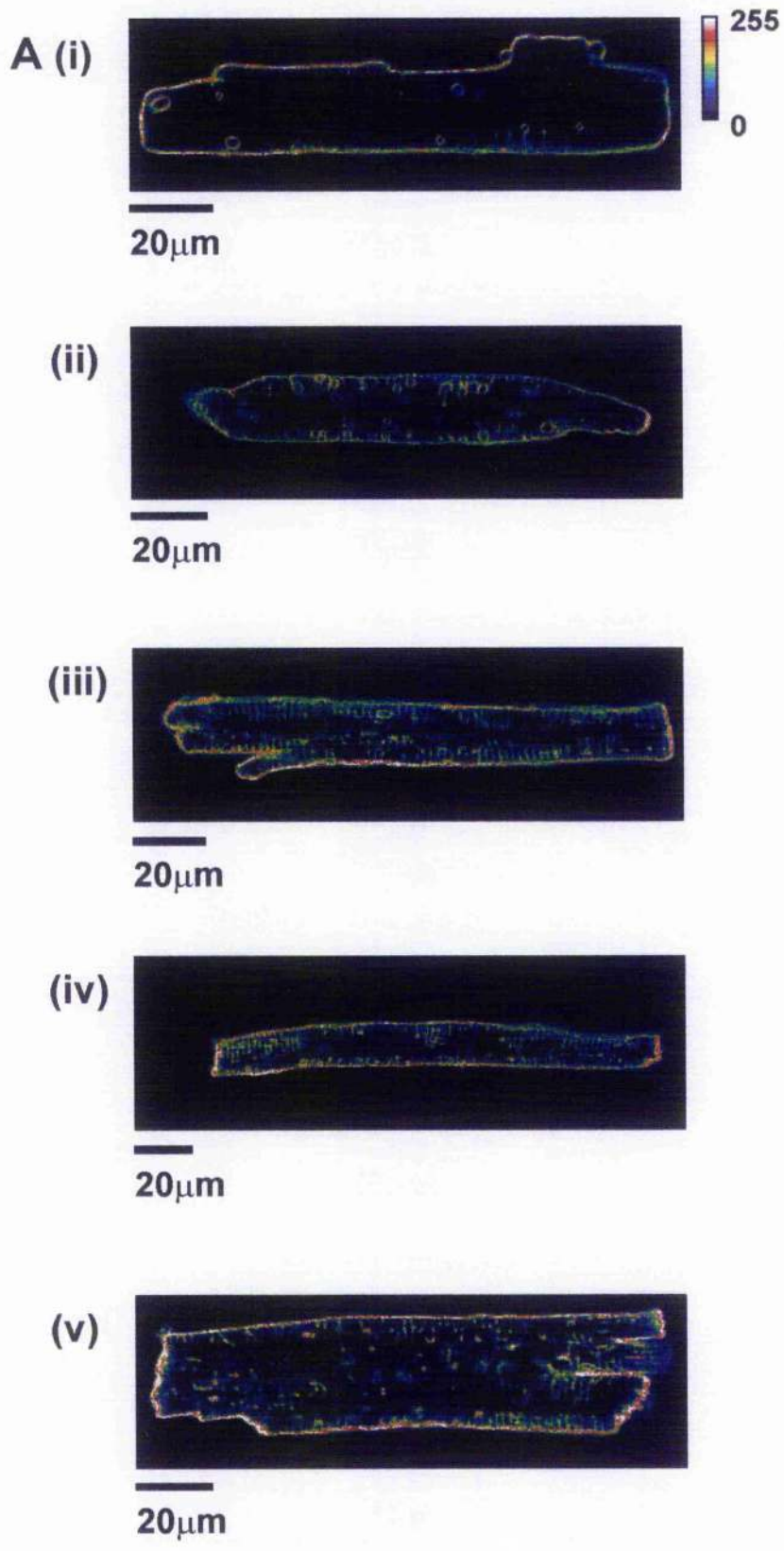

Figure 3.7 Patterns of detubulation following formamide treatment.

A (i) - (iii) Confocal sections showing varying patterns of formamide-induced detubulation in intact isolated left ventricular rabbit cardiomyocytes stained with di-8-ANNEPS.

(i) Cardiomyocyte with almost complete detubulation. **(ii)** Cardiomyocyte with almost complete detubulation but with the presence of small intracellular vacuoles. **(iii)** Cell showing detubulation mainly in the centre of the section; t-tubules remain apparent running perpendicular to the surface sarcolemma. **(iv)** Section showing a pattern similar to (i) with absence of t-tubules in the centre, however remaining t-tubules appear in clusters along the length of the periphery. **(v)** Cell showing much more uniform detubulation throughout the section. Remaining t-tubules are regularly spaced.

As a result of this variation in t-tubule distribution patterns, the relative t-tubule area was examined for the individual sections which had been analysed for each cell. This was performed for the five sections above and five sections below the median section for each cell. The aim of this was to determine if there was a relationship between the relative t-tubule area and depth of section. The results obtained are presented below in Figure 3.8. The plot shows that there was no preferential loss of t-tubules in individual sections analysed in formamide-treated cells compared to controls. No significant differences in relative t-tubule area existed within the sections in each group ($p>0.05$).

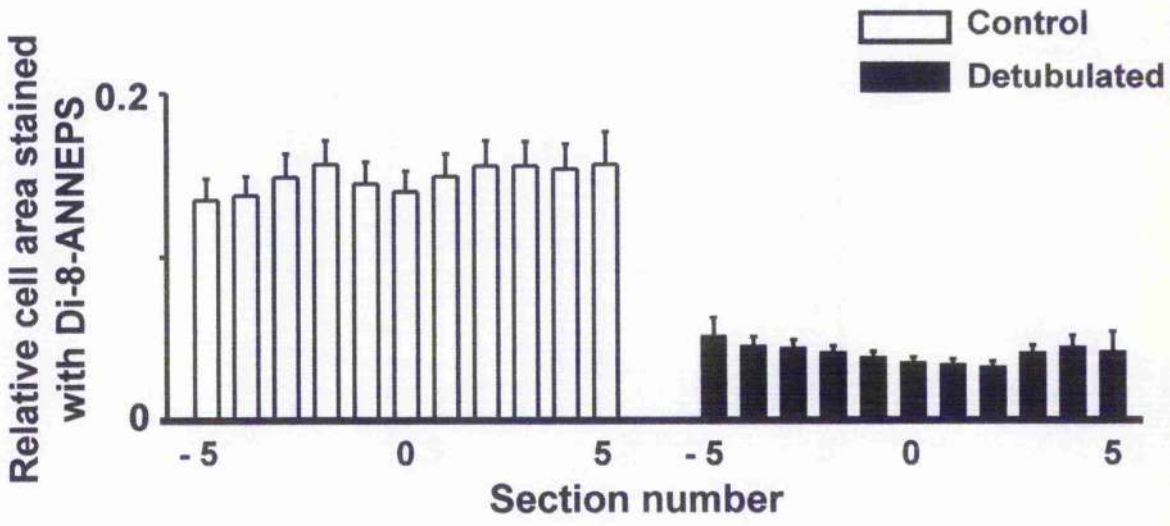

Figure 3.8 Relative t-tubule area in each confocal section analysed (z-axis).

Graph showing relative t-tubule area in each confocal section in control (white; n=32 cells) and detubulated (black; n=16 cells) isolated intact cardiomyocytes. Sections that were five above and below the central section analysed were examined. The bar corresponding to the median section in each group is denoted 0.

Relative t-tubule area was assessed in permeabilised cells detubulated with formamide. This aimed to establish that the depleted t-tubules were still capable of being detected within the cell using the permeabilisation and di-8-ANNEPS technique. This is expected as the mechanism of action of formamide-induced detubulation involves pinching off the t-tubule mouth and subsequent resealing within the cell (see 3.1.4.3). The results are presented below in Figure 3.9. No major differences existed between relative t-tubule area in permeabilised control and detubulated cardiomyocytes indicating that the protocol was capable of detecting internalised t-tubules.

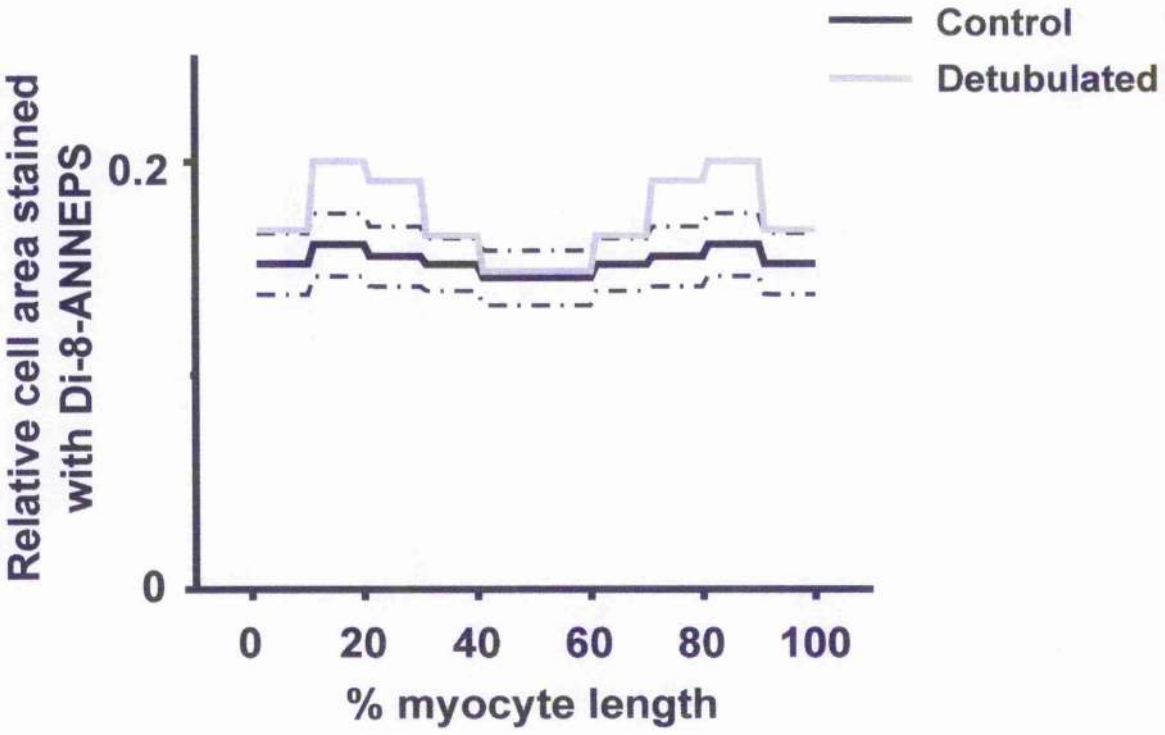

Figure 3.9 T-tubule profile in permeabilised control and detubulated cardiomyocytes.

Graph showing the relative cell area stained with di-8-ANNEPS along the cell length of permeabilised left ventricular rabbit cardiomyocytes in control (black; n=28 cells) and formamide-treated cardiomyocytes (grey; n=2 cells). Dashed lines represent ± SEM values (control only). Formamide-treated cells show no major difference in the relative t-tubule area *vs.* control, indicating that t-tubules were still present following formamide exposure. The general distribution of t-tubule staining along the cell length was similar in both groups.

3.4.4 *T-tubule area in intact cardiomyocytes*

The relative t-tubule area was assessed in isolated intact cells from sham and LVD rabbits. Example images of cells stained with di-8-ANNEPS are presented in Figure 3.10 A(i) and (ii). Di-8-ANNEPS staining of sham myocytes revealed a regular array of intracellular staining. This became more disorganised in LVD cells with the appearance of gaps in the stain predominantly towards the cell ends. Corresponding binary images produced by the analysis algorithm accompany in Figure 3.10 B(i) and (ii). The analysis was performed for the 10-15 central sections of the cell which spanned the full length; the t-tubule area in each section was then summed and averaged for the cell.

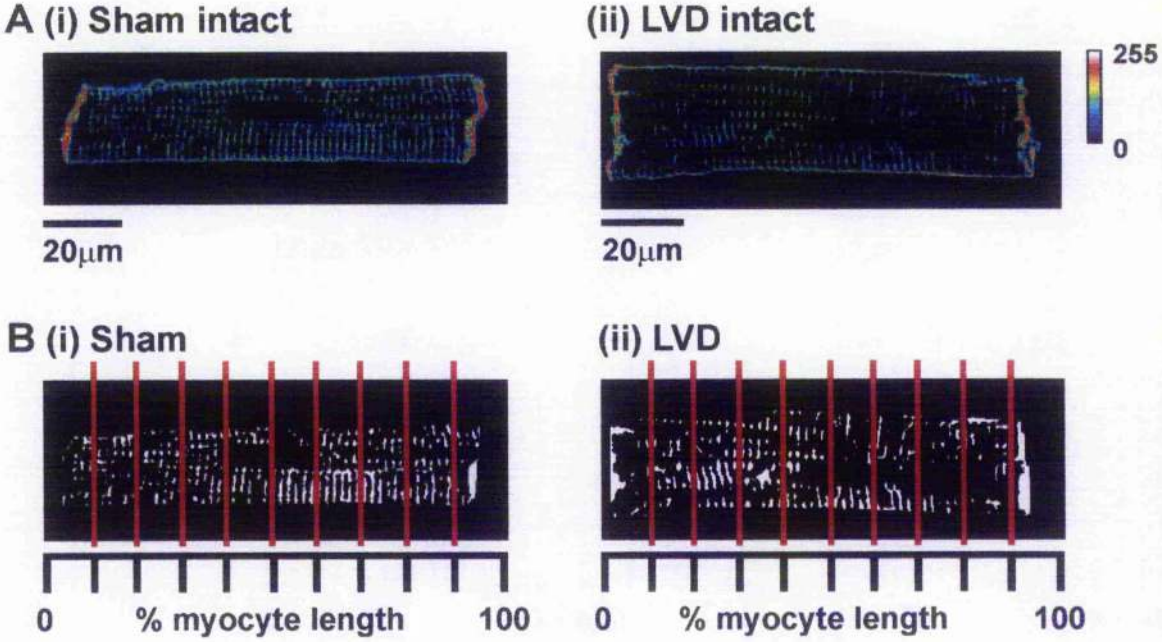

Figure 3.10 Di-8-ANNEPS staining in intact ventricular cardiomyocytes.

A Examples of fluorescence di-8-ANNEPS images taken from intact **(i)** sham and **(ii)** LVD ventricular cardiomyocytes.

B Corresponding binary images produced from these same cells; red lines denote the division of the cell into ten sections for the purposes of analysis.

3.4.5 T-tubule area in permeable cardiomyocytes

Relative t-tubule area was also assessed in the sham and LVD groups in cells which had had their surface membranes permeabilised by exposure to β-escin. This allowed access of di-8-ANNEPS into the cell interior thus enabling any t-tubules which did not have access to the extracellular space to become labelled and hence visualised for analysis. Example images of permeable sham and LVD isolated cardiomyocytes are shown in Figure 3.11 A(i) and (ii) respectively; the corresponding binary images are presented in Figure 3.11 B(i) and (ii). Additional nuclear membrane staining was visible in the permeable group; this was considered to be of an approximately consistent amount between all permeable cells and mean t-tubule area was calculated as for intact cells.

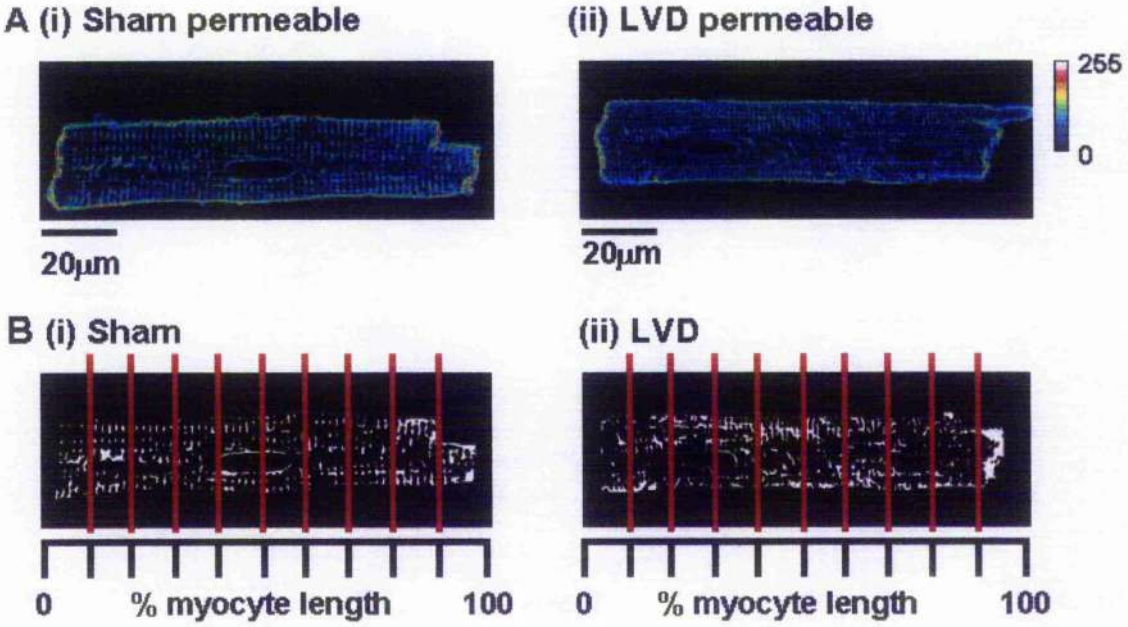

Figure 3.11 Di-8-ANNEPS staining in permeable ventricular cardiomyocytes.

A Examples of fluorescence di-8-ANNEPS images taken from permeabilised **(i)** sham and **(ii)** LVD ventricular cardiomyocytes. Additional nuclear membrane staining is revealed due to intracellular access of di-8-ANNEPS.

B Corresponding binary images produced from these same cells; red lines denote the division of the cell into ten sections for the purposes of analysis.

3.4.6 Assessment of nuclear staining

A degree of nuclear membrane staining by di-8-ANNEPS was observed in many of the permeable cells whilst in intact cells the nucleus was visible as an area devoid of staining. In order to assess whether the nuclear region may be significantly contributing to t-tubule area, a subset of intact and permeable LVD cells were analysed with and without exclusion of the nuclear region. The relative t-tubule areas for intact and permeable cells are displayed below in Figure 3.12.

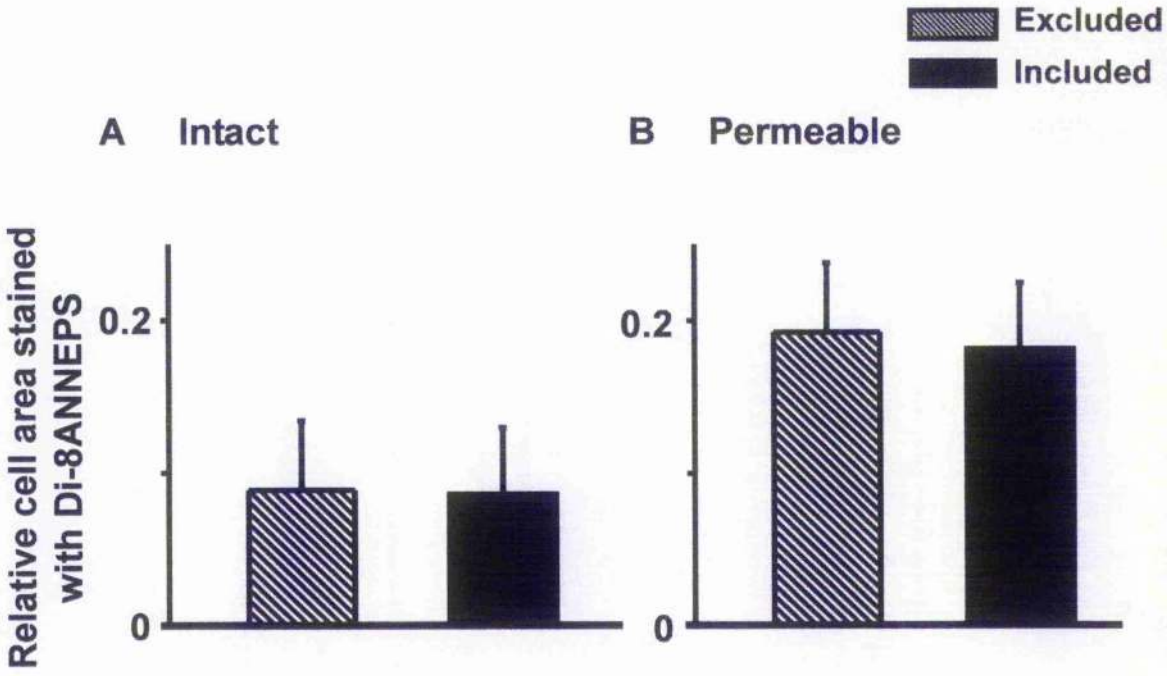

Figure 3.12 Contribution of the nuclear region to relative t-tubule area.

Relative cell area stained with di-8-ANNEPS (t-tubule area) in LVD **A** intact cells analysed with and without nuclear exclusion (n=6 cells) **B** permeable cells analysed with and without nuclear exclusion (n=6 cells).

Comparison of the relative t-tubule area with and without exclusion of the nuclear region revealed no significant difference in either intact or permeable groups. All subsequent analysis of t-tubule area therefore included the nuclear region.

3.4.7 Relative t-tubule area in isolated cardiomyocytes

The relative t-tubule area was determined for each group studied. Findings revealed a significant decrease in relative t-tubule area in intact LVD cardiomyocytes compared to intact sham cardiomyocytes (0.12 ± 0.008 *vs.* 0.16 ± 0.009; $p<0.05$) (Figure 3.13). No significant differences were detected between the two permeable groups.

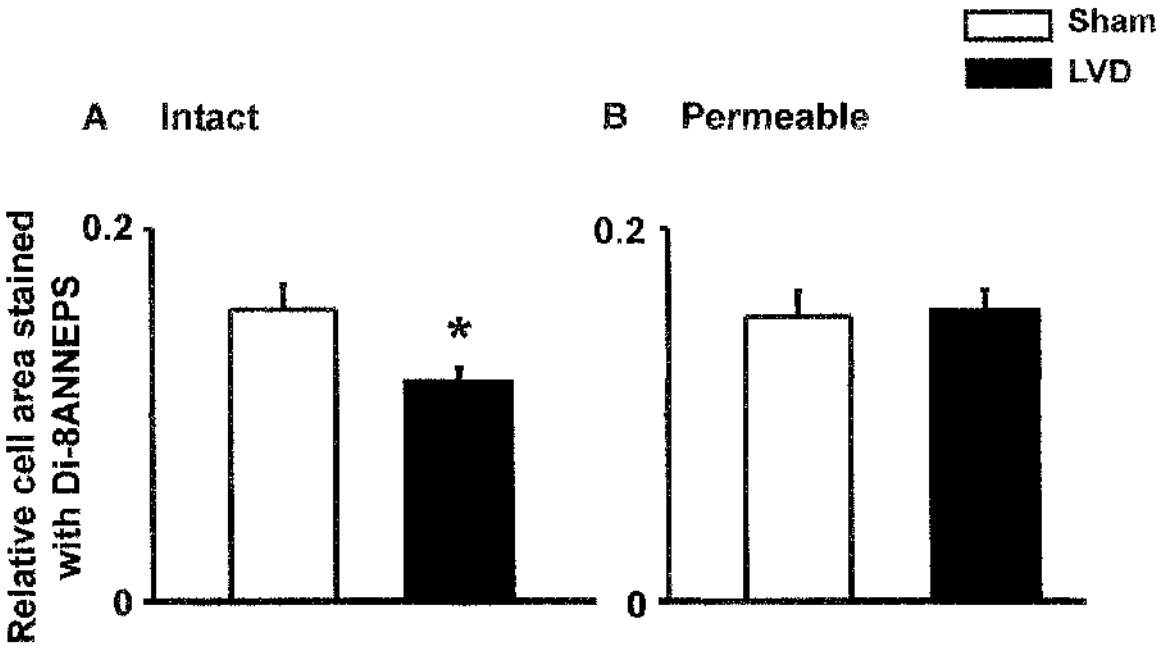

Figure 3.13 Relative t-tubule area in sham and LVD isolated ventricular cardiomyocytes.

Relative cell area stained with di-8-ANNEPS (t-tubule area) in A intact sham (n=32 cells) and LVD (n=49 cells) cardiomyocytes and B permeable sham (n=28 cells) and LVD (n=45 cells) cardiomyocytes. Relative t-tubule area was significantly decreased in intact LVD cardiomyocytes compared to intact sham cardiomyocytes (0.12 *vs.* 0.16; * $p<0.05$). No significant differences existed between the relative t-tubule areas in permeable cardiomyocytes.

3.4.8 T-tubule distribution

A profile of the mean t-tubule staining along the x-axis of cardiomyocytes was produced for intact and permeabilised cells in both sham and LVD groups (Figure 3.14). The distribution of t-tubule staining along the cell length was most markedly different in the intact cells. This presented as the lowest value at the cell ends in both sham and LVD cells and then, in the LVD group, as stepped

increases towards the cell centre. Permeable cells from sham and LVD both exhibited a similar pattern with a generally more uniform distribution of t-tubules along the cell length and cell ends.

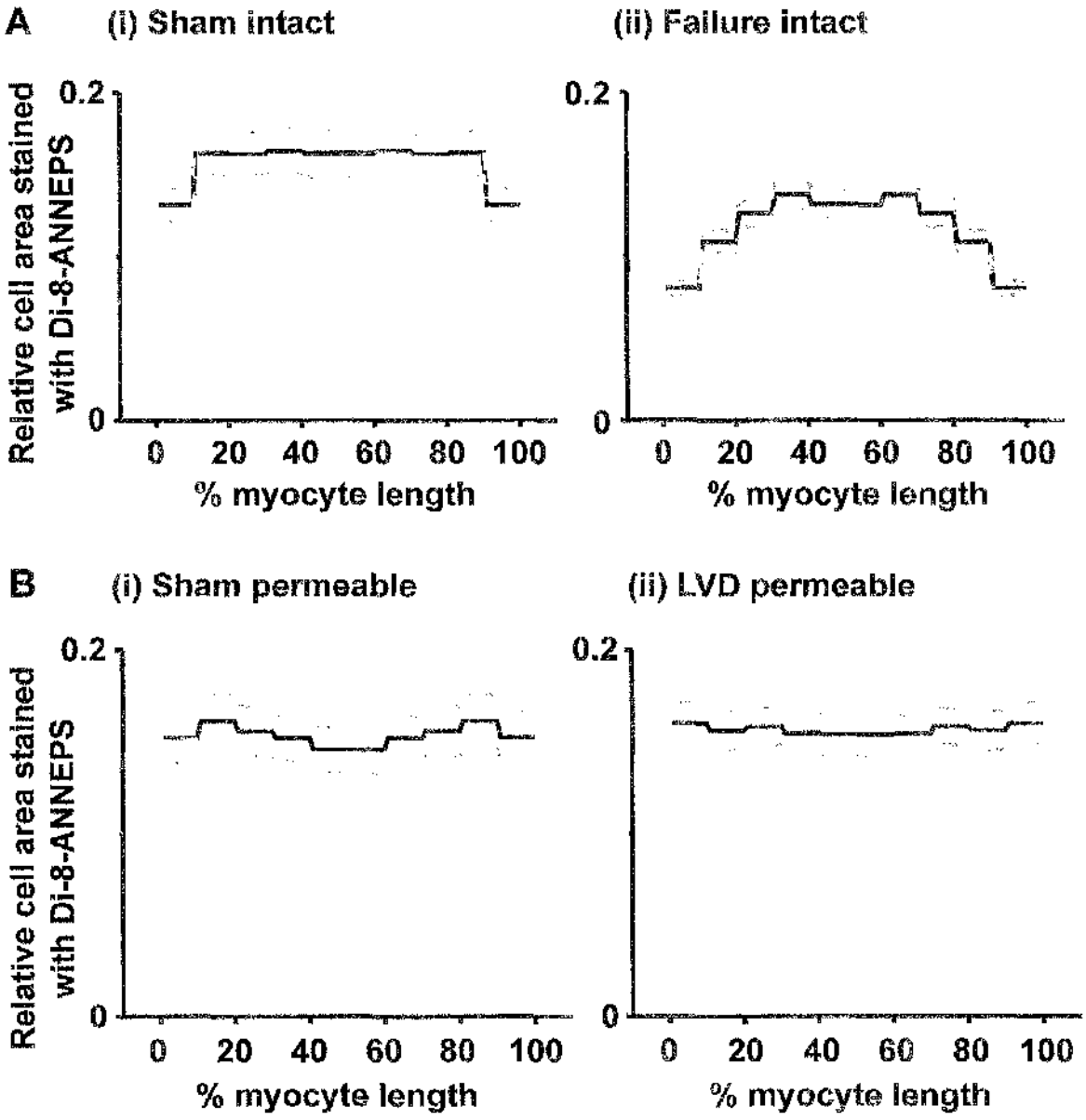

Figure 3.14 Profile of t-tubule staining along the cardiomyocyte length.

A Profile of t-tubule staining along the length of intact (i) sham and (ii) LVD ventricular cardiomyocytes (n=32 and 49 cells respectively); dashed grey lines represent ± SEM values. B Profile as in A (i) and (ii) but for cells permeabilised using β-escin (n=28 and 45 cells respectively). No major differences in the distribution of t-tubule staining along the length of both permeable groups are apparent.

In order to explore further these differences in t-tubule distribution in intact cells, the relative t-tubule area in sections 1-10, 10-20 and 40-50 of the percentage cell length were examined. These represented the cell end, the length immediately adjacent to the cell end and cell centre respectively; results for sham and LVD are presented in Figure 3.15. There were no significant differences in relative t-tubule area for the three cell lengths studied in intact sham cells. In the LVD intact group there was a significant decrease in relative cell area at the cell ends (1-10) when compared to the cell centre (40-50) ($p<0.001$).

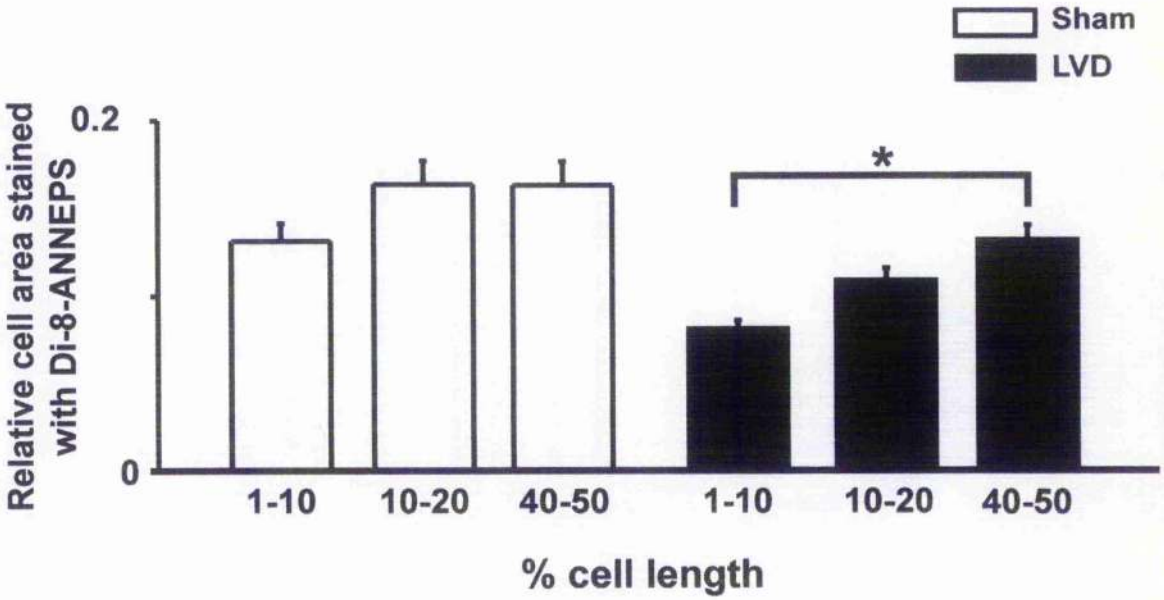

Figure 3.15 Examination of relative t-tubule area along the cell length in intact cardiomyocytes.

Graph of relative t-tubule area in sham (white; n=32 cells) and LVD (black; n=49 cells) intact isolated cardiomyocytes for 1-10, 10-20 and 40-50 percent of the cell length. LVD intact cells showed a significant decrease in relative t-tubule area at the cell ends (1-10) compared to the cell centre (40-50), * $p<0.001$; no significant differences were detected in the sham group.

3.4.9 NCX distribution

The pattern of NCX distribution was determined in isolated ventricular myocytes from sham and LVD hearts using an immunocytochemical staining technique. Images obtained from sham and LVD cells are presented in Figure 3.16.

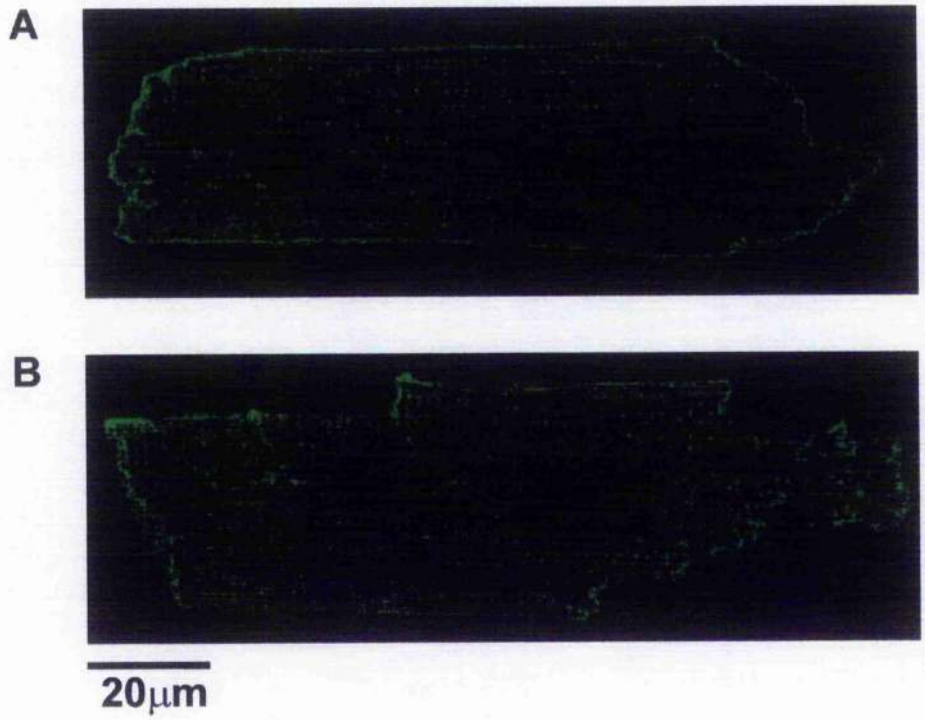

Figure 3.16 NCX distribution pattern.

Immunocytochemical staining for NCX protein in **A** sham and **B** LVD isolated ventricular rabbit myocytes.

A broadly similar pattern of NCX distribution was obtained in sham and LVD cardiomyocytes. NCX staining was apparent in the surface sarcolemma, the intercalated disc region and the t-tubule network.

In order to confirm the presence of NCX in the t-tubule network, a fast Fourier Transform analysis was applied to the images in Figure 3.16. This was performed using a programme created by Prof. Godfrey Smith in IDL by a method similar to that of Brette *et al.* (2002). The analysis was also applied to a di-8-ANNEPS stained ventricular myocyte as a reference frequency profile for the t-tubule network. The fluorescence frequency profiles obtained are shown in Figure 3.17 on the following page.

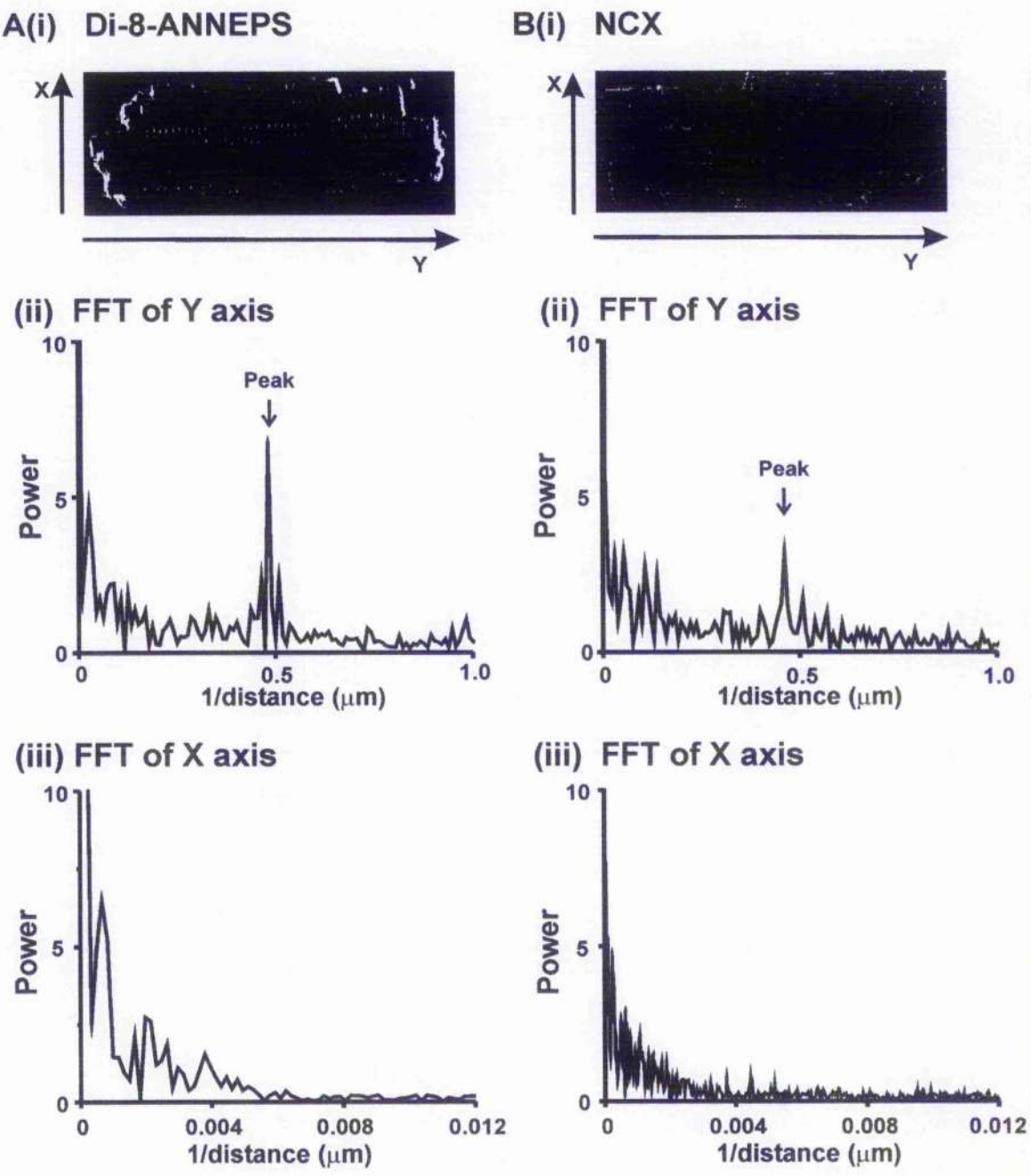

Figure 3.17 Fluorescence frequency profiles for di-8-ANNEPS and NCX staining.

A(i) Confocal image of an LVD ventricular myocyte labelled with di-8-ANNEPS; X and Y axes are labelled, **(ii)** fast Fourier Transform and resulting frequency profile of fluorescence along the Y axis and **(iii)** fast Fourier Transform and resulting frequency profile of fluorescence along the X axis.

B (i) Confocal image of an LVD ventricular myocyte labelled immunocytochemically for NCX; X and Y axes are labelled, **(ii)** and **(iii)** as in A.

The Fourier transform of the average fluorescence signal along the Y axis of a di-8-ANNEPS stained LVD ventricular myocyte exhibited one clear peak at a frequency of approximately 2 μm corresponding to the regularly spaced t-tubules. Fast Fourier transform of the NCX immunocytochemically labelled LVD myocyte also revealed a peak fluorescence frequency at approximately 2 μm. A similar plot was obtained for the NCX labelled sham myocyte shown in Figure 3.16 (data not shown). No periodicity was evident in the profile along the X axis in any of the cells under study. These results support a localisation of NCX in the t-tubule network of left ventricular myocytes from the rabbit. Furthermore, they confirm that there is no gross change in the distribution of NCX protein in sham and LVD ventricular myocytes.

3.5 Discussion

This chapter has quantified the relative cell area occupied by the t-tubule network (relative t-tubule area) in isolated ventricular cardiomyocytes from rabbits with and without LVD. The t-tubule network was visualised using the membrane selective fluorophore di-8-ANNEPS and confocal microscopy in both intact and permeabilised cardiomyocytes. Subsequent quantitative analysis revealed a significant decrease in relative t-tubule area in intact LVD cardiomyocytes. LVD cardiomyocytes were also shown to exhibit a significant degree of cellular hypertrophy versus sham. In addition, a protocol for detubulation was adapted and applied to intact cardiomyocytes to deplete the t-tubule network thus establishing a proof of principle for the technique in detecting internalised t-tubules. This study is the first to produce successful detubulation of the t-tubule network in isolated rabbit ventricular myocytes.

3.5.1 Visualisation and quantification of the t-tubule network

Di-8-ANNEPS is a lipophilic dye which remains in the outer leaflet of the plasma membrane. Consequently, it does not cross the membrane and incubation with intact isolated cardiomyocytes leads to staining of all membrane in contact with the extracellular space. As the lumen of the t-tubule is continuous with the extracellular space, di-8-ANNEPS can access through the t-tubule mouth and successfully label all membrane contained within the tubule.

Application of the di-8-ANNEPS protocol to control intact ventricular myocytes stained the surface sarcolemma, the intercalated disc and intracellular structures. The highest intensity of signal was detected at the intercalated disc which is to be expected due to the high degree of membrane in this region (Page, 1978; Kieval *et al.*, 1992). The intracellular staining was present as a regular array of dots, corresponding to t-tubules viewed in cross section, and lines, corresponding to t-tubules in the focal plane which ran perpendicular to the surface membrane. This pattern of staining is consistent with all previous reports of t-tubule distribution in ventricular myocytes (Shacklock *et al.*, 1995; Soeller & Cannell, 1999; He *et al.*, 2001; Balijepalli *et al.*, 2003). Di-8-ANNEPS

staining appeared more disorganised in LVD ventricular myocytes and was visibly reduced towards the cell ends.

The relative t-tubule area was assessed by quantifying the di-8-ANNEPS staining using a specifically designed algorithm. The cardiac myocyte is reported to be approximately 20 μm thick (Bers, 2001) therefore approximately 30-40 sections (at 0.5 μm) in the z-stacks performed in the present study would be obtained. From these, only the most central 10-15 sections which encompassed the full cell length were analysed and therefore each section was at least 10 μm from the cell top or bottom. As a consequence, these sections were of reproducible dimensions and the intracellular staining was consistently attributable to only the t-tubule network from image to image and not to any interfering surface sarcolemma from above or below (Kieval *et al.*, 1992). This ensured that an accurate and robust analysis method was performed in order to limit artefactual results and variability.

3.5.2 Hypertrophy of failing isolated cardiomyocytes

Measurement of the dimensions of isolated left ventricular myocytes demonstrated a significant increase in both cell length and width in LVD myocytes when compared to sham. The presence of significant cellular hypertrophy in the LVD ventricular myocytes is characteristic of the development of heart failure in these animals 8 weeks post-operatively (Pye & Cobbe, 1996).

In the failing heart, such as that produced in our coronary ligation model of LVD, cardiac performance is decreased (due to myocyte loss and/or mechanical stress) and is therefore unable to maintain the cardiac output. Initially, this loss or stress is compensated for by the heart increasing stroke volume through two main routes (i) an increase in end-diastolic pressure leading to stretching of the myocardium and higher contractile energy (via Starling's law of the heart) and (ii) by an increase in the level of β-adrenergic stimulation. Both of these will lead to a positive inotropic response (Levick, 2003). In addition, these changes in haemodynamic load and circulating hormone levels also act as pathophysiological stimuli for hypertrophy (Bers, 2001).

Cardiomyocytes are terminally differentiated and are thus incapable of cell division to replace functional cells lost through necrosis/apoptosis. As a result, the surviving cardiomyocytes respond by increasing in size in order to generate more contractile force in the face of falling cardiac output. Commonly, hypertrophy is classified as either being (i) compensated, where the hypertrophy enables the heart to meet the demands of the body or (ii) decompensated, where the hypertrophy is insufficient to overcome the compromised function of the heart and the demands of the body cannot be met; this then progresses onto the syndrome of heart failure. The specific way in which the dimensions of the cardiomyocyte and heart itself are physically remodelled has led to two hypertrophy classifications. Concentric remodelling occurs when cardiomyocyte width is greatly increased but little alteration in length occurs. At the whole heart level, this leads to a thickening of the left ventricle wall with no dilation of the chamber. On the other hand, eccentric remodelling involves a large increase in cardiomyocyte length which produces a dilation of the chamber. The hypertrophy in our model is best described as compensated and a combination of concentric and eccentric. Discussion of the mechanisms of hypertrophy is presented in 3.5.7.

3.5.3 Detubulation of isolated rabbit cardiomyocytes

This is the first study to report successful detubulation of isolated rabbit ventricular myocytes using the membrane permeable agent formamide. The method employed to detubulated ventricular myocytes in the present chapter was a modification of a well characterised protocol first described by Kawai *et al.*, (1999). The modification involved the inclusion of BDM in order to prevent cellular contraction and through this a significant detubulation of isolated rabbit ventricular myocytes was produced. Subsequent permeabilisation of these cells revealed no apparent difference between detubulated and control myocytes. This indicated that t-tubules had sealed off within the cell interior in response to formamide exposure in keeping with previous findings in the rat (Brette *et al.*, 2002). A level of variation in the extent of detubulation occurred which is also consistent with previous reports (approximately 20% of rat cells are not detubulated by formamide) (Brette *et al.*, 2002). The fact that the same staining and analysis steps as employed in the study of sham and LVD myocytes

were capable of detecting a loss of t-tubules provided a proof of principle for the mechanism of loss of t-tubules in LVD.

3.5.4 T-tubule network in sham cardiomyocytes

Quantification of the relative t-tubule area in sham intact and permeabilised ventricular myocytes showed no significant difference. Examination of the distribution profiles of relative t-tubule area along the length of intact myocytes revealed a greater abundance of t-tubules in the cell centre compared with the edges. In intact sham myocytes, relative t-tubule area decreased from approximately 16% in the cell centre to 13% towards the cell ends; this pattern was also observed by Quinn *et al.* (2003). However, the distribution profile for permeable sham cells demonstrated a uniform t-tubule area along the length of the cell indicating that t-tubules are present at the cell ends. The ends of each apposing cardiomyocyte interdigitate to form the intercalated disc which is densely populated with structural proteins involved in the mechanical and electrical connection between neighbouring cells. Decreased t-tubule area towards the cell ends in the intact cell may reflect an absence of t-tubules due to the space limitations in this structurally unique region of the cardiomyocyte. Consequently, these t-tubules would limit the access of di-8-ANNEPS to their lumens in the intact cell. This obstruction would be overcome once the cell was permeabilised as di-8-ANNEPS would have access to the tubule membrane via the cytoplasm. There is a concern that di-8-ANNEPS may be labelling a substantial proportion of intracellular membrane in the permeable cell (as was evident for the nuclear membrane). This does not seem to be significant as the relative t-tubule areas in intact and permeable sham cells are approximately equal. In addition, the short exposure time to di-8-ANNEPS (5 min) would be expected to limit labelling of intracellular structures.

3.5.5 T-tubule network in failing cardiomyocytes

Quantification of the relative t-tubule area in intact rabbit ventricular myocytes revealed an overall 25% decrease in the LVD group compared to sham. Three main hypotheses exist to explain the mechanism behind this reduction in intact LVD cardiomyocytes. Firstly, the t-tubules in LVD cells may become narrowed,

analogous to the situation proposed at the ends of sham intact cells (see above 3.5.4); this narrowing of t-tubule lumen would limit di-8-ANNEPS access in the intact cell. Secondly, the t-tubules may simply pinch off from the surface sarcolemma, become internalised and reseal within the cell to form tubules isolated from the extracellular space. In the third scenario, the t-tubules again become internalised within the cardiomyocyte but are then degraded leading to a true loss of t-tubules from the cell. In order to distinguish between the latter two mechanisms of t-tubule loss in LVD, the cell permeabilisation technique with β-escin was utilised.

On permeabilisation of sham and LVD groups, the 25% difference in relative t-tubule area was negated and there was no significant difference between LVD and sham. The return of relative t-tubule area to control values upon permeabilisation suggests that the loss of t-tubules in this model of heart failure is a result of t-tubules pinching off from the surface sarcolemma and resealing within the cardiomyocyte. This mechanism is in contradiction with a similar study which detected a comparable loss (24%) of t-tubules in a canine tachycardia induced heart failure model (Balijepalli *et al.*, 2003). In this model the mechanism of loss of t-tubules was attributed to a true depletion of the internalised tubules as evidenced by the loss of membrane associated proteins assayed using both confocal microscopy and biochemical membrane fractionation and immunolabeling techniques. Precisely how the t-tubules were degraded once internalised was not alluded to in the paper (Balijepalli *et al.*, 2003).

Examination of the distribution profile of relative t-tubule area along the length of intact LVD myocytes shows that t-tubules are lost from the cell in a step-wise fashion from the cell centre towards the cell end where the value is lowest. Comparison of the relative t-tubule area at the cell ends (1-10%) and cell centre (40-50%) demonstrated that this loss was significant ($p<0.05$). This pattern of pronounced t-tubule loss from the cell ends is in agreement with findings in canine tachycardia-induced failing cardiomyocytes (Balijepalli *et al.*, 2003). In the current study, the 25% decrease in the intact LVD group compared to sham is much lower than the 40% reported previously by our group from the same model (Quinn *et al.*, 2003). The discrepancy is most likely due to differences in the

operation of analysis techniques. Although the t-tubule quantification by Quinn and colleagues used the same analysis method as here, areas of the cell interior thought not to be due to t-tubules were discarded from the image at the discretion of the user and were not included in the intracellular pixel counting procedure. The analysis method employed in the present chapter included all intracellular staining for each cell and there was no subjective decision made as to what represented "t-tubule" and what did not. In addition, cells in this study were randomised and analysis was performed blind such that the user was unaware of which group the cell belonged to and the number of cells included in this study was higher. The disagreement in the mechanism of t-tubule network loss with the work of Balijepalli *et al.*, (2003) seems most probably due to the species differences (rabbit *vs.* dog) and method of induction/degree of heart failure in each study. Although Satoh and colleagues (1996) did not directly study canine ventricular myocytes, they did define that there was variation in the number and/or size of t-tubules between species. This species variation may also extend into how the t-tubule network is maintained and/or depleted in the pathological setting. It may be unwarranted, therefore, to compare these two studies in order to try to define a common mechanism of t-tubule loss in heart failure.

As mentioned previously, (3.5.4) the increase in relative t-tubule area on permeabilisation of LVD cells is not considered to be artefactual. Although nuclear staining was evident in permeabilised cells, this was very minor and is not considered to contribute a substantial degree of staining to the analysis and quantification of t-tubule area. In support of this, no significant difference was evident when comparing intact and permeable sham cells. Thus it is concluded that a level of detubulation has occurred preferentially towards the cell ends in intact LVD cells. Alternatively, as may be occurring in the sham cell ends, t-tubules here may be narrower and are therefore less accessible to di-8-ANNEPS.

In order to determine if the mechanism behind t-tubule reduction in intact LVD cardiomyocytes is attributable to narrowing of the tubule lumen, a series of experiments examining the exchange time of di-8-ANNEPS would be appropriate. A narrower lumen would be expected to present a longer diffusion delay to di-8-ANNEPS down the tubule. Employing longer incubation times with the dye (for

example 5, 10, 30, 60 min) and quantifying the relative t-tubule area along the length of the cell would determine if this mechanism was present. It is, however, not considered that t-tubule narrowing is the predominant mechanism behind t-tubule reduction in LVD cells in the present study. From the same rabbit model of LVD, Quinn *et al* (2003) made estimates of the mean surface area to volume ratio (SA/V) in sham and LVD groups based on the ratio of mean cell capacitance and mean cell volume (Quinn *et al.*, 2003). These showed that SA/V ratio in LVD cells was reduced to approximately 80% of sham thus indicating that there was a loss in cell surface area in LVD cells. This suggests that t-tubules were indeed lost in LVD cells instead of becoming narrowed as the latter would still contribute to cell capacitance measurements. It is also possible that, as cell area was significantly greater in LVD *vs.* sham cells, the hypertrophy in LVD cells was not accompanied by the addition of t-tubules (see 3.5.7.2).

3.5.6 Consequences of t-tubule remodeling in heart failure

Regardless of the mechanism by which t-tubules are lost in heart failure, a depletion of the t-tubule network would be expected to have profound consequences on the efficiency of EC coupling and ultimately the contractile function of the cell. The potential significance of alterations in the t-tubule network has been determined by a number of studies.

It is well accepted that remodelling of the t-tubule network in response to hypertrophy or failure leads to a disruption of normal Ca^{2+} fluxes and a reduction the temporal and spatial efficiency of CICR (Gomez *et al.*, 1997; Brette & Orchard, 2003; Louch *et al.*, 2004; Louch *et al.*, 2006; Song *et al.*, 2006). As stated previously, the t-tubules are the main site at which Ca^{2+} sparks originate due to the high concentration of LTCC and junctional couplings of LTCC and RyR2. A reduction in the number of t-tubules leads to areas of isolated SR in which the RyR2s are uncoupled from LTCCs. As I_{Ca} is the major physiological trigger for Ca^{2+} sparks, these regions are incapable of normal CICR and instead exhibit delayed release which is stimulated through propagated CICR. The resulting whole cell Ca^{2+} transient will be of reduced amplitude and display characteristic biphasic kinetics attributable to normal CICR and propagated Ca^{2+}

release. This conclusion is supported by the following studies of cell types with reduced or absent t-tubule networks: cultured ventricular myocytes (Lipp *et al.*, 1996; Mitcheson *et al.*, 1996; Louch *et al.*, 2004), detubulated ventricular myocytes (Kawai *et al.*, 1999; Brette *et al.*, 2002), Purkinje cells (Cordeiro *et al.*, 2001), atrial myocytes (Huser *et al.*, 1996) and neonatal ventricular myocytes (Haddock *et al.*, 1999; Seki *et al.*, 2003).

The consequence of pathological t-tubule remodeling on NCX function is of particular reference to the current thesis. Immunocytochemical staining for NCX showed no gross difference in the distribution pattern between sham and LVD cells. Although no attempt was made to quantify NCX levels using these images, it did not appear that there was a substantial reordering of NCX protein in LVD cells. NCX is reported, however, to be more concentrated in the t-tubules (see 3.1.5.2). Frequency profiles produced from these cells confirmed a periodicity of NCX fluorescence at approximately 2 μm which corresponds with a t-tubular location on the long axis of the cell. Reduction of the t-tubule network would therefore be expected to decrease the percentage of functional NCX in contact with the extracellular space.

3.5.7 Mechanism of remodeling in failing cardiomyocytes

It is well established that cardiomyocytes undergo a physical remodeling in response to the mechanical stresses leading to heart failure. Of relevance to the work presented in the current chapter is the remodeling of cell size and the t-tubule network.

3.5.7.1 Remodeling of cell size

Two classifications for hypertrophy exist based on the particular phenotype of the cardiomyocyte. An early study of LV wall stress in humans undergoing cardiac catheterisation defined a relationship between haemodynamic stimuli and the resulting overall type of hypertrophy produced (Grossman *et al.*, 1975). The hypothesis shown in Figure 3.18 was suggested from the results obtained.

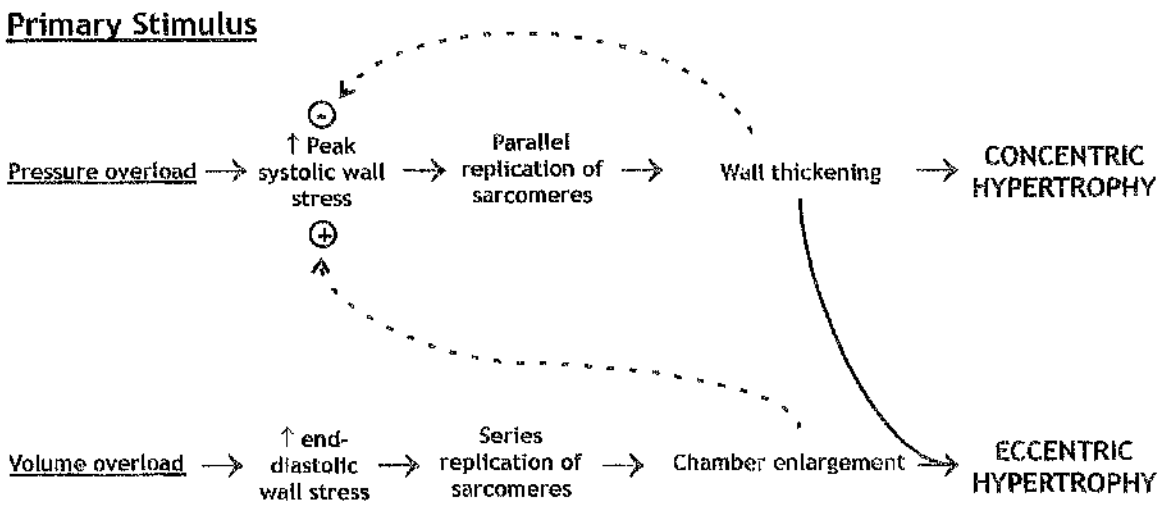

Figure 3.18 Hypothesis relating haemodynamic stimulus and patterns of hypertrophy.

Diagram showing the progression from primary haemodynamic stimulus through to overall type of ventricular hypertrophy. Redrawn from Grossman *et al.*, (1975).

In this it was proposed that concentric hypertrophy resulted from the parallel replication of sarcomeres whilst eccentric hypertrophy resulted from the series replication of sarcomeres. In a study of human ischaemic cardiomyopathy (ICM), a significant increase in left ventricular myocyte length was detected compared to control whilst sarcomere length in the two groups was comparable. This therefore supports the addition of sarcomeres as a mechanism by which myocytes' length is increased during hypertrophy (Gerdes *et al.*, 1992). The data presented in the current chapter suggest that the hypertrophy in our model is a combination of concentric and eccentric. On average, cardiomyocytes from LVD animals were shown to undergo an 11% increase in length and a 10% increase in width compared to sham operated animals. Previous investigation in rat of the ventricular remodeling which follows myocardial infarction has also shown the presence of a combination of concentric and eccentric remodeling (Anversa *et al.*, 1985). This study revealed a 14% increase in cell length and 6% increase in cell diameter. Predominantly eccentric remodeling has been determined in a sheep model of myocardial infarction (Kramer *et al.*, 1998) and human ICM (Gerdes *et al.*, 1992). However, it has been established that the degree and type of hypertrophy (concentric *vs.* eccentric) is related to the size of infarct and so comparison between studies may be precluded (Olivetti *et al.*, 1991).

In the most basic terms, ventricular mass is determined by the net difference between contractile protein synthesis and degradation. Hypertrophy will occur when synthesis is greater than degradation (Carabello, 2002). The precise mechanism by which this imbalance occurs is extremely complex and is considered to involve multiple pathways or mediators, most of which are poorly understood. Various studies have attempted to define the pathway to cellular remodelling and hypertrophy; the general theme involved is shown in Figure 3.19.

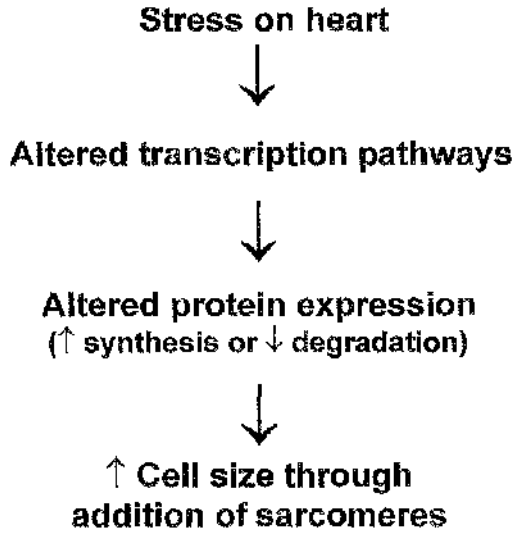

Figure 3.19 General theme of the pathway to hypertrophy.

The primary stimulus for hypertrophy leads to an alteration in transcription pathways in the cell which proceed to alter the balance in protein expression such that extra sarcomeres are manufactured and added onto the cell to increase its size.

The exact signalling pathways which have been proposed to link the initial hypertrophic signal/stress to the alteration of transcription and translation are beyond the scope of this work. They have been suggested to include the mitogen-activated protein kinase (MAPK) pathways via G-protein coupled receptors or stretch leading to the phosphorylation of nuclear transcription factors and alterations in intracellular Ca^{2+} signalling via CaMK (Bers, 2001).

3.5.7.2 Remodelling of the t-tubule network in failing cardiomyocytes

The present study has demonstrated that a significant remodeling of the t-tubule network occurs in failing left ventricular myocytes from the rabbit. A significant

proportion of these tubules have become pinched off from the surface sarcolemma and then resealed within the cell interior. Cardiomyocytes from LVD hearts are also significantly longer and wider than sham, 111 and 110% of sham respectively. This hypertrophy is considered to be as a result of both parallel and series addition of sarcomeres. The reduction in relative t-tubule area was particularly profound at the cell ends. It therefore appears that whilst the cardiomyocyte has undergone the addition of new contractile units these have not been equipped with an accompanying complete t-tubule network. Although the myocyte dimensions have increased in an attempt to normalise ventricular function, it is unlikely that these cells exhibit optimal contractile function due to the lag in growth of the t-tubule network.

It has been suggested that hypertrophy in adult cardiomyocytes during disease states and dysfunction is a programmed reversion towards a more foetal-like form and phenotype (Bers, 2001; Poindexter *et al.*, 2001). Many of the features associated with a loss of t-tubule network parallel the situation in embryonic cardiomyocytes. As detailed earlier (3.1.2.1) embryonic cells possess a reduced SERCA2a but increased NCX abundance, relying mainly on trans-sarcolemmal Ca^{2+} fluxes, and have a substantially reduced t-tubule network compared to adult cells. This regression has been termed de-differentiation and may therefore occur as a protective mechanism to return cardiomyocytes to a stage where cell proliferation can occur again (Poindexter *et al.*, 2001). This hypothesis requires further investigation and it is probable that many other signaling pathways contribute to the remodeling of the t-tubule network in heart failure.

3.5.8 Limitations and future work

Precise estimation of relative t-tubule area is extremely difficult due to the complexity of the t-tubule system, the access of indicators to the t-tubule lumen and the precision and reproducibility of analysis methods. In the present study, every effort was made to control for variables within both the experimental protocol and analysis procedure to produce as accurate an estimation of the relative cell area occupied by the t-tubule network. It is recognised, however, that the following variables may have influenced the results obtained.

(i) T-tubule diameters are known to vary considerably within cardiomyocytes (Ogata & Yamasaki, 1990; Soeller & Cannell, 1999) therefore the fluorescence signal from each t-tubule may vary with the diameter of the individual t-tubule.

(ii) T-tubules have been shown to become dilated in situations of heart failure (Kostin *et al.*, 1998). It is possible that although the abundance of t-tubules decreases in heart failure, the remaining tubules may increase in diameter thereby allowing proportionately more access to di-8-ANNEPS. This would lead to an overestimation of t-tubule area and underestimate the depletion of the t-tubule network in LVD.

(iii) The isolation procedure used to obtain single cardiomyocytes may produce cells with varying amounts of cellular damage to their structure. It may be the case that relative t-tubule area is comparable in sham and LVD ventricular cells in the whole heart and that the t-tubule network in failing hearts is simply more susceptible to this damage. This could underlie the reduction in t-tubule network in LVD single cardiomyocytes and requires further investigation.

Soeller and Cannell (1999) examined the t-tubule network in the rat by immersing the cardiomyocyte in dextran-linked fluorescein solution before imaging using two-photon microscopy. Complex deconvolution techniques were then applied to reduce distortion of the image by the point spread function in order to produce an approximate three dimensional model of the t-tubule network (Soeller & Cannell, 1999). Although their approach proved successful in determining precise characteristics of the network it is unlikely that this type of image processing is practically applicable to large data sets due to its very long time and complexity. By comparison, the method presented in the current chapter is considered to be technically quick and easy to perform. It has resulted in an acceptably reproducible method of estimating relative t-tubule area in isolated ventricular myocytes.

Future work must aim to determine what happens to the t-tubule network during heart failure in intact tissue in order to determine the consequences to the whole heart. Of great interest would be to assess the regional distribution of ventricular myocytes undergoing depletion of t-tubule network in response to

heart failure and how the severity of this varies with distance from the infarcted region.

3.6 Summary

This study has provided a detailed quantification of relative t-tubule area in isolated rabbit ventricular myocytes and determined a significant reduction in LVD. In addition, it is the first to report a robust method for detubulating isolated cardiomyocytes from the rabbit using the agent formamide. The loss of t-tubule network in failing cells will slow the rate of SR Ca^{2+} release and decrease cell shortening which, at the level of the whole heart, would be expected to reduce cardiac force and rate of contraction.

As NCX protein is reported to be concentrated in the t-tubules, the depletion of the t-tubule network in failing cells would limit the fraction of NCX in contact with the extracellular fluid, thereby decreasing the amount of functional exchanger. This may explain the reduction in NCX activity in spite of increased NCX protein seen previously in our model and contribute to depressed contractility. Previous work in isolated detubulated rat cardiomyocytes has suggested that NCX may still be capable of functioning, although at a much reduced level, in the internalised t-tubules (Despa *et al.*, 2003). It is presumed, however, that NCX function was assessed in these cells within a few hours of the detubulating event. The question of whether the ionic gradient required for NCX function would be maintained for longer periods or whether these would run down as intra-tubular composition equilibrated with the cytosol remains to be answered.

Reduction of the t-tubule network may not be the entire cause for reduced NCX activity in our model. Defects other than myocyte structure are abundance, location and regulation of proteins. Detection and quantification of t-tubule morphology may however, be used as an indicator of the cellular pathology accompanying heart failure.

CHAPTER 4
QUANTIFICATION OF SORCIN

4.1 Introduction and review of sorcin

Sorcin (SOluble Resistance-related Calcium-binding proteIN) is a 21.6 kDa calcium-binding protein first isolated from the cytoplasmic extract of multi-drug resistant cells (Hamada *et al.*, 1988). The acquisition of drug resistance in these cells is due to over-expression of the membrane-bound drug transporter P-glycoprotein. The close genetic linkage of regions coding for P-glycoprotein and sorcin was considered to lead to the concomitant amplification of sorcin protein (Meyers *et al.*, 1995a).

The expression of sorcin *in vivo* is widespread. High levels are present in the heart while substantial amounts have been shown to exist also in the brain, kidney, adrenal medulla and skeletal muscle (Meyers *et al.*, 1995a; Meyers *et al.*, 1995b). The precise role for sorcin in the heart is far from confirmed but most research agrees that it is involved in Ca^{2+} homeostasis. Studies have found that sorcin associates with four major cardiac Ca^{2+}-handling proteins; the SR Ca^{2+}-release channel or ryanodine receptor (RyR2) (Meyers *et al.*, 1995a), L-Type Ca^{2+} channel (LTCC) (Meyers *et al.*, 1998), Na^{+}-Ca^{2+} exchanger (NCX) (Seidler *et al.*, 2003) and more recently the sarcoplasmic/endoplasmic reticulum Ca^{2+}-ATPase (SERCA2a) (Matsumoto *et al.*, 2005).

Sorcin is a member of the Penta-Elongation Factor (PEF) family of proteins (five EF-hand domains) which contains other high affinity Ca^{2+}-binding proteins such as grancalcin, calpain (small and large subunits), peflin and the apoptosis-linked gene-2 protein (ALG-2) (Kitaura *et al.*, 2001; Ilari *et al.*, 2002; Mella *et al.*, 2003; Maki *et al.*, 2002). PEF family proteins have been divided into two main functional classes: (i) regulatory, involved in intracellular signalling and (ii) structural, involved in regulation of intracellular calcium. Sorcin has been assigned to the former.

The term "EF-hand" (Figure 4.1) was first coined as it could be described using the right hand with index finger and thumb outstretched to represent the incoming and outgoing alpha helices respectively; the three remaining curled

fingers represent the calcium binding loop with the ion held in its palm (Tufty & Kretsinger, 1975).

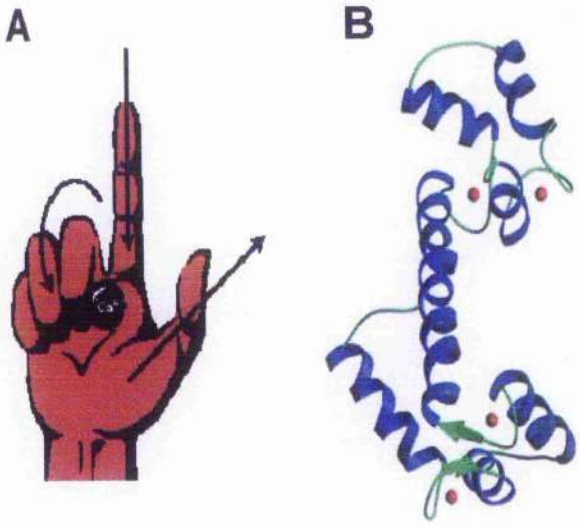

Figure 4.1 The EF hand.

A Cartoon of the EF "hand". Index finger and thumb represent the α-helices whist the curled fingers correspond to the Ca^{2+}-binding loop; the Ca^{2+} ion can be seen in the palm.

B Ribbon diagram of the EF hand domain. Figure taken from The Pawson Lab., http://www.mshri.on.ca/pawson.eFh.html.

Typically, the EF-hand is characterised by a helix-loop-helix structure - two perpendicular α-helices (ten-twelve amino acids each) connected by an interhelical loop of twelve amino acids. The loop structure is the region involved in binding calcium; within this, residues 1, 3, 5, 7 and 9 provide ligands to coordinate Ca^{2+} whilst residue 12, commonly glutamate and often referred to as the bidentate ligand, provides two oxygen atoms for the binding of calcium (Ilari *et al.*, 2002). The EF-hands (EF-) of sorcin occur in adjacent pairs linked via short stranded β-sheets (Xie *et al.*, 2001). In the case of sorcin, EF-1 pairs with EF-2 and EF-3 pairs with EF-4 (both in a "canonical" manner) whilst EF-5 remains unpaired in the monomer. EF-5 can pair with another EF-5 from a second sorcin monomer during dimer formation. Sorcin therefore comprises eight α-helices in total (A-H), two of which are long six-turn α-helices joining EF-2 to EF-3 (D-helix) and EF-4 to EF-5 (G-helix) thereby promoting overall stability of the molecule (Zamparelli *et al.*, 2000; Ilari *et al.*, 2002; Mella *et al.*, 2003;

Zamparelli *et al.*, 2000; Xie *et al.*, 2001). The sorcin molecule contains two main domains (Figure 4.2); the N-terminus (residues 1-32) and the C-terminus (residues 33-198; containing the EF-hands). The flexible N-terminus domain (residues 1-32) is rich in glycine and proline residues and is involved in dimerisation. Binding sites for two calcium ions and two phosphorylation sites for cAMP-dependent protein kinase (PKA) are present in the C-terminus. The potential function of sorcin may therefore be regulated both by intracellular [Ca^{2+}] and [cAMP], thus altering Ca^{2+}-binding and phosphorylation status respectively (Hamada *et al.*, 1988; Meyers *et al.*, 1995b; Zamparelli *et al.*, 1997; Ilari *et al.*, 2002; Mella *et al.*, 2003). Both of these properties will be discussed.

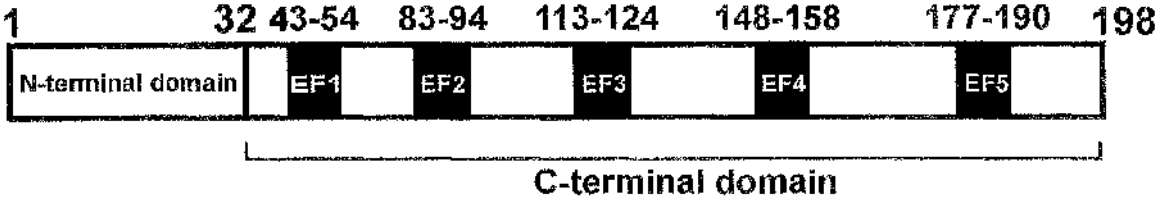

Figure 4.2 Schematic representation of the structure of sorcin.

Map of the N- and C-terminals of sorcin (residues 1-32 and 33-198 respectively). EF-hands 1-5 (■) are located in the C-terminus of the protein; numbers above each indicate the residues contained within each EF-hand. Redrawn from Matsumoto *et al*, (2005).

4.1.1 Calcium binding and translocation to membrane

Originally considered to be purely a cytosolic protein, it is now widely accepted that sorcin undergoes a Ca^{2+}-dependent translocation to membranes. This feature is common to all PEF proteins (Maki *et al.*, 2002). Sorcin binds two calcium ions per monomer in the first three EF-hand domains localised to the C-terminus. This occurs at micromolar Ca^{2+} concentrations (K_d,Ca ~ 1 μmol/L) which is of pertinence to cardiac EC coupling (Meyers *et al.*, 1995b; Zamparelli *et al.*, 1997). Early studies demonstrated the translocation phenomenon using Western blotting in membrane and supernatant fractions from cardiac homogenates, multi-drug resistant cells and *E.coli* over-expressing recombinant sorcin. On addition of Ca^{2+}, sorcin was detected only in membrane fractions; this translocation was reversible upon addition of EGTA (to reduce intracellular [Ca^{2+}]) and sorcin protein was detected only in supernatant fractions.

Additionally, it was found that the process was Ca^{2+}-specific and did not occur in response to other divalent cations such as Mg^{2+}, a result of relevance as many PEF proteins are capable of binding Mg^{2+} also (Meyers *et al.*, 1995b; Jia *et al.*, 2000). The first insight into the mode of interaction with membrane was also demonstrated in this study. Sorcin was shown to partition into the detergent phase of Triton X-100 at high [Ca^{2+}] therefore suggesting a form of association with hydrophobic lipid components within the membrane (Meyers *et al.*, 1995b). Knowing that all PEF proteins undergo a conformational change on binding Ca^{2+}, leading to the exposure of hydrophobic regions, it was hypothesised that translocation was not due to a direct interaction with lipid (Meyers *et al.*, 1995b). Further studies explored the Ca^{2+} and pH dependence of the translocation process. These revealed that upon saturation with Ca^{2+}, sorcin underwent a rearrangement of aromatic residues, particularly of hydrophobic tryptophan residues, leading to their exposure to surrounding solvent and thereby favouring movement of the molecule into membrane. In the absence of membrane and at physiological pH, sorcin formed high molecular weight aggregates in excess calcium which could be prevented when membrane was present due to the stabilisation of the interaction with the membrane by carboxylate groups. This also was deemed to confer specificity to the interaction with the target.

Further understanding of the mode of Ca^{2+} binding and translocation was gained when the crystal structure of sorcin was produced using the x-ray coordinates of calpain as a template. This was then subsequently divided into two: (i) the sorcin calcium binding domain (SCBD) which lacks the N-terminus and (ii) the 90-198 fragment which lacks EF-1 and EF-2. Fluorescence titration experiments using the fluorophore Quin 2 determined that removal of these first two EF hands (fragment 90-198) abolished the ability to bind Ca^{2+}. In addition, this fragment did not translocate to E.Coli. membrane even when [Ca^{2+}] was raised to 10 mmol/L. Binding of Ca^{2+} to EF-1 and 2 was thus deemed necessary for the activation of sorcin and subsequent translocation to membrane (Zamparelli *et al.*, 2000). Using the same crystal structure of the SCBD and computer modelling, it was later suggested that, in Ca^{2+}-free sorcin, the N-terminal domain is bound to the SCBD between EF4 and EF5 covering the hydrophobic tryptophans (Trp-99 and Trp-105) located on the D-helix between EF-2 and 3 in

the C-terminus. There is no significant conformational change in the SCBD on Ca^{2+}-binding and only the flexible N-terminus is re-positioned with respect to the SCBD, leading to the exposure of the hydrophobic residues. In line with this theory is sorcin's intrinsic fluorescence, attributable to Trp-99 and Trp-105 on the D helix in the SCBD. Most PEF proteins exhibit enhanced fluorescence on binding of Ca^{2+} yet this was not found to be true for sorcin. At saturating [Ca^{2+}], intrinsic fluorescence is quenched in native sorcin due to re-alignment of the flexible N-terminus and exposure of the tryptophans by Ca^{2+}-binding, whilst in the SCBD fragment fluorescence is unaffected due to the absence of the N-terminus (Ilari *et al.*, 2002).

A more recent study by the same group produced three site-specific mutants of sorcin in which the bidentate glutamate (E) in the interhelical loops of EF-hands one, two or three was replaced by either glutamine (Q) or alanine (A) giving rise to E53Q-, E94A- and E124A-sorcin respectively. The mutated forms could not bind Ca^{2+} in that particular EF-hand as substitution of the glutamate rendered the hand unable to co-ordinate Ca^{2+} sufficiently for binding. EF hands four and five were not mutated as they do not possess the required ligands to bind Ca^{2+}. Only the E124A-sorcin mutant showed structural alteration due to the participation of residue 124 in a network of interactions in the D-helix. The mutants determined that EF-hands one, two and three are capable of binding Ca^{2+} and that the affinity for binding to Ca^{2+} and two well established protein targets for sorcin (RyR and annexin VII) followed the order wild-type > E53Q- > E94A- > E124A-sorcin. This indicated that a mutation in EF-3 had the largest functional impact. Two binding sites for Ca^{2+} were identified for wild type sorcin with dissociation constants of 0.42×10^{-6} mol/L and 6.3×10^{-6} mol/L. Of these, EF-3 was shown to have the highest affinity for Ca^{2+}-binding as it possesses four acidic Ca^{2+} co-ordinating residues and is the most conserved EF-hand within the PEF family in terms of these residues. The importance of EF-3 as the major EF-hand superseded previous incorrect reports that EF-pairs 1 and 2 (through their structural coupling) were the physiologically relevant Ca^{2+}-binding sites in sorcin (Zamparelli *et al.*, 2000; Xie *et al.*, 2001).

This work has led to the current proposed mechanism of Ca^{2+}-binding and translocation to membrane of sorcin which states that Ca^{2+} binds primarily to EF-

3, activating the protein. This then produces a conformational change at glutamate in position 124 (due to loss of hydrogen bonding with neighbouring aspartate residues) which is transmitted to EF-2 via re-arrangement of the packing order of the hydrophobic core of the D-helix. The original Ca^{2+}-binding signal at EF3 is then conveyed via the canonical structural pairing which exists between EF-1 and EF-2 to EF-1. Thus it has now been concluded that EF-2 and EF-3 are the functionally relevant Ca^{2+} binding sites and that the conformational alteration seen in EF-1 occurs as a secondary consequence via the D-helix (Mella *et al.*, 2003). In keeping with earlier work, this conformational change in EF-1 would then be expected to lead to the loosening and re-orientation of the N-terminus with respect to the C-terminus, thereby uncovering hydrophobic domains below and allowing interaction of sorcin with target proteins (Ilari *et al.*, 2002).

The Ca^{2+} dependence of the translocation of sorcin to membrane has been assessed in permeabilised rat cardiomyocytes. It revealed an EC_{50} of 202 μmol/L for translocation; the authors state this Ca^{2+} concentration would only be achieved at the dyadic junction (Farrell *et al.*, 2003). This result is surprisingly high by comparison with the less than 1 μmol/L and 10 μmol/L reported by Meyers *et al* (1995b) and Zamparelli *et al* (2000) which are more in agreement with each other.

A more novel proposal is the effect of PKA-phosphorylation on Ca^{2+} binding and translocation. A constitutively phosphorylated mutant of sorcin was produced by substitution of serine 178 for aspartate. Using the fluorescence shift which occurs on Ca^{2+} binding, it was shown that the phosphorylated mutant had an increased Ca^{2+} sensitivity compared to wild-type sorcin. Furthermore it was shown that phosphorylation induced by the infusion of 1 μmol/L isoproterenol in control hearts led to an increase in sorcin in SR membrane fractions versus whole homogenates. Thus it has been suggested that translocation to membranes such as the SR may occur in response PKA-mediated phosphorylation as well as in response to $[Ca^{2+}]$ (Matsumoto *et al.*, 2005).

4.1.2 Dimerisation

All PEF family proteins posses the common feature of dimerisation (Maki *et al.*, 2002). Sorcin has been known to exist as a dimer since its discovery and is stabilised through the pairing of unpaired or "uneven" EF-5 hands. Subsequent work has shown that the protein can form both homodimers (with another sorcin monomer) and heterodimers with grancalcin, the latter in a Ca^{2+}-independent manner (Kitaura *et al.*, 2001; Xie *et al.*, 2001; Ilari *et al.*, 2002; Hansen *et al.*, 2003). Only the formation of sorcin homodimers is relevant in the cardiac cell as grancalcin is found only in cells originating from bone marrow (Jia *et al.*, 2000). Throughout this thesis, "dimer" will be used in place of homodimer to represent the sorcin-sorcin dimer.

A molecular model of the sorcin dimer has been produced and used to determine the nature of the linkage. At the dimer interface, helices G and H associated with each EF-5 form a four-helix bundle and the loops form an antiparallel β-sheet, all of which is stabilised via buried hydrophobic interactions between neighbouring side chains. Sorcin dimers are structurally asymmetrical due to the differing orientations of sub-domains from each monomer (Zamparelli *et al.*, 2000; Xie *et al.*, 2001; Ilari *et al.*, 2002; Maki *et al.*, 2002). At first it was believed that dimerisation arose via a non-covalent linkage as the molecule could be denatured into constituent monomers by SDS treatment (Hamada *et al.*, 1988). This was later discovered to be untrue and in fact the dimer interactions were of the covalent type (Meyers *et al.*, 1995a).

Physiologically, dimerisation provides stability to the molecule through the pairing of the only unpaired EF-hand (EF-5). The exact functional consequence/significance of dimerisation in PEF proteins is largely unknown but four main proposals exist; dimerisation: (i) will provide a new interface for target interaction (ii) may alter function of hetereodimeric forms e.g. heterodimers of the small and large subunits of calpain form an active protease (iii) may fine tune the Ca^{2+} signalling role provided by the PEF proteins and (iv) may modulate the action on the target protein (Hansen *et al.*, 2003). Studies on other members of the PEF family (ALG-2 and peflin) have suggested that the monomeric forms are more susceptible to proteolysis, hence highlighting the

desirability for PEF members to form dimers in physiological conditions. In addition, mutated PEF proteins lacking the fifth EF-hand motif are unable to dimerise and undergo rapid degradation, reinforcing the critical role for EF-5 in this process (Kitaura *et al.*, 2001).

Sedimentation velocity experiments revealed that sorcin and the SCBD fragment were capable of forming stable dimers at pH 7.5 in the presence of 2 mmol/L EGTA. Ca^{2+}-bound sorcin tended to precipitate in the absence of membrane. At acidic pH's (6.0) and high temperatures (35-40 °C), sorcin was capable of Ca^{2+}-linked tetramer formation. This process was in competition with Ca^{2+}-dependent translocation to membranes as an overall decrease in hydrophobicity occurred due to the aromatic residues (tryptophan and tyrosine) involved in Ca^{2+}-dependent translocation becoming buried at the dimer-dimer interface (Zamparelli *et al.*, 1997; Ilari *et al.*, 2002). Even once tetramerised, potential sites for further oligomerisation of sorcin remain available, explaining the tendency for sorcin to precipitate at higher concentrations (1-2 mg/mL) (Ilari *et al.*, 2002). In addition, sorcin may complex with unknown macromolecules as has been suggested for ALG-2 (Kitaura *et al.*, 2001). Hence the behaviour of sorcin in the cardiac cell appears to be very labile in response to varying cellular conditions.

4.1.3 Sorcin and target interaction

Sorcin is proposed to interact with its targets via either its C- or N-terminals in a Ca^{2+}-dependent manner (Mella *et al.*, 2003). Interaction with membrane-bound targets has been linked to its ability to translocate to membranes in its dimeric form due to exposure of hydrophobic domains on the surface of the molecule (Zamparelli *et al.*, 1997). Of these hydrophobic residues, Trp-99 is considered especially important as it is more exposed to solvent than Trp-105 (Mella *et al.*, 2003). However, it has also been suggested that, at physiological pH, Ca^{2+}-free sorcin may already expose sufficient hydrophobic domains to enable it also to interact with membrane-bound targets as has been established for calmodulin (Zamparelli *et al.*, 1997).

As is the case with all EF-hand proteins, sorcin can interact with multiple targets. The most widely evidenced cellular targets for sorcin in the cardiac cell are (i) RyR2, (ii) LTCC, (iii) NCX, (iv) SERCA2a and (v) annexin VII. The investigation of their interaction and the potential functional implications for EC coupling are discussed below.

4.1.3.1 Ryanodine receptor

The ryanodine receptor (RyR2) is the SR-associated membrane protein responsible for release of stored Ca^{2+} during excitation-contraction coupling. It was the first and now most extensively characterised membrane bound target for sorcin in the cardiac cell (Meyers *et al.*, 1995a).

This early work, using immunoelectron microscopy in rat cardiomyocytes, demonstrated that sorcin was localised to the dyadic junction of the T-tubules and the SR (Meyers *et al.*, 1995a), a finding supported by numerous subsequent studies. Critically, an association between RyR2 and sorcin was shown following complementary immunoprecipitation with both RyR2 and sorcin antibodies. In addition, the forced expression of sorcin in RyR2-negative, non-excitable cells led to the simultaneous expression of RyR2 protein. On application of caffeine, these cells exhibited a rapid and transient rise in intracellular Ca^{2+}, thus implying that the expressed RyR2 was organised into working release units. The cellular site of the interaction between the two proteins was suggested to be within the SR membrane as the link was resistant to proteolysis by proteinase K. This study failed to address whether the interaction of sorcin and RyR is direct or via an intermediary protein or anchoring protein. It did hint, however, at the possibility of a disulphide link existing between the two as RyR could not be detected when cardiomyocytes were lysed in the presence of the reducing agent β-mercaptoethanol (Meyers *et al.*, 1995a). In the SR-rich fraction of isolated rat cardiomyocytes over-expressing sorcin via adenoviral gene transfer, a 71% increase in RyR2 protein was detected (Suarez *et al.*, 2004). This further strengthens the early work by Meyer's group on the interaction of the two proteins and implies that their expression/targeting in the cell may be linked.

The functional consequences of the interaction of sorcin and RyR2 were initially explored using radiolabelled ryanodine binding experiments in SR microsomes and single channel recordings from isolated RyR2 channels incorporated into lipid bilayers. Recombinant sorcin significantly decreased the open probability of RyR2 when applied to the cytoplasmic side of the channel (IC_{50} ~ 480 nmol/L) and completely inhibited ryanodine binding at higher concentrations (IC_{50} ~ 700 nmol/L). This was in contrast to skeletal muscle, where sorcin had a stimulatory effect on RyR1 (the skeletal muscle isoform). The inhibitory effect on RyR2 was shown to be dose-dependent, Ca^{2+}-independent and was alleviated when sorcin was phosphorylated by the catalytic subunit of PKA. No alteration of RyR2's affinity for Ca^{2+} was detected. The association between sorcin and RyR2 was unaffected by calmodulin or calpain, which also inhibit RyR2, thereby indicating a different mechanism for sorcin's effect; the precise mechanism remains unknown (Lokuta *et al.*, 1997). The possibility that sorcin may interact with RyR2 using either its N- or C-terminal was investigated using truncated forms of sorcin. The SCBD fragment associated with RYR2 in the same manner as native sorcin at physiological [Ca^{2+}] and so it was proposed that the interaction occurred via the C-terminal of sorcin (Zamparelli *et al.*, 2000). This too was shown to be negated by phosphorylation. The 90-198 fragment which lacks EF-1 and EF-2 did not associate with RyR2, a finding most probably explained due to the requirement of these hands for Ca^{2+} binding and translocation (Ilari *et al.*, 2002).

The consequences of the physical and functional association of sorcin and RyR2 in the cardiac cell are well documented in the literature. The characterisation of spontaneous Ca^{2+} sparks in response to sorcin provides a direct measure of the modulation of RyR2 activity (Seidler *et al.*, 2003). This has been performed in both permeabilised isolated rabbit cardiomyocytes over-expressing sorcin (Seidler *et al.*, 2003) and in permeabilised isolated mouse cardiomyocytes exposed to exogenous sorcin (Farrell *et al.*, 2003). In the rabbit, over-expression of sorcin led to a significant decrease in Ca^{2+} spark amplitude, frequency, width and duration compared to LacZ controls (all $p<0.05$). The SR Ca^{2+} content was comparable for both groups (Seidler *et al.*, 2003). A similar result was obtained in the mouse by including 1 μmol/L recombinant sorcin in the patch pipette. This led to a significant decrease in Ca^{2+} spark frequency

($p<0.05$), amplitude, width and duration compared to control (all $p<0.001$). These alterations were reversible on removal of sorcin. Unfortunately, this study failed to determined if SR Ca^{2+} content was the same in the absence and presence of sorcin (Farrell *et al.*, 2003). These functional studies therefore confirm the inhibitory effect of sorcin on RyR2 activity in situ.

A novel theory which has emerged is that sorcin may serve as a modulator of RyR2 in the same way as has been proposed for FKBP. Over-expression of FKBP 12.6 was shown to reduce SR leak by reducing RyR2 open probability, stabilising it in the closed configuration and thereby increasing SR Ca^{2+} load (Prestle *et al.*, 2001). It is suggested that sorcin may decrease SR leak via its inhibitory effect on RyR2 (Suarez *et al.*, 2004). Further to this, RyR2 inhibition by sorcin may serve to contribute to the termination of RyR2 release (Meyers *et al.*, 1995a; Lokuta *et al.*, 1997; Farrell *et al.*, 2003). Initially Meyers *et al.* (1995a) concluded that the association of sorcin with RyR2 stabilised the RyR protein and retarded its degradation. Building on this was the idea that, at low $[Ca^{2+}]_i$, sorcin would be present predominantly in the cytoplasm but, at higher $[Ca^{2+}]_i$, sorcin would translocate to membrane, interact with RyR2 and limit further release so as to reduce SR depletion (Lokuta *et al.*, 1997). It is proposed that sorcin interacts with RyR2 at rest, as evidenced by the inhibition of Ca^{2+} sparks, as well as when activated by rises in $[Ca^{2+}]_i$ during the transient (Farrell *et al.*, 2003). The ability of sorcin to inhibit RyR2 is very rapid and experimental artefacts preclude precise determination of the kinetics. Currently, the best estimation of the time-scale of sorcin's inhibitory action on a single RyR2 is ≤ 20 ms, a result which is suggested to be reasonable for modulating SR release and EC coupling gain on a beat to beat basis (Farrell *et al.*, 2003).

4.1.3.2 L-type Ca^{2+} channel

The second intracellular target identified for sorcin in the heart was the L-type Ca^{2+} channel (LTCC). The LTCC links the incident action potential and SR by providing the trigger for SR Ca^{2+} release via RyR2. The initial indication that sorcin may also associate with LTCC was provided by immunoprecipitation of RyR using antibodies directed against sorcin. These also detected an unknown protein of approximately 220 kDa protein (Meyers *et al.*, 1995a). Further

suggestion that an interaction with LTCC's was spatially plausible was provided by the cellular localisation of sorcin at the dyadic junction. In confirmation of this, a subsequent immunoprecipitation study using specific antibodies showed sorcin to interact with the cardiac α_1 pore-forming subunit of the L-type Ca^{2+} channel (α_{1C}) (Meyers *et al.*, 1998). LTCC exists in two forms in cardiac membrane; a small fraction exists as the full length protein (240 kDa) whilst the majority is in the form of a truncated version lacking the C-terminus. Only the full length protein was recovered using anti-sorcin antibodies, indicative of a cytoplasmically orientated C-terminal sorcin-binding domain on the α_{1C} subunit. Investigations using HIS_6-tagged fragments of the α_{1C} C-terminus localised the site of sorcin binding to residues 1622-1748. This is a region of α_{1C} overlapping with the region responsible for Ca^{2+}-dependent inactivation in the native protein and the same area that calmodulin binds to which also inactivates I_{Ca} (Meyers *et al.*, 1998).

Functionally, the effects of sorcin on I_{Ca} are conflicting. The rapid component of inactivation (T_{fast}) of I_{Ca} was shown to be significantly faster in isolated cardiomyocytes from transgenic mice over-expressing sorcin compared to control mice. This occurred both in the presence and absence of Ca^{2+}-induced inactivation. LTCC protein expression, I_{Ca} density and I_{Ca} activation characteristics were unaltered compared to wild type animals. Examination of I_{Ca} in oocytes co-expressing LTCC subunits and sorcin found that there was a 27% increase in the rate of inactivation versus control. In these experiments, Ba^{2+} was used as the charge carrier, thereby indicating that the effect of sorcin was not solely Ca^{2+}-dependent (Meyers *et al.*, 2003). Taken together, these data suggest that sorcin interacts with LTCC directly to affect inactivation kinetics independent of Ca^{2+}. However, single cell studies of I_{Ca} from other groups using either exogenous recombinant sorcin (3 μmol/L) or adenoviral-mediated over-expression of sorcin report no effect on the parameters of I_{Ca} (Farrell *et al.*, 2003; Seidler *et al.*, 2003). In summary, a role for sorcin in the regulation of interchannel communication between LTCC and RyR2 has been suggested but this remains controversial (Meyers *et al.*, 1998).

4.1.3.3 NCX

The sodium-calcium exchanger (NCX) is the major Ca^{2+} extrusion pathway in the cardiac cell. Its stimulation by sorcin was discovered in isolated rabbit cardiomyocytes over-expressing sorcin via adenoviral gene transfer (MOI=100, 24 hr culture). Under whole cell voltage-clamp conditions, depolarisation-induced Ca^{2+} transients were smaller and peak-systolic and end-diastolic $[Ca^{2+}]_i$ were both significantly decreased ($p<0.05$) in sorcin over-expressing cells. This was accompanied by a significant decrease in action potential duration ($p<0.05$) assessed using current injection. No effect of sorcin on either the amplitude of I_{Ca} or integral of the current was detected. The rapid application of 10 mmol/L caffeine revealed significantly decreased SR Ca^{2+} release in sorcin over-expressing cells compared to LacZ (528 ± 32 nmol/L *vs.* 895 ± 70 nmol/L respectively; $p<0.01$) indicating a reduced SR Ca^{2+} content. The rate constant for the decay of the caffeine-induced Ca^{2+} release and I_{NCX} were significantly increased in sorcin over-expressing cells ($p<0.01$) demonstrating a more rapid extrusion of Ca^{2+} via NCX (Seidler *et al.*, 2003). This finding was verified by assessing the NCX current-voltage (I-V) relationship, which was significantly increased between 10 - 80 mV ($p<0.01$). An increase in NCX-mediated efflux would be expected to decrease $[Ca^{2+}]_i$, thereby limiting the amount available for re-uptake to the SR and reducing SR Ca^{2+} content. In turn, this would explain the decrease in Ca^{2+} transient amplitude in sorcin over-expressing cells. Additional measurements on EC coupling gain were performed by assessing the relationship between SR Ca^{2+} content and Ca^{2+} transient amplitude in both sorcin over-expressing and LacZ cardiomyocytes; these revealed no effect of sorcin. Significantly decreased Ca^{2+} spark characteristics (frequency, amplitude, duration and width) were detected in the presence of sorcin but no alteration in SR content was produced. Together these data implied that the decrease in Ca^{2+} transient amplitude could be attributed predominantly to a decreased SR Ca^{2+} content, which is itself a sole consequence of the stimulation of NCX-mediated Ca^{2+} efflux by sorcin.

A physical association of the two proteins has been demonstrated by co-immunoprecipitation studies using NCX antiserum (Smith *et al.*, 2005a). The nature of the interaction of sorcin with NCX was revealed using the SCBD

fragment of sorcin (residues 33 - 198) which was shown to reduce I_{NCX} at more positive potentials in a similar manner to native sorcin. As this fragment lacks the N-terminus, it was concluded that sorcin interacts with NCX using the C-terminus as with RyR2 (Smith *et al.*, 2005a).

4.1.3.4 SERCA2a

The most novel target suggested for sorcin is the SR Ca^{2+}-ATPase, SERCA2a (Matsumoto *et al.*, 2005). The evidence supporting a possible interaction between sorcin and SERCA2a is weakened by the fact that no co-immunoprecipitation data exist to demonstrate a physical association of the two. In spite of this, the relevant functional evidence from this paper will be discussed.

Single isolated rat cardiomyocytes over-expressing sorcin (MOI=20, 48 hr culture) were produced and shown to exhibit a significant increase in the amplitude and rate of decay of the Ca^{2+} transient compared to GFP over-expressing controls. In addition, the amplitude of the caffeine-induced Ca^{2+} transient showed a 43% increase in the SR content in cells over-expressing sorcin. To account for the influence of phospholamban (PLB) on SERCA2a activity, the expression of PLB and its phosphorylated form were assessed in over-expressing cells and found to be unchanged. Using an oxalate-facilitated Ca^{2+} uptake assay in SR vesicles, it was shown that sorcin increased SR uptake via SERCA2a in a dose-dependent manner; the EC_{50} for this effect was 0.52 μmol/L. The addition of 1 μmol/L recombinant sorcin increased the maximal rate of Ca^{2+} uptake by 34% compared to control. The increase in SR uptake was also shown to be Ca^{2+} dependent. The authors conclude that sorcin stimulates SERCA2a indicating a role for sorcin in the maintenance of SR load and Ca^{2+} homeostasis. The stimulatory effect of sorcin on SERCA2a can be criticised, however, for being speculative as the absence of a measure of I_{Ca} or the action potential duration limit an isolated effect of sorcin on the parameters of the Ca^{2+} transient via SERCA2a and SR load. A second study of the effects of over-expression of sorcin in adult rat cardiomyocytes (MOI=20, 48 hr culture) also revealed a significant increase in the Ca^{2+} transient and a 49% increase in SR load. In an attempt to propose a

mechanism for the result, the authors hypothesised that this could be due, in part, to an increase in SERCA2a activity and/or expression (Suarez *et al.*, 2004).

4.1.3.5 Annexin VII

Annexin VII is a member of the annexin family of proteins which is expressed in the heart and, like sorcin, binds to phospholipid membranes in a Ca^{2+}-dependent manner (Brownawell & Creutz, 1997). It has been proposed that the annexin family of proteins exert their effects *in vivo* through their interaction with other proteins. Each annexin has a unique N-terminus sequence and so the interacting protein for each is specific. In the adrenal medulla, the interaction of sorcin with annexin VII (also referred to as synexin) leads to the translocation of sorcin to chromaffin granule membrane where it mediates the inhibition of annexin VII-mediated chromaffin granule aggregation. This association was first shown using extracts of bovine adrenal medulla on an immobilised construct containing annexin VII and overlay procedures using recombinant sorcin. Using deletion mutants, the site of interaction was mapped to the first 31 amino acids of the N-terminus of annexin VII (Brownawell & Creutz, 1997). Similarly, the involvement of the N-terminus of sorcin (residues 1-32) in the interaction with annexin VII was shown using surface plasmon resonance and overlay assay techniques (Verzili *et al.*, 2000). These identified that the SCBD did not associate with annexin VII, therefore indicating the sorcin N-terminal domain as the site of interaction. The binding of sorcin with immobilised annexin VII was shown to be highly dependent on $[Ca^{2+}]$. This was optimal at 6 μmol/L with an equilibrium dissociation constant (K_D) of 0.63 μmol/L but was rapidly reduced as $[Ca^{2+}]$ was decreased to 3 μmol/L. No interaction occurred in the presence of EGTA highlighting that Ca^{2+} is essential for the process. These results reveal that the interaction between sorcin and annexin VII is possible at Ca^{2+} concentrations achieved in subcellular areas such as the dyad or directly below the membrane during the cardiac cycle (Verzili *et al.*, 2000).

The role of the annexin VII-sorcin interaction in the cardiomyocyte is unclear. One suggestion is that annexin VII may regulate sorcin by recruiting it to membrane and localising it to its membrane-bound targets with which it can then associate using its free C-terminus (Brownawell & Creutz, 1997). In

striated muscle, annexin VII is present in the plasma membrane and the T-tubules (Selbert *et al.*, 1995). It has been implicated in the fusion of membranes leading to the possibility that it may order and stabilise membrane into discrete microdomain rafts (Clemen *et al.*, 1999; Gerke & Moss, 2002). One such domain, the lipid raft, exists as a lateral assembly of membrane patches rich in glycolipid and cholesterol and many membrane-associated proteins including annexins are concentrated here (Carozzi *et al.*, 2000; Gerke & Moss, 2002). Lipid rafts may also occur in caveolae which are specialised flask-shaped, sarcolemmal invaginations containing the caveolin proteins; this theory however, remains controversial (Carozzi *et al.*, 2000; Meder & Simons, 2006). The main isoform of caveolae-contained protein expressed in muscle is caveolin-3 (Parton *et al.*, 1997). Caveolae are dense in cholesterol and use of cholesterol-binding agents such as filipin or nystatin leads to the dramatic loss of membrane caveolae indicating their absolute requirement for cholesterol (Carozzi *et al.*, 2000; Bossuyt *et al.*, 2002). The t-tubular system, present in all striated muscle, may be a highly exaggerated form of caveolae and its formation has been reported to involve caveolin mediated raft stabilisation and repeated caveolae formation leading to a distinctly organised membrane region with highly specific lipid and protein composition (Carozzi *et al.*, 2000).

Annexin VII has been shown to co-localise with caveolin-3 and sorcin (Clemen *et al.*, 1999). In addition studies on bovine cardiac membrane vesicles have demonstrated that NCX and caveolin-3 co-immunoprecipitate. NCX possesses five potential caveolin-3 binding sites in the XIP domain and depletion of cholesterol (via β-cyclodextrin) leads to a reduction in the NCX-caveolin-3 interaction and NCX activity (Bossuyt *et al.*, 2002). Together, these findings suggest that a subset of the NCX1 population may be present in membrane caveolae of the cardiomyocyte. This evidence supports a role for annexin VII in the heart of membrane organisation and recruitment of sorcin to caveolae and perhaps t-tubules and may contribute to its regulatory effect on NCX1.

To date, two studies have examined the role of annexin VII using an annexin VII knockout mouse (Srivastava *et al.*, 1999; Herr *et al.*, 2001). The first of these found that complete knockout of the annexin VII gene was lethal at embryonic day 10 due to cerebral haemorrhage (Srivastava *et al.*, 1999). The second study

produced a viable mouse in which complete gene knockout was achieved. On examination of early embryonic isolated cardiomyocytes from these animals, no alteration in resting [Ca^{2+}], Ca^{2+} transient amplitude or [peak Ca^{2+}] were detected. By contrast, adult isolated cardiomyocytes demonstrated a significantly decreased cell shortening-frequency as stimulation frequency was increased compared to controls. The authors suggest that this depression may be attributable to annexin VII's interaction with sorcin and its inhibitory action on RyR2 and LTCC. Although an altered pattern of force-frequency was detected in the knockout compared to the wild type animal, the study provides insufficient data on other parameters involved in EC coupling to attribute the alteration to a specific cause (Herr *et al.*, 2001).

4.1.4 Phosphorylation

Sorcin is the only PEF protein to possess sites for cAMP-dependent protein kinase (PKA) which are localised to the C-terminus (Van der Bliek *et al.*, 1986). Early work by Meyers showed positive phosphorylation of sorcin through the incorporation of ^{32}P when the protein was incubated with PKA (Meyers, 1989). Two putative phosphorylation sites exist here: (i) RYS (residues 147-149) which lies between the F helix and the loop of EF-4 and (ii) RRDS (residues 175-178) which accounts for the last three residues of the G helix and the loop of EF-5. It is most probable that RRDS is the main site for phosphorylation by PKA as it is exposed to solvent and accessible to PKA whilst the other site (RYS) is embedded at the dimer interface. RRDS is in close apposition to an additional arginine (residue 84) which, along with the two contained in the site sequence itself, provide the specificity for the coordination of a phosphate anion. This is then within interacting distance of serine residue 172. By contrast, the RYS phosphorylation site lacks the neighbouring arginine residues for the coordination of phosphate (Ilari *et al.*, 2002). The crystal structures of sorcin and the SCBD suggested that the presence of the N-terminal would decrease the accessibility of the phosphorylation site to solvent, therefore reducing phosphorylation (Zamparelli *et al.*, 2000; Ilari *et al.*, 2002). This theory was tested using back-phosphorylation assays, confirming that this was indeed the case. Native sorcin was phosphorylated approximately twofold slower than the

SCBD indicating that the presence of the N-terminus hinders access of PKA and phosphorylation of sorcin (Ilari *et al.*, 2002; Zamparelli *et al.*, 2000).

Functionally, phosphorylation of sorcin using PKA has been shown to decrease its inhibition of RyR2 in [3H]ryanodine binding assays (Lokuta *et al.*, 1997; Zamparelli *et al.*, 2000; Farrell *et al.*, 2003). This effect was challenged, however, as isolated rat cardiomyocytes over-expressing sorcin showed comparable increases in cell shortening to controls upon exposure to forskolin. Specific inhibition of RyR2 using ryanodine resulted in a decreased cell shortening in these cells and so it was proposed that the modulation of RyR2 by sorcin was, in part, independent of phosphorylation (Frank *et al.*, 2005). It is conceivable that the work of Lokuta *et al.* (1997) is more appropriate as they positively demonstrate phosphorylation of exogenous sorcin by PKA treatment by autoradiography. In addition, the absence of endogenous sorcin in the isolated pig microsomes verified that all sorcin added during experiments was indeed of the phosphorylated form. In the study by Frank *et al.* (2005), phosphorylation of sorcin was not confirmed and interpretation of the result is complicated by the possibility of phosphorylation of other cellular targets such as LTCC.

A recent study has suggested that phosphorylation of sorcin may also regulate the ability to translocate to membrane. This work showed that protein phosphatase 1 (PP1) was capable of de-phosphorylating purified recombinant sorcin in a dose-dependent manner (Matsumoto *et al.*, 2005). Thus phosphorylation/de-phosphorylation processes may modulate the ability of sorcin to interact with membrane-bound targets and account in part for the functional effects observed in response to alterations in phosphorylation status.

4.1.5 Sorcin and the Ca^{2+} transient

The effects of sorcin on the Ca^{2+} transient are controversial and, to date, no one clear message has been determined. Of the five major studies examining the effect of sorcin on the Ca^{2+} transient, three found a decrease (Farrell *et al.*, 2003; Meyers *et al.*, 2003; Seidler *et al.*, 2003) whilst two found an increase (Suarez *et al.*, 2004; Matsumoto *et al.*, 2005). Each of these draws on different

membrane-bound targets for sorcin in an attempt to provide explanation for the observed effect.

Whole-cell patch clamp recordings in isolated mouse ventricular cardiomyocytes revealed a significant decrease in the amplitude and duration of the Ca^{2+} transient and cell shortening when 3 μmol/L sorcin was included in the pipette solution (Farrell *et al.*, 2003). As no significant differences were detected in any parameter of I_{Ca}, the authors speculated that the effect of sorcin on the Ca^{2+} transient was attributable solely to inhibition of RyR2 function and thus sorcin acted to reduce the gain of EC coupling. The study failed to address the contribution of SR Ca^{2+} content to the results and so it is not clear if they were due to an isolated effect on RyR2 or were the result of cumulative alterations in EC coupling. Similarly, whole-cell patch clamp measurements in isolated rabbit cardiomyocytes over-expressing sorcin (MOI=100, 24 hr culture) showed a significant decrease in Ca^{2+} transient amplitude compared to controls ($p<0.05$) (Seidler *et al.*, 2003). The cause for this effect was a reduced SR Ca^{2+} content in sorcin over-expressing cells as a result of increased NCX activity. This was verified by EC coupling gain and Ca^{2+} spark experiments (Seidler *et al.*, 2003). At the single cell level, transgenic mice over-expressing sorcin (20 fold) also demonstrated a significant decrease in Ca^{2+} transient amplitude ($p<0.05$), compared to wild type, using field stimulation over a range of frequencies (e.g. F/F_0 at 0.5Hz; 4.4 ± 0.26 *vs.* 2.4 ± 0.14 respectively $p<0.05$) (Meyers *et al.*, 2003). Increased inactivation of I_{Ca} was detected but once more SR Ca^{2+} content was not measured. It was concluded that acceleration of LTCC inactivation by sorcin would therefore be expected to limit the amount of trigger Ca^{2+} for SR release and, along with sorcin's previously shown inhibitory effect on RyR2 open probability, explain the reduced Ca^{2+} transient amplitude in the model.

Contrary to the above, over-expression of sorcin in adult rat cardiomyocytes (MOI=20, 48 hr culture) revealed a significant increase in the Ca^{2+} transient and a 49% increase in SR load. In sorcin over-expressing cells, the half-time of $[Ca^{2+}]_i$ decline of the transient was significantly reduced (0.32 ± 0.016 *vs.* 0.375 ± 0.018; $p<0.05$) and the time to reach peak systolic Ca^{2+} was significantly increased (0.194 ± 0.004 *vs.* 0.172 ± 0.007; $p<0.001$) compared to controls. Examination of protein expression in the SR rich fraction of these cells revealed

a 71% increase in RyR2, a 3 fold increase in SERCA2a and a 66% increase in PLB. Suggested mechanisms for the increased transient following sorcin over-expression centred on the increased SR load and, in order to account for this, alluded to RyR2 inhibition and a stimulation of SERCA2a activity and/or expression. The authors suggest that sorcin may modulate RyR2 in an analogous way to FKBP (by decreasing RyR2 open probability), reducing SR diastolic leak and thereby further increasing SR Ca^{2+} content leading to a larger transient (Suarez *et al.*, 2004). No direct measurements of RyR2 or SR function were performed in support of this theory and so it remains to be confirmed or refuted (Suarez *et al.*, 2004). In a similar over-expression study in rat cardiomyocytes (MOI=20, 48 hr culture), a significant increase in Ca^{2+} transient amplitude was detected. This was accompanied by a significantly faster time constant of decline of the Ca^{2+} transient in sorcin over-expressing cells compared to controls (0.18 ± 0.01 *vs.* 0.21 ± 0.01 respectively; $p<0.01$). A 43% increase in SR load was also shown in sorcin over-expressing cells and together these results were attributed to a stimulation of SERCA2a by sorcin and increased SR Ca^{2+} load. (Matsumoto *et al.*, 2005). Measurements of I_{Ca} or the action potential duration, which can both alter SR content independently of SERCA2a, were not performed.

4.1.6 Sorcin effects in vivo

Mice from the transgenic mouse model created by Meyers *et al* (2003) exhibited cardiac contractile abnormalities, alluding to a role for sorcin in control of normal contractile functioning *in vivo*. These manifest as a significant decrease in LV contractile and relaxation parameters compared to control. No hypertrophy or alteration in expression of LTCC, RyR2, SERCA2a or PLB occurred in the model and the defects were attributed to RyR2 inhibition and increased inactivation of I_{Ca} (Meyers *et al.*, 2003).

An acute over-expression of sorcin was achieved in mouse whole hearts using adenoviral gene transfer directly into the LV wall (Suarez *et al.*, 2004). This resulted in a 274% increase in sorcin protein expression and a marked increase in contractile functioning of the heart. Hearts over-expressing sorcin exhibited significant increases in peak LV systolic pressure (40%), maximum dP/dt (54%), minimum dP/dt (72%) with no alteration in SERCA2a, RyR2 or PLB levels when

compared to controls. The suggested mechanism for this effect was an increase in Ca^{2+} transient amplitude following sorcin over-expression.

Repeated coronary artery injection (12 days) of sorcin contained within an adenoviral vector led to the production of an in vivo rat model of sorcin over-expression (1.7 fold increase) (Frank *et al.*, 2005). Echocardiography measurements revealed an improved cardiac contractility in animals over-expressing sorcin compared to controls which was independent of β-adrenergic stimulation.

4.1.7 Sorcin in heart failure and cardiomyopathy

The ability of sorcin to modulate intracellular Ca^{2+} in the cardiac cell is well established, yet its precise role in the altered Ca^{2+} handling which occurs in cardiomyopathy and heart failure is complex and poorly understood.

In the spontaneously hypertensive heart failure (SHHF) rat heart it was shown that sorcin and RyR2 did not co-localise at the dyadic junction as occurs in the normal animal. This disorganisation suggested that sorcin may contribute to the altered Ca^{2+} homeostasis in heart failure through an alteration in its effects on the target Ca^{2+} handling proteins (Meyers *et al.*, 2003). The improvements seen by Suarez *et al.* (2004) in the normal mouse led them to explore whether a similar over-expression (adenoviral gene transfer directly into the LV wall) could reverse the contractile abnormalities apparent in the diabetic mouse model of cardiomyopathy. The over-expression procedure resulted in an improvement of contractile function (5 days post-infection) to those comparable with levels in the normal mouse. The effects were most significant in measurements of percentage fractional shortening and velocity of fibre shortening which are in contrast to the transgenic study. The results obtained in single cells over-expressing sorcin showing increased SR Ca^{2+} content were extrapolated up to the whole heart level and proposed as a mechanism for the observed contractile improvement in the diabetic mouse. Increases in SERCA2a and/or inhibition of RyR2 mediated SR leak would serve to increase SR Ca^{2+} load and Ca^{2+} transient amplitude and correct the contractile defect in the diabetic mouse (Suarez *et al.*, 2004).

Additional evidence as to the altered state of sorcin in the failing heart was provided using human left ventricular tissue from patients with and without dilated cardiomyopathy (Frank *et al.*, 2004). Sorcin protein expression was significantly reduced by 35% in whole homogenates from failing hearts compared to controls, yet the amount of sorcin associated with RyR2, assessed by co-immunoprecipitation, was significantly increased ($p<0.05$). Application of recombinant sorcin during ryanodine binding assays revealed a significantly increased inhibition of RyR2 in failing hearts compared to control, indicating that RyR2 in the failing heart was more susceptible to inhibition by sorcin perhaps through the increased association. These findings may contribute to the altered Ca^{2+} homeostasis in dilated cardiomyopathy (Frank *et al.*, 2004). A 33% reduction in sorcin protein was detected in whole homogenates from a rabbit coronary artery ligation model of LVD compared to sham operated animals (Smith *et al.*, 2006). The model also displayed a decrease in NCX activity (Quinn *et al.*, 2003). Work by the same group using adenoviral-mediated gene over-expression in the rabbit showed that sorcin decreased SR content via stimulation of NCX. The lower sorcin expression in LVD may therefore account for the decrease in NCX activity in LVD.

Investigation of the UM-X7.1 cardiomyopathic hamster heart, a model of end-stage heart failure, revealed decreased sorcin expression in whole homogenates (64% *vs.* controls) compared to increased sorcin expression when the SR fraction was examined (105% *vs.* control) (Matsumoto *et al.*, 2005). This finding was also confirmed in Dahl salt-sensitive rats. Expression of RyR2 and SERCA2a were decreased in keeping with previously established data from the same model. Translocation to membrane was shown to occur in response to PKA-mediated phosphorylation (by isoproterenol) which is known to be stimulated in heart failure due to the increased sympathetic drive. PKA-mediated phosphorylation of immunoprecipitated endogenous sorcin from UM-X7.1 hamster hearts was increased compared to control hearts, thus suggesting hyperphosphorylation of sorcin as a mechanism for the increased translocation of sorcin to membrane fractions. This study suggested that sorcin had a stimulatory effect on SERCA2a. An increase in sorcin in SR fractions from heart failure hearts would increase SERCA2a activity, and may contribute as a compensatory mechanism to restore the SR content and help to normalise Ca^{2+} handling in heart failure (Matsumoto

et al., 2005). Significantly increased sorcin (39% *vs.* control) was also detected in a fast paced canine model of heart failure which was associated with a decrease in contractility. Inhibition of RyR2 by the elevated levels of sorcin (as previously shown by (Lokuta *et al.*, 1997)) was presumed to account for a 32% decrease in SR Ca^{2+} release in heart failure cells and hence the depressed contractility present in the model (Farrell *et al.*, 2000). In a rat-aorta banding model of heart failure, sorcin protein expression was increased 3 fold in failing hearts. In an attempt to determine if this increased sorcin was beneficial or detrimental in failing cells, a Herpes Simplex Virus was used as a vehicle to deliver sorcin (to over-express) or its antisense (to reduce expression). Twelve hours following over-expression, Ca^{2+} transients were decreased whereas, at 36 hours post-infection, Ca^{2+} transients were increased compared to controls; ablation of sorcin led to a reduced Ca^{2+} transient amplitude. In this model, it appears that sorcin over-expression may improve EC coupling but that the effect may be time-dependent (Zhu *et al.*, 2003).

Interestingly, a naturally occurring mutation of sorcin (F112L) has been identified in patients from two genetically independent backgrounds with familial hypertrophic cardiomyopathy (FHC) and hypertension. This mutation was shown to cause a reduction in sorcin's translocation to membrane, had no effect on RyR2 channel conductance and demonstrated limited inhibition of SR Ca^{2+} release compared to wild type sorcin (Mohiddin *et al.*, 2002). The mutant's three-dimensional structure was shown to possess a very different conformation to the native protein. The mutation, which exists within EF-3, destabilises the molecule such that the number of hydrophobic residues is reduced, which then leads to the rearrangement of the adjacent EF-hands (Valdivia *et al.*, 2004). This phenylalanine residue at position 112 (F112) in EF-3, the hand established to be critically involved in the coordination of Ca^{2+} by sorcin, would therefore be expected to reduce the binding of Ca^{2+}, interaction with RyR2 and may account for the cardiac abnormalities observed. Further work is required to characterise the effects of this mutation on the processes of EC coupling.

4.1.8 Effect of sorcin - Summary

In general, the literature on the effects of sorcin on contractility and EC coupling is divergent. Table 4.1 on the following page summarises the experimental models, methods and data obtained from the major studies detailed in the previous sections.

Table 4.1 Summary table of sorcin in the normal heart (upper half) and in heart failure/cardiomyopathy (lower half).

References: 1 (Meyers *et al.*, 2003); 2 (Farrell *et al.*, 2003); 3 (Seidler *et al.*, 2003); 4 (Suarez *et al.*, 2004); 5 (Matsumoto *et al.*, 2005); 6 (Frank *et al.*, 2005); 7 (Smith *et al.*, 2006); 8 (Zhu *et al.*, 2003); 9 (Farrell *et al.*, 2000); 10 (Frank *et al.*, 2004). Abbreviations: WH whole homogenate; HSV Herpes Simplex Virus; ? indicates where mechanisms are speculative and no evidence exists in the study to support them. Data on sorcin expression levels are expressed as a fold change *vs.* control.

Species / Model	Sorcin expression level	Contractility	Intracellular targets & effects
Mouse / Transgenic *(in vivo)* [1]	↑ (20x)	↓	↓ RyR2 activity, ↑ LTCC inactivation
Mouse / Recombinant [2]	N/A (exogenously applied)	↓	↓ RyR2 activity
Rabbit / Ad/Sorc [3]	↑ (6x)	↓	RyR2, ↑ NCX activity
Rat / Ad/Sorc [4]	↑ (5x)	↑	↑SR LOAD - ↓ RyR2 activity ∴ ↓ SR leak and ↑ SERCA2a activity &/or expression ?
Rat / Ad/Sorc [5]	↑ (not quantified)	↑	↑ SERCA2a activity
Rat / Ad/Sorc *(in vivo)* [6]	↑ (1.7x)	↑	Modulation of RyR2 or LTCC ?
Mouse / Cardiomyopathy / Ad/Sorc [4]	↑ (3x)	↑	↑SR LOAD - ↓ RyR2 activity ∴ ↓ SR leak and ↑ SERCA2a activity &/or expression ?
Rabbit / LVD [7]	↓ (33 %)	↓	↓ NCX activity
Rat / HF / HSV/Sorc [8]	↑ (not quantified)	12hrs↓, 36hrs↑	Modulation of RyR2 activity
Hamster / Cardiomyopathy [5]	WH ↓ (64 %); SR ↑ (105 %)	↓	^ SERCA2a activity ?
Canine / HF [9]	↑ (39%)	↓	↓ RyR2 activity
Human / HF [10]	↓ (35 %)	↓	↓ RyR2 inhibition

4.1.9 Disparities in the effects of sorcin

The disparities in the reported effects of sorcin are wide (see Table 4.1); possible explanations for the main differences are detailed below.

4.1.9.1 Failure to assess SR Ca^{2+} content

It is generally accepted that sorcin modulates RyR2 function yet a major flaw of some studies investigating the effects of sorcin on cardiac contractility and the Ca^{2+} transient is their lack of information on the Ca^{2+} content of the SR (Meyers *et al.*, 2003; Farrell *et al.*, 2003). In the steady state, the magnitude of the Ca^{2+} transient is regulated by I_{Ca} and SR Ca^{2+} content as well as by the properties of RyR2 (Eisner & Trafford, 2000). It is therefore imperative to assess the SR content when determining the effect an intervention, in this case sorcin, has on the Ca^{2+} transient. The Ca^{2+} contained within the SR has a direct impact on the open probability of RyR2 and hence the amount of Ca^{2+} it releases in response to the $[Ca^{2+}]$ of I_{Ca} (Gyorke & Gyorke, 1998). A higher SR content will increase sensitivity of RyR2 to the cytosolic $[Ca^{2+}]$ trigger. Therefore, in order to say that sorcin exerts an effect on the transient via RyR2 alone, one must determine if there are parallel changes in SR content. Again, it is difficult to support suggestions that sorcin affects the "gain" of EC coupling (Farrell *et al.*, 2003) in the absence of data on SR content as gain is determined by both I_{Ca} and SR content.

Factors which themselves contribute to SR content have not been assessed in a number of studies. Firstly, the action potential duration was not determined in cardiomyocytes in which transients were measured without the use of voltage-clamp (Meyers *et al.*, 2003; Suarez *et al.*, 2004; Matsumoto *et al.*, 2005). An alteration in action potential duration can affect the SR content via Ca^{2+} flux on NCX. For example, a decrease in action potential duration in response to sorcin, as seen by Seidler *et al.*, (2003), would be expected to increase efflux as the period of time at negative potentials would be greater. Secondly, the properties of I_{Ca} were not assessed in both papers reporting an increase in transient/contractility in response to sorcin (Suarez *et al.*, 2004; Matsumoto *et al.*, 2005). The characteristics of I_{Ca} are fundamental to the transient and affect

SR content via $[Ca^{2+}]_i$. I_{Ca} must be measured in order to account for alterations in the amount of trigger Ca^{2+} which would also affect the degree of activation of RyR2-mediated SR release. The failure of the above studies to investigate all the integral processes contributing to Ca^{2+} cycling precludes a direct comparison of their results on contractility.

4.1.9.2 Experimental method

The experimental method and exposure time used to introduce sorcin protein in each study varies enormously (i.e. acute *vs.* chronic exposure). This may also contribute to some of the differences in the results obtained. Three studies utilised *adenoviral-mediated over-expression* in single isolated ventricular cardiomyocytes over either 24 or 48 hr (Seidler *et al.*, 2003; Suarez *et al.*, 2004; Matsumoto *et al.*, 2005). The *transgenic approach*, adopted by Meyers *et al*, (2003) involved a prolonged exposure to sorcin throughout the mouse's development up to the age of sacrifice (4-6 months) (Meyers *et al.*, 2003). Although the expression levels of many of the Ca^{2+} regulatory proteins (RyR2, SERCA2a, PLB, Cav1.2 subunit of LTCC and CSQ) were reported to exhibit no significant changes, the authors do state that significance was not reached in all comparisons. Additional adaptive changes in the transgenic mouse compared to the wild-type cannot be ruled out as the gene for sorcin is up-regulated from the mouse's conception. The relative contribution of this genetically modified gene throughout development may lead to alterations other than sorcin over-expression in the adult, thereby making the transgenics difficult to interpret. More invasive methods have also been used to over-express sorcin via *adenoviral-mediated transfer* in order to assess *in vivo* effects (Suarez *et al.*, 2004; Matsumoto *et al.*, 2005; Frank *et al.*, 2005). The coronary artery injection technique employed by Frank *et al*, (2005) in the rat took place over twelve days using a catheter inserted into the aorta. Mice with diabetic cardiomyopathy were administered a bolus dose of adenovirus into five sites of the LV wall (Suarez *et al.*, 2004).

In addition to the differing methods used to introduce sorcin, differences also exist in the methods used to assess the effect of sorcin on contractility. Ca^{2+} transients in single cells were measured using two main approaches: (i)

fluorescence and field stimulation (Meyers *et al.*, 2003; Suarez *et al.*, 2004; Matsumoto *et al.*, 2005) and (ii) fluorescence and voltage-clamp (Farrell *et al.*, 2003; Seidler *et al.*, 2003). Field stimulated studies of the Ca^{2+} transient have involved confocal microscopy and fluo-3 AM (Meyers *et al.*, 2003), epifluorescence microscopy and indo-1 (Suarez *et al.*, 2004) and dual fluorescence with fura-2 AM (Matsumoto *et al.*, 2005). As previously mentioned, this approach does not allow for variations in action potential duration which can alter the Ca^{2+} transient. The use of voltage-clamp provides a more robust indication of alterations to the transient as action potential duration is fixed by the protocol (Farrell *et al.*, 2003; Seidler *et al.*, 2003). Frank *et al*, (2005) only provided fractional shortening data in response to sorcin over-expression which, in the absence of measurement of the Ca^{2+} transient, are insufficient to determine an increase in contractility (Frank *et al.*, 2005).

Of the *in vivo* studies, Suarez *et al.*, (2004) assessed contractility in the isolated Langendorff perfused heart 5 days post sorcin transfection. The heart was electrically paced at 400 beats/min and pressures were assessed via an intraventricular balloon. Frank *et al*, (2005) used only echocardiography to assess contractile function and whilst other studies also utilised this technique, information on the Ca^{2+} transient was also presented (Meyers *et al.*, 2003).

Finally, the cause of heart failure or cardiomyopathy may affect the results relating to sorcin expression. Of the studies conducted, no two have employed the same type of heart failure/cardiomyopathy or species.

4.1.9.3 Concentration of sorcin

The concentration of sorcin achieved in the cardiomyocyte is yet another potential variable between studies. Extremely high levels of sorcin were achieved using the transgenic method (20 x higher than wild-type) (Meyers *et al.*, 2003). This far exceeds any of the other studies examining sorcin's effects (see Table 4.1). Two of the investigations of adenoviral-mediated over-expression in single cells yielded comparable levels of over-expression (5-6 fold increase *vs.* control) whilst sorcin protein expression was not quantified in the third (Seidler *et al.*, 2003; Suarez *et al.*, 2004). On the other hand, the study by

Frank *et al*, (2005) led to a surprisingly low level of sorcin over-expression (1.7 x increase) using an adenoviral method. This variability has been drawn on by authors in an attempt to explain the inconsistencies between results (Frank *et al.*, 2005). It has been proposed that sorcin may exhibit a "dose-related effect" where low levels such as Suarez *et al*, (2004) and Frank *et al*, (2005) may increase Ca^{2+} release whilst higher levels such as Meyers *et al*, (2003) may reduce release. Such an elementary explanation seems improbable as both Suarez *et al*, (2004) and Seidler *et al*, (2003) achieved comparable levels of protein with opposing effects on Ca^{2+} release. Some degree of dose-dependence may contribute to the effect of sorcin, however, as the inhibition of RyR2 has been shown to be dose-dependent (Lokuta *et al.*, 1997).

4.1.9.4 Species variation

The use of different species to study the effects of sorcin further complicates the comparison of results. For example, many of the targets for sorcin have only been shown in one particular species (e.g. SERCA2a, NCX, I_{Ca}), therefore there may be alternative targets for sorcin to interact with in different species. Differences in the Ca^{2+} handling between species also exist. For example, during systole in the rabbit approximately 70% of the $[Ca^{2+}]_i$ is released from the SR; in the rat this figure is increased to approximately 90% (Bers, 2001). The relative importance sorcin has to contractility may be dependent on the Ca^{2+} handling of each particular species.

4.2 Aims

The aims of the present chapter were as follows:

1. To quantify endogenous sorcin levels in the whole LV homogenates from rabbits with and without LVD using quantitative Western blotting techniques.

2. To assess whether sorcin protein expression is altered in LVD compared to sham.

3. To ascertain if a physical interaction exists between sorcin and NCX in the cardiomyocyte.

4.3 Methods

4.3.1 Quantification of sorcin expression – experimental approach

The study of sorcin protein expression in rabbit left ventricular homogenates (sham operated and LVD) was carried out using two different primary antibodies directed against sorcin. Firstly, a commercially available monoclonal mouse anti-sorcin primary (Zymed, raised against the N-terminus) and secondly a rabbit anti-sorcin primary antibody (gifted from H.H.Valdivia, University of Wisconsin-Madison, raised against the C-terminus). With the gel system and buffers employed, the sorcin monomer ran at approximately 22 kDa whilst the sorcin dimer ran at approximately 44 kDa. The monoclonal primary only detected the sorcin dimer with negligible signal at the level of the monomer. This primary was unstable throughout the course of the investigation and was subject to substantial degradation. The study was repeated using the polyclonal primary which detected both sorcin monomer and dimer.

Sorcin bands detected using both antibodies were normalised to the 52 kDa band of the protein GAPDH from the same lane as an internal standard (see 2.3.1.1). A sample of purified recombinant sorcin (gifted from E.Chiancone, Universita' La Sapienza, Rome) was used as a positive control for verification of signals.

Details of homogenate preparation, estimation of protein content and all solutions used are listed in Chapter 2, General methods. An overview of the techniques of quantitative western blotting and co-immunoprecipitation can also be found there (2.3.1.1 and 2.3.3 respectively).

4.3.2 Production of recombinant sorcin

The recombinant sorcin was produced by Prof. Emilia Chiancone's group (Universita' La Sapienza, Rome) according to methods detailed previously (Meyers *et al.*, 1995b).

Full-length sorcin cDNA was obtained from a colchicine-resistant Chinese hamster ovary library. This was then amplified by polymerase chain reaction (PCR), digested using restriction enzymes and ligated into the T7 expression vector (Figure 4.3).

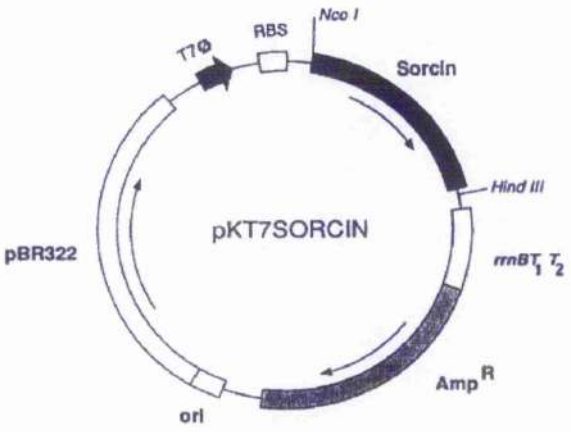

Figure 4.3 Sorcin prokaryotic vector pKT7SORCIN.

Plasmid diagram showing insert of sorcin gene (black). Ori-plasmid origin of replication; Amp^R-ampicillin resistance gene; rrnBT1T2-transcript terminators; T7∅-T7 promoter. Figure taken from Meyers *et al.*, (1995b).

The pKT7SORCIN construct was then transformed in *E.Coli* and PCR was used to verify inclusion of the correct insert. Bacteria were grown and harvested. Sorcin protein was purified via chromatography and frozen at -80 °C until required. The concentration of the recombinant protein was determined spectrophotometrically at 280 nm.

4.3.3 Electrophoresis and quantitative Western blot analysis

Electrophoresis was carried out according to the method of Laemmli (1970); 10 well 10% Bis-Tris gels were used throughout. All homogenate and recombinant samples were prepared in 4 X Laemmli sample buffer and were exposed to 70 °C for approximately 10 min prior to loading to ensure proteins were run under reducing conditions. Molecular weight markers (Invitrogen Ltd., U.K.) were added (5 μl) typically into lane one of the gel in order to identify bands and also to provide a marker (52 kDa) under which membranes were later cut following transfer.

In the case of the monoclonal primary, sham and LVD samples were assigned into pairs in a random fashion. Onto each gel, a sham sample (4, 6, 8 and 10 μg loads) and its corresponding LVD sample (4, 6, 8 and 10 μg loads) were loaded. A sample of recombinant sorcin (5 ng) was added into the final lane.

SDS-PAGE was performed by exposure of each gel to a constant voltage of 200 V for 45 min on ice. Protein transfer to a nitrocellulose membrane was achieved using a wet blotter in transfer buffer. The membrane was notched at the level of the 52 kDa marker and blocked for 1 hour at room temperature in blocking buffer. The membrane was then cut in half horizontally in line with the 52 kDa notch. Blots were incubated at 4 ^{o}C overnight in (i) monoclonal mouse anti-sorcin primary antibody (1:1000, Zymed) for the lower half of the membrane and (ii) monoclonal mouse anti-GAPDH antibody (1:20000, Abcam) for the upper half both in antibody incubation buffer.

The following day membranes were washed for three five-minute periods in the order rinse buffer, high-salt rinse buffer, rinse buffer. Both halves of membrane were incubated separately at room temperature for 1 hour in anti-mouse horseradish peroxidase conjugated secondary antibody (1:10000, Amersham) in antibody incubation buffer. After this time had elapsed, membranes were washed three times (as before). Detection and visualisation of bands was performed using chemiluminescence (Enhanced chemiluminescence (ECL) detection system, 1 min, Amersham) and autoradiographic film. Exposure time was commonly 15 min and films were developed using a Kodak X-OMAT (ME-3). Technical staff from a neighbouring department performed a regular quality assurance programme on the developer.

Studies utilising the polyclonal primary were carried out exactly as above with the following alterations:

- Gels were run with only one load of each sample (10 μg) due to time constraints of the project. LVD and sham samples were alternated across each gel in order to minimise variance attributable to the gel itself or to the efficiency of transfer. The n number was increased from 8 (in the monoclonal

study) to 15 due to the production of additional samples in the time between the two studies.

- The primary antibody used for the lower half of the membrane was polyclonal rabbit anti-sorcin (1:6000) in antibody incubation buffer.

- The secondary antibody used for the lower half of the blot was anti-rabbit horseradish peroxidase (1:10000, Sigma) in antibody incubation buffer.

4.3.4 Densitometry and analysis for sorcin

Quantification of the monomeric (polyclonal primary only) and dimeric forms of sorcin (both primaries), which run at approximately 22 and 44 kDa respectively using this gel system, was performed by scanning developed immunoblots into an Imaging Densitometer. The files containing the scans were then imported into Quantity One (BioRad), analysed and a mean optical density for each band was produced. All signals were normalised against the corresponding GAPDH band (52 kDa) from the same lane.

4.3.5 Statistical analysis

Results for protein quantification were expressed as the mean fraction of LVD:sham. A two-tailed paired Student's T-test (monoclonal study) and a two-tailed unpaired Student's T-test (polyclonal study) were used to indicate statistical significance between each sham and LVD group ($p<0.05$).

4.3.6 Sorcin-NCX co-immunoprecipitation

Investigation of the physical interaction between sorcin and NCX using Co-immunoprecipitation was performed by Dr Susan Currie, University of Glasgow.

Left ventricular whole homogenates were produced as previously described for sorcin (section 2.3.5.1 and 2.3.6.1) with the inclusion of 1% glycerol in the buffer according to the methods of Currie *et al.*, (2004). The homogenate was centrifuged at 45 000 *g* for 10 min at 4 °C, the supernatant was removed and the pellet was re-suspended in solubilisation buffer (50 mmol/L HEPES, 100mmol/L

NaCl, 1% CHAPS, 1% glycerol and 100 µl protease inhibitors) (Currie *et al.*, 2004). From this, membrane associated proteins were extracted using the ProteoExtract native membrane protein extraction kit (Calbiochem). This is a highly selective method of yielding membrane-associated proteins in their native state. Protein G-sepharose was produced by adhering protein G onto sepharose beads in order to immobilise it on an insoluble matrix. The extracts for immunoprecipitation were first pre-cleared with protein G and sepharose beads. Pre-clearing aims to purify the extract and lower the amount of non-specific contaminants (proteins with high affinity for protein G). A set of extracts which did not undergo the pre-clearing step were run also as a control. NCX protein was immunoprecipitated from samples by incubating them with NCX antiserum (1:5000, Swant) overnight at 4 °C. It is generally the case that polyclonal antibodies work best for immunoprecipitation as they have greater affinity for protein G; in keeping with this, a monoclonal antibody from Swant was found to be ineffective for the protocol.

Immunoprecipitated protein was captured using the protein G-sepharose beads. After several high-stringency washes, the immunoprecipitated protein was extracted from beads by heating at 75 °C for 15 min. Immunoprecipitates were subject to SDS-PAGE using the NuPAGE system (Invitrogen Ltd., U.K.) on either 3-8% Tris-Acetate gels for NCX with monoclonal anti-NCX (1:1000, Swant) or 12% Bis-Tris gels for sorcin with polyclonal anti-sorcin (1:6000, gift from H.H. Valdivia).

Further controls were produced by running non-immunoprecipitated extracts from the same samples in parallel on both gels and probed for either NCX or sorcin as above.

4.4 Results

Assessment of total protein in left ventricular homogenates from sham and LVD rabbits was performed using the Bradford Assay as detailed in General methods (see 2.3.6.3). The average total protein in the left ventricular homogenates produced was 10.7 ± 0.6 mg/mL.

Antibody dilutions and exposure times were optimised for immunoblotting using each primary and corresponding secondary such that blots were clear and non-specific binding was minimised.

4.4.1 Detection of sorcin in ventricular homogenates

To determine the full profile of signals detected by each primary antibody, ventricular homogenates were subject to SDS-PAGE and the entire membrane was probed with either the monoclonal or polyclonal primary and corresponding secondary antibody. Through inclusion of recombinant sorcin protein and molecular weight markers, the bands corresponding to monomeric and dimeric sorcin were established from each. Both monoclonal and polyclonal primary antibodies detected a spectrum of bands from the homogenate as shown in Figure 4.4. Strong signals for the sorcin dimer were obtained using both primaries yet only the polyclonal detected sorcin monomer from the homogenate sample. Bands of molecular weights other than these were also highlighted; in particular a band was obtained at approximately 52 kDa by the polyclonal. Using both antibodies, the recombinant sorcin was detected predominantly as monomer.

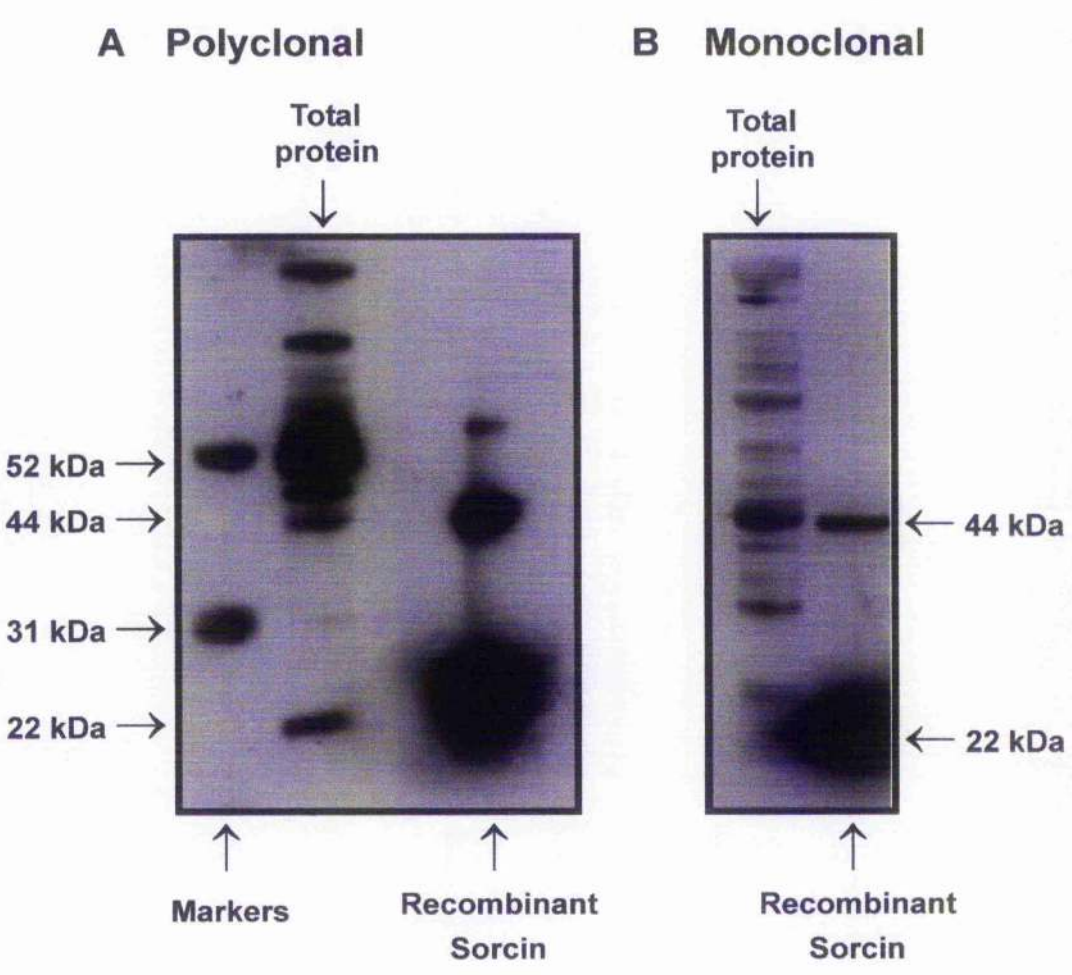

Figure 4.4 Comparison of complete banding profile obtained when probing rabbit left ventricular homogenate with monoclonal and polyclonal anti-sorcin antibodies.

A The immunoblot shows a sample of left ventricular homogenate (total protein, 10 μg) probed with a polyclonal anti-sorcin primary antibody. Molecular weight markers (lane 1) and recombinant sorcin (lane 4; 100 ng) were included. Arrows at 44 and 22 kDa represent the level of sorcin dimer and monomer respectively. Marker bands at 52 and 31 kDa are included for orientation.

B As A; immunoblot with homogenate (10 μg) loaded in lane 1 and recombinant protein (100 ng) in lane 2 but probed with a monoclonal anti-sorcin primary antibody. 44 and 22 kDa arrows indicate positions of sorcin dimer and monomer respectively. A band corresponding to the sorcin monomer (22 kDa) was absent in the homogenate sample.

4.4.2 Verification of denaturing conditions

The inability of the monoclonal anti-sorcin primary to detect sorcin monomer from homogenate may have been due to insufficient denaturing of proteins prior to gel electrophoresis. This was investigated through the inclusion of 5% (w/v)

beta-mercaptoethanol (β-ME) in the sample buffer. β-ME is an alternative reducing agent often employed in Western blotting protocols instead of DTT. An example of an immunoblot in which β-ME was included is presented below in Figure 4.5.

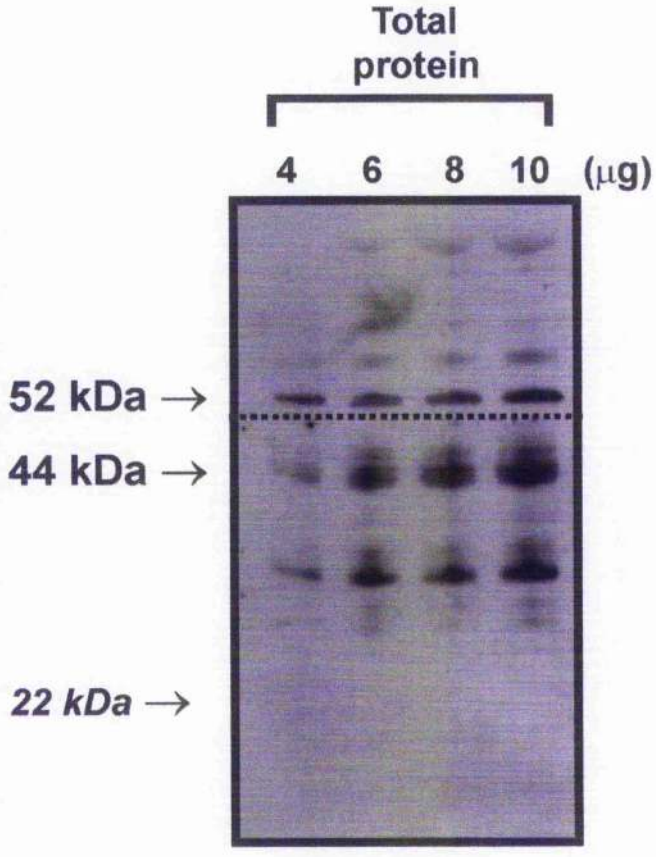

Figure 4.5 Efficiency of β-mercaptoethanol at denaturing the sorcin dimer.

Example immunoblot in which β-mercaptoethanol (β-ME; 5%) was added to the sample buffer prior to electrophoresis. Total protein was loaded into each of the four lanes as indicated (4-10 μg) and the membrane was probed with monoclonal anti-sorcin primary (bottom half) and anti-GAPDH (top half). Clear bands corresponding to the sorcin dimer (44 kDa) and GAPDH (52 kDa) are shown; arrows as previously. The inclusion of β-ME did not yield a detectable monomer signal (22 kDa level).

The inclusion of the additional reducing agent β-ME to the homogenate sample did not result in a detectable monomer signal. As it was of no advantage, this step was omitted from all subsequent Western blots.

4.4.3 Degradation of monoclonal anti-sorcin primary

The study began using the commercially available monoclonal anti-sorcin primary. However, a deterioration of the signals obtained became apparent approximately eight months into the study compared with those from the beginning. This difference was demonstrated by producing blots using the same sample probed at the start of the study then seven months on following storage at -80 °C as shown in Figure 4.6.

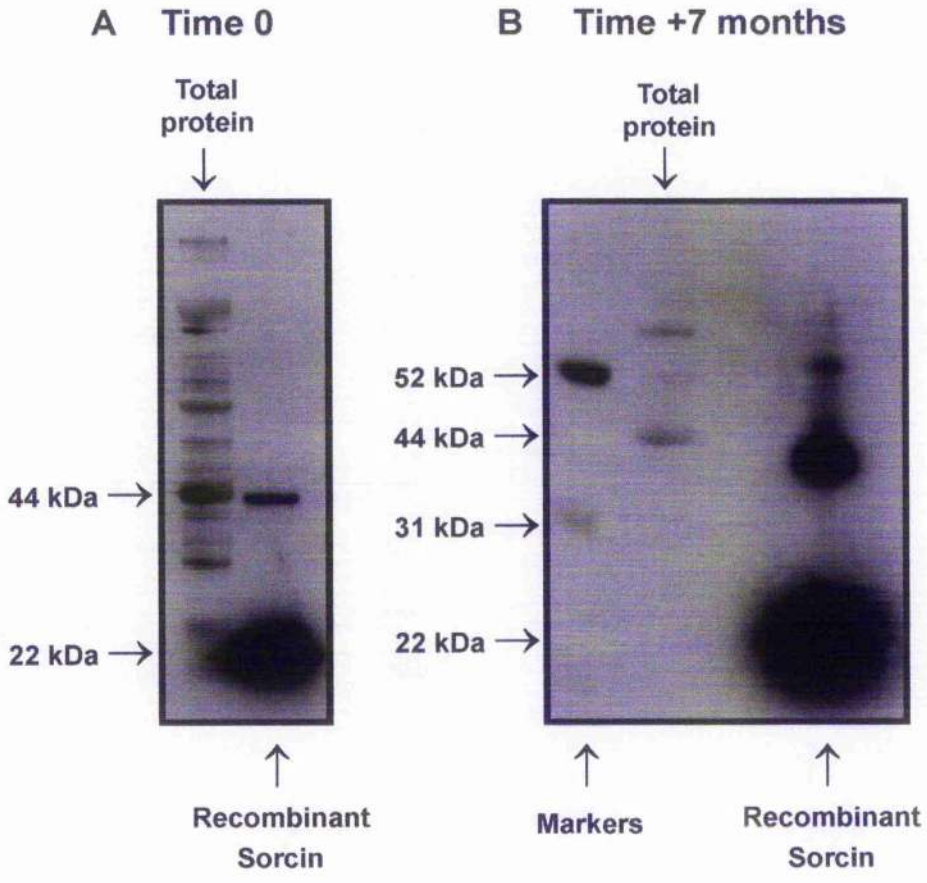

Figure 4.6 Degradation of the monoclonal primary.

A Example immunoblot of the complete profile obtained when probing ventricular total protein homogenate (10 μg) with the monoclonal anti-sorcin primary at the start of the study (Time 0). Recombinant protein and arrows at 44 and 22 kDa indicating sorcin dimer and monomer as previously.

B Immunoblot of the same total protein homogenate preparation (lane 2), molecular weight markers (lane 1) and recombinant protein (lane 4) probed for sorcin using the monoclonal primary antibody 7 months into the study (Time 7 months). Arrows as previously.

Barely any bands were obtained after 7 months storage. One explanation for the discrepancy was the possibility that homogenate samples were degrading whilst stored at -80 °C over this timescale. In order to investigate this, an immunoblot was performed using a sample which had been freshly prepared and samples which had been stored for varying time periods (5, 8 and 10 months) with the polyclonal anti-sorcin primary (Figure 4.7).

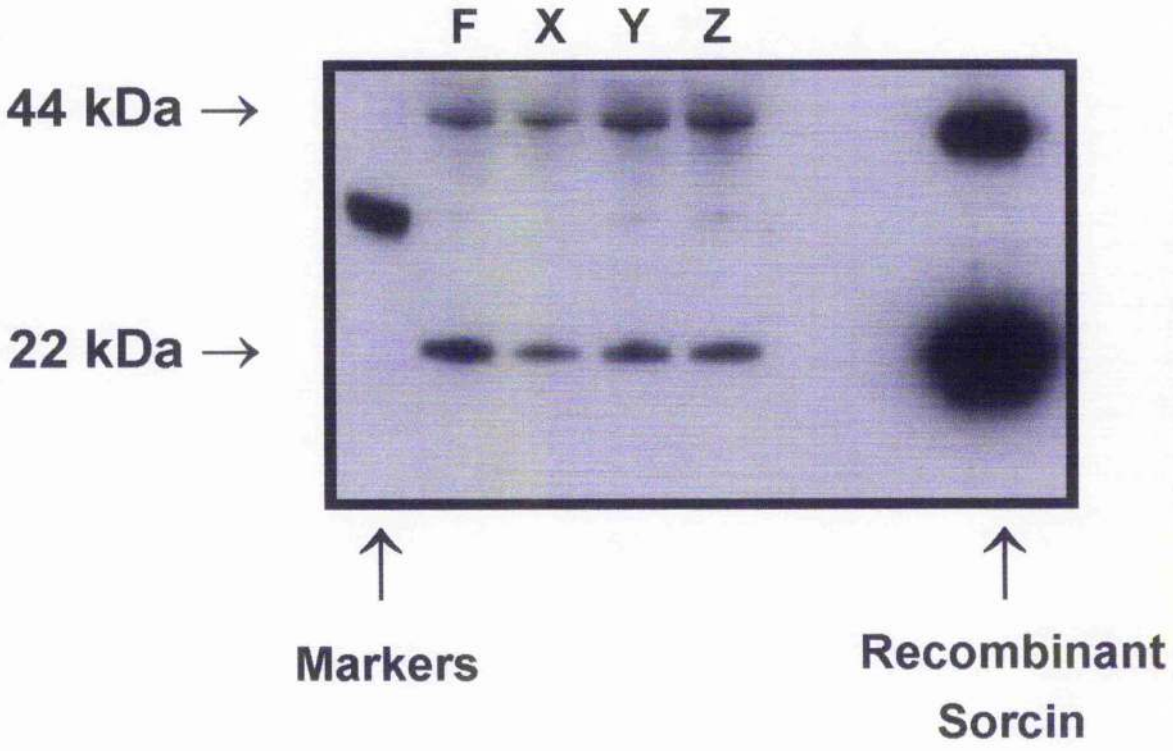

Figure 4.7 Effect of storing homogenates at - 80 °C.

Immunoblot shows a fresh homogenate preparation **(F)** and three prepared previously and stored at -80 °C for 11 months **(X)**, 8 months **(Y)** and 5 months **(Z)** (lanes 2-5) probed for sorcin using the polyclonal primary antibody. Markers and recombinant sorcin (220 ng) were included in lanes 1 and 8 for reference. Bands at 22 and 44 kDa correspond to sorcin dimer and monomer respectively.

The results showed no signs of deterioration in the intensity of monomer and dimer bands following long-term storage and thus the effects seen in Figure 4.6 could be attributed to the monoclonal anti-sorcin primary antibody itself.

4.4.4 Quantification of sorcin expression using a monoclonal primary

Western blotting using the monoclonal anti-sorcin antibody was performed on left ventricular homogenate samples from sham and LVD rabbits as described previously. A typical blot is shown in Figure 4.8; bands for sorcin and GAPDH are labelled. As no significant signals were detected at the level of the monomer using this primary, only the dimer signal was normalised and quantified.

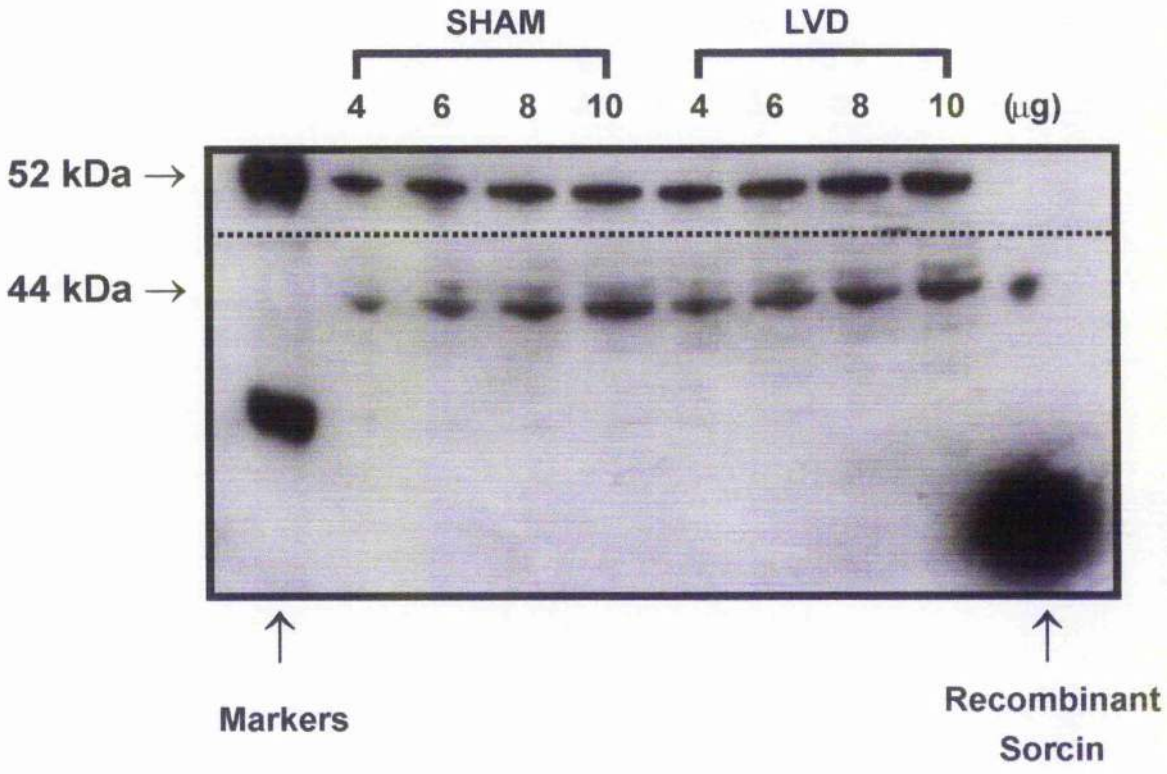

Figure 4.8 Typical immunoblot probed for sorcin and GAPDH using a monoclonal primary antibody.

The blot shows left ventricular homogenates from sham and LVD rabbits (lanes 2-9) in increasing loads (4-10 μg as indicated). Molecular weight markers (lane 1) and recombinant sorcin (lane 10, 50 ng) were included. The area above the dotted line was probed with anti-GAPDH primary antibody; the area beneath was probed with a monoclonal anti-sorcin primary antibody. Bands visible at the 44 kDa level represent the sorcin dimer; no signals were obtained for sorcin monomer. The line of bands at 52 kDa represent the corresponding GAPDH signals to which all sorcin bands were normalised.

4.4.5 Quantification of sorcin expression using a polyclonal primary

Once it had been established that the monoclonal primary was unstable an alternative in-house polyclonal anti-sorcin primary antibody was selected. The quantification study was then repeated using this as described earlier in 4.3.3. Figure 4.9 is an example immunoblot showing the bands obtained. The polyclonal primary detected the monomer and dimer, so both these signals were quantified and normalised

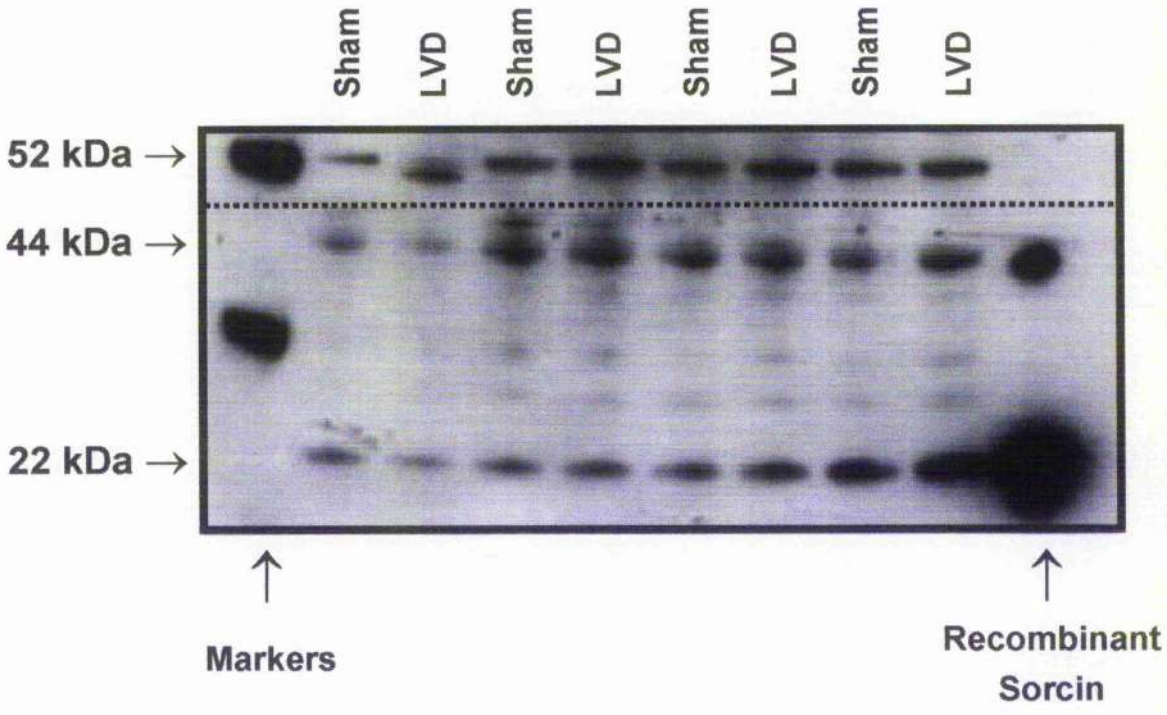

Figure 4.9 Typical immunoblot probed for sorcin and GAPDH using a polyclonal primary antibody.

The blot shows left ventricular homogenates from sham and LVD rabbits (alternate lanes 2-9, all 10 μg). Molecular weight markers (lane 1) and recombinant sorcin (lane 10, 100 ng) were included. The area above the dotted line was probed with anti-GAPDH primary antibody; the area beneath was probed with a polyclonal anti-sorcin primary antibody. Bands visible at the 44 kDa and 22 kDa levels represent the sorcin dimer and monomer respectively. The bands at 52 kDa represent the corresponding GAPDH signal to which all sorcin bands were normalised.

4.4.6 Sorcin expression levels in ventricular homogenates

The data from a number of experiments using both antibodies were analysed and subject to statistical testing as detailed previously 4.3.5.

The overall results obtained for sorcin protein expression using each primary antibody are presented in Figure 4.10. A significant decrease in sorcin dimer expression in LVD *vs.* sham was detected when probing ventricular homogenates with both anti-sorcin primary antibodies. Each primary antibody detected a comparable decrease in sorcin dimer of approximately 33% *vs.* sham (± 0.11; n=8 for the monoclonal; ± 0.05; n=15 for the polyclonal). There was no significant difference in the levels of sorcin monomer between sham and LVD (polyclonal only) although a trend to decrease in LVD was observed.

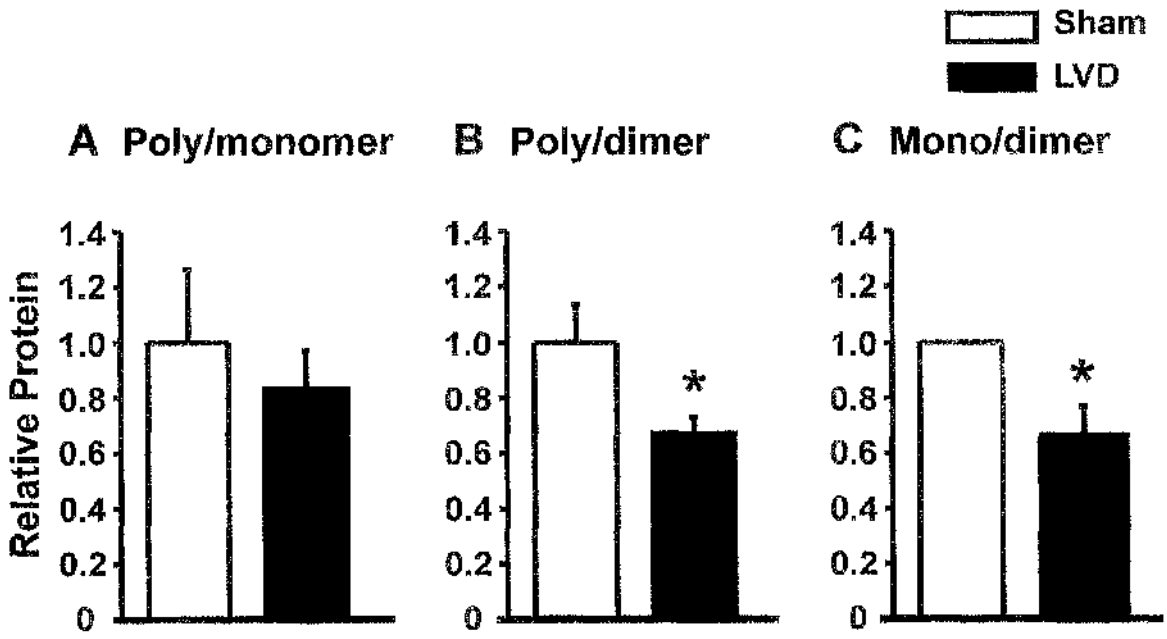

Figure 4.10 Sorcin protein expression relative to GAPDH in sham and LVD left ventricular homogenates based on immunoblot density.

Mean ± SEM sorcin protein expression in left ventricular homogenates (sham in white and LVD in black) assessed by immunoblot using two types of primary antibody. All sorcin protein levels were normalised to GAPDH. **A** sorcin monomer expression using a polyclonal primary (n = 15), **B** sorcin dimer expression using a polyclonal primary (n = 15) and **C** sorcin dimer expression using a monoclonal primary (n = 8).

4.4.7 Echocardiographic parameters

Following a post-operative eight-week recovery period, the rabbits' *in vivo* echocardiographic parameters were assessed as detailed in general methods (2.1.1). Of the measurements taken, % ejection fraction (EF), left atrial dimension (LAD) and left ventricular end diastolic dimension (LVEDD) are the most commonly cited parameters to indicate morphological changes and thus cardiac function. The data from each sham and LVD group for each antibody were averaged and are presented in Figure 4.11 for comparison.

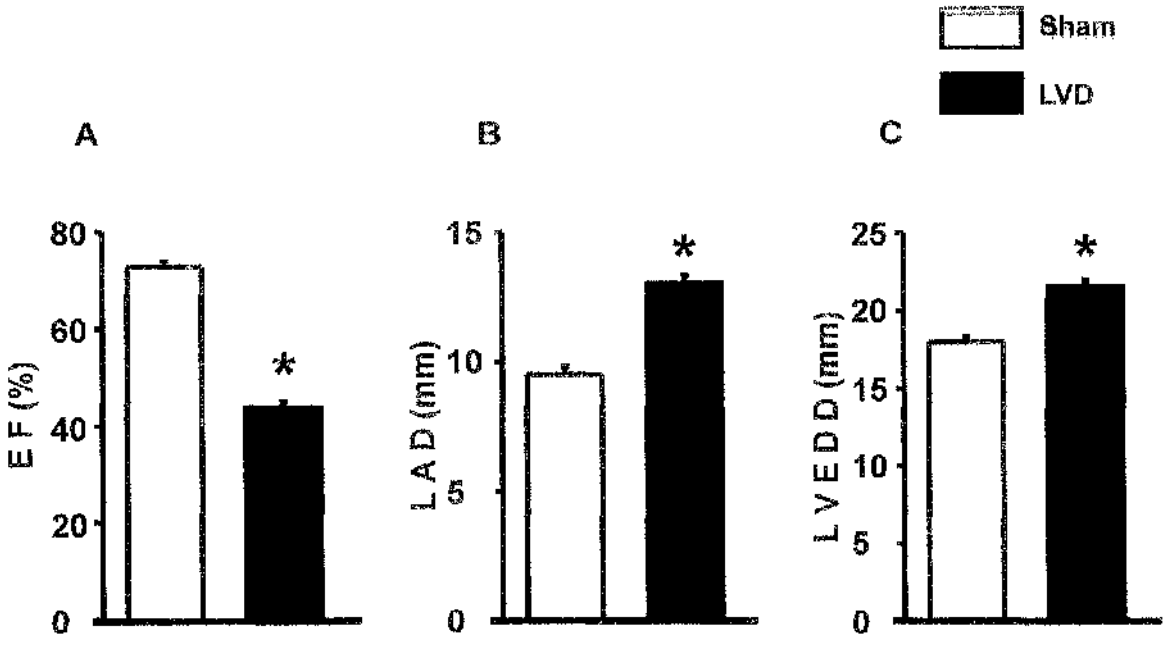

Figure 4.11 Comparison of echocardiographic parameters of sham and LVD animals.

Graphs of sham *vs.* LVD means for A Ejection fraction (%; EF), B Left atrial dimension (mm; LAD) and C Left ventricular end diastolic dimension (mm; LVEDD). LVD was characterised by a significantly decreased EF and significantly increased LAD and LVEDD; * $p<0.001$ in all cases.

The three main echocardiographic parameters (EF, LAD and LVEDD) were plotted for the animals used in the monoclonal (Figure 4.12) and polyclonal (Figure 4.13) sorcin expression studies to see if any correlations existed between sorcin levels and the degree of failure. As can be seen from these figures, no relationship between sorcin protein and EF, LAD or LVEDD was evident. No significant differences existed between sham and LVD for the echocardiographic parameters of hearts used for sorcin expression measurements in either the

monoclonal or polyclonal antibody studies (p=0.35-0.98). As Figure 4.11 shows, significant differences existed between sham and LVD means for EF, LAD and LVEDD indicating substantial impairment in cardiac function in the LVD group vs. sham.

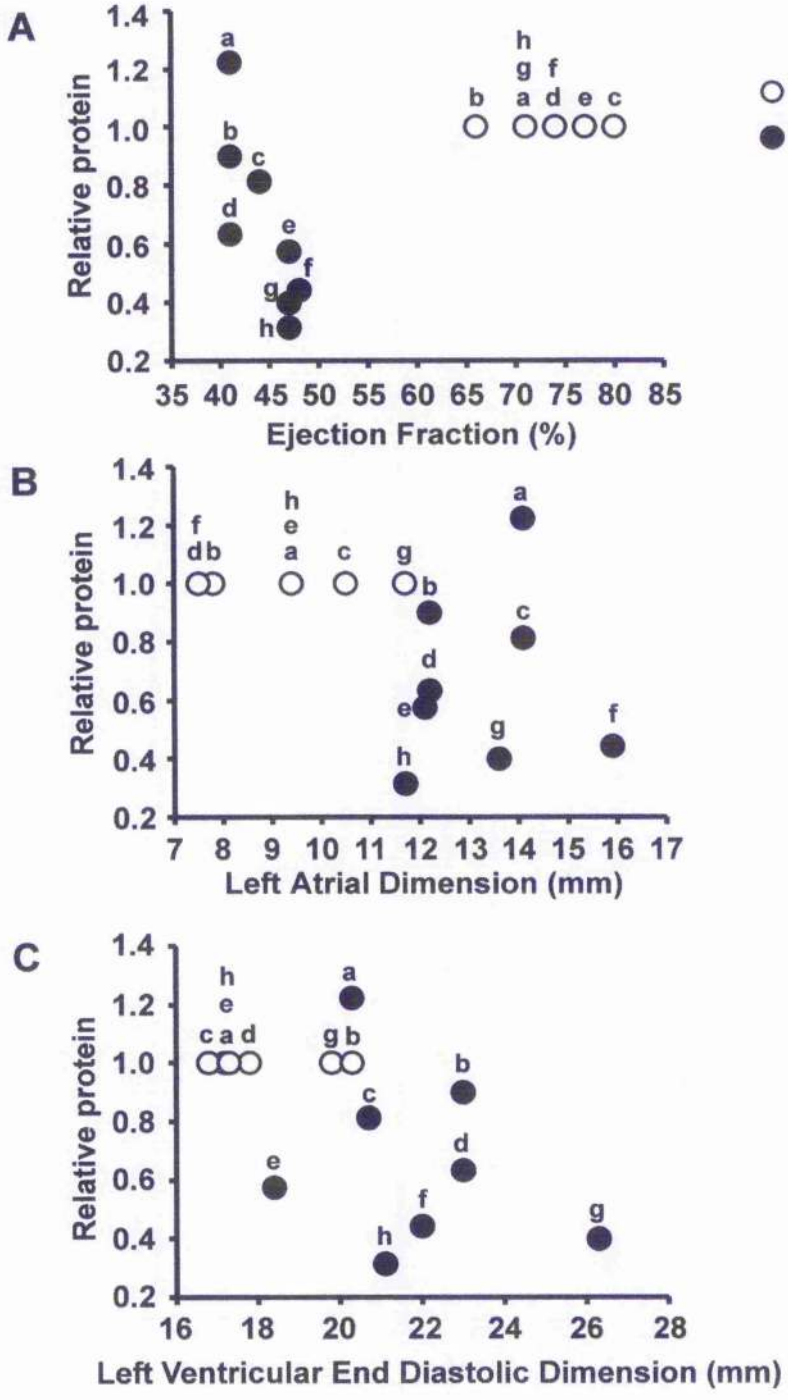

Figure 4.12 Relationship between sorcin and echocardiographic parameters in the monoclonal study.

Graphs of relative protein *vs.* **A** % ejection fraction, **B** left atrial dimension (mm) and **C** left ventricular end diastolic dimension (mm) for each animal used in the monoclonal sorcin expression study. Sham (o) and LVD (•) animals were paired up on each gel and LVD protein was expressed as a fraction of sham; letters (a-h) denote paired animals on Western blot. No significant correlations exist between sorcin expression levels detected using the monoclonal primary and any of the parameters (EF, LAD or LVEDD).

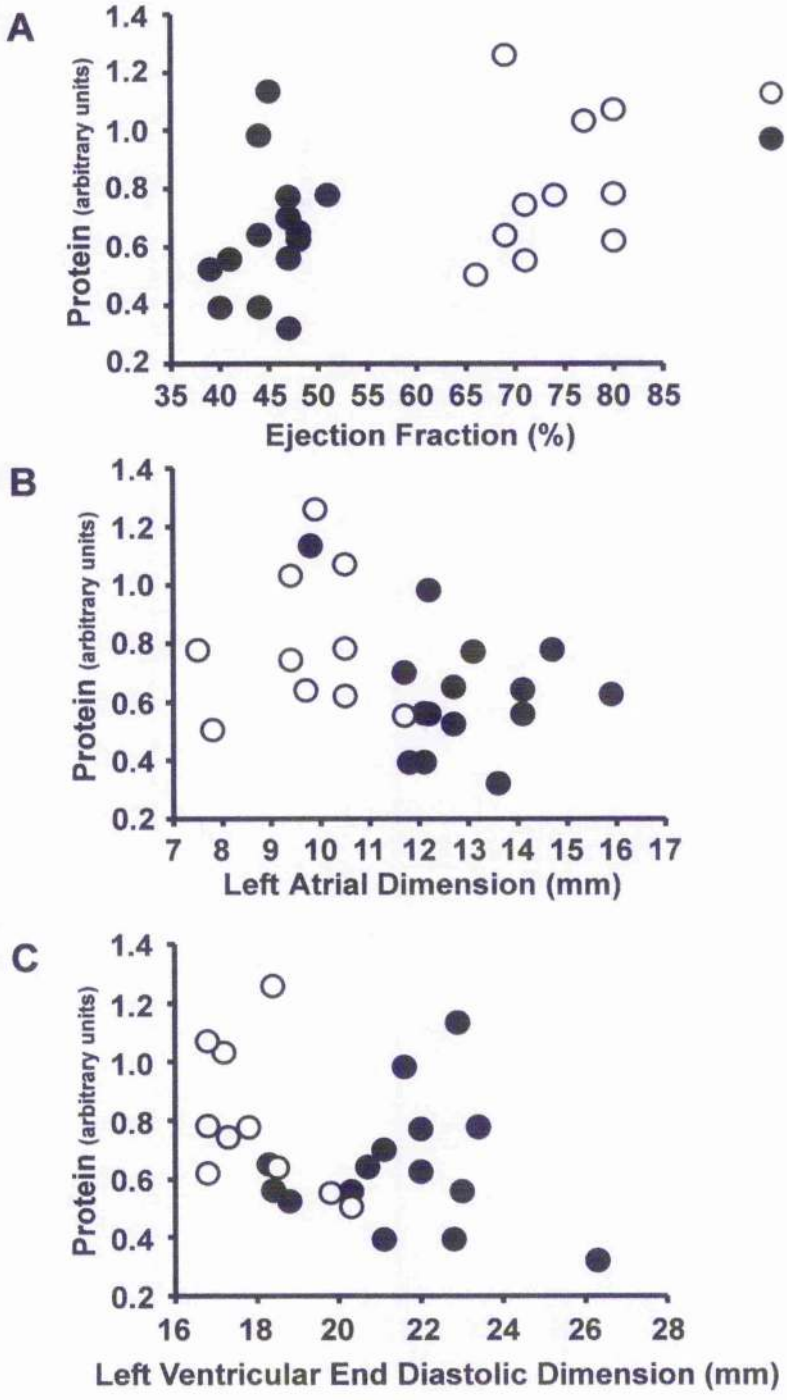

Figure 4.13 Relationship between sorcin and echocardiographic parameters in the polyclonal study.

Graphs of protein (arbitrary units) *vs.* **A** % ejection fraction, **B** left atrial dimension (mm) and **C** left ventricular end diastolic dimension (mm) for each animal used in the monoclonal sorcin expression study. Sham (o) and LVD (•) animals were not paired in this study. No significant correlations exist between sorcin expression levels detected using the polyclonal primary and any of the parameters (EF, LAD or LVEDD).

4.4.8 Sorcin and NCX co-immunoprecipitation

Sorcin expression levels have previously been shown to modulate NCX activity in rabbit cardiomyocytes. It was therefore investigated whether sorcin and NCX are physically associated in the cardiomyocyte using the co-immunoprecipitation technique. The preliminary results obtained are presented in Figure 4.14 below with the permission of Dr Susan Currie, University of Glasgow.

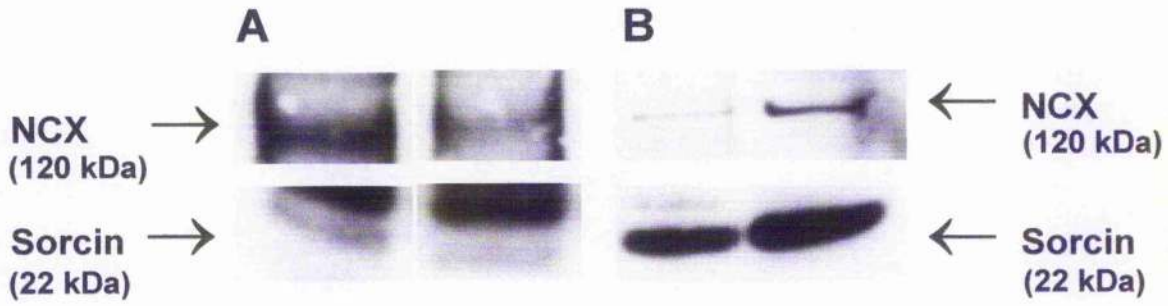

Figure 4.14 Sorcin-NCX co-immunoprecipitation.

A Blot showing bands obtained when probing a sorcin-immunoprecipitated sample using NCX antiserum both with pre-clearing step (left) and without pre-clearing step (right). The top bands represent the 120 kDa mature form of NCX whilst the lower band represents the 22 kDa sorcin monomer.

B Blot showing bands recovered from a non-immunoprecipitated membrane sample (left) and a solubilised sample (right) indicating that both sorcin and NCX are present and detectable in the ventricular extract. Bands are as in A above.

Bands for both NCX and sorcin were recovered from the immunoprecipitate (Figure 4.14 A) therefore indicating that sorcin and NCX physically interact in the rabbit ventricular cardiomyocyte.

4.5 Discussion

This chapter has quantified the endogenous levels of sorcin in left ventricular homogenates from rabbits with and without LVD. This was performed using two different primary antibodies directed against sorcin. In addition, some preliminary work on the interaction between sorcin and NCX has been presented.

4.5.1 Sorcin expression levels are altered in heart failure

The data obtained from the present study indicate that sorcin expression levels are significantly decreased in heart failure. This was, however, only found to be true for the dimeric form of sorcin and that monomer levels were not significantly changed. Comparable decreases in dimer levels were detected using two different primary antibodies (33%), thus reinforcing the validity of the result. The sorcin monomer was undetectable using the monoclonal primary even in the presence of strongly reducing conditions. This highlights the variability in the affinities of the two antibodies used. Previous studies in the literature report only on the levels of sorcin monomer with no mention of dimer. Consequently, this is the first study to quantify sorcin dimer expression levels in cardiac tissue and investigate their changes in response to pathology.

In the same rabbit model of LVD, a decreased NCX activity was shown to be accompanied by an increase in NCX protein (Quinn *et al.*, 2003). Work by this group also revealed that over-expression of sorcin stimulated NCX activity (Seidler *et al.*, 2003). A mechanism for the NCX dichotomy is therefore provided by the present study. The decreased levels of sorcin dimer may account for the decreased NCX activity present in LVD (Smith *et al.*, 2006). This conclusion is strengthened by the finding that sorcin and NCX physically interact within the rabbit ventricular cardiomyocyte as shown by co-immunoprecipitation (Smith *et al.*, 2005b). The modulatory effect of sorcin on NCX function occurs in spite of elevated NCX protein levels.

Mean echocardiographic parameters confirmed that the hearts used in the LVD groups for each study had impaired cardiac function compared to the sham

group. This was manifest as a significant decrease in EF and significant increases in LAD and LVEDD. The absence of any clear correlation between echocardiographic parameters and sorcin expression suggests that sorcin levels are not the predominant factor determining mechanical performance of the heart following myocardial infarction and subsequent LVD. The high degree of variability in both the degree of LVD and protein levels in each animal may prevent a correlation becoming evident.

4.5.2 Sorcin's effects in the cardiomyocyte

The inability to define a common effect of sorcin in the heart is mainly attributable to the multiple target proteins for sorcin and the conflicting results obtained. Some studies suggest that sorcin improves contractile functioning (Suarez *et al.*, 2004; Frank *et al.*, 2004; Frank *et al.*, 2005) whilst others suggest it depresses it (Meyers *et al.*, 2003; Farrell *et al.*, 2003; Seidler *et al.*, 2003). The identified targets for sorcin in the cardiomyocyte are all critical to EC coupling and are fundamental in the maintenance of $[Ca^{2+}]_i$. It is unclear whether sorcin acts independently on each target or whether there is a co-ordinated action to produce the whole-cell effect.

The highly Ca^{2+}-dependent changes in sorcin's conformation make it difficult to predict its interaction with targets and subsequent behaviour. For example, local Ca^{2+} gradients exist within the cardiomyocyte at the dyadic cleft following CICR and beneath the membrane due to intrinsic leaks in the membrane (Zamparelli *et al.*, 1997). This may alter the translocation ability of sorcin at distinct locations in the cell favouring spatially and temporally different functional effects.

Sorcin is a highly versatile protein. The consensus of opinion at present leans toward the sorcin dimer as the functional player in target interaction (Brownawell & Creutz, 1997; Meyers *et al.*, 2003). As sorcin can interact with either C- or N-terminals it may therefore bind simultaneously to two distinct targets and couple processes. In addition, it has been suggested that alterations in sorcin protein may affect expression levels of other cardiac proteins. The over-expression of sorcin in cells with undetectable levels of RyR2 led to the

subsequent appearance of RyR2 protein (Meyers *et al.*, 1995a). It therefore appears that sorcin may also be capable of modulating the expression levels of its targets as well as their activity. In the same model of LVD as used in this thesis, a significantly decreased level of RyR2 protein exists (Currie *et al.*, 2005) which may be linked with the parallel decrease in sorcin protein. In keeping with this theory, altered NCX levels in LVD may be part of this effect, but this remains to be shown definitively.

4.5.3 Monomer vs. dimer ?

It is well established that sorcin exists as both a monomer and dimer within the cardiac cell. One possible explanation for a decrease in sorcin dimer expression in LVD in this study (as initially detected using the monoclonal antibody) would have been a dissociation of the dimer into monomer (as then undetectable). This possibility was ruled out by further investigations using the polyclonal which showed no significant change in monomer levels. The quantification data on endogenous sorcin in the literature reports only on the sorcin monomer. Their diagrams fail to present the entire gel and instead cut out the bands at the level of the monomer (22 kDa), hence preventing determination of whether additional higher molecular weight bands were detected. The study by Meyers *et al*, (1995) adopted this approach, yet the discussion states that "higher molecular weight bands were also observed" (Meyers *et al.*, 1995a). Although absent from their publications, correspondence with both the Meyers and Chiancone groups revealed that they detected a 44 kDa band when probing for sorcin (M.B. Meyers & E.Chiancone; personal communication).

A monomer-dimer association constant of 3×10^5 M^{-1} has been determined for sorcin from sedimentation equilibrium data obtained at pH 7.5 (Zamparelli *et al.*, 2000).

The following equation can be produced using this value:

$$K = \frac{[S_2]}{[S] \times [S]}$$

K	-	association constant
[S]	-	monomer concentration
[S_2]	-	dimer concentration

$$\rightarrow \quad [S_2] = [S] \times [S] \times (3 \times 10^5)$$

So, for example if [S] = 1 μM

$$[S_2] = 10^{-6} \times 10^{-6} \times (3 \times 10^5)$$

$$= \underline{0.3\ \mu M}$$

The equation can be used to calculate the steady state relationship between monomer and dimer as shown in Figure 4.15.

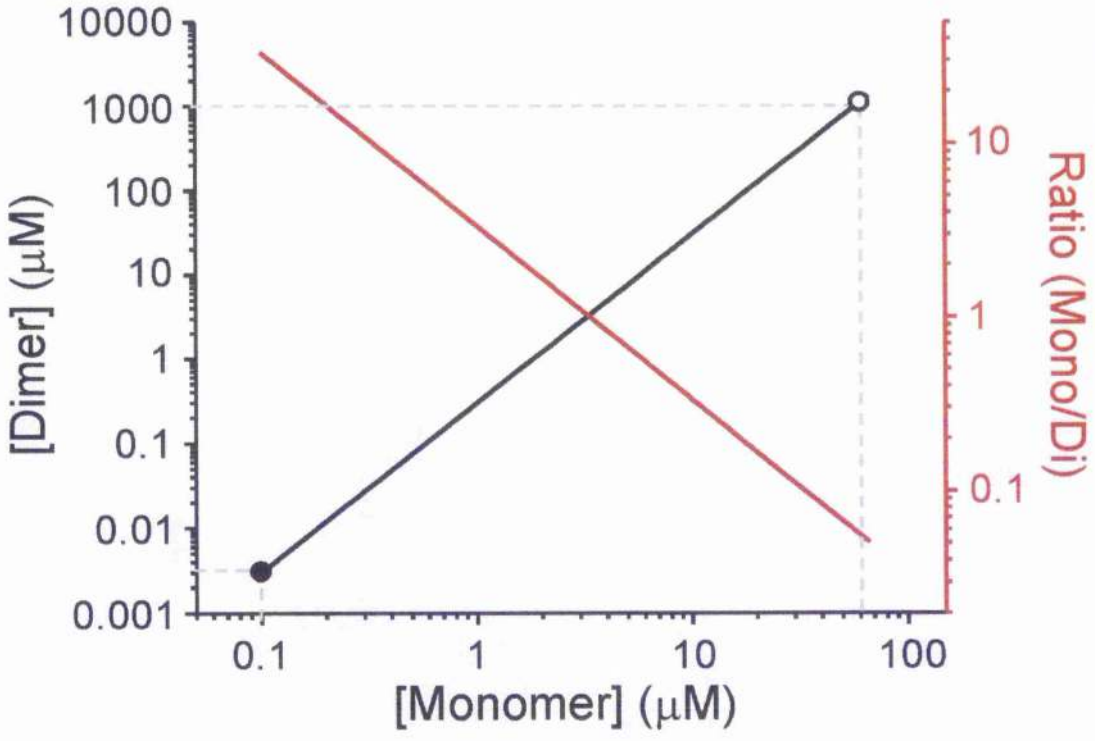

Figure 4.15 The relationship between sorcin monomer and dimer concentrations.

Plot relating monomer concentration with the corresponding dimer concentration calculated using the association-dissociation constant determined by Zamparelli *et al*, (2000) (**Black**). A plot of the monomer:dimer ratio is also included (**Red**). Grey dashed lines correspond to examples described in the text.

It is therefore possible to make an inference about the physiological relationship of sorcin dimerisation within the cell. For example, when the sorcin monomer concentration is at 0.1 μmol/L, the predicted dimer concentration will be 3 nmol/L with a monomer:dimer ratio of 33.3 (see grey lines in Figure 4.15). When monomer concentration is increased to 62 μmol/L, the dimer concentration is dramatically increased to 1 mmol/L and the monomer:dimer ratio is reduced to 0.05 (see grey lines in Figure 4.15). Thus it is evident that the relationship between sorcin monomer:dimer is non-linear.

The monomer:dimer ratios obtained from the Western data in the present study were 0.85 ± 0.14 and 1.04 ± 0.13 for sham and LVD groups respectively ($p>0.05$) indicating there were no gross changes in monomer and dimer levels in each group. It was only possible to obtain such a ratio using the polyclonal primary as the monoclonal did not detect sorcin monomer at quantifiable levels. A 33% decrease in dimer expression levels was detected in the LVD group. Assuming that the relationship shown in Figure 4.15 is the dominant factor in determining the monomer:dimer ratio in the cytosol, a prediction of the monomer:dimer ratio and the level of monomer in response to this decrease in dimer can be made. Decreasing the dimer concentration will produce a decrease in monomer (although by a proportionately smaller amount), an increase in the monomer:dimer ratio and an overall decrease in total sorcin in the cytoplasm.

The equilibrium factor, described by Zamparelli *et al*, (2000), may not be the predominant factor in determining the overall ratio of sorcin monomer:dimer within the tissue and other factors may contribute.

4.5.3.1 Factors which may alter the monomer:dimer ratio

The homogenate samples used in this study were detected as both monomer and dimer whereas the recombinant sorcin was mainly identified as monomer. A recombinant protein is by nature an ultra pure preparation of the protein. The presence of membrane fragments in the rabbit homogenates may have promoted dimerisation of sorcin; the probability of dimerisation would be reduced in the recombinant due to the absence of membrane. The membrane present in the homogenate would act as a sink for the dimer, thereby stabilising it in this form.

As demonstrated above, sorcin monomer and dimer levels are in a specific association:dissociation equilibrium and hence the level of dimerisation will depend on the level of monomer. If the total concentration of sorcin in the homogenates was high, the sorcin dimer would be favoured as predicted by Figure 4.15. Although the precise concentration of sorcin in the cytoplasm is unknown it may be comparable to the 6 μmol/L figure previously determined for calmodulin, another PEF Ca^{2+}-binding protein (Haiech *et al.*, 1981). If so, then sorcin would exist as approximately 2 μmol/L dimer and 1 μmol/L monomer. This is not inconsistent with the Western data which revealed both monomer and dimer in the homogenates. Finally, sorcin has been shown to be mainly dimeric in the presence of 2 mmol/L EGTA at pH 7.5 using sedimentation velocity experiments (Zamparelli *et al.*, 1997). As these conditions were present in the homogenate, it seems unsurprising that dimer was detected as well as monomer. Alterations in the monomer make any changes in the dimer difficult to predict (and vice versa); this may therefore make any suggestion of the functional effects of the alterations difficult.

4.5.4 Interaction between Sorcin-NCX

The co-immunoprecipitation data presented in this study have demonstrated for the first time that a physical interaction exists between sorcin and NCX. They do not, however, determine if this interaction occurs directly or indirectly. The structure of NCX has been determined and, within this, two potential binding sites exist for sorcin to interact directly. These sites are (i) the calmodulin binding domain and (ii) the XIP region of the cytoplasmic loop. NCX has been suggested to form part of a macromolecular complex in the sarcolemma as has previously been reported for RyR2 in the SR membrane. In order to determine if direct or indirect, techniques such as mass spectroscopy must be employed.

4.6 Summary

The decreased sorcin dimer levels in this rabbit model of LVD may account for previously demonstrated decreases in NCX activity. As mentioned previously, the dimer is considered to be the most functionally relevant form of sorcin. It therefore appears imperative that dimer levels are quantified as well as monomer levels to obtain an accurate picture of endogenous sorcin in order to investigate its effects in health and disease.

Although an effect on RyR2 is accepted, effects on I_{Ca} (Meyers *et al.*, 1998) and NCX (Seidler *et al.*, 2003) remain to be reproduced and an effect on SERCA2a is weakened through absence of co-immunoprecipitation data. With so many intracellular targets for sorcin in the cardiomyocyte, it is unclear as to whether sorcin's action on these targets works independently or synergistically to produce a whole-cell effect. Considerable ambiguity remains as to sorcin's effects in the heart and its potential value as a therapeutic target. Further studies are therefore required to resolve this.

CHAPTER 5
PHOSPHOLEMMAN

5.1 Introduction

Phospholemman (PLM) is an approximately 8 kDa, 72 amino acid, phosphoprotein (Palmer *et al.*, 1991). First identified in purified cardiac sarcolemmal vesicles, PLM commonly runs at 15 kDa during SDS-PAGE (Manalan & Jones, 1982). Structural analysis has shown PLM possesses a single transmembrane domain (residues 18-37) composed of a tetramer of α-helices (Palmer *et al.*, 1991; Beevers & Kukol, 2006). The intracellular C-terminus of the protein (residues 38-72) is positively charged and contains numerous phosphorylation sites whilst the N-terminus (residues 1-18) is negatively charged and extracellular (Palmer *et al.*, 1991; Chen *et al.*, 1998). PLM belongs to the FXYD gene family of small ion transport regulators all of which contain an invariant motif of FXYD. The family contains 7 members and as PLM was the first member of the family to be sequenced it was denoted FXYD1. The gene sequence has been determined for PLM and expression studies have shown it to be present in skeletal muscle, smooth muscle and liver whilst the highest levels are found in the heart (Palmer *et al.*, 1991; Bogaev *et al.*, 2001). The name "phospholemman" was given to this protein as a reflection of its multiple phosphorylation sites and presence in the membrane (Palmer *et al.*, 1991).

5.1.1 Association of PLM with membrane

PLM is known to be anchored into the plasma membrane via a single membrane-spanning domain (Palmer *et al.*, 1991). The C-terminal of PLM is proposed to further stabilise this incorporation by binding to the surface of plasma membrane lipids (Clayton *et al.*, 2005). Originally, PLM was considered an entirely surface membrane-associated protein but recent work has suggested that it may localise to the membrane of the endoplasmic reticulum through its C-terminal (Lansbery *et al.*, 2006). It appeared that when PLM was expressed in Madin-Darby canine kidney cells, phosphorylation was required for its translocation to the surface membrane; the presence of a negative charge at threonine residue 69 in the cytoplasmic domain has been shown to be crucial for this effect (Lansbery *et al.*, 2006). A predominantly sarcolemmal origin for phosphorylated PLM has previously been demonstrated (Presti *et al.*, 1985),

therefore phosphorylation may be a pre-requisite for PLM to incorporate into the plasma membrane but the relevance of this study to cardiac tissue remains to be confirmed. Indeed, immunocytochemical analysis of the non-phosphorylated form of PLM in rat cardiomyocytes has located it to the surface sarcolemma, intercalated discs and t-tubules (Zhang *et al.*, 2003). A final point regarding PLMs behaviour in membrane was determined when it was shown that PLM preferentially associated with anionic lipids in a mixed lipid membrane environment This raises the possibility that PLM may also participate in membrane organisation functions (Clayton *et al.*, 2005).

5.1.2 Phosphorylation of PLM

The phosphorylation of a 15 kDa sarcolemmal protein by PKA was first shown to occur in purified sarcolemmal vesicles from canine left ventricular tissue. Exogenous application of the ionophore alamethicin and PKA to these vesicles revealed that phosphorylation occurred via the cytoplasmic domain (Manalan & Jones, 1982). Incorporation of radiolabelled phosphate (^{32}P) to the same protein was demonstrated shortly after this when intact guinea-pig ventricular tissue was exposed to isoprenaline. This was shown to be accompanied by an increased force of contraction as is characteristic of general β-adrenergic stimulation of the myocyte (Presti *et al.*, 1985). Later identified as PLM, this protein has been shown to be the major sarcolemmal substrate in cardiac membrane for both PKA and PKC. The C-terminal of PLM contains sequences for both these kinases as well as for cGMP kinase and CaMK although it is not considered a substrate for the latter two (Palmer *et al.*, 1991). PLM is known to possess two physiologically relevant phosphorylation sites in the C-terminal portion of the protein - one at Serine 63 (Ser63), the other at Serine 68 (Ser68); PKA phosphorylates Ser68 whilst PKC phosphorylates both Ser63 and Ser68 as well as threonine at position 69 (Palmer *et al.*, 1991; Walaas *et al.*, 1994). Further to this, studies in skeletal muscle have shown that insulin and adrenaline stimulate phosphorylation of PLM at these sites indicating hormonal regulation of this process may also occur (Walaas *et al.*, 1994). Phosphorylation of PLM may be required for PLM to insert in the sarcolemma (Lansbery *et al.*, 2006). Functionally, the phosphorylation status of PLM has been shown to account for

the modulatory effect of PLM on membrane-bound targets (Silverman *et al.*, 2005; Song *et al.*, 2005).

PLM is rapidly phosphorylated *in vivo* in response to adrenergic stimulation (Presti *et al.*, 1985; Palmer *et al.*, 1991) and can be dephosphorylated by protein phosphatases types 1 and 2A (Neumann *et al.*, 1999). The regulation of phosphorylation status of PLM therefore becomes complicated in situations of heart failure where kinase and phosphatase levels are commonly altered. Estimations of the basal level of phosphorylation of PLM at its two main sites have been produced using phosphospecific antibodies. In rat, approximately 40% of the total PLM was found to be phosphorylated at Ser68 (Song *et al.*, 2005; Zhang *et al.*, 2006a) whilst this was reduced to approximately 15% at Ser63 (Song *et al.*, 2005); in guinea-pig, 25% of PLM was phosphorylated at Ser68 (Silverman *et al.*, 2005). It appears, therefore, that a large reserve of unphosphorylated PLM remains in the cardiomyocyte for regulation by cellular kinases.

5.1.3 Functions of PLM

In vivo, PLM resides in membrane and is implicated in the following functional roles: (i) channel formation and ion conductivity (ii) osmotic regulation and (ii) regulation of the rate of ion translocation through pumps and exchangers (Zhang *et al.*, 2003).

The concept of PLM functioning as a channel was first proposed following the determination of its sequence (Palmer *et al.*, 1991). Shortly after this, PLM expression in *Xenopus* oocytes was shown to induce a Cl^--selective current in excised patches of membrane. This current was referred to as $I_{Cl(PLM)}$ and was shown to activate at hyperpolarising voltages with extremely slow kinetics. Mutations of residues within the single transmembrane region of PLM (18-37) were performed to disrupt the aqueous pore of the proposed channel. This led to alterations in the kinetic properties of $I_{Cl(PLM)}$ indicating that PLM in the bilayers was indeed forming an ion channel as opposed to regulating an existing one (Moorman *et al.*, 1992). To further confirm this role, purified PLM was incorporated into phospholipid bilayers, where it was also shown to produce a similar ion channel to $I_{Cl(PLM)}$ in oocytes (Moorman *et al.*, 1995). Recently, the

secondary structure of the transmembrane domain has been characterised and was shown to support the role of ion channel activity (Beevers & Kukol, 2006).

The high permeability of $I_{Cl(PLM)}$ to the amino acid taurine then led to the proposal that PLM may function in volume regulation (Moorman *et al.*, 1995). Cell swelling is known to produce compensatory effluxes of osmolytes such as taurine and Cl^- in order to maintain cell volume. Using embryonic kidney cells as a model system, PLM over-expression was shown to increase swelling-activated ion currents (Davis *et al.*, 2004). PLM may therefore take part in the complex and multiple pathways by which cell volume is controlled.

The regulation of ion channels and transporters by PLM in the cardiac cell was anticipated due to its similarity in C-terminal with the SERCA2a regulator phospholamban and has since been well characterised experimentally (Palmer *et al.*, 1991; Chen *et al.*, 1998). PLM is known to affect cardiac contractility via modulation of NCX and the Na^+/K^+-ATPase. Evidence supporting the regulation of these two by PLM and phosphorylated PLM will be discussed below. As the modulation of NCX by PLM is the subject of the current chapter, particular attention will be focussed on NCX regulation.

5.1.4 Interaction of PLM with NCX

PLM inhibits NCX function via a mechanism which requires its phosphorylation at Ser68 (Song *et al.*, 2005; Zhang *et al.*, 2006a).

The modulation of NCX was first demonstrated in rat ventricular myocytes over-expressing PLM. $[Ca^{2+}]_o$ was varied between 0.6-5 mmol/L in order to assess the effect of PLM on contractility and Ca^{2+} transients. Compared to controls, at low $[Ca^{2+}]_o$, where Ca^{2+} *efflux* on NCX is favoured, PLM over-expressing cells exhibited increased contraction whilst at high $[Ca^{2+}]_o$, where Ca^{2+} *influx* on NCX is favoured, Ca^{2+} transient amplitudes were decreased (Song *et al.*, 2002; Zhang *et al.*, 2003). These cells exhibited no alterations in NCX, calsequestrin and SERCA2a protein levels or SERCA2a activity when compared to controls. From this, it was proposed that PLM affected Ca^{2+} influx and efflux pathways via modulation of NCX activity (Song *et al.*, 2002).

Direct investigation of this hypothesis has confirmed that PLM inhibits NCX function (Zhang *et al.*, 2003). PLM over-expressing cells demonstrated significantly decreased NCX activity in both forward mode and reverse NCX modes, as evidenced by 1.8 fold prolongation in half-time of relaxation from the caffeine-induced Ca^{2+} transient and reverse I_{NCX} respectively. Co-over-expression of PLM with NCX was shown to reverse all these effects. Over-expression of PLM was accompanied by no alteration in resting membrane potential, action potential amplitude or duration or dimensions of the myocyte. Down-regulation of PLM protein, through the introduction of antisense PLM to rat cardiomyocytes, resulted in significant increases in the rate of decline from caffeine-induced Ca^{2+} transients and I_{NCX} and lower diastolic $[Ca^{2+}]_i$. In down-regulating PLM, NCX activity was increased through relief of the basal level of NCX inhibition by PLM (Mirza *et al.*, 2004). Similar to this, PLM knock-out mice have been shown to exhibit significantly higher I_{NCX} (Tucker *et al.*, 2006; Zhang *et al.*, 2006a). Co-expression of NCX and PLM in human embryonic kidney cells (HEK293 cells) revealed significantly decreased I_{NCX} and Na^+-dependent $^{45}Ca^{2+}$ uptake compared to controls. As this expression system is devoid of endogenous NCX and PLM, this demonstrated unambiguously inhibition of NCX function by PLM in the absence of other proteins (Ahlers *et al.*, 2005).

The Ser68 phosphorylation site in the C-terminal is critical for the inhibitory effect of PLM on NCX. A constitutively de-phosphorylated PLM mutant, in which Ser68 was substituted for alanine (PLMS68A), was shown to negate completely PLM inhibition of NCX in both rat cardiomyocytes (Song *et al.*, 2005) and HEK293 cells (Ahlers *et al.*, 2005; Zhang *et al.*, 2006a). Conversely, a constitutively phosphorylated PLM mutant, in which Ser68 was substituted for glutamate, resulted in an enhanced inhibition of I_{NCX} (Zhang *et al.*, 2006a). This was not due a lack of physical association between the mutants and NCX as they still co-immunoprecipitated (Ahlers *et al.*, 2005). Ser63 phosphorylation has also been shown to inhibit NCX activity but to a much lesser extent than Ser68 phosphorylation, thereby indicating that functionally the latter predominates (Zhang *et al.*, 2006a)

PLM and NCX were shown to co-localise in the sarcolemma, intercalated discs and t-tubule membrane, thus supporting their functional interaction (Zhang *et*

al., 2003). Further to this, a physical interaction of PLM and NCX through co-immunoprecipitation has been demonstrated in rat cardiomyocytes (Mirza *et al.*, 2004) and HEK293 cells (Ahlers *et al.*, 2005). As PLM modulates Na^+/K^+-ATPase activity (see section 5.1.5 following), this would alter $[Na^+]_i$ which may be argued to modulate NCX as a secondary effect through alterations in the driving force on NCX. This is, however, not the case as inhibition of I_{NCX} was shown in HEK co-expressing PLM and NCX where K^+, Ca^{2+}, Cl^- and Na^+/K^+-ATPase currents were blocked (Ahlers *et al.*, 2005). In addition, $[Na^+]_i$ was similar in PLM knock-out and wild-type mice lending further support for a primary effect of PLM on NCX activity (Tucker *et al.*, 2006). The mechanism of action of PLM on contractility and Ca^{2+} transients can be explained by alterations in SR Ca^{2+} content via the altered NCX activity; this was verified in PLM knock-out mice. These cells were shown to have significantly lower SR contents at low $[Ca^{2+}]_o$ and significantly higher SR contents at high $[Ca^{2+}]_o$ which mirrored the changes in contractile amplitudes and Ca^{2+} transients (Tucker *et al.*, 2006).

5.1.5 Interaction of PLM with Na^+/K^+-ATPase

The Na^+/K^+-ATPase is the membrane pump responsible for the maintenance of the ionic gradients (high $[K^+]_i$ and low $[Na^+]_i$) which are essential for normal cellular excitability. PLM in its unphosphorylated form is inhibitory on Na^+/K^+-ATPase function, which is then reversed upon phosphorylation of PLM at Ser68 and Na^+/K^+-ATPase activity is stimulated (Fuller *et al.*, 2004).

Expression studies in *Xenopus* oocytes first showed that PLM and Na^+/K^+-ATPase physically interacted through co-immunoprecipitation experiments (Crambert *et al.*, 2002). Later work in rabbit determined that PLM associates with all three α-subunits of the Na^+/K^+-ATPase (Bossuyt *et al.*, 2005). The association of PLM and Na^+/K^+-ATPase occurs through a hydrophobic interaction of the two proteins' transmembrane domains whilst Na^+/K^+-ATPase activity is modulated via the two proteins C-terminal cytoplasmic domains. In *Xenopus* oocytes co-expression of Na^+/K^+-ATPase and PLM resulted in an approximately 2-fold decrease in the affinity for $[Na^+]_i$ and a small reduction in the affinity for $[K^+]_o$ (Crambert *et al.*, 2002). PKA stimulation of Na^+/K^+-ATPase in PLM knock-out mice was shown not to occur directly but instead through phosphorylation of PLM (Despa *et al.*,

2005). The affinity for $[Na^+]_i$ was reduced in the knock-out compared to the wild-type but this difference was nulled on phosphorylation of PLM. PKA-dependent phosphorylation of PLM leads to a substantial stimulation of Na^+/K^+-ATPase in rat (Fuller *et al.*, 2004) and PLM knock-out mouse cardiomyocytes (Despa *et al.*, 2005). This is of greater magnitude than that predicted by relief of inhibition and so it appears that PLM phosphorylation stimulates Na^+/K^+-ATPase activity (Fuller *et al.*, 2004). Application of forskolin significantly increased Na^+ current in line with phosphorylation of PLM (Silverman *et al.*, 2005). Interestingly, phosphorylation and subsequent relief of inhibition (and potentially stimulation) of Na^+/K^+-ATPase has been shown to occur following ischaemia in the rat (Fuller *et al.*, 2004). In vascular smooth muscle, however, phosphorylation of PLM at Ser68 has been shown to induce relaxation through stimulation of Na^+/K^+-ATPase (Rembold *et al.*, 2005). Another anomalous finding is that the PLM knock-out mouse showed a 50% reduction in Na^+/K^+-ATPase activity. This was attributed to compensatory (related to the significant hypertrophy) rather than PLM-mediated mechanisms, although this was unsubstantiated experimentally (Jia *et al.*, 2005). The action of PLM on the cardiac Na^+/K^+-ATPase is therefore analogous to the regulation of SERCA2a by phospholamban.

As well as modulating Na^+/K^+-ATPase activity via interacting with the protein itself, it has been suggested that PLM may be involved in membrane organisation, leading to the segregation of anionic lipids and thereby maximising Na^+/K^+-ATPase function (Clayton *et al.*, 2005). Long-term regulation of cell volume is achieved through the maintenance of ionic gradients by Na^+/K^+-ATPase and hence there may be an additional role in volume regulation for PLM at this level (Davis *et al.*, 2004).

5.2 Aims

The aims of the present chapter were as follows:

1. To quantify the endogenous phosphorylation status of PLM in sham and LVD-operated rabbit myocardium.

2. To quantify the expression levels of total PLM protein in sham and LVD-operated rabbit myocardium

3. To assess whether the phosphorylation status of PLM and expression levels of total PLM are altered in LVD compared to sham in a way that may explain the depressed NCX activity observed in LVD.

5.3 Methods

5.3.1 Quantification of PLM expression – experimental approach

Quantification of phospholemman and its two phosphorylated forms in rabbit cardiac homogenates was performed in collaboration with Professor Michael Shattock's group, King's College London. Details of homogenate preparation, estimation of protein content and all solutions used are listed in General methods (2.3.5.1 and 2.3.6.1). An overview of the technique of quantitative Western blotting can be found there also.

The study utilised three antibodies for the Western blotting step, one directed against total PLM protein and two directed against each of the phosphorylation sites (Ser63 and Ser68). Antibodies were as follows: (i) chicken anti-PLM antibody (Fuller *et al.*, 2004); raised against the C-terminus), (ii) phosphorylation site-specific CP-63 rabbit anti-PLM antibody and (iii) phosphorylation site-specific CP-68 rabbit anti-PLM antibody (both produced by J.R.Moorman and colleagues, University of Virginia, VA (Silverman *et al.*, 2005); raised against the C-terminus). With the gel system and buffers employed, PLM ran at approximately 10 kDa for each antibody. This combination was found optimal as it reduced background exposure levels and resolved sharper bands for PLM.

5.3.2 Electrophoresis and quantitative Western blot analysis

Electrophoresis was performed according to the method of Laemmli (1970); 12 well 15% Tris-tricine gels were used throughout. All homogenate samples were prepared in 4 X Laemmli sample buffer and were exposed to 70 °C for approximately 10 min prior to loading to ensure proteins were run under reducing conditions. A consistent total protein load was pipetted into each well in alternating LVD/sham order across each gel. This alternating pattern aimed to minimise variance attributable to the gel itself or to the efficiency of transfer across the width of the gel.

SDS-PAGE was performed by exposure of each gel to a constant voltage of 200 V for 45 min on ice. Protein transfer to polyvinylidene fluoride (PVDF) membranes was performed using a semi-dry blotter in transfer buffer; these were then blocked in blocking buffer. Membranes were incubated at 4 °C overnight in (i) chicken anti-PLM antibody for total PLM or rabbit anti-PLM antibody CP63 or CP68 - phosphospecific for either (ii) serine 63 or (iii) serine 68 all at 1:2000 dilution in antibody incubation buffer. The following day, membranes were washed for three five-minute periods in the order rinse buffer, high-salt rinse buffer, rinse buffer. Incubation in secondary antibody at room temperature for 1 hour was as follows: membrane (i) in anti-chicken horseradish peroxidase conjugate (1:1000; Promega); membranes (ii) and (iii) in anti-rabbit horseradish peroxidase (1:5000; Amersham) all in antibody incubation buffer. After this, membranes were washed three times as described above. Detection and visualisation of bands was performed using chemiluminescence (ECL detection system, 1 min, Amersham) and exposure to autoradiographic film followed by development.

5.3.3 Densitometry and analysis for phospholemman

Quantification of bands representing Ser63 phosphorylated PLM, Ser68 phosphorylated PLM and total PLM (monomeric form) was performed by scanning developed immunoblots into an Imaging Densitometer. The files containing the scans were then imported into N.I.H. Image software (Freeware, N.I.H., Baltimore, MD) and analysed. The optical density for each band was produced by normalising the densitometry value to that of the band in lane 1 (containing a randomly selected sample). The results from a number of experiments were then averaged to produce the mean optical density in each group. Additionally, total PLM blots were used as a standard to which both phosphospecific bands were normalised. After images had been obtained, PVDF membranes were stripped of antibodies and Coomassie stained for total homogenate protein. This was performed in order to ensure a consistent pattern of banding for each sample.

Results were expressed as the mean of a number of experiments and a two-tailed unpaired Student's T-test was used to indicate statistical significance between sham and LVD groups ($p<0.05$).

5.4 Results

5.4.1 Detection of PLM and its phosphorylated forms in ventricular homogenates

Quantification of the phosphorylation status of PLM and expression of total PLM in sham and LVD-operated rabbit myocardium was performed using a non-phosphospecific antibody - for total PLM protein - and two phosphospecific antibodies directed at its known sites of phosphorylation - serine 63 and serine 68. Example blots obtained when probing whole left ventricular homogenates using each antibody are presented below in Figure 5.1.

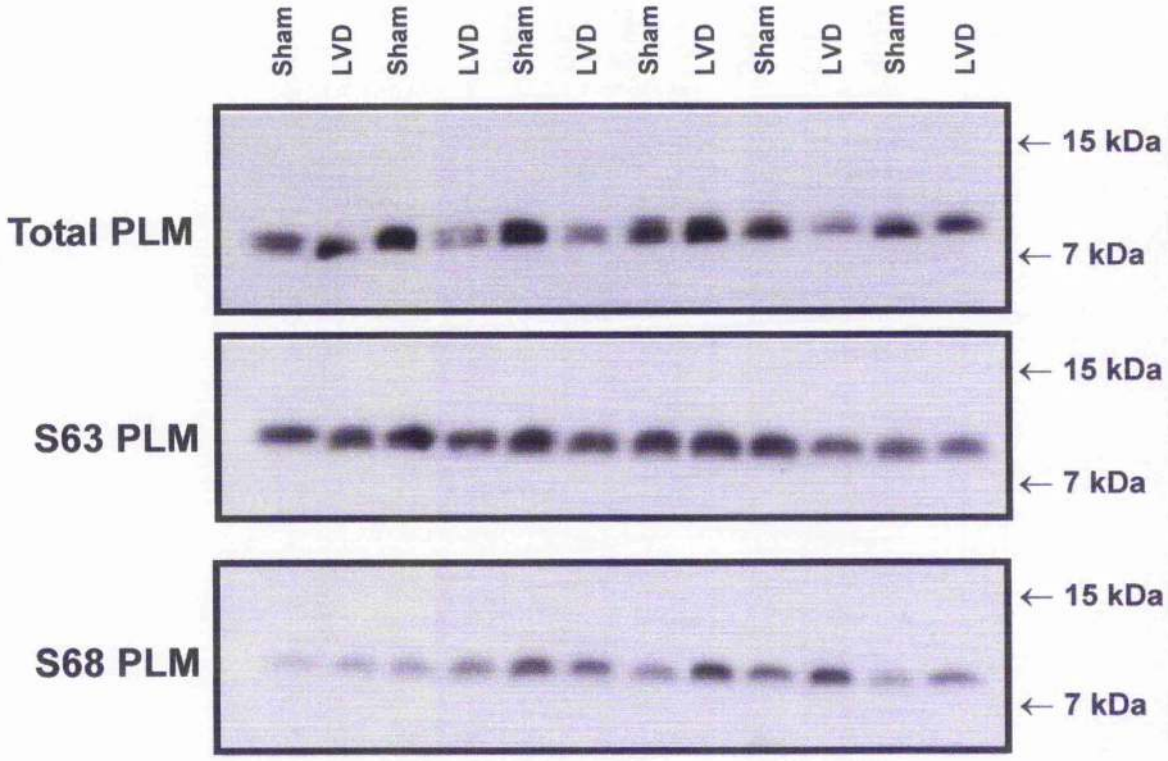

Figure 5.1 Typical Western blots for PLM and its phosphorylated forms.

Example signals obtained when probing whole left ventricular samples with antibodies directed against total PLM, Ser63 phosphorylated PLM or Ser68 phosphorylated PLM (as labelled). Samples were alternated along the length of the gel as denoted at the top of the diagram. PLM consistently ran at approximately 10 kDa with each antibody; arrows to the left of each blot demonstrate the level of molecular weight markers (not shown).

5.4.2 PLM expression levels in ventricular homogenates

The mean data obtained for total PLM protein expression, Ser63 phosphorylated PLM expression and Ser68 phosphorylated PLM are presented below in Table 5.1. The top three rows in this table represent values for total PLM, Ser63 PLM and Ser68 PLM normalised to total homogenate protein whilst the bottom two rows represent Ser63 PLM Ser68 PLM further normalised to total PLM protein (Ser63 PLM/Total PLM and Ser68 PLM/Total PLM).

Table 5.1 Mean densitometry values for total PLM, Ser68 phosphorylated PLM and Ser63 phosphorylated PLM.

Mean densitometry measurements obtained when probing for total PLM and the two phosphorylated forms of PLM in sham and LVD myocardium (n=7 and n=9 respectively).

	Sham	SEM	LVD	SEM
Total PLM	**1.14**	0.13	**1.03**	0.12
Ser63 PLM	**1.3**	0.1	**1.31**	0.11
Ser68 PLM	**1.99**	0.22	**1.77**	0.23
Ser63 PLM / Total PLM	**1.18**	0.07	**1.41**	0.17
Ser68 PLM / Total PLM	**1.78**	0.12	**1.86**	0.29

The mean data have also been presented as a chart in Figure 5.2 on the following page.

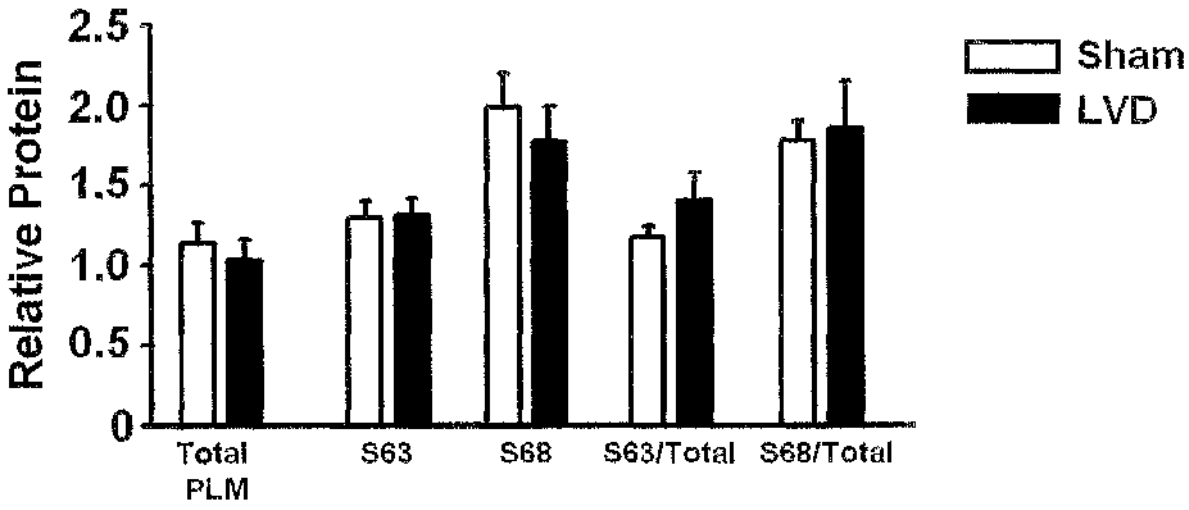

Figure 5.2 Chart of mean densitometry for PLM and its phosphorylated forms in sham and LVD myocardium.

Mean ± SEM densitometry data for sham (white; n=7) and LVD (black; n=9) when probing using antibodies directed against total PLM, Ser63 phosphorylated PLM or Ser68 phosphorylated PLM. Also presented in the last two columns on the right hand side are data for Ser63 phosphorylated PLM and Ser68 phosphorylated PLM normalised to total PLM. No significant differences were detected between the groups using any of the antibodies or normalisation methods ($p>0.05$).

As can be seen from Table 5.1 and Figure 5.2 no significant differences in the phosphorylation status of PLM between sham and LVD groups were detected when data were normalised either to total protein or to total PLM.

5.5 Discussion

The present chapter aimed to determine whether alterations in the phosphorylation status of PLM or total PLM levels existed between sham and LVD myocardium. The phosphorylation status of PLM was investigated in the present thesis due to its established inhibition of NCX activity which predominantly occurs through the Ser68 phosphorylated form. An increase in Ser68 PLM would therefore be expected to contribute to decreased NCX activity seen in this model.

5.5.1 Phosphorylation of PLM and expression levels of total PLM are unaltered in heart failure

Quantification of the phosphorylation of status of PLM in whole homogenates from rabbit left ventricle was performed using two phosphospecific antibodies directed against the two main phosphorylation sites in the PLM sequence -Ser63 and Ser68. The findings of this study revealed no significant difference in the phosphorylation status of PLM at either Ser63 or Ser68 in LVD compared to sham-operated tissue. Similarly, no significant difference was found between total PLM protein in LVD and sham-operated homogenates. When the mean densitometry data from the phosphospecific antibodies were normalised to total PLM, again, no significant differences were apparent.

Investigation of PLM protein levels and phosphorylation status in heart failure has produced variable results. Profiling of the gene expression pattern following myocardial infarction in rats has shown increased PLM mRNA (Sehl *et al.*, 2000). In keeping with this, over-expression of PLM led to cells which exhibited similar aspects of $[Ca^{2+}]$ handling to those seen in post-infarction myocytes such as prolonged relaxation from caffeine-induced contractures and depressed NCX function (Song *et al.*, 2002). In a different rabbit model of heart failure, induced by aortic insufficiency and stenosis, total PLM expression levels were reduced by approximately 45%, yet the fraction of PLM phosphorylated at Ser68 was significantly increased (Bossuyt *et al.*, 2005). A two- to fourfold increase in total PLM expression has recently been detected in post-myocardial infarction rat cardiomyocytes (Zhang *et al.*, 2006b). The rabbit model of LVD used in this

study showed no significant difference in the expression of PLM protein or its phosphorylation levels at either Se63 or Ser68. This indicates that PLM does not contribute to the decreased NCX activity or depressed contractile function.

5.5.2 Detection of an additional band using Ser68 phosphospecific primary

In some preliminary gels, an additional band at approximately 25 kDa was evident when probing with the phosphospecific Ser68 primary antibody (CP68). Quantification of this band was performed and the mean densitometries for both sham and LVD myocardium are presented below in Table 5.2.

Table 5.2 Mean densitometry values for an additional band detected by the Ser68 phosphospecific antibody.

Mean densitometry measurements for an additional band recovered when probing with the Ser68 phosphospecific anti-PLM antibody in both sham and LVD tissue homogenates (n = 3 for each).

	Sham	SEM	**LVD**	SEM
Ser68	**2.33**	0.82	**7.01**	1.21

It is considered that this additional band corresponds to the SR-associated phosphoprotein phospholamban (PLB) which forms a homopentamer of approximately 22 kDa (Tada *et al.*, 1975; Tada & Katz, 1982). It is conceivable that this would be detected by the Ser68 phosphospecific antibody due to (i) non-specific cross-reactivity with other protein sequences and (ii) the impurity of the sample i.e. the presence of SR membrane in whole homogenates. PLB was also detected in an early phosphorylation study of PLM in sarcolemma-enriched membrane vesicles (Presti *et al.*, 1985). PLB was detected at 27 and 11 kDa and was shown to be a distinct protein from PLM in that (i) boiling of the membrane preparation in 3% SDS prior to electrophoresis converted all PLB to the 11 kDa form, (ii) increasing the degree of phosphorylation of PLB reduced its electrophoretic mobility and (iii) unlike PLM, it could be detected by PLB antiserum. These findings were in keeping with similar studies of endogenous PKA substrates in sarcolemmal vesicles (Manalan & Jones, 1982) and PLB

phosphorylation in isolated SR membrane (Lindemann *et al.*, 1983). Interestingly, these studies also identified a phosphoprotein of 15 kDa which, in the latter study, was confirmed to be sarcolemmal in origin due to the accompanying Na^+/K^+-ATPase activity from samples (Lindemann *et al.*, 1983). These therefore support the conclusion that the additional band detected by CP68 corresponds to PLB.

PLM and PLB are somewhat similar in nature as they are both small phosphoproteins possessing a single transmembrane domain with phosphorylation sites located cytoplasmically regulating P-type ATPases (Palmer *et al.*, 1991). Of particular relevance to the current study is that they share a high degree of sequence similarity in a section of 9 amino acids which includes Ser68 of PLM as shown below in Figure 5.3.

Phospholemman - R S S I R R L **S** T R R R ^{72}

Phospholamban - R S A I R R A **S** T I E M ^{20}

Figure 5.3 Sequence similarities between PLM and PLB.

The single letter amino acid sequences of PLM and PLB are shown. The regions of sequence homology of 9 consecutive residues in PLM and PLB are enclosed within the box. The parallel positioning of Ser68 of PLM and Ser16 of PLB within this sequence are highlighted in bold (S); both of these residues are major targets for PKA-mediated phosphorylation. Diagram redrawn from Palmer *et al.*, (1991).

In this section, 7 of the 9 amino acids are identical. Ser68 of PLM is a major target for phosphorylation by PKA; similarly, Ser16 of PLB is a major phosphorylation target for PKA. The parallel positioning of Ser16 in PLB with Ser68 of PLM in this conserved region further strengthens the conclusion that the additional band resolved at approximately 25 kDa is PLB which is detected due to cross-reactivity of the CP68 antibody in this region. Thr17 is also phosphorylated in the cardiomyocyte by CaMK; phosphorylation at this site may have also resulted in cross-reactivity with CP68 due to the sequence similarities in this region.

It is evident from Table 5.2 that PLB exhibits higher phosphorylation levels in LVD samples. This finding is in agreement with an earlier study which demonstrated a significantly higher degree of phosphorylation of PLB in the same rabbit model of heart failure as the current thesis (Currie & Smith, 1999). In this study, mean PLB phosphorylation state (Ser16 and Thr17 phosphorylation) was significantly increased in LVD compared to sham (4.0 ± 1.7 *vs.* 8.3 ± 0.42 respectively; $p<0.001$). Additionally, SERCA2a and total PLB were significantly reduced in LVD *vs.* sham (Currie & Smith, 1999). It is well established that β-adrenergic stimulation leads to phosphorylation of PLB which relieves its inhibition on SERCA2a. This in turn promotes sequestration of Ca^{2+} into the SR and increases the amount available for release during EC coupling. Heart failure is characterised by altered β-adrenergic signalling. The cellular basis for these changes is unknown but they include upregulation of cellular kinases and downregulation of β-adrenoceptor density (Bristow *et al.*, 1982; Currie & Smith, 1999). The finding of enhanced phosphorylation of PLB is consistent with other animal models of heart failure (Boateng *et al.*, 1997). The cause of increased phosphorylation of PLB is unclear due to the variable and complex balance between levels of kinases and phosphatases in heart failure.

A potential mechanism for the regulation of SERCA2a by PLB relates to the structure of its cytoplasmic C-terminal. This has been suggested to act as a conformational switch which, in the absence of SERCA2a, interacts with the membrane but in its presence allows PLB to directly interact with SERCA2a (Clayton *et al.*, 2005). A similar mode of operation in the regulation of Na^+/K^+-ATPase and NCX has been proposed for PLM.

5.5.3 Limitations

The quantitative Western blotting protocol and analysis employed in this thesis failed to include an internal standard. The value of an internal standard and the difficulties associated with their selection is highlighted in General methods 2.3.1.1. A more accurate method would have been to run an internal standard such that variation between the signals obtained from each sample could be minimised.

5.6 Summary

The unaltered phosphorylation status of PLM (Ser63/Ser68) or of total PLM expression levels revealed by this study suggest that PLM would not significantly inhibit NCX activity in LVD cardiomyocytes. It is therefore concluded that PLM does not account for, or contribute to, the previously demonstrated decreases in NCX activity despite increased NCX protein levels in this rabbit model of LVD. The lack of a significant finding may reflect compensatory changes in phosphorylation/expression levels in line with their 8 week recovery period. A previous study of gene expression alterations following myocardial infarction showed that PLM levels returned to normal at both 6 and 12 weeks post myocardial infarction in spite of being significantly raised at 2 weeks (Sehl *et al.*, 2000). Mechanisms other than increased PLM inhibition of NCX are considered to account for the reduction in NCX activity in this rabbit model of LVD.

CHAPTER 6
NCX PHOSPHORYLATION

6.1 Introduction

The regulation of NCX transport activity is highly complex and occurs in response to a variety of factors including phosphorylation. Phosphorylation is a well recognised and powerful modulator of the activity of a number of proteins within the cardiomyocyte. The current chapter focuses on the phosphorylation status of NCX in sham and LVD rabbit hearts and the relation this may have to NCX function.

The concept that phosphorylation may regulate NCX activity was first suggested through stimulation of the exchanger by ATP in bovine sarcolemmal vesicles (Caroni & Carafoli, 1983), isolated rat cardiomyocytes (Haworth *et al.*, 1987) and the squid axon (DiPolo & Beauge, 1987). Following this, experiments were undertaken to determine the mechanism behind the ATP effect. Using giant excised sarcolemmal patches from guinea-pig, rabbit and mouse (Collins *et al.*, 1992) and heterogeneously expressed NCX (Condrescu *et al.*, 1995; Linck *et al.*, 1998), the mechanism was found to be independent of protein kinases and phosphorylation of NCX. The ATP effect was shown to occur in response to the generation of PIP_2 and attenuation of Na^+-dependent inactivation (Hilgemann & Ball, 1996; He *et al.*, 2000; Philipson & Nicoll, 2000).

The *potential* for phosphorylation of NCX was confirmed when the NCX gene was cloned and shown to contain putative phosphorylation sites within the sequence encoding for the intracellular loop region (Nicoll *et al.*, 1990). Shortly after this, evidence in the literature arose in support of NCX phosphorylation in mammalian Purkinje fibres (Han & Ferrier, 1995), in smooth muscle (Iwamoto *et al.*, 1995) and in cardiac NCX expressed in baby hamster kidney cells (BHK) (Linck *et al.*, 1998). In contradiction to this, single cell voltage clamp experiments in guinea-pig ventricular myocytes found no effect on NCX activity in response to β-adrenergic stimulation (Main *et al.*, 1997). To the present day, phosphorylation of NCX and the subsequent modulation of its function remain controversial. Studies have evaluated potential phosphorylation of NCX via either PKA- or PKC-mediated pathways and these will be reviewed separately.

NCX phosphorylation in the ventricular myocyte has been widely examined through the use of the β-adrenergic agonist, isoprenaline. Although isoprenaline is a non-selective agonist at β-adrenoceptors, the range of effects of isoprenaline in the heart all arise through the activation of β_1-adrenoceptors as β_2-adrenoceptors are absent in cardiac tissue. Through this G-protein coupled receptor system, isoprenaline application leads to an increase in the cytoplasmic cAMP concentration ($[cAMP]_i$) which stimulates PKA to initiate phosphorylation of its intracellular target proteins. These studies involving isoprenaline will therefore be discussed under PKA-mediated phosphorylation.

6.1.1 PKC-mediated phosphorylation of NCX

The regulation of NCX activity by PKC-mediated phosphorylation was first suggested in the squid axon by a mechanism proposed to involve PKC and an increased affinity for $[Ca^{2+}]_i$ and $[Na^+]_o$ (DiPolo & Beauge, 1987). Evidence of phosphorylation of mammalian NCX via the PKC pathway did not arise until some time after from work using cultured rat smooth muscle cells (Iwamoto *et al.*, 1995). Upon labelling these cells with ^{32}P, a phosphorylated form of NCX was identified. The extent of phosphorylation could be increased by exposure to PMA which was associated with enhanced reverse NCX activity (Iwamoto *et al.*, 1995).

PKC-mediated phosphorylation and regulation of NCX activity were then shown in cardiac mammalian NCX protein immunoprecipitated from CCL39 fibroblasts (expressing cloned canine cardiac NCX) and neonatal rat cardiomyocytes (Iwamoto *et al.*, 1996). Using autoradiography, phosphorylation was shown to be significantly increased by approximately 50% (*vs.* basal levels) in response to phorbol 12-myristate 13-acetate (PMA; a PKC agonist at 0.3 μmol/L) and okadaic acid (a protein phosphatase inhibitor at 1 μmol/L) which was accompanied by a concomitant increase in both forward and reverse NCX activity by approximately 15% of control. Conversely, treatment with kinase inhibitors reduced phosphorylation levels. Phosphomapping identified sites residing on the intracellular loop of the NCX molecule for phosphorylation by PKC (Iwamoto *et al.*, 1996). A similar effect of PKC-mediated phosphorylation of rat NCX was

achieved using the α_1-agonist phenylephrine. Measurement of $^{45}Ca^{2+}$ uptake into rat sarcolemmal vesicles revealed that application of phenylephrine (100 μmol/L) significantly increased NCX uptake activity by 111% (Ballard & Schaffer, 1996). The PKC inhibitor chelerythrine (CLT; a PKC inhibitor) and the α_1-antagonist prazosin significantly reduced the ability of phenylephrine to increase exchanger function. Thus, the effects of these interventions pointed towards a mechanism of action of phenylephrine which occurred through stimulation of phospholipase C and activation of PKC (Ballard & Schaffer, 1996). A 31% increase of I_{NCX} was induced by phenylephrine (80 μmol/L) in intact rat ventricular myocytes (Stengl *et al.*, 1998).

Collectively, these studies indicated that phosphorylation of mammalian cardiac NCX could occur through a PKC-dependent mechanism most probably involving the intracellular loop region of the molecule leading to increased exchanger function (Ballard & Schaffer, 1996; Iwamoto *et al.*, 1996; Stengl *et al.*, 1998). It was, however, unclear if this effect was due to direct phosphorylation of residues on the intracellular loop or an additional protein. Further work by Shigekawa's group used CCL39 fibroblasts expressing NCX mutants which underwent phosphorylation via PMA treatment (Iwamoto *et al.*, 1998). The NCX mutants were formed by substituting one of the nine serine candidate phosphorylation sites for alanine, thus rendering it incapable of being phosphorylated at that site. Three of these residues (Ser-249, Ser-250 and Ser-357) were shown to be phosphorylated by PKC. When NCX was mutated at all three sites and expressed in CCL39, the increase in activity in response to PMA was maintained. An additional NCX mutant, in which the most central cytoplasmic loop (residues 246-672) was removed, showed a loss of enhanced exchanger activity on exposure to PMA. From this it was concluded that PKC-dependent regulation of NCX did not require the direct phosphorylation of the NCX molecule (Iwamoto *et al.*, 1998).

6.1.2 PKA-mediated phosphorylation of NCX

The subject of PKA-mediated phosphorylation of NCX is one of intense debate. A growing body of evidence has emerged in support of NCX phosphorylation via the PKA pathway yet this has been met with strong resistance from reports which refute this effect. Phosphorylation of NCX via the PKA pathway has been examined functionally through measurement of exchanger function in response to β-adrenergic stimulation and directly using biochemical techniques.

The ability of PKA to phosphorylate NCX was demonstrated using *in vitro* phosphorylation of a fusion protein of the cytoplasmic domain of canine cardiac NCX (Iwamoto *et al.*, 1996). Two early studies then went on to examine NCX activity in response to PKA stimulation and each yielded a contradictory result (Main *et al.*, 1997; Han & Ferrier, 1995). Measurement of I_{NCX} and $[Ca^{2+}]_i$ (with SR and sarcolemmal ion channels inhibited) in guinea-pig ventricular myocytes indicated no effect on application of 1 μmol/L isoprenaline (Main *et al.*, 1997). In two-electrode voltage clamped Purkinje fibres from the rabbit, isoprenaline application (0.1 μmol/L) was shown to significantly enhance I_{NCX}, an effect which could be mimicked by forskolin (Han & Ferrier, 1995). The result was attributed to β-adrenoceptor-initiated phosphorylation of NCX. In frog ventricular myocytes, however, isoprenaline was shown to inhibit NCX activity resulting in a reduction of I_{NCX} by 40-80% of the control current (Fan *et al.*, 1996). As direct activation of cAMP with forskolin mimicked the reduction, the effect of isoprenaline was assigned to the adenylate cyclase-cAMP-PKA pathway. Experiments in oocytes later showed the isoprenaline effect occurred through a specific exon sequence unique to the frog (Shuba *et al.*, 1998) thus the opposing effect of isoprenaline in frog may be due to a species-specific difference in the gene sequence between the amphibians and mammals.

Recent works have focussed on whether phosphorylation of mammalian cardiac NCX occurs through the PKA-system and the potential this may have in the regulation of NCX function. Of these latest studies, two have reported no effect of β-adrenergic stimulation (Ginsburg & Bers, 2005; Lin *et al.*, 2006). The modulatory effect of isoprenaline on NCX activity was investigated in intact rabbit ventricular myocytes using three different experimental approaches.

These involved measurement of Ca^{2+} removal from caffeine-induced transients during field stimulation and electrophysiological measurement of I_{NCX} with perforated and whole cell ruptured patch techniques. The results demonstrated no alteration in the $[Ca^{2+}]_i$ dependence of NCX function or in the Ni^{2+}-sensitive current (I_{NCX}) and therefore each approach agreed that isoprenaline did not alter NCX function (Ginsburg & Bers, 2005). A similar lack of effect of isoprenaline on the Ni^{2+}-sensitive current (I_{NCX}) has recently been reported using guinea-pig, mouse and rat ventricular myocytes (Lin *et al.*, 2006).

Phosphorylation of NCX by the PKA pathway was positively demonstrated in *Xenopus* oocytes expressing neuronal NCX (He *et al.*, 1998). The first detailed study to then show this effect on the mammalian exchanger was performed in oocytes expressing the cardiac exchanger from the rat and in native rat ventricular myocytes (Ruknudin *et al.*, 2000). Upon application of a "cAMP-dependent protein kinase-activating cocktail" a 40% increase in Na^+-dependent $^{45}Ca^{2+}$ uptake in the oocyte preparation occurred; this effect was mimicked in isolated ventricular rat myocytes. Similarly, measurement of I_{NCX} revealed that isoprenaline increased the outward current by approximately 100%. Application of KT5720, a PKA antagonist, nulled this effect. Cardiac NCX was immunoprecipitated from these preparations and *in vitro* back-phosphorylation work demonstrated this was indeed as a result of direct PKA-mediated phosphorylation of the NCX protein (Ruknudin *et al.*, 2000). The ability to phosphorylate NCX *in vitro* using the catalytic subunit of PKA was also confirmed in a later paper from the same group (Schulze *et al.*, 2003).

A stimulatory effect of isoprenaline has been demonstrated in pig ventricular myocytes (Wei *et al.*, 2003). Application of 2 μmol/L isoprenaline resulted an approximately 100% increase in the Ni^{2+}-sensitive I_{NCX} activity with no alteration in the reversal potential of the current (Wei *et al.*, 2003). In contrast to findings in the guinea-pig by Main and co-workers (1997), isoprenaline was more recently shown to significantly increase Ni^{2+}-sensitive I_{NCX} in this species in both forward and reverse modes by between 25 -100% of control values (Perchenet *et al.*, 2000; Zhang *et al.*, 2001). This was mimicked by the application of forskolin (Perchenet *et al.*, 2000) and almost completely inhibited in the presence of adenosine (which activates an inhibitory G-protein thereby decreasing $[cAMP]_i$)

indicating a direct dependence on increased $[cAMP]_i$ for NCX augmentation (Zhang *et al.*, 2001). Co-incubation of guinea-pig myocytes with isoprenaline and PMA did not change the stimulatory effect of isoprenaline on NCX function and similarly no effect was seen with the inclusion of CLT. Both of these approaches ruled out the possibility of a PKC-mediated effect and confirmed the mechanism of stimulation of NCX activity to occur by way of the PKA pathway (Perchenet *et al.*, 2000; Zhang *et al.*, 2001).

The stimulatory effect of isoprenaline on NCX function in the guinea-pig reported by these two latter studies has recently been contested (Lin *et al.*, 2006). In voltage-clamped guinea-pig ventricular myocytes, application of 1 μmol/L isoprenaline augmented the Ni^{2+}-sensistive current by approximately 32%. It was shown, however, that the mechanism of this increase was solely due to a contaminating increase in the PKA-activated cystic fibrosis trans-membrane conductor regulator (CFTR) chloride current ($I_{CFTR-Cl}$) and *not* through any significant alteration in I_{NCX} (Lin *et al.*, 2006). Using voltage-clamped guinea-pig ventricular myocytes, exchanger function was "removed" (0 $[Ca^{2+}]_o$; Ca^{2+} and Na^+-free pipette solution composition) and cells were subjected to 1 μmol/L isoprenaline to stimulate $I_{CFTR-Cl}$. Further application of 5 mmol/L Ni^{2+} inhibited $I_{CFTR-Cl}$ with a half-maximal concentration of 0.5 mmol/L indicating that $I_{CFTR-Cl}$ was also sensitive to Ni^{2+}. Additionally, when I_{NCX} was assessed in a low Cl^- solution at the reversal potential for $I_{CFTR-Cl}$ (designed to minimise the contamination by $I_{CFTR-Cl}$), application of 1 μmol/L isoprenaline produced no change in the Ni^{2+}-sensitive I_{NCX} confirming the conclusion that NCX function was unaltered (Lin *et al.*, 2006). No evidence of contamination of I_{NCX} by $I_{CFTR-Cl}$ occurred in the swine study by Wei *et al.* (2003) as evidenced by a subset of experiments in which niflumic acid was included (Wei *et al.*, 2003; Haigney *et al.*, 2006). The presence of a large $I_{CFTR-Cl}$ conductance is well established in guinea-pig cardiomyocytes yet it is practically absent in larger animals and thus its contamination may not be a factor in other species when assessing effects of β-adrenergic stimulation on the Ni^{2+}-sensitive I_{NCX} (Haigney *et al.*, 2006).

A physical basis to support PKA-mediated phosphorylation of NCX has recently been suggested by Schulze and colleagues (2003). They proposed that NCX existed in a macromolecular complex of kinases and phosphatases as has

previously been shown for both the cardiac LTCC and RyR2 (Schulze *et al.*, 2003). The study involved the determination of protein-protein interactions between NCX and the proteins previously implicated to be involved in NCX phosphorylation. NCX protein was immunoprecipitated from rat heart and shown to contain both the catalytic and regulatory subunits (RA1 but not RAII) of PKA, PKC and protein phosphatases 1 and 2A. Critically, the additional presence of A Kinase Anchoring Protein (mAKAP) (300 kDa form) was detected in the NCX immunoprecipitate. Further immunolocalisation studies in intact rat ventricular myocytes revealed a colocalisation of the mAKAP with NCX and PKA-RA1 and therefore confirmed a scaffolding mechanism through which PKA could be linked with NCX. By analogy with the RyR2 macromolecular configuration, several leucine/isoleucine zipper regions were highlighted in the intracellular loop sequence of NCX as a means of providing the link in the NCX structure with mAKAP. No linker molecule was proposed for the association of NCX with PKC and further investigation of the spatial organisation if the intracellular loop region of NCX is required to determine this interaction. An additional protein, ankyrin, was assumed to participate in the complex as a method by which the NCX macromolecular complex could interact with the cytoskeleton and be guided to the appropriate locations within the cell such as the t-tubule membrane (Schulze *et al.*, 2003).

6.1.3 NCX phosphorylation in heart failure

To date, only one study has been undertaken to examine the phosphorylation status of NCX in heart failure. Wei and co-workers used a pig model of tachycardia-induced heart failure in which to assess both the basal phosphorylation status of NCX and its responsiveness to β-adrenergic stimulation (Wei *et al.*, 2003). NCX protein levels and activity were characterised in the model and shown to be increased by 149% and 500% of control values respectively. Despite the increased protein levels in failing cells, application of isoprenaline (2 μmol/L) resulted in a modest 100% increase in mean peak I_{NCX} in failing cells compared to a 500% increase induced in control cells. The diminished reserve of phosphorylatable NCX in failing cells was shown to be independent of decreased β-adrenoceptor numbers or downregulated adenylate cyclase activity as application of forskolin and 8-Br-cAMP resulted in a similar

magnitude of increase in failing cells as isoprenaline. Direct assessment of the PKA-phosphorylation status of NCX in control and failing swine cardiomyocytes was performed using *in vitro* back-phosphorylation. The resulting data indicated that the NCX protein from control hearts was phosphorylated by twice as much *in vitro* and thus NCX from the failing heart was hyperphosphorylated. A proportionately higher reduction in mean peak I_{NCX} in failing cells (73%) compared to controls cells (20%) by protein phosphatase 1 application verified this result and indicated reduced protein phosphatase activity as a possible mechanism behind the enhanced phosphorylation status in failing cells. In conclusion the authors stated that hyperphosphorylation of NCX may account for the disproportionate increase in NCX activity (500% *vs.* control) despite the modest increases in NCX protein levels (149% *vs.* control) in their heart failure model (Wei *et al.*, 2003).

6.2 Aims

The aims of the present chapter were as follows:

1. To quantify the endogenous phosphorylation levels of NCX in cardiac extracts from rabbits with and without LVD using *in vitro* back-phosphorylation techniques.

2. To quantify endogenous NCX protein levels in cardiac extracts from rabbits with and without LVD using quantitative Western blotting.

3. To assess whether the NCX phosphorylation status was altered in LVD compared to sham.

6.3 Methods

Quantification of the PKA-mediated phosphorylation status of endogenous NCX protein from rabbit cardiac extracts (sham and LVD) was performed in collaboration with Dr Dan Schulze's group, University of Maryland, Baltimore. In addition, quantitative Western blotting was performed to assess differences in NCX protein in cardiac lysates from sham and LVD. Details of the extract preparation are listed in General methods (2.3.5.1 and 2.3.6.2). A brief overview of the technique of *in vivo* back-phosphorylation can also be found there (2.3.4).

6.3.1 Solutions for in vitro back-phosphorylation of NCX

The solutions given below were freshly prepared for each experimental run. All concentrations are in mmol/L except where stated otherwise; pH correction was performed at room temperature (20-21 °C).

Phosphorylation buffer - HEPES (25), $MgCl_2$ (5), EGTA (5), 2% Triton X-100; pH 7.4.

RIA buffer - sodium phosphate buffer (50), KF (50), NaCl (75), EDTA (2.5), Tris (25), 0.01% NaN_3.

6.3.2 In vitro back-phosphorylation of NCX

The cardiac extract was centrifuged at 100 g for 10 min to remove any undissolved cell fragments. The supernatant was concentrated 3-fold using Microcon-50 (Millipore) and the total protein concentration was assayed (Bio-Rad protein assay kit). Samples were incubated with NCX polyclonal antibody 11-13 (1:200, Swant, Bellinzona, Switzerland) overnight at 4 °C. The antigen-antibody complex was precipitated by mixing with protein A-Sepharose beads (Sigma) for 2-4 hr at 4 °C followed by centrifugation which yielded a pellet. *In vitro* phosphorylation was performed by incubation of the pellet with 1 μg of the catalytic subunit of PKA (PKA-CS reconstituted in 5 mmol/L DTT) and 370 kBq of

[^{32}P]ATP (111 TBq/mmol) in phosphorylation buffer for 10 min at 37 °C. The reaction was stopped by washing with RIA buffer.

Gel electrophoresis and Western blot analysis were used in order to detect (i) total NCX protein from the cardiac lysates and (ii) incorporation of labelled phosphate from the immunoprecipitate. The protocol followed was similar to that of the sorcin study with exception of the following:

Samples were prepared in loading buffer containing 100 mmol/L DTT, heated at 75 °C for 3 min and loaded onto 8% polyacrylamide gels. Membranes were incubated with polyclonal rabbit anti-NCX1 primary antibody (1:500, Swant) in antibody incubation buffer at room temperature for 3 hr and HRP-conjugated anti-rabbit secondary antibody (1:2000, Jackson Immunoresearch Laboratories, PA, U.S.A) in antibody incubation buffer at room temperature for 1 hr. Membranes were developed by peroxidise-catalysed chemiluminescence of luminol (Amersham). Signals were detected with Hyperfilm-ECL. Band intensity for each of the samples was digitised using computer software and corrected for protein loading.

Results were expressed as the mean of a number of experiments and a two-tailed unpaired Student's T-test was used to indicate statistical significance between sham and LVD groups ($p<0.05$).

6.4 Results

6.4.1 Detection of NCX from cardiac samples

Quantitative Western blotting was performed for total NCX protein in ventricular samples from sham and LVD rabbits using an immuno-specific antibody. A representative blot obtained from these experiments is presented below in Figure 6.1A. The endogenous phosphorylation status of NCX protein was also assessed in samples from sham and LVD rabbits using *in vitro* back-phosphorylation and incorporation of [^{32}P]; typical autoradiographs obtained are presented below in Figure 6.1B.

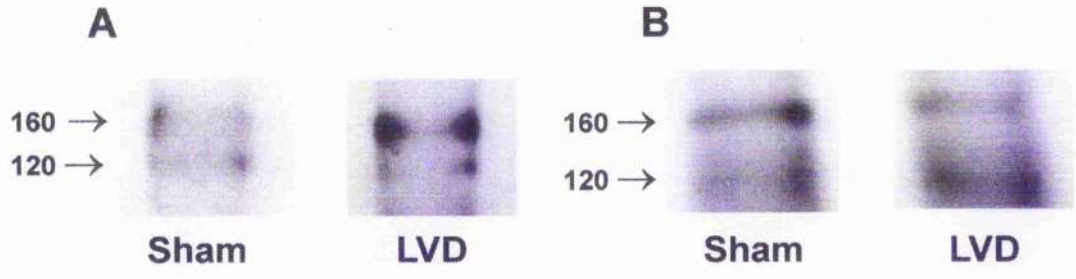

Figure 6.1 Typical blots of NCX protein and back-phosphorylation in sham and LVD.

Example signals obtained **A** when probing ventricular samples from sham (left) and LVD (right) for total NCX protein and **B** from back-phosphorylation in immunoprecipitated NCX from samples of sham (left) and LVD (right) incorporating [^{32}P]; arrows to the left of **A** and **B** indicate the 120 and 160 kDa bands used for quantification.

Each blot in Figure 6.1 A and B shows two bands representing the 120 and 160 kDa forms of NCX. These were quantified and summed to produce a mean values for protein (Figure 6.1 A) and back-phosphorylation (Figure 6.1 B) in sham and LVD samples.

6.4.2 Increased NCX protein and hyperphosphorylation in LVD

The mean data obtained for total NCX protein and PKA-mediated back-phosphorylation in sham and LVD groups are shown in Figure 6.2.

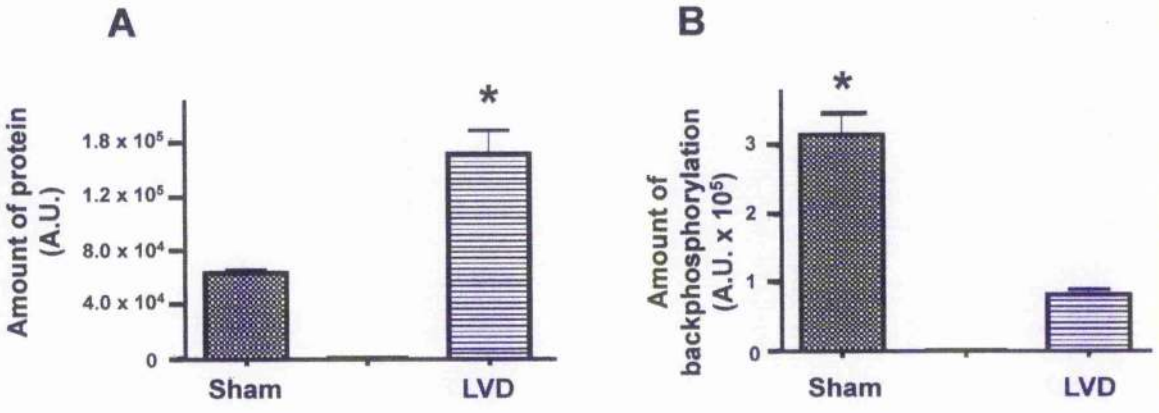

Figure 6.2 Mean NCX protein and back-phosphorylation by PKA in sham and LVD.

Mean ± SEM densitometry data for **A** NCX total protein in sham (hatched; n=6) and LVD (lined; n=6) and **B** back-phosphorylation in sham (hatched; n=3) and LVD (lined; n=3). NCX total protein was significantly higher in the LVD group *vs.* sham whilst a significantly higher incorporation of ^{32}P in the sham group indicated a significantly higher basal level of phosphorylation in the LVD group. Asterisks indicate $p<0.001$.

The graph in Figure 6.2 shows that total NCX protein was significantly higher in the LVD group compared to sham. The degree of incorporation of ^{32}P is inversely related to endogenous phosphorylation levels thus the significantly higher incorporation in the sham group *vs.* the LVD group (Figure 6.2 B) is indicative of a significantly higher level of basal phosphorylation in LVD compared to sham. Basal phosphorylation in LVD was in the order of three-fold higher than sham.

6.5 Discussion

Previous studies have suggested an up-regulation of mammalian NCX activity in response to PKA-mediated phosphorylation of NCX (Han & Ferrier, 1995; Perchenet *et al.*, 2000; Ruknudin *et al.*, 2000; Zhang *et al.*, 2001; Schulze *et al.*, 2003; Wei *et al.*, 2003). Recently in a tachycardia-induced pig model of heart failure, hyperphosphorylation of NCX was detected which was associated with significantly increased basal NCX function (Wei *et al.*, 2003). In the rabbit model of LVD used in the current thesis, Quinn and co-workers (2003) found NCX protein to be significantly increased (132% of sham) whilst NCX function was reduced to 75% of sham values. The phosphorylation-dependent regulation of NCX function has been demonstrated by many different groups and so the work presented in the current chapter aimed to determine if a decrease in the phosphorylation status of NCX could account for the reduced NCX activity despite increased protein previously demonstrated in the rabbit model of LVD (Quinn *et al.*, 2003).

6.5.1 Hyperphosphorylation of NCX in LVD

Quantification of total NCX protein revealed a significantly higher level of NCX expression in LVD *vs.* sham. This is in keeping with previous data gleaned from the same animal model (Quinn *et al.*, 2003). Quantification of the endogenous phosphorylation status of NCX from sham and LVD cardiac samples was achieved by measuring the incorporation of radiolabelled phosphate by the catalytic subunit of PKA. Although the existence of PKA-mediated phosphorylation in the rabbit has been contested (Ginsburg & Bers, 2005), the data in Figure 6.1 and 6.2 show a positive incorporation of the radiolabel into rabbit samples from both sham and LVD. These results also reveal that sham samples were subject to a significantly greater degree of back-phosphorylation by PKA, approximately 3-fold, thus indicating a significantly higher basal level of phosphorylation in LVD. Hyperphosphorylation of NCX has previously been detected in a pig model of heart failure (Wei *et al.*, 2003).

6.5.2 Disparities in the effect of NCX phosphorylation

Under normal circumstances, sympathetic stimulation of the heart is mediated by β_1-adrenergic stimulation which is well known to produce a positive inotropic and chronotropic response. This is achieved through the phosphorylation and modulation of the activity of the key Ca^{2+}-handling proteins such as LTCC, SERCA2a and RyR2. There is, however, no clear consensus in the literature as to whether NCX phosphorylation occurs under physiological conditions *in vivo* or the regulatory effect this may have on exchanger function.

Discrepancies in the legitimacy of phosphorylation of NCX via PKA may reflect the type of preparation used in each study. Many studies have employed giant excised patches or heterogeneous expression systems to study NCX regulation by phosphorylation which clearly are well removed from the situation in the intact cell. If indeed NCX does exist in a macromolecular complex (Schulze *et al.*, 2003), it is unclear whether the integrity of the complex would be maintained in these preparations. Another major variable between investigations is species difference. For example, as has been pointed out by Lin and colleagues (2006) in their latest paper, the expression levels of contaminating ion conductances may vary from species to species and lead to differential interpretation of conclusions regarding NCX phosphorylation. The differences in the effects of phosphorylation-induced modulation of NCX activity may also be linked with the level of tonic phosphorylation of the endogenous exchanger between species such that β-adrenergic stimulation may have little or no additional phosphorylation effect. The phosphorylation of intracellular proteins is a dynamic process which involves a balance between kinase and phosphatase and, as these are commonly altered in pathological situations, will further compound the true phosphorylation status of NCX in heart failure. It must additionally be noted that application of isoprenaline to ventricular myocytes will increase $[Ca^{2+}]_i$ levels which may also lead to the activation of CaMK and potentially phosphorylation. A search of the literature failed to find a study to date which has directly examined the effect of CaMK on NCX function.

6.5.3 Limitations

A recognised major short-coming of the technique developed by Ruknudin *et al.*, (2000) is the absence of a detergent in the homogenisation buffer used to purify sarcolemmal membrane preparations from the ventricular extract (see 2.3.5.1 and 2.3.6.2 in General methods). When isolating a membrane preparation from a whole-cell sample, a percentage of detergent is used in order to break down the phospholipid membrane and release the protein of interest into solution prior to centrifugation. Incomplete lysis of cells may lead to contamination of the preparation with proteins other than NCX such as cytoplasmic contents. Consequently, the hyperphosphorylation detected may reflect inappropriate back-phosphorylation of proteins other than NCX and lead to an artefactually high level of endogenous phosphorylation. Confirmation of this result with the inclusion of detergents in the lysis step is therefore required to eliminate this possibility. Ruknudin has defended his work stating that the use of detergents increases proteolysis of the fragile NCX protein tertiary structure and leads to loss of phosphorylation sites through their altered conformation (personal communication). This caveat in the back-phosphorylation protocol has further added to the controversy surrounding PKA-mediated phosphorylation of NCX.

6.6 Summary

The findings of the present chapter indicate that NCX is hyperphosphorylated via a PKA-dependent process in LVD. NCX activity has been shown to be reduced in the model of LVD employed in the current work therefore this result is inconsistent with that of Wei *et al.* (2003) who proposed that hyperphosphorylation of NCX was associated with enhanced activity. Only one account of PKA-mediated phosphorylation *reducing* NCX activity has been reported (Shuba *et al.*, 1998). This was obtained in amphibian cardiac tissue and to date no comparable effect has been suggested to occur in mammalian cardiac NCX and such an effect, although not impossible, seems unlikely. It has also been suggested that there may be a shift in the isoform of NCX expressed during heart failure (Wei *et al.*, 2003). These exchangers may then have an altered propensity to PKA-mediated phosphorylation which may further

compound the overall effects of altered NCX protein levels and activity in heart failure.

In conclusion, further work is required to ascertain the precise functional effect of hyperphosphorylation in order to assess its contribution to the reduction in NCX activity in the rabbit model of heart failure. Additionally, the phosphorylation status must be confirmed in the more physiological setting of intact ventricular myocytes through functional measurements in response to PKA-activators and/or inhibitors.

CHAPTER 7

ELECTROPHYSIOLOGICAL STUDIES OF SORCIN

7.1 Introduction

The current chapter employed an electrophysiological approach to assess the modulation of NCX function by sorcin with particular reference to EC coupling and the consequences of sorcin phosphorylation. Detailed accounts of sorcin's modulation of NCX and the alteration in sorcin's effects in response to phosphorylation have been reviewed previously in Chapter 4 (4.1.3.3 and 4.1.4 respectively); only a brief summary of each will be presented here to reiterate the main points.

7.1.1 Sorcin and NCX

The stimulatory effect of sorcin on NCX function was demonstrated in whole-cell voltage clamped in rabbit ventricular myocytes over-expressing sorcin (5-fold) via adenoviral gene transfer (Seidler *et al.*, 2003). This comprehensive study also identified effects of sorcin on EC coupling many of which were in agreement with the findings of other groups (see 4.1.5). The sorcin-mediated effects included:

(i) Decreased Ca^{2+} transient amplitude compared to controls

(ii) Decreased peak-systolic and end-diastolic $[Ca^{2+}]_i$.

(iii) Significantly decreased action potential duration.

(iv) Reduced SR Ca^{2+} content.

(v) Increased I_{NCX} and rate constant for the decay from caffeine-induced Ca^{2+} release.

Of the effects listed, the stimulation of NCX function by sorcin was a novel finding. The I-V relationship for NCX current density in sorcin over-expressing and control cardiomyocytes produced the following plot shown in Figure 7.1.

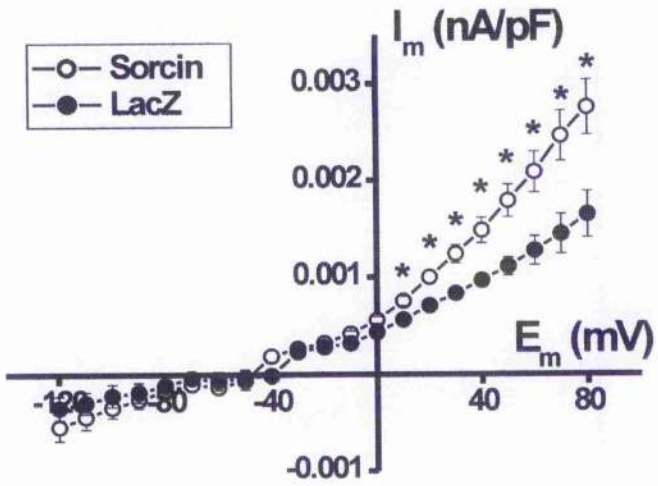

Figure 7.1 Effect of sorcin on the NCX I-V relationship.

Mean I-V relationship of the Ni^{2+}-sensitive NCX current in LacZ control (closed circles) and sorcin over-expressing (open circles) rabbit cardiomyocytes at R.T. Figure taken from Seidler *et al.*, (2003).

It was concluded that the mechanism by which sorcin reduced the Ca^{2+} transient amplitude involved a reduction in SR Ca^{2+} load through stimulation of NCX function (Seidler *et al.*, 2003). This study is the only to report an effect of sorcin on NCX and the result has yet to be confirmed by alternative routes to introduce/enhance sorcin levels in cardiomyocytes.

7.1.2 Phosphorylation of sorcin

Sorcin is phosphorylated by PKA predominantly at the RRDS region (Meyers, 1989). In the native protein, the presence of the N-terminus partially occludes this site and impedes the access of PKA (Zamparelli *et al.*, 2000; Ilari *et al.*, 2002). Phosphorylation of sorcin in response to cellular kinases other than PKA has not been reported in the literature.

Evidence exists to suggest the following responses to phosphorylation of sorcin:

(i) Reduction in the inhibition of RyR2 open probability which occurs with non-phosphorylated sorcin (Lokuta *et al.*, 1997; Farrell *et al.*, 2003).

(ii) Abolition of the interaction of sorcin and RyR2 at the molecular level (Zamparelli *et al.*, 2000).

(iii) Enhanced ability to translocate to membrane (Matsumoto *et al.*, 2005).

The effect of phosphorylated sorcin on the modulation of other target proteins such as NCX has not been investigated.

7.2 Aims

The aims of the present chapter were as follows:

1. To confirm the stimulatory effect of sorcin on NCX activity in rabbit cardiomyocytes using exogenously applied recombinant sorcin.

2. To determine the effect of sorcin phosphorylation on NCX function in rabbit cardiomyocytes.

7.3 Methods

In order to address the aims of this chapter, two sets of voltage-clamp experiments using rabbit cardiomyocytes were carried out.

The first set of experiments utilised freshly isolated cells. The effect of the inclusion of recombinant sorcin in the patch pipette solution on the membrane currents in response to an EC coupling protocol was assessed. The second group of experiments employed short-term culture of cardiomyocytes in which exogenous sorcin mutants were introduced by adenoviral-mediated delivery. Two phospho-mutants were produced by introducing a point mutation at the threonine in position 178 and replacing it with either glutamic acid (E) or alanine (A). In doing so, this created a constitutively phosphorylated form of sorcin, SorcinT178E, and a constitutively de-phosphorylated form of sorcin, SorcinT178A respectively. A control group was produced along side this using a vector containing the gene for β-galactosidase (LacZ). The protocol for the production of these follows (7.3.4.2). The NCX I-V relationship was then assessed in each group of cells.

7.3.1 Electrophysiology of single rabbit cardiomyocytes

7.3.1.1 Principles of voltage clamp

The experimental technique of voltage clamp utilises the electrical properties of biological membrane in order to measure the currents produced by the flux of ions through membrane channels. During this, voltage is held constant and current is measured. The voltage clamp setup prevents these membrane currents from influencing membrane potential by injection of current which is of an exactly equal magnitude but opposite direction to the current flowing through the channels.

Electrical control of the myocyte is achieved by gaining access to the intracellular environment of the cell via a glass micropipette (approximately 0.5 μm tip diameter) which contains conductive solution and an electrode connected to external circuitry. The latter comprises two amplifiers (voltage follower and

differential amplifier). Through this voltage can be measured and current injected either simultaneously (continuous) or alternately (discontinuous). The membrane acts as a parallel plate capacitor thus accumulates charge on either side leading to production of capacitive currents when membrane voltage is changing. By keeping membrane voltage constant these can be eliminated and current attributable to ion flow through channels can be measured in isolation.

The use of specially designed voltage protocols, membrane channel voltage inactivation potentials and selective blockers of ion channels allows the recording from subsets of ion channel populations.

The investigations carried out in the present thesis utilised the whole cell patch or dialysed cell configuration. The cell membrane was ruptured following formation of a gigaseal with the micropipette and suction thereby gaining access to the interior and allowing subsequent dialysis with pipette solution.

7.3.1.2 Apparatus

Micropipettes were pulled from borosilicate glass capillary tubes (0.69 mm I.D.; 1.2 mm O.D.) using pre-programmed protocols on a Flaming/Brown micropipette puller (Sutter Instrument 6, model P-97) and lightly heat polished. The electrode consisted of thin piece of silver wire which was coated at regular intervals throughout each experimental run using a chloride-rich solution.

Cells were contained within a perspex bath situated above the objective of an inverted microscope (Nikon, Diaphot 200) and viewed using a X 40 oil lens. Connection of a CCD camera to a monitor allowed the field of view to be visualised throughout. The solution inflow (left hand side of the bath) was provided by an multi-tube pen (MPRE8 multi-tube, Cell MicroControls, Norfolk, VA, U.S.A.) connected to a series of 50 mL syringes which were gravity fed through thin diameter tubing and controlled by solenoid valves and switching set (6-7 μl dead space). This system allowed for fairly rapid solution switching (less than 1 sec). The outflow (right hand side of the bath) consisted of a capillary tube pulled to a narrow diameter tip connected to a length of tubing which was suction fed from the tap; the bath reference electrode was positioned alongside. The microscope was placed on an air table within a Faraday cage to reduce

vibration and electrical noise respectively. An HS-2A headstage with a current gain of 0.1 (Axon Instruments, Foster City, CA, U.S.A.) was held by a clamp attached to the stage and controlled via coarse and micro-manipulators (Narishige International Ltd.). Clampex 8.0 software and an Axoclamp-2B microelectrode voltage clamp amplifier (both Axon Instruments, Foster City, CA, U.S.A.) were used to elicit and record output from protocols. Analogue to digital conversion of the signal output was performed using a digidata board (model 1320A) before being fed in to a computer.

7.3.2 Electrophysiology solutions

Solutions were freshly prepared for each experimental run. All concentrations are in (mmol/L) except where stated otherwise; pH correction was performed at room temperature (20-21 °C).

7.3.2.1 E-C coupling studies

Normal Tyrode's (NT) superfusate - NaCl (140), KCl (4), HEPES (5), $MgCl_2$ (1), $CaCl_2$ (1.8), glucose (11.1) with 4-aminopyridine (5) and niflumic acid (0.1) added to block K^+ and Ca^{2+}-activated Cl^- currents respectively; pH 7.4 with NaOH.

Control pipette solution - KCl (20), K aspartate (100), tetraethylammonium chloride (TEACl, 20, to block Ca^{2+}-dependent K^+ channels), HEPES (10), $MgCl_2$ (4.5, calculated free [Mg] ≈ 0.9 mmol/L), disodium ATP (4), disodium creatine phosphate (1), EGTA (0.01) with the extra addition of TRIS (771 μmol/L) and EGTA (15.4 μmol/L) to account for the storage constituents of the recombinant sorcin; pH 7.25 with KOH.

Sorcin-containing pipette solution - as for control but with the extra addition of recombinant sorcin (3 μmol/L) only; pH 7.25 with KOH.

7.3.2.2 NCX current density studies

K^+-free superfusate - NaCl (140), CsCl (4), HEPES (5), $MgCl_2$ (1), $CaCl_2$ (1.8), glucose (11.1) with N-acetylstrophanthidin (0.01) and nifedipine (0.01) added to block the Na^+-K^+ pump and L-type Ca^{2+} channel respectively; pH 7.4 with CsOH.

Pipette solution - CsCl (45), EGTA/Ca^{2+}EGTA (Cs 100, EGTA 50, Ca^{2+} 25, calculated free [Ca] ≈ 250 nmol/L), HEPES (20), $MgCl_2$ (11, calculated free [Mg] ≈ 1.2 mmol/L), disodium ATP (10); pH 7.25 with CsOH.

7.3.3 Electrophysiology protocols

In all experiments, voltage-clamp was achieved using whole-cell ruptured patch technique and currents were measured in discontinuous (switch clamp) mode; all protocols were pre-programmed into Clampex 8.0 software.

Isolated cardiomyocytes were bathed in normal Tyrode's at room temperature (20-21 °C). Micropipettes were filled with the appropriate solution which had been filtered (0.2 μm, Whatman) prior to use. The pipette was lowered into the bath under positive pressure in order to prevent extracellular solution travelling up into the lumen. The amplifier was set to bridge mode. The bridge and input offset were balanced to compensate for microelectrode voltage drop whilst passing current and to zero the tip potential respectively. The resistance of the pipette was read off the bridge dial (average resistance of 7 mΩ).

SEVC mode was selected and the pipette was positioned directly over cell and lowered onto surface using the micro-manipulator under positive pressure. A holding potential of -80 mV was used at this time. Once in contact with the sarcolemma, suction (negative pressure) was applied until a gigaohm seal was achieved. Membrane capacitance was corrected for at this stage. Short bursts of suction were applied to the back of the pipette to rupture the sarcolemma directly under the pipette tip and the bath perfusion was commenced. dSEVC mode was selected. Anti-alias filtering was applied to reduce noise and the gain of the amplifier was optimised until a stable whole cell voltage clamp at -80 mV was established. Sampling rate was typically 4 kHz. The appropriate voltage

clamp protocol was then applied and the integrity of the clamp was monitored throughout.

7.3.3.1 Fura-2 Ca^{2+} measurements and optical setup

In order to assess changes in intracellular Ca^{2+} during EC coupling protocols, the ratiometric Ca^{2+} indicator Fura-2 acetoxymethyl ester (AM) was used. The ability of Fura-2 to perform this function is provided by its shift in excitation spectrum on binding Ca^{2+}. When exciting at 340 nm an increase in $[Ca^{2+}]$ produces an increase in fluorescence above 500 nm; when exciting at 380 nm an increase in $[Ca^{2+}]$ produces a decrease in fluorescence above 500 nm. The ratio of these two signals is then measured. As $[Ca^{2+}]$ has opposing effects on emission when excited at 340 and 380 nm only true alterations attributable to $[Ca^{2+}]$ will produce changes in the fluorescence ratio; factors other than $[Ca^{2+}]$ that cause alterations in fluorescent measurement will be cancelled out. Consequently, the ratiometric approach accurately reports $[Ca^{2+}]_i$ independent of dye concentration or motion artefacts.

Fura-2 AM was prepared at a stock concentration of 1 mmol/L in anhydrous dimethylsulphoxide (DMSO) and frozen at -4 °C until required. Immediately prior to experiments, cells were incubated with 5 μmol/L for 12 min. During this time Fura-2 AM crosses the sarcolemma where it is rapidly hydrolysed by plasma esterases into its active, cell impermeant form. Incubation was terminated by the addition of excess normal Tyrode's.

Once a suitable cell was selected from the bath a black rectangle was manoeuvred round the periphery of the cell such that it was contained within this box and interfering light from the surroundings was excluded. A high arc lamp was used to produce light which was diffracted through a monochromator (Cairn Research Ltd., Kent, U.K.) to yield the specific wavelengths for excitation of Fura-2 AM. This was then passed to the microscope via a light guide, reflected by a dichroic mirror and focussed onto the myocyte in the box using a 40X oil lens. Emitted light was captured and passed through the dichroic mirror. Signals were received and amplified by a PMT and then measured using an Optoscan (Cairn Research Ltd., Kent, U.K.). The output (raw 340 and 380 signals

and a 340/380 ratio signal) were analogue to digital converted (Digidata 1320A, Axon Instruments, Foster City, CA, U.S.A.) and output on computer.

7.3.3.2 Calibration of the Fura-2 fluorescence ratio

Non-cellular background fluorescence was assessed by moving the box off the cell and onto an adjacent region of the bath devoid of any cells or debris. This reading was then used to zero the outputs of each wavelength on the optoscan. The minimum (R_{min}) and maximum (R_{max}) fluorescence ratios for each cell were determined at the beginning and end of the protocol respectively. R_{min} was taken as the Fura-2 fluorescence ratio in the quiescent cell before any stimulation was applied. R_{max} was determined from the peak Fura-2 fluorescence ratio following impalement of the cell with the micropipette at the end of the experiment.

7.3.3.3 EC coupling and recombinant sorcin

Myocytes were perfused with normal Tyrode's superfusate at room temperature (20-21 °C) and were whole cell voltage clamped as described above. Pipettes were filled with either control or sorcin-containing solution; the latter was not filtered due to short supply of recombinant sorcin. Cells were held at -80 mV before application of a voltage step to -40 mV for 150 ms in the presence of 5 μmol/L tetrodotoxin (TTX) in order to inhibit the inward sodium current (I_{Na}). The voltage was then stepped to 0 mV for 150 ms before returning to -80 mV. The protocol was repeated at 1 Hz for 60 s in order to achieve steady state Ca^{2+} transients. Rapid switching to perfusate containing 10 mmol/L caffeine following the protocol caused SR Ca^{2+} release from which SR content and NCX activity could be assessed.

7.3.3.4 NCX current densities in cells over-expressing sorcin mutants

Myocytes were perfused with K^+-free superfusate at room temperature (20-21 °C) and were whole cell voltage clamped at a holding potential of -80 mV. From here a 3 s ascending ramp was applied from -120 mV to +80 mV at 0.1 Hz. Myocytes were subject to 12 successive ramps during the protocol and steady

state currents were achieved. Of these, ramps 7 - 12 were performed in the presence of 5 mmol/L nickel chloride (Ni^{2+}) which is known to block NCX thus all currents recorded are as a result of alternative extrusion pathways. Subtraction of these gave the current attributable solely to NCX. Data at each potential were averaged and plotted as I-V curves.

An ascending ramp was chosen since this has been shown to cause less perturbation of sub-sarcolemmal [Ca^{2+}] than a descending ramp and the resulting currents are closer to those obtained using a voltage step protocol (Convery and Hancox, 1999).

7.3.4 Adenoviral mediated over-expression of proteins

This procedure was performed using replication-deficient adenoviral vectors containing the genes encoding for the two sorcin mutants (SorcinT178E and SorcinT178A) and LacZ.

7.3.4.1 Principles

The process of introducing genetic material into cardiac myocytes has been hindered by their inherent terminal differentiation. This has been circumvented through the use of replication-deficient adenoviruses to obtain very high expression levels of proteins of interest. Adenoviral mediated gene transfer is well suited to this task as the adenovirus possesses high infectivity efficiency (near 100%), can accommodate up to 7.5 kb of foreign genetic material and can generate high levels of protein expression within the target host.

Since their discovery in 1953, 40 distinct serotypes of human adenovirus have been isolated. These have been split into 6 subgroups of which serotype 5 is the most extensively developed and optimised as a vector for gene delivery.

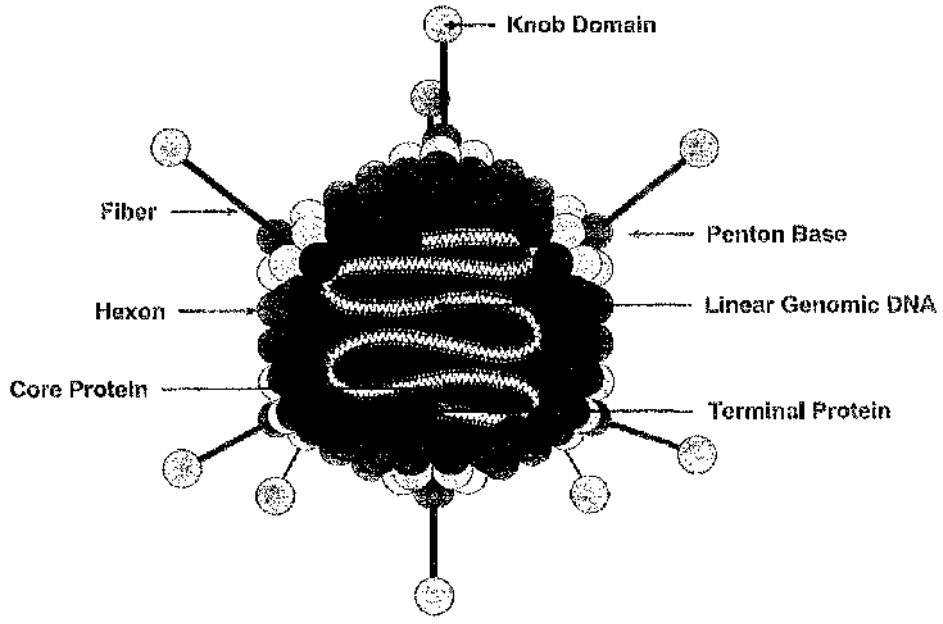

Figure 7.2 Structure of adenovirus serotype 5

Taken from Adenovator™ Q Biogene applications manual, version 1.1.

Adenoviruses exist as non-enveloped, icosahedral particles (Figure 7.2). Their structure is centred around the core which contains linear, double stranded, genomic DNA of approximately 30-40 kb. Within this are 9 transcription units which are expressed at either early or late stages of the infection cycle (early E1-E4 and late L1-L5). E1A is the first of these to be expressed in the cycle and undergoes alternative splicing which gives rise to proteins required for viral replication. Deletion of this E1 region from adenovirus in hamster embryonic kidney cells (HEK 293) was performed yielding a replication deficient virus capable of infecting other cells but not of replicating itself (Graham 1977,Becker 1994). Sites where deletions have taken place in the viral genome are then used to incorporate the foreign DNA of interest.

7.3.4.2 Production of recombinant adenoviral vectors

The adenoviral vectors were generated by Dr Tim Seidler, Dr Jurgen. Prestle (University of Goettingham) and Dr Debbie Reynolds (University of Glasgow) according to previously described methods (Becker *et al.*, 1994).

cDNA of the protein of interest was cloned and purified and the relevant mutation was introduced. A ligated construct was then formed by subjecting the vector pACCMV.pLpA to restriction digestion with *Eco*RI and *Hind*III. cDNA from the protein of interest was then ligated downstream from an immediate-early cytomegalovirus (CMV) promoter within the vector. This is a strong promoter sequence which allows transcription of the protein of interest to be initiated. The ligated construct was then transformed in E.Coli and mass produced.

The constructs and pJM17 plasmids were used to co-transfect HEK 293 cells where they underwent homologous recombination to form the functional replication-deficient recombinant adenovirus.

7.3.4.3 Transfection with recombinant adenoviral vectors

Freshly dissociated rabbit cardiac myocytes were obtained using a protocol similar to that previously stated in General methods (2.2.1) but with alterations to ensure aseptic technique. All solutions used were sterile filtered, all instruments used were autoclaved and all plastic ware was of sterile standard. The procedures were carried out in a laminar flow cabinet.

The ventricle was cut down into a sterile dish with BSA solution (0.125 mmol/L Ca^{2+}). The basal left ventricular tissue and interventricular septum were removed with care to avoid the infarct (in animals with LVD) and chopped using scissors. The tissue mixture was transferred to tissue culture grade sterile flasks and shaken at room temperature for 1 hr in order to yield single myocytes.

The cell suspension was then gradually transferred through the steps detailed previously to BSA solution containing a final concentration of 1 mmol/L $CaCl_2$. Cells were allowed to sediment by gravity and were re-suspended in M199 medium (supplemented with 312.5 mg Taurine, 500 mg D, L Carnitine, 327.5 mg creatine, 5 mL penicillin/streptomycin per 500 mL).

The cell count was assessed using haemocytometer slides and adjusted to 1×10^5 cells/mL in M199 solution. This value was previously calculated experimentally and represented the optimum cell density for culture (Debbie Reynolds, doctoral thesis, 2003). M199 cell suspension was added to a small cell culture dish in a

Class II biological safety cabinet and the appropriate volume of adenovirus was added at a multiplicity of infection of 100. Dishes were incubated at 37 °C for a period of 24 hr.

7.3.5 Statistical analysis

ANOVA multiple comparison with Tukey post-test correction was used to determine significance between groups for points on the NCX I-V curves in LacZ, T178A and T178E over-expressing cells (Figure 7.7). Statistical significance was taken as $p<0.05$.

7.4 Results

7.4.1 EC coupling studies using recombinant sorcin

The aim of this set of experiments was to assess the effects of sorcin on the currents generated by an EC coupling protocol in rabbit cardiomyocytes and compare these to control. Recombinant sorcin (3 μmol/L) was to be included in the patch pipette solution and from there dialyse into the cell. This approach proved unsuccessful as the patch pipettes containing sorcin would not maintain a seal onto the cell surface. The following modifications were made in an attempt to preserve a seal when sorcin was included in the pipette solution:

(i) sorcin concentration in the pipette solution was reduced to from 3 μmol/L to 1 μmol/L.

(ii) EGTA concentration in the pipette solution was increased from 25 μmol/L to 125 μmol/L.

(iii) "backfilling" of the pipette tip with control solution.

The alteration of EGTA concentration did not enhance sealing when sorcin was included in the pipette solution. Whilst the modifications in (i) and (iii) initially formed a seal, neither enabled it to be maintained for the duration of the protocol in order to assess stable steady-state Ca^{2+} transients or NCX-mediated extrusion from caffeine-induced transients.

Example traces from a cell using control pipette solution (control cell) and in those in which alterations in sorcin concentration and backfilling were applied are presented in Figures 7.3, 7.4 and 7.5. Each figure shows the initial 25 s of the protocol (25 sweeps) and includes traces of voltage (mV), Fura ratio and membrane current (nA). The mean membrane current (nA) and Fura ratio from a number of steady state transients (indicated in each figure) are also presented.

In control cells, the seal between the pipette and cell surface was successfully maintained throughout the EC coupling protocol (n=6). Figure 7.3 shows a set of example traces obtained from a control cell in response to the protocol indicated in Figure 7.3 A(i). As evidenced by the membrane current trace in Figure 7.3 A(iii), when the cell was held at -80 mV in between stimuli virtually no current flowed indicating a negligible leak around the pipette tip and a good quality seal. Reproducible steady state Ca^{2+} transients were obtained and I_{Ca} exhibited a characteristic biphasic inactivation. The average time constant of an exponential fit to the decay phase of the averaged steady state Ca^{2+} transient in control cells was 419 ± 2.8 ms (n=6).

Experiments were then attempted including 3 μmol/L recombinant sorcin in the patch pipette solution. These were unsuccessful as a seal between the pipette tip and surface membrane could not be maintained for long enough to establish the stable whole cell voltage-clamp configuration.

Previous work from our group applied 3 μmol/L recombinant sorcin in an NCX patch pipette solution which comprises a greater EGTA concentration than used in this set of experiments (Stewart Miller, doctoral thesis, 2003; see 7.3.2.2 for its composition). As $[Ca^{2+}]_i$ was highly buffered in that particular pipette solution, it was postulated that the inability to seal may be Ca^{2+}-dependent. In an attempt to overcome this problem, the EGTA concentration was increased from 25 μmol/L to 125 μmol/L. This was a modest increase by comparison with the NCX pipette solution such that Ca^{2+} transients could still be assessed. Modification of the EGTA concentration did not prolong sealing of the pipette when sorcin (3 μmol/L) was present in the solution.

The next adjustment in pipette solution composition involved reducing the sorcin concentration to 1 μmol/L. A typical recording yielded from this type of experiment is shown in Figure 7.4. As can be seen in Figure 7.4 A(iii), although a seal was initially achieved this broke down after approximately seven sweeps of the protocol which lead to loss of voltage control of the cardiomyocyte.

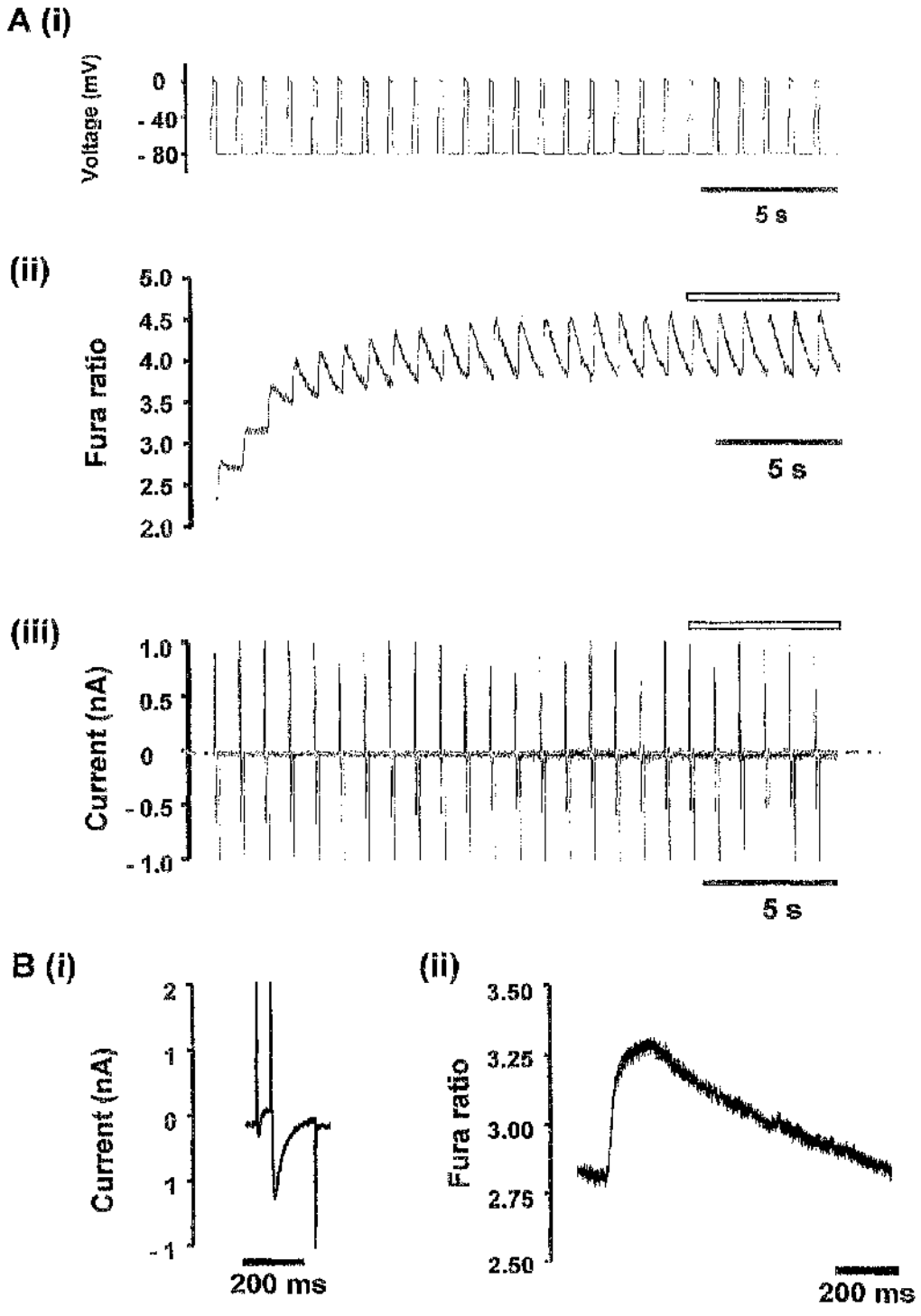

Figure 7.3 EC coupling protocol in response to control pipette solution.

A Recordings of **(i)** membrane voltage (mV); **(ii)** Fura ratio and **(iii)** membrane current (nA) during the initial 25 sweeps of an EC coupling protocol at 1 Hz; timescales are indicated beneath each. **B (i)** Mean membrane current (nA) and **(ii)** Fura ratio produced by averaging the 6 steady state signals indicated by the hollow bars above **A (ii) and (iii)** respectively.

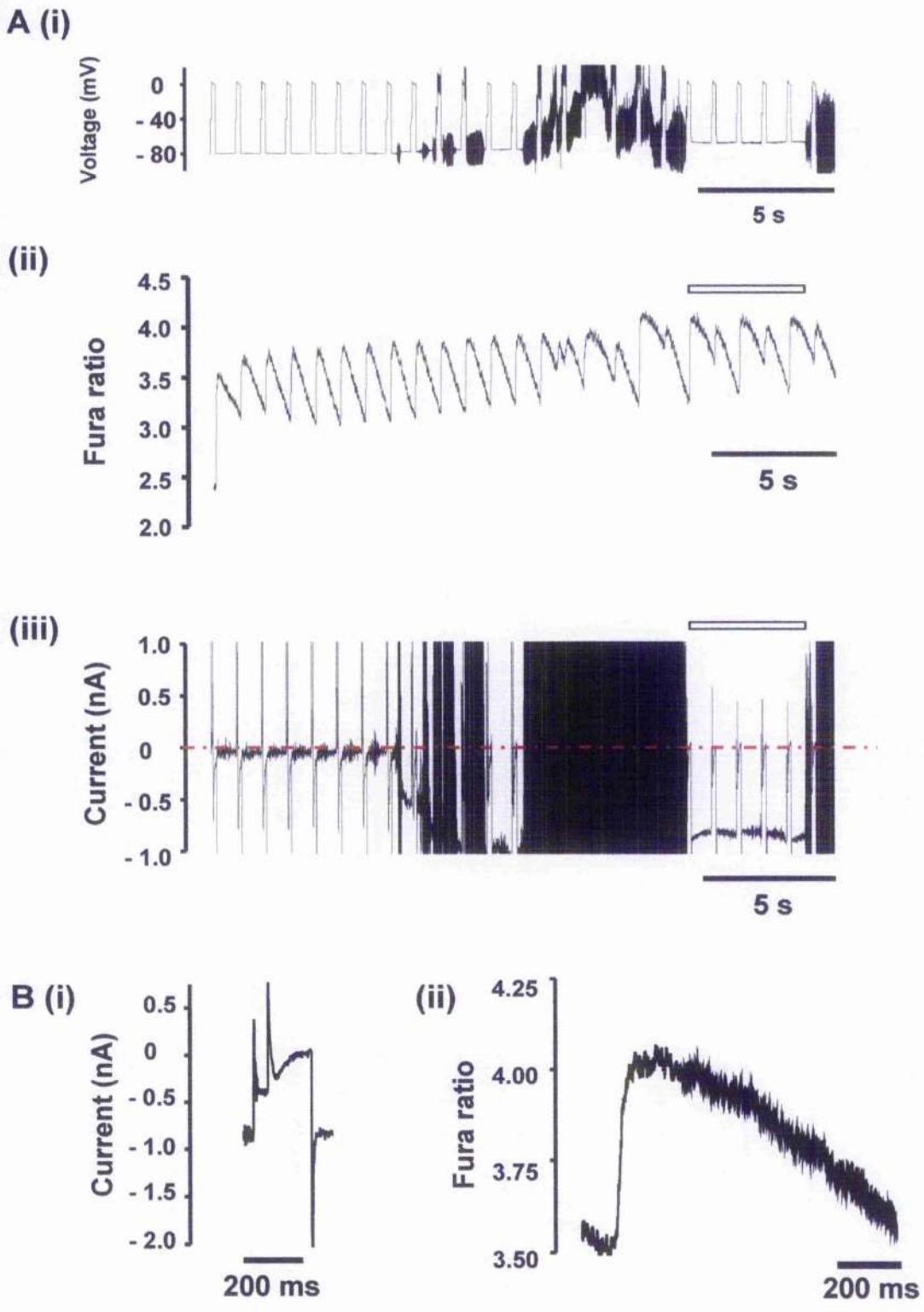

Figure 7.4 EC coupling protocol in response to 1 μmol/L sorcin pipette solution.

A Recordings as in Figure 7.3 but with the addition of 1 μmol/L recombinant sorcin in the pipette solution. **B** again as in Figure 7.3, signals were produced by averaging the 4 signals indicated by the hollow bars above **A (ii) and (iii)** respectively due to excessive noise and loss of voltage control either side.

The final adjustment made to facilitate sealing when sorcin was present in the pipette solution was to "backfill" the pipette tip. This intervention involved filling the pipette tip only with control solution and the remaining pipette lumen with sorcin-containing solution (3 μmol/L). This aimed to initially promote seal formation through the control solution, allow the membrane to be ruptured and gain access to the cell interior whilst promoting a stable seal before sorcin began dialysing into the cell. This approach also failed to maintain a seal and Figure 7.5 was the only recording achieved using this method. The membrane current signal in Figure 7.5 A(iii) shows that following rupturing of the cell membrane, the pipette seal was lost immediately on starting the protocol. As a result, the leak current became so large that voltage control of the cell could not be maintained.

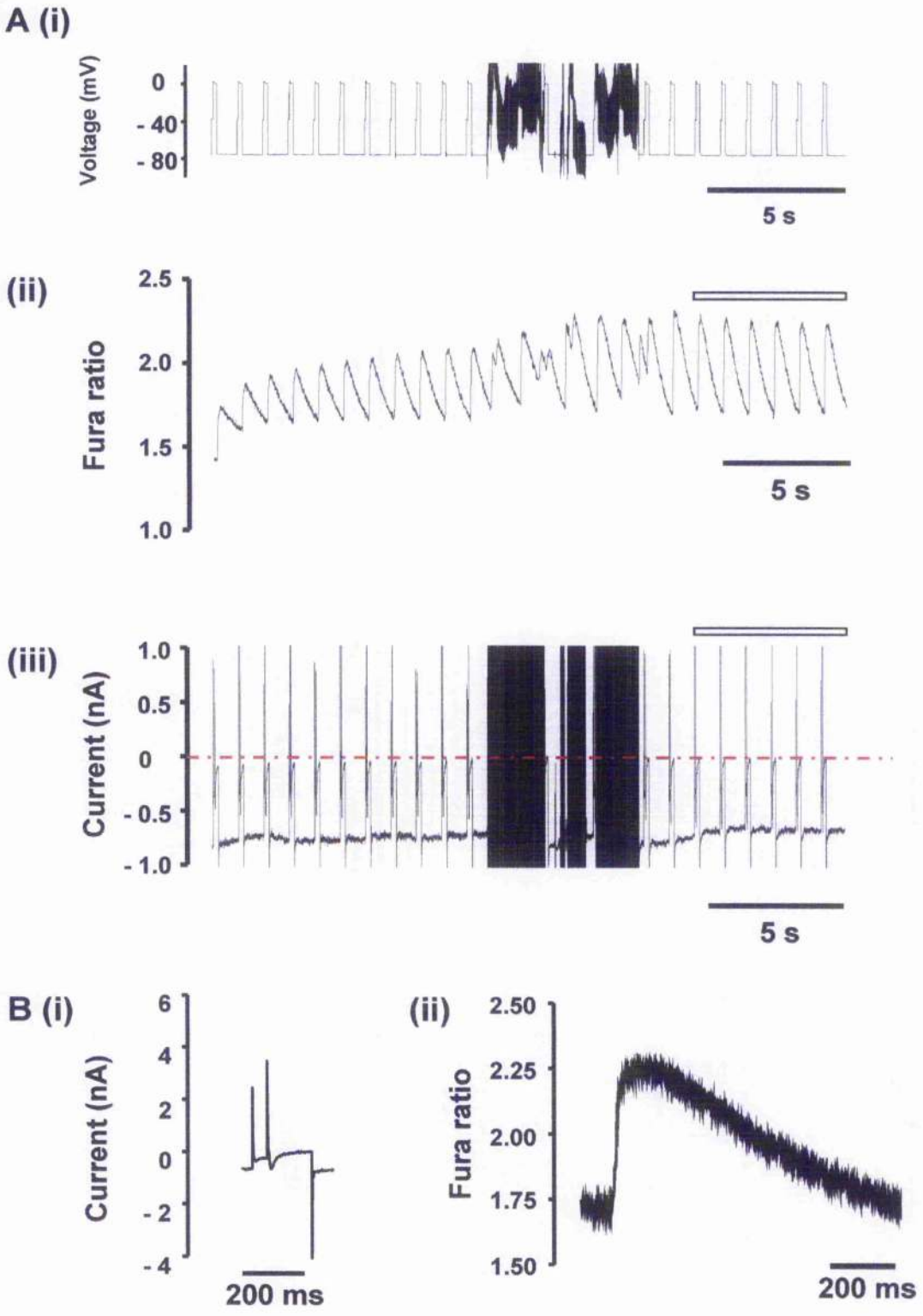

Figure 7.5 EC coupling protocol in response to 3 μmol/L sorcin backfilled pipette solution.

A Recordings as in Figure 7.3 but with the addition of 3 μmol/L recombinant sorcin in the pipette solution. **B** again as in Figure 7.3; signals were produced by averaging the 6 signals indicated by the hollow bars above **A (ii) and (iii)** respectively due to excessive noise and loss of voltage control.

7.4.2 Effect of sorcin phosphorylation on NCX activity

The effect of phosphorylation of sorcin on the stimulation of NCX function was assessed using constitutively phosphorylated (T178E) and de-phosphorylated (T178A) sorcin mutants in 24 hr cultured cells; LacZ (LZ) cells formed a control group. Membrane currents were recorded in response to an ascending ramp in the absence and presence of 5 mmol/L Ni^{2+}. A diagrammatic representation of this protocol is shown in Figure 7.6.

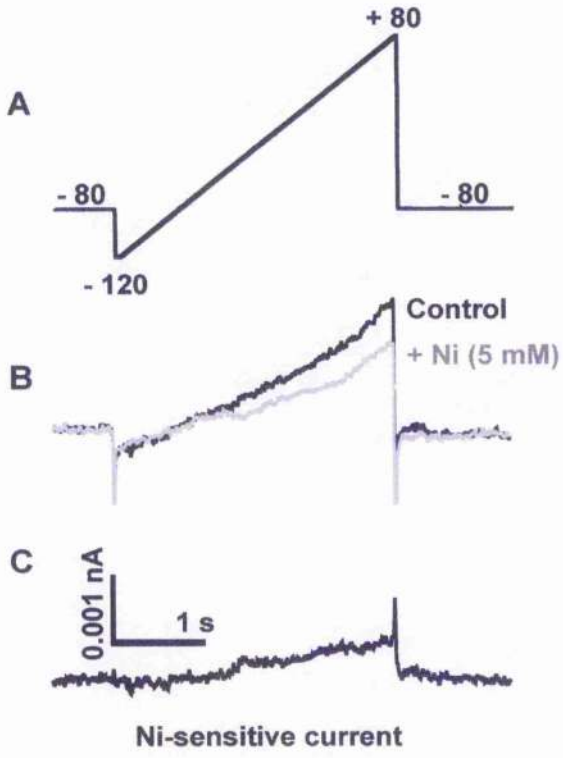

Figure 7.6 Protocol for measuring NCX density.

A Cells were held at -80 then ramped from -120 to +80 before returning to -80; all values are in mV. **B** Currents measured in response to the ramp in the absence (control) and presence (+ Ni) of nickel. **C** The Ni-sensitive current which represents NCX current density.

This eliminated currents not attributable to NCX and thus the difference current represented NCX current density. The experimental conditions were designed such that ionic conditions were strictly controlled (in the pipette solution $[Ca^{2+}]_i$ was buffered at 250 nmol/L using 50 mmol/L EGTA and $[Na^+]_i$ was set at 20 mmol/L). The difference current was plotted against voltage to construct the NCX I-V relationship for each group; these are presented in Figure 7.7.

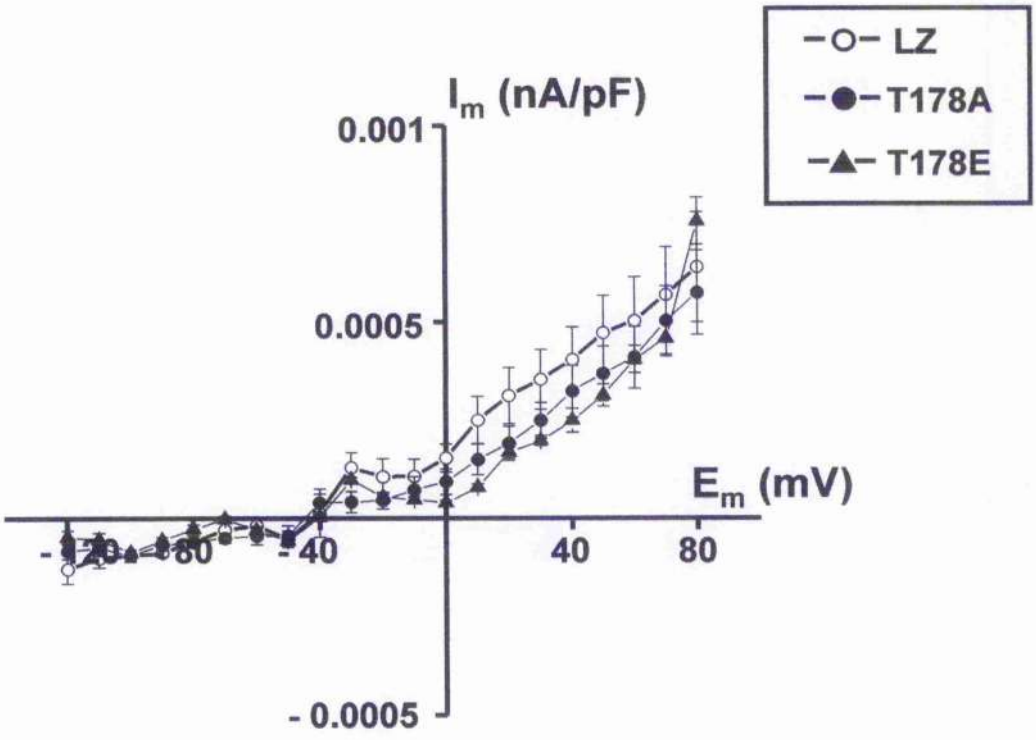

Figure 7.7 Effect of sorcin phospho-mutants on the NCX I-V relationship.

Mean I-V relationship of the Ni^{2+}-sensitive NCX current in LacZ control (open circles; n=9 cells), sorcinT178A (closed circles; n=10 cells) and sorcinT178E (closed triangles; n=6 cells) over-expressing rabbit cardiomyocytes.

The I-V relationships for each group were almost superimposable and no significant differences existed in the currents at any voltage ($p>0.05$). The reversal potential was consistent for all groups studied and lay at approximately -40 mV in keeping with previous studies using the same experimental conditions (Seidler *et al.*, 2003). In order to control for an effect of virus transfection, an additional control group of untransfected cells (no adenovirus) was also investigated and was not significantly different from LacZ (data not shown).

7.5 Discussion

7.5.1 EC coupling studies with recombinant sorcin

The failure to maintain a seal between the pipette tip and cell surface when sorcin was included in the filling solution was an unforeseen difficulty in the investigation of the effect of exogenous sorcin on EC coupling.

Previous work in the group had applied 3 μmol/L recombinant sorcin (from the same batch as used here) when measuring the NCX I-V relationship in rabbit cardiomyocytes in response to the ramp protocol described in Figure 7.6 (Stewart Miller, doctoral thesis, 2003). One major difference in the NCX current density pipette solution composition is its EGTA concentration (50 mmol/L) compared to that used in the current chapter (25 μmol/L). Higher sorcin and $[Ca^{2+}]_i$ concentrations immediately beside the membrane compared to the bulk cytoplasm may contribute to the loss of seal formation. Although the precise mechanism which would link these phenomena is unknown, the following speculation may in part contribute to the inability to maintain a seal with the conditions used in the present chapter.

As stated previously in Chapter 4, many of the process involving sorcin are highly sensitive to $[Ca^{2+}]_i$. Any fluctuations in $[Ca^{2+}]_i$ occurring due to the currents flowing during the protocol or intrinsic leaks over the sarcolemma may have produced elevated local $[Ca^{2+}]_i$ gradients in the sub-sarcolemmal space *vs.* the bulk cytoplasm. These would then differentially regulate sorcin's behaviour in the cytoplasm near to the membrane. It is well established that the translocation of sorcin to membrane is Ca^{2+}-dependent (see 4.1.1). On dialysing into the cell, the concentration of sorcin will be highest in the sub-sarcolemmal region and thus will amplify the population of sorcin susceptible to regulation by this elevated $[Ca^{2+}]_i$. This may effectively draw sorcin towards the region below the surface membrane during this initial phase following cell rupturing. Verzili *et al.*, (2000) highlight the critical dependence on $[Ca^{2+}]_i$ for the interaction between sorcin and annexin VII with optimal binding reported to occur at 6 μmol/L (Verzili *et al.*, 2000). Annexin VII has also been implicated to recruit to the membrane upon binding its target protein sorcin (Brownawell & Creutz, 1997). Once localised to the membrane, a re-ordering of the membrane can occur with formation of microdomains such as lipid rafts (Clemen *et al.*, 1999; Carozzi *et al.*, 2000; Gerke & Moss, 2002). Thus, through elevated sub-sarcolemmal sorcin and/or annexin VII produced by the $[Ca^{2+}]_i$ gradient (due to lack of buffering by EGTA) a re-organisation of the membrane environment may occur when sorcin dialyses into the cell. Disruption of the phospholipid membrane surrounding the pipette tip may then lead to a loss of the seal

between this and the membrane of the cardiomyocyte soon after its formation. This theory remains to be tested.

A study by Valdivia's group on the effects of sorcin on EC coupling included experiments in voltage-clamped murine cardiomyocytes with application of exogenous recombinant sorcin (3 μmol/L) via the pipette solution (Farrell *et al.*, 2003). These appeared to be successful and no mention was made in the paper regarding difficulty in maintaining patch pipette seals. The origin of the recombinant sorcin and patch pipette solution composition differed from that of the current study. Compounded by the species difference, in which the mouse cardiomyocyte membrane may be more robust to the effect of sorcin, these differences could account for the variable experimental success between the study of Farrell and co-workers (2003) and the study presented in this chapter.

At the time of this study, difficulties associated with optimising a new enzyme for cell isolation were experienced. Poor yields and membrane quality of the single isolated cardiomyocytes obtained is thought to have added to the difficulty in sealing pipettes in these experiments.

7.5.2 Phosphorylation

Phosphorylation of sorcin has been shown to partially reverse both the functional inhibition of RyR2 activity (Lokuta *et al.*, 1997; Farrell *et al.*, 2003) and the biochemical interaction between sorcin and RyR2 (Zamparelli *et al.*, 2000). More recently it was suggested that phosphorylation of sorcin enhanced its ability to translocate to membrane (Matsumoto *et al.*, 2005)

As the phosphorylation state has been implicated in altering the effect of wild-type sorcin it was anticipated that one of the phospho-mutants would produce a deviation in the effect of native sorcin on the NCX I-V relationship. However, the I-V relationships from cells expressing LacZ, and a constitutively phosphorylated or de-phosphorylated sorcin mutant showed no significant difference. Although the reversal potential was maintained at approximately -40 mV, the currents obtained at all potentials were approximately half the size of those measured in the study by Seidler and colleagues (2003). NCX activity is

known to be highly temperature sensitive (Bersohn *et al.*, 1991; Vornanen *et al.*, 1994) therefore repeating these experiments at 37 °C may yield larger currents and also may be important in the mediating the effects of sorcin on NCX.

The lack of effect of either sorcin phospho-mutants may lie in the construct of the mutants themselves. It is conceivable that mutating a region such as a phosphorylation site which relies critically on its tertiary structure in order to correctly to coordinate the phosphate ion in the native state would be particularly sensitive to perturbations in protein structure produced by amino acid substitution. It may be, therefore, that a point mutation at this site alters the conformation of the protein rendering it non-functional in terms of its interaction with NCX. Matsumoto *et al.*, (2005) made a point mutation at this site and produced a constitutively phosphorylated mutant of sorcin through substitution with aspartate (Matsumoto *et al.*, 2005). This was shown to alter the intrinsic fluorescence of the protein, a sign that the mutation induced significant changes in the tertiary structure of the protein. The relevance of this substitution to the functional interaction with membrane-bound targets was not investigated.

7.6 Summary

Through the use of an electrophysiological approach, the work in this chapter aimed to assess the effect of exogenously applied sorcin on EC coupling in rabbit cardiomyocytes. This was not possible as cells could not be whole cell voltage clamped under the experimental conditions used. Further work is therefore required on this to revise pipette solution composition such that cell seals can be maintained. In addition, an alternative batch of recombinant sorcin could be sourced to use with the current experimental conditions.

Assessment of the consequences of sorcin phosphorylation on NCX function in isolated cardiomyocytes failed to show any statistically significant difference. This may have been due to significant alterations in the proteins conformation by substitution at the chosen residue. Residue 178 may be involved in the interaction with NCX but this requires additional investigation. Alternative routes to phosphorylate sorcin should be investigated such as incubating the protein with PKA prior to voltage-clamp experiments. As with all proteins subject to phosphorylation, the endogenous phosphorylation state of sorcin will reflect the intricate balance of kinases and phosphatases in the cardiomyocyte. It is therefore of great importance to ascertain the functional significance of phosphorylation of sorcin on the stimulation of NCX function.

CHAPTER 8
CONCLUSIONS

8.1 Factors affecting NCX

The general aim of this thesis was to investigate the sub-cellular basis for the observed dichotomy between NCX activity and protein levels in a rabbit model of LVD. In order to address this aim, a number of candidate factors which could account for the dichotomy were investigated. These included t-tubule density, the proteins sorcin and phospholemman and the phosphorylation status of NCX. The main findings of this investigation are discussed below.

T-tubule density in LVD.....

Quantification of the relative cell area attributable to the t-tubule network revealed a significant decrease in LVD. The mechanism for this loss was shown to be due to partial detubulation of the cardiomyocyte in which some t-tubule mouths had pinched off from the surface sarcolemma therefore closing off their luminal connection to the extracellular space. Narrowing of t-tubules may also have occurred. As NCX protein is predominantly located in the t-tubule network some of the NCX population will be enclosed in the internalised t-tubules reducing the functional percentage available for ion exchange. A method for detubulating rabbit cells with the agent formamide was developed and cells were permeabilised with β-escin to provide a proof of concept for this technique.

Sorcin expression in LVD.....

A comprehensive study of sorcin protein expression determined that sorcin dimer expression was significantly reduced in LVD. This finding was verified using two different primary antibodies. As sorcin has been shown to interact with NCX leading to a stimulation of exchanger function, a down-regulation of sorcin protein would be expected to act to reduce NCX activity.

Effect of phosphorylation of sorcin on NCX activity .....

Using an electrophysiological approach, the role of modulation of NCX through phosphorylation of sorcin was assessed. Neither a constitutively phosphorylated or de-phosphorylated mutant of sorcin had a significant effect on NCX activity. This may have been due to a significant conformational change in sorcin's tertiary structure in response to the mutation which prevented their interaction with NCX.

Phosphorylation status of phospholemman in LVD.....

Quantification of the endogenous phosphorylation status of the protein phospholemman at two separate sites revealed no significant difference in LVD. Alterations in phospholemman phosphorylation do not appear to contribute to reduced NCX activity in LVD.

Phosphorylation status of NCX in LVD.....

Biochemical analysis of the phosphorylation status revealed NCX protein in LVD was hyperphosphorylated compared to control. As phosphorylation of NCX has been associated with increased activity, the hyperphosphorylation in LVD does not account for decreased NCX function. This subject requires confirmation using an alternative experimental approach.

8.2 Relative contribution to NCX dichotomy

In summary, quantitative changes in (i) t-tubule network, (ii) sorcin expression and (iii) NCX phosphorylation status were detected in LVD. In the rabbit model of LVD, NCX protein expression is increased by 32% whereas NCX activity is decreased by 25% (Quinn *et al.*, 2003). In order to speculate on the relative contribution the quantitative changes in these factors has on NCX activity or protein in the model a series of simplified estimations have been made. This aims to highlight the relevance of each of these three factors to the NCX dichotomy in LVD. The estimations utilise the appropriate previously published values for NCX (where stated) to relate the quantitative change for each factor to the dichotomy. It also assumes that the increased protein in LVD is capable

of functioning and is appropriately targeted to the correct sub-cellular areas of the membrane.

Relative to sham, in order to achieve 75% of total NCX activity from 132% protein, 57% of this protein must be active ([1/1.32]*75).

Detubulation.....

A 63% concentration of NCX protein has been reported to exist within the t-tubule network in rat (Despa *et al.*, 2003). In this thesis, a 25% loss of t-tubules was shown to occur in the rabbit model of LVD. Using the concentration value calculated by Despa *et al.*, (2003) this reduction in t-tubule network would result in a 16% loss of functional NCX protein in contact with the extracellular space. As NCX activity was reduced by 25% of sham in the rabbit, detubulation does not fully account for the reduction in protein activity.

NCX hyperphosphorylation.....

Wei *et al.*, (2003) produced the only existing study examining NCX phosphorylation in an animal model of heart failure (Wei *et al.*, 2003). In this model, the endogenous NCX of failing cells was phosphorylated 2-fold compared to sham. An accompanying 500% increase in NCX activity in LVD was determined.

In LVD protein is 32% higher than sham and if hyperphosphorylation results in a 500% increase in NCX activity (*vs.* sham) then we would expect this protein to be 660% (132*5) active yet NCX activity in our model was determined to be 75%. Therefore a large percentage of inhibition is unaccounted for. The hyperphosphorylation hypothesis predicts 660% activity but we observe 75% activity. By comparison with the study of Wei *et al.*, (2003), this relationship would predict the NCX protein in our model would to inhibited to 11% of sham (75/660). This is would require profound inhibition of NCX activity by factors independent of phosphorylation which seems highly unlikely, e.g. T-tubule remodelling predicts only a 16% reduction.

Sorcin down-regulation.....

Seidler *et al.*, (2003) over-expressed sorcin five times in the rabbit which was associated with a 2-fold increase in NCX activity (Seidler *et al.*, 2003). Work in the present thesis identified endogenous sorcin dimer levels were decreased by 33% compared to sham. Assuming a linear relationship between sorcin concentration and NCX activity where 5 times concentration of sorcin gives 2 times NCX activity, a 33% reduction in the sorcin concentration would produce an 8% reduction in NCX activity.

Thus, if the percentage effects on NCX activity of detubulation and sorcin are combined a 23% reduction in NCX function is accounted for (0.92 (sorcin) * 0.84 (t-tubule) = 0.77). The data from Quinn *et al.*, (2003) indicated a 57% reduction in activity due to the accompanying increase in NCX protein. A further 20% therefore must be as a result of additional factors to those investigated in the current thesis.

In conclusion, it appears that no factor in isolation that was investigated in the present study can account for the NCX dichotomy in the rabbit model of LVD. Of these, the most likely candidate which was shown to alter is the t-tubule network in that a partial detubulation will lead to a reduction in the fraction of functional exchanger. While it is difficult to attribute relative importance to the factors studied, perhaps more importantly are the results of this work that eliminate potential factors in the modulation of NCX in LVD.

BIBLIOGRAPHY

Ahlers, B. A., Zhang, X. Q., Moorman, J. R., Rothblum, L. I., Carl, L. L., Song, J., Wang, J., Geddis, L. M., Tucker, A. L., Mounsey, J. P., & Cheung, J. Y. (2005). Identification of an endogenous inhibitor of the cardiac Na^+/Ca^{2+} exchanger, phospholemman. *J.Biol.Chem.* **280**, 19875-19882.

Allen, D. G. & Smith, G. L. (1987). The effects of hypertonicity on tension and intracellular calcium concentration in ferret ventricular muscle. *J.Physiol* **383**, 425-439.

Anversa, P., Loud, A. V., Levicky, V., & Guideri, G. (1985). Left ventricular failure induced by myocardial infarction. I. Myocyte hypertrophy. *Am.J.Physiol* **248**, H876-H882.

Argiro, V. (1981). Excitation-contraction uncoupling of striated muscle fibres by formamide treatment: evidence of detubulation. *J.Muscle Res.Cell Motil.* **2**, 283-294.

Balaguru, D., Haddock, P. S., Puglisi, J. L., Bers, D. M., Coetzee, W. A., & Artman, M. (1997). Role of the sarcoplasmic reticulum in contraction and relaxation of immature rabbit ventricular myocytes. *J.Mol.Cell Cardiol.* **29**, 2747-2757.

Balijepalli, R. C., Lokuta, A. J., Maertz, N. A., Buck, J. M., Haworth, R. A., Valdivia, H. H., & Kamp, T. J. (2003). Depletion of T-tubules and specific subcellular changes in sarcolemmal proteins in tachycardia-induced heart failure. *Cardiovasc.Res.* **59**, 67-77.

Ballard, C. & Schaffer, S. (1996). Stimulation of the Na^+/Ca^{2+} exchanger by phenylephrine, angiotensin II and endothelin 1. *J.Mol.Cell Cardiol.* **28**, 11-17.

Bassani, J. W., Bassani, R. A., & Bers, D. M. (1994). Relaxation in rabbit and rat cardiac cells: species-dependent differences in cellular mechanisms. *J.Physiol* **476**, 279-293.

Bassani, R. A., Bassani, J. W., & Bers, D. M. (1992). Mitochondrial and sarcolemmal Ca^{2+} transport reduce $[Ca^{2+}]_i$ during caffeine contractures in rabbit cardiac myocytes. *J.Physiol* **453**, 591-608.

Bean, B. P. & Rios, E. (1989). Nonlinear charge movement in mammalian cardiac ventricular cells. Components from Na and Ca channel gating. *J.Gen.Physiol* **94**, 65-93.

Becker, T. C., Noel, R. J., Coats, W. S., Gomez-Foix, A. M., Alam, T., Gerard, R. D., & Newgard, C. B. (1994). Use of recombinant adenovirus for metabolic engineering of mammalian cells. *Methods Cell Biol.* **43 Pt A**, 161-189.

Beevers, A. J. & Kukol, A. (2006). Secondary structure, orientation, and oligomerization of phospholemman, a cardiac transmembrane protein. *Protein Sci.* **15**, 1127-1132.

Bers, D. M. (2001). Excitation-contraction coupling and cardiac contractile force., Second ed. Kluwer Academic Publishers, Netherlands.

Bers, D. M. (2002). Cardiac excitation-contraction coupling. *Nature* **415**, 198-205.

Bersohn, M. M., Vemuri, R., Schuil, D. W., Weiss, R. S., & Philipson, K. D. (1991). Effect of temperature on sodium-calcium exchange in sarcolemma from mammalian and amphibian hearts. *Biochim.Biophys.Acta* **1062**, 19-23.

Beuckelmann, D. J. & Wier, W. G. (1988). Mechanism of release of calcium from sarcoplasmic reticulum of guinea-pig cardiac cells. *J.Physiol* **405**, 233-255.

Boateng, S., Seymour, A. M., Dunn, M., Yacoub, M., & Boheler, K. (1997). Inhibition of endogenous cardiac phosphatase activity and measurement of sarcoplasmic reticulum calcium uptake: a possible role of phospholamban phosphorylation in the hypertrophied myocardium. *Biochem.Biophys.Res.Commun.* **239**, 701-705.

Bogaev, R. C., Jia, L. G., Kobayashi, Y. M., Palmer, C. J., Mounsey, J. P., Moorman, J. R., Jones, L. R., & Tucker, A. L. (2001). Gene structure and expression of phospholemman in mouse. *Gene* **271**, 69-79.

Bossuyt, J., Ai, X., Moorman, J. R., Pogwizd, S. M., & Bers, D. M. (2005). Expression and phosphorylation of the na-pump regulatory subunit phospholemman in heart failure. *Circ.Res.* **97**, 558-565.

Bossuyt, J., Taylor, B. E., James-Kracke, M., & Hale, C. C. (2002). Evidence for cardiac sodium-calcium exchanger association with caveolin-3. *FEBS Lett.* **511**, 113-117.

Brette, F., Komukai, K., & Orchard, C. H. (2002). Validation of formamide as a detubulation agent in isolated rat cardiac cells. *Am.J.Physiol Heart Circ.Physiol* **283**, H1720-H1728.

Brette, F. & Orchard, C. (2003). T-tubule function in mammalian cardiac myocytes. *Circulation Research* **92**, 1182-1192.

Brette, F., Salle, L., & Orchard, C. H. (2004). Differential modulation of L-type Ca^{2+} current by SR Ca^{2+} release at the T-tubules and surface membrane of rat ventricular myocytes. *Circ.Res.* **95**, e1-e7.

Brette, F., Salle, L., & Orchard, C. H. (2006). Quantification of calcium entry at the T-tubules and surface membrane in rat ventricular myocytes. *Biophys.J.* **90**, 381-389.

Bristow, M. R., Ginsburg, R., Minobe, W., Cubicciotti, R. S., Sageman, W. S., Lurie, K., Billingham, M. E., Harrison, D. C., & Stinson, E. B. (1982). Decreased catecholamine sensitivity and beta-adrenergic-receptor density in failing human hearts. *N.Engl.J.Med.* **307**, 205-211.

Brownawell, A. M. & Creutz, C. E. (1997). Calcium-dependent binding of sorcin to the N-terminal domain of synexin (annexin VII). *J.Biol.Chem.* **272**, 22182-22190.

Carabello, B. A. (2002). Concentric versus eccentric remodeling. *J.Card Fail.* **8**, S258-S263.

Carafoli, E. (1994). Biogenesis: plasma membrane calcium ATPase: 15 years of work on the purified enzyme. *FASEB J.* **8**, 993-1002.

Carl, S. L., Felix, K., Caswell, A. H., Brandt, N. R., Ball, W. J., Jr., Vaghy, P. L., Meissner, G., & Ferguson, D. G. (1995). Immunolocalization of sarcolemmal dihydropyridine receptor and sarcoplasmic reticular triadin and ryanodine receptor in rabbit ventricle and atrium. *J.Cell Biol.* **129**, 672-682.

Caroni, P. & Carafoli, E. (1983). The regulation of the Na^+ -Ca^{2+} exchanger of heart sarcolemma. *Eur.J.Biochem.* **132**, 451-460.

Carozzi, A. J., Ikonen, E., Lindsay, M. R., & Parton, R. G. (2000). Role of cholesterol in developing T-tubules: analogous mechanisms for T-tubule and caveolae biogenesis. *Traffic.* **1**, 326-341.

Chen, F., Mottino, G., Klitzner, T. S., Philipson, K. D., & Frank, J. S. (1995). Distribution of the Na^+/Ca^{2+} exchange protein in developing rabbit myocytes. *Am.J.Physiol* **268**, C1126-C1132.

Chen, Z., Jones, L. R., O'Brian, J. J., Moorman, J. R., & Cala, S. E. (1998). Structural domains in phospholemman: a possible role for the carboxyl terminus in channel inactivation. *Circ.Res.* **82**, 367-374.

Cheng, H., Lederer, W. J., & Cannell, M. B. (1993). Calcium sparks: elementary events underlying excitation-contraction coupling in heart muscle. *Science* **262**, 740-744.

Clayton, J. C., Hughes, E., & Middleton, D. A. (2005). The cytoplasmic domains of phospholamban and phospholemman associate with phospholipid membrane surfaces. *Biochemistry* **44**, 17016-17026.

Clemen, C. S., Hofmann, A., Zamparelli, C., & Noegel, A. A. (1999). Expression and localisation of annexin VII (synexin) isoforms in differentiating myoblasts. *J.Muscle Res.Cell Motil.* **20**, 669-679.

Collins, A., Somlyo, A. V., & Hilgemann, D. W. (1992). The giant cardiac membrane patch method: stimulation of outward Na^+-Ca^{2+} exchange current by MgATP. *J.Physiol* **454**, 27-57.

Condrescu, M., Gardner, J. P., Chernaya, G., Aceto, J. F., Kroupis, C., & Reeves, J. P. (1995). ATP-dependent regulation of sodium-calcium exchange in Chinese hamster ovary cells transfected with the bovine cardiac sodium-calcium exchanger. *J.Biol.Chem.* **270**, 9137-9146.

Cordeiro, J. M., Spitzer, K. W., Giles, W. R., Ershler, P. E., Cannell, M. B., & Bridge, J. H. (2001). Location of the initiation site of calcium transients and sparks in rabbit heart Purkinje cells. *J.Physiol* **531**, 301-314.

Crambert, G., Fuzesi, M., Garty, H., Karlish, S., & Geering, K. (2002). Phospholemman (FXYD1) associates with Na,K-ATPase and regulates its transport properties. *Proc.Natl.Acad.Sci.U.S.A* **99**, 11476-11481.

Currie, S., Loughrey, C. M., Craig, M. A., & Smith, G. L. (2004). Calcium/calmodulin-dependent protein kinase IIdelta associates with the ryanodine receptor complex and regulates channel function in rabbit heart. *Biochem.J.* **377**, 357-366.

Currie, S., Quinn, F. R., Sayeed, R. A., Duncan, A. M., Kettlewell, S., & Smith, G. L. (2005). Selective down-regulation of sub-endocardial ryanodine receptor expression in a rabbit model of left ventricular dysfunction. *J.Mol.Cell Cardiol.* **39**, 309-317.

Currie, S. & Smith, G. L. (1999). Enhanced phosphorylation of phospholamban and downregulation of sarco/endoplasmic reticulum Ca^{2+} ATPase type 2 (SERCA 2) in cardiac sarcoplasmic reticulum from rabbits with heart failure. *Cardiovasc.Res.* **41**, 135-146.

Davis, C. E., Patel, M. K., Miller, J. R., John, J. E., III, Jones, L. R., Tucker, A. L., Mounsey, J. P., & Moorman, J. R. (2004). Effects of phospholemman expression on swelling-activated ion currents and volume regulation in embryonic kidney cells. *Neurochem.Res.* **29**, 177-187.

Delbridge, L. M., Bassani, J. W., & Bers, D. M. (1996). Steady-state twitch Ca^{2+} fluxes and cytosolic Ca^{2+} buffering in rabbit ventricular myocytes. *Am.J.Physiol* **270**, C192-C199.

Despa, S., Bossuyt, J., Han, F., Ginsburg, K. S., Jia, L. G., Kutchai, H., Tucker, A. L., & Bers, D. M. (2005). Phospholemman-phosphorylation mediates the beta-adrenergic effects on Na/K pump function in cardiac myocytes. *Circ.Res.* **97**, 252-259.

Despa, S., Brette, F., Orchard, C. H., & Bers, D. M. (2003). Na/Ca exchange and Na/K-ATPase function are equally concentrated in transverse tubules of rat ventricular myocytes. *Biophys.J.* **85**, 3388-3396.

DiPolo, R. & Beauge, L. (1987). In squid axons, ATP modulates Na^{+}-Ca^{2+} exchange by a $[Ca^{2+}]_i$-dependent phosphorylation. *Biochim.Biophys.Acta* **897**, 347-354.

Eisner, D. A., Choi, H. S., Diaz, M. E., O'Neill, S. C., & Trafford, A. W. (2000). Integrative analysis of calcium cycling in cardiac muscle. *Circ.Res.* **87**, 1087-1094.

Eisner, D. A. & Trafford, A. W. (2000). No Role for the Ryanodine Receptor in Regulating Cardiac Contraction? *News Physiol Sci.* **15**, 275-279.

Fabiato, A. (1985). Time and Calcium Dependence of Activation and Inactivation of Calcium-Induced Release of Calcium from the Sarcoplasmic-Reticulum of A Skinned Canine Cardiac Purkinje-Cell. *Journal of General Physiology* **85**, 247-289.

Fan, J., Shuba, Y. M., & Morad, M. (1996). Regulation of cardiac sodium-calcium exchanger by beta-adrenergic agonists. *Proc.Natl.Acad.Sci.U.S.A* **93**, 5527-5532.

Farrell, E. F., Antaramian, A., Rueda, A., Gomez, A. M., & Valdivia, H. H. (2003). Sorcin inhibits calcium release and modulates excitation-contraction coupling in the heart. *J.Biol.Chem.* **278**, 34660-34666.

Farrell, E. F., Meyers, M. B., Lokuta, A. J., Jiang, M. T., Wolff, M. R., & Valdivia, H. H. Abnormal expression of sorcin, a Ca^{2+}-binding protein regulator of cardiac ryanodine receptors, may be an underlying component of depressed Ca2+ release in heart failure cells. American Heart Association . 2000.
Ref Type: Abstract

Flucher, B. E. (1992). Structural analysis of muscle development: transverse tubules, sarcoplasmic reticulum, and the triad. *Dev.Biol.* **154**, 245-260.

Forbes, M. S., Hawkey, L. A., & Sperelakis, N. (1984). The transverse-axial tubular system (TATS) of mouse myocardium: its morphology in the developing and adult animal. *Am.J.Anat.* **170**, 143-162.

Fosset, M., Jaimovich, E., Delpont, E., & Lazdunski, M. (1983). [^{3}H]nitrendipine receptors in skeletal muscle. *J.Biol.Chem.* **258**, 6086-6092.

Frank, J. S., Mottino, G., Chen, F., Peri, V., Holland, P., & Tuana, B. S. (1994). Subcellular distribution of dystrophin in isolated adult and neonatal cardiac myocytes. *Am.J.Physiol* **267**, C1707-C1716.

Frank, J. S., Mottino, G., Reid, D., Molday, R. S., & Philipson, K. D. (1992). Distribution of the Na^+-Ca^{2+} exchange protein in mammalian cardiac myocytes: an immunofluorescence and immunocolloidal gold-labeling study. *J.Cell Biol.* **117**, 337-345.

Frank, K., Boelck, B., Hattebuhr, N., Malik, A., & Schwinger, R. H. Decreased expression and strengthened connection of sorcin to the ryanodine receptor channel of human insufficient myocardium. Z Kardiol 93[Supplement 3]. 2004. Ref Type: Abstract

Frank, K. F., Bolck, B., Ding, Z., Krause, D., Hattebuhr, N., Malik, A., Brixius, K., Hajjar, R. J., Schrader, J., & Schwinger, R. H. (2005). Overexpression of sorcin enhances cardiac contractility in vivo and in vitro. *J.Mol.Cell Cardiol.* **38**, 607-615.

Franzini-Armstrong, C. (1991). Simultaneous maturation of transverse tubules and sarcoplasmic reticulum during muscle differentiation in the mouse. *Dev.Biol.* **146**, 353-363.

Fuller, W., Eaton, P., Bell, J. R., & Shattock, M. J. (2004). Ischemia-induced phosphorylation of phospholemman directly activates rat cardiac Na/K-ATPase. *FASEB J.* **18**, 197-199.

Gage, P. W. & Eisenberg, R. S. (1969). Action potentials, afterpotentials, and excitation-contraction coupling in frog sartorius fibers without transverse tubules. *J.Gen.Physiol* **53**, 298-310.

Gallagher, F. A. & Huang, C. L. (1997). Osmotic 'detubulation' in frog muscle arises from a reversible vacuolation process. *J.Muscle Res.Cell Motil.* **18**, 305-321.

Gathercole, D. V., Colling, D. J., Skepper, J. N., Takagishi, Y., Levi, A. J., & Severs, N. J. (2000). Immunogold-labeled L-type calcium channels are clustered in the surface plasma membrane overlying junctional sarcoplasmic reticulum in guinea-pig myocytes-implications for excitation-contraction coupling in cardiac muscle. *J.Mol.Cell Cardiol.* **32**, 1981-1994.

Gerdes, A. M., Kellerman, S. E., Moore, J. A., Muffly, K. E., Clark, L. C., Reaves, P. Y., Malec, K. B., McKeown, P. P., & Schocken, D. D. (1992). Structural remodeling of cardiac myocytes in patients with ischemic cardiomyopathy. *Circulation* **86**, 426-430.

Gerke, V. & Moss, S. E. (2002). Annexins: from structure to function. *Physiol Rev.* **82**, 331-371.

Ginsburg, K. S. & Bers, D. M. (2005). Isoproterenol does not enhance Ca-dependent Na/Ca exchange current in intact rabbit ventricular myocytes. *J.Mol.Cell Cardiol.* **39**, 972-981.

Goddette, D. W. & Frieden, C. (1986). Actin polymerization. The mechanism of action of cytochalasin D. *J.Biol.Chem.* **261**, 15974-15980.

Gomez, A. M., Schwaller, B., Porzig, H., Vassort, G., Niggli, E., & Egger, M. (2002). Increased exchange current but normal Ca^{2+} transport via Na^{+}-Ca^{2+} exchange during cardiac hypertrophy after myocardial infarction. *Circ.Res.* **91**, 323-330.

Gomez, A. M., Valdivia, H. H., Cheng, H., Lederer, M. R., Santana, L. F., Cannell, M. B., McCune, S. A., Altschuld, R. A., & Lederer, W. J. (1997). Defective excitation-contraction coupling in experimental cardiac hypertrophy and heart failure. *Science* **276**, 800-806.

Grossman, W., Jones, D., & McLaurin, L. P. (1975). Wall stress and patterns of hypertrophy in the human left ventricle. *J.Clin.Invest* **56**, 56-64.

Gu, Y., Gorelik, J., Spohr, H. A., Shevchuk, A., Lab, M. J., Harding, S. E., Vodyanoy, I., Klenerman, D., & Korchev, Y. E. (2002). High-resolution scanning patch-clamp: new insights into cell function. *FASEB J.* **16**, 748-750.

Gunter, T. E., Buntinas, L., Sparagna, G., Eliseev, R., & Gunter, K. (2000). Mitochondrial calcium transport: mechanisms and functions. *Cell Calcium* **28**, 285-296.

Gyorke, I. & Gyorke, S. (1998). Regulation of the cardiac ryanodine receptor channel by luminal Ca^{2+} involves luminal Ca^{2+} sensing sites. *Biophys.J.* **75**, 2801-2810.

Haddock, P. S., Coetzee, W. A., Cho, E., Porter, L., Katoh, H., Bers, D. M., Jafri, M. S., & Artman, M. (1999). Subcellular $[Ca^{2+}]_i$ gradients during excitation-contraction coupling in newborn rabbit ventricular myocytes. *Circ.Res.* **85**, 415-427.

Haiech, J., Klee, C. B., & Demaille, J. G. (1981). Effects of cations on affinity of calmodulin for calcium: ordered binding of calcium ions allows the specific activation of calmodulin-stimulated enzymes. *Biochemistry* **20**, 3890-3897.

Haigney, M. C., Wei, S. K., Schulze, D. H., Ruknudin, A. M., & Matsuoka, S. (2006). Response to "beta-adrenergic stimulation does not activate Na^+/Ca^{2+} exchange current in guinea pig, mouse, and rat ventricular myocytes". *Am.J.Physiol Cell Physiol* **290**, C1271-C1272.

Hamada, H., Okochi, E., Oh-hara, T., & Tsuruo, T. (1988). Purification of the Mr 22,000 calcium-binding protein (sorcin) associated with multidrug resistance and its detection with monoclonal antibodies. *Cancer Res.* **48**, 3173-3178.

Han, X. & Ferrier, G. R. (1995). Contribution of Na^+-Ca^{2+} exchange to stimulation of transient inward current by isoproterenol in rabbit cardiac Purkinje fibers. *Circ.Res.* **76**, 664-674.

Hansen, C., Tarabykina, S., la Cour, J. M., Lollike, K., & Berchtold, M. W. (2003). The PEF family proteins sorcin and grancalcin interact in vivo and in vitro. *FEBS Lett.* **545**, 151-154.

Hasenfuss, G., Reinecke, H., Studer, R., Pieske, B., Meyer, M., Drexler, H., & Just, H. (1996). Calcium cycling proteins and force-frequency relationship in heart failure. *Basic Res.Cardiol.* **91 Suppl 2**, 17-22.

Hasenfuss, G., Schillinger, W., Lehnart, S. E., Preuss, M., Pieske, B., Maier, L. S., Prestle, J., Minami, K., & Just, H. (1999). Relationship between Na^+-Ca^{2+}-exchanger protein levels and diastolic function of failing human myocardium. *Circulation* **99**, 641-648.

Haworth, R. A., Goknur, A. B., Hunter, D. R., Hegge, J. O., & Berkoff, H. A. (1987). Inhibition of calcium influx in isolated adult rat heart cells by ATP depletion. *Circ.Res.* **60**, 586-594.

He, J., Conklin, M. W., Foell, J. D., Wolff, M. R., Haworth, R. A., Coronado, R., & Kamp, T. J. (2001). Reduction in density of transverse tubules and L-type Ca^{2+} channels in canine tachycardia-induced heart failure. *Cardiovasc.Res.* **49**, 298-307.

He, S., Ruknudin, A., Bambrick, L. L., Lederer, W. J., & Schulze, D. H. (1998). Isoform-specific regulation of the Na^+/Ca^{2+} exchanger in rat astrocytes and neurons by PKA. *J.Neurosci.* **18**, 4833-4841.

He, Z., Feng, S., Tong, Q., Hilgemann, D. W., & Philipson, K. D. (2000). Interaction of PIP(2) with the XIP region of the cardiac Na/Ca exchanger. *Am.J.Physiol Cell Physiol* **278**, C661-C666.

Herr, C., Smyth, N., Ullrich, S., Yun, F., Sasse, P., Hescheler, J., Fleischmann, B., Lasek, K., Brixius, K., Schwinger, R. H., Fassler, R., Schroder, R., & Noegel, A. A. (2001). Loss of annexin A7 leads to alterations in frequency-induced shortening of isolated murine cardiomyocytes. *Mol.Cell Biol.* **21**, 4119-4128.

Hilgemann, D. W. (1990). Regulation and deregulation of cardiac Na^+-Ca^{2+} exchange in giant excised sarcolemmal membrane patches. *Nature* **344**, 242-245.

Hilgemann, D. W. & Ball, R. (1996). Regulation of cardiac Na^+/Ca^{2+} exchange and KATP potassium channels by PIP2. *Science* **273**, 956-959.

Huser, J., Lipsius, S. L., & Blatter, L. A. (1996). Calcium gradients during excitation-contraction coupling in cat atrial myocytes. *J.Physiol* **494 (Pt 3)**, 641-651.

Ilari, A., Johnson, K. A., Nastopoulos, V., Verzili, D., Zamparelli, C., Colotti, G., Tsernoglou, D., & Chiancone, E. (2002). The crystal structure of the sorcin calcium binding domain provides a model of Ca^{2+}-dependent processes in the full-length protein. *J.Mol.Biol.* **317**, 447-458.

Iwamoto, T., Pan, Y., Nakamura, T. Y., Wakabayashi, S., & Shigekawa, M. (1998). Protein kinase C-dependent regulation of Na^+/Ca^{2+} exchanger isoforms NCX1 and NCX3 does not require their direct phosphorylation. *Biochemistry* **37**, 17230-17238.

Iwamoto, T., Pan, Y., Wakabayashi, S., Imagawa, T., Yamanaka, H. I., & Shigekawa, M. (1996). Phosphorylation-dependent regulation of cardiac Na^+/Ca^{2+} exchanger via protein kinase C. *J.Biol.Chem.* **271**, 13609-13615.

Iwamoto, T., Wakabayashi, S., & Shigekawa, M. (1995). Growth factor-induced phosphorylation and activation of aortic smooth muscle Na^+/Ca^{2+} exchanger. *J.Biol.Chem.* **270**, 8996-9001.

Jia, J., Han, Q., Borregaard, N., Lollike, K., & Cygler, M. (2000). Crystal structure of human grancalcin, a member of the penta-EF-hand protein family. *J.Mol.Biol.* **300**, 1271-1281.

Jia, L. G., Donnet, C., Bogaev, R. C., Blatt, R. J., McKinney, C. E., Day, K. H., Berr, S. S., Jones, L. R., Moorman, J. R., Sweadner, K. J., & Tucker, A. L. (2005). Hypertrophy, increased ejection fraction, and reduced Na-K-ATPase activity in phospholemman-deficient mice. *Am.J.Physiol Heart Circ.Physiol* **288**, H1982-H1988.

Jorgensen, A. O., Shen, A. C., Arnold, W., Leung, A. T., & Campbell, K. P. (1989). Subcellular distribution of the 1,4-dihydropyridine receptor in rabbit skeletal muscle in situ: an immunofluorescence and immunocolloidal gold-labeling study. *J.Cell Biol.* **109**, 135-147.

Kaprielian, R. R., Stevenson, S., Rothery, S. M., Cullen, M. J., & Severs, N. J. (2000). Distinct patterns of dystrophin organization in myocyte sarcolemma and transverse tubules of normal and diseased human myocardium. *Circulation* **101**, 2586-2594.

Kass, R. S., Lederer, W. J., Tsien, R. W., & Weingart, R. (1978). Role of calcium ions in transient inward currents and aftercontractions induced by strophanthidin in cardiac Purkinje fibres. *J.Physiol* **281**, 187-208.

Kawai, M., Hussain, M., & Orchard, C. H. (1999). Excitation-contraction coupling in rat ventricular myocytes after formamide-induced detubulation. *Am.J.Physiol* **277**, H603-H609.

Khan, K. N., Skepper, J. N., Hockaday, A. R., Burgess, A. J., & Huang, C. L. (2000). Loop diuretics inhibit detubulation and vacuolation in amphibian muscle fibres exposed to osmotic shock. *J.Muscle Res.Cell Motil.* **21**, 79-90.

Kieval, R. S., Bloch, R. J., Lindenmayer, G. E., Ambesi, A., & Lederer, W. J. (1992). Immunofluorescence localization of the Na-Ca exchanger in heart cells. *Am.J.Physiol* **263**, C545-C550.

Kitaura, Y., Matsumoto, S., Satoh, H., Hitomi, K., & Maki, M. (2001). Peflin and ALG-2, members of the penta-EF-hand protein family, form a heterodimer that dissociates in a Ca^{2+}-dependent manner. *J.Biol.Chem.* **276**, 14053-14058.

Kostin, S., Scholz, D., Shimada, T., Maeno, Y., Mollnau, H., Hein, S., & Schaper, J. (1998). The internal and external protein scaffold of the T-tubular system in cardiomyocytes. *Cell Tissue Res.* **294**, 449-460.

Koutsis, G., Philippides, A., & Huang, C. L. (1995). The afterdepolarization in Rana temporaria muscle fibres following osmotic shock. *J.Muscle Res.Cell Motil.* **16**, 519-528.

Kramer, C. M., Rogers, W. J., Park, C. S., Seibel, P. S., Shaffer, A., Theobald, T. M., Reichek, N., Onodera, T., & Gerdes, A. M. (1998). Regional myocyte hypertrophy parallels regional myocardial dysfunction during post-infarct remodeling. *J.Mol.Cell Cardiol.* **30**, 1773-1778.

Krolenko, S. A. (1969). Changes in the T-system of muscle fibres under the influence of influx and efflux of glycerol. *Nature* **221**, 966-968.

Lansbery, K. L., Burcea, L. C., Mendenhall, M. L., & Mercer, R. W. (2006). Cytoplasmic targeting signals mediate delivery of phospholemman to the plasma membrane. *Am.J.Physiol Cell Physiol* **290**, C1275-C1286.

Leach, R. N., Desai, J. C., & Orchard, C. H. (2005). Effect of cytoskeleton disruptors on L-type Ca channel distribution in rat ventricular myocytes. *Cell Calcium* **38**, 515-526.

Levick, J. R. (2003). An introduction to cardiovascular physiology., Fourth ed. Arnold.

Lim, H. W. & Molkentin, J. D. (1999). Calcineurin and human heart failure. *Nat.Med.* **5**, 246-247.

Lin, X., Jo, H., Sakakibara, Y., Tambara, K., Kim, B., Komeda, M., & Matsuoka, S. (2006). Beta-adrenergic stimulation does not activate Na^+/Ca^{2+} exchange current in guinea pig, mouse, and rat ventricular myocytes. *Am.J.Physiol Cell Physiol* **290**, C601-C608.

Linck, B., Qiu, Z., He, Z., Tong, Q., Hilgemann, D. W., & Philipson, K. D. (1998). Functional comparison of the three isoforms of the Na^+/Ca^{2+} exchanger (NCX1, NCX2, NCX3). *Am.J.Physiol* **274**, C415-C423.

Lindemann, J. P., Jones, L. R., Hathaway, D. R., Henry, B. G., & Watanabe, A. M. (1983). beta-Adrenergic stimulation of phospholamban phosphorylation and Ca^{2+}-ATPase activity in guinea pig ventricles. *J.Biol.Chem.* **258**, 464-471.

Lipp, P., Huser, J., Pott, L., & Niggli, E. (1996). Spatially non-uniform Ca^{2+} signals induced by the reduction of transverse tubules in citrate-loaded guinea-pig ventricular myocytes in culture. *J.Physiol* **497 (Pt 3)**, 589-597.

Litwin, S. E. & Bridge, J. H. (1997). Enhanced Na^+-Ca^{2+} exchange in the infarcted heart. Implications for excitation-contraction coupling. *Circ.Res.* **81**, 1083-1093.

Lokuta, A. J., Meyers, M. B., Sander, P. R., Fishman, G. I., & Valdivia, H. H. (1997). Modulation of cardiac ryanodine receptors by sorcin. *J.Biol.Chem.* **272**, 25333-25338.

Louch, W. E., Bito, V., Heinzel, F. R., Macianskiene, R., Vanhaecke, J., Flameng, W., Mubagwa, K., & Sipido, K. R. (2004). Reduced synchrony of Ca^{2+} release with loss of T-tubules-a comparison to Ca^{2+} release in human failing cardiomyocytes. *Cardiovasc.Res.* **62**, 63-73.

Louch, W. E., Mork, H. K., Sexton, J., Stromme, T. A., Laake, P., Sjaastad, I., & Sejersted, O. M. (2006). T-tubule disorganization and reduced synchrony of Ca^{2+} release in murine cardiomyocytes following myocardial infarction. *J.Physiol.*

Loughrey, C. M., MacEachern, K. E., Neary, P., & Smith, G. L. (2002). The relationship between intracellular [Ca^{2+}] and Ca^{2+} wave characteristics in permeabilised cardiomyocytes from the rabbit. *J.Physiol* **543**, 859-870.

Main, M. J., Grantham, C. J., & Cannell, M. B. (1997). Changes in subsarcolemmal sodium concentration measured by Na-Ca exchanger activity during Na-pump inhibition and beta-adrenergic stimulation in guinea-pig ventricular myocytes. *Pflugers Arch.* **435**, 112-118.

Maki, M., Kitaura, Y., Satoh, H., Ohkouchi, S., & Shibata, H. (2002). Structures, functions and molecular evolution of the penta-EF-hand Ca^{2+}-binding proteins. *Biochim.Biophys.Acta* **1600**, 51-60.

Manalan, A. S. & Jones, L. R. (1982). Characterization of the intrinsic cAMP-dependent protein kinase activity and endogenous substrates in highly purified cardiac sarcolemmal vesicles. *J.Biol.Chem.* **257**, 10052-10062.

Marban, E., Robinson, S. W., & Wier, W. G. (1986). Mechanisms of arrhythmogenic delayed and early afterdepolarizations in ferret ventricular muscle. *J.Clin.Invest* **78**, 1185-1192.

Matsumoto, T., Hisamatsu, Y., Ohkusa, T., Inoue, N., Sato, T., Suzuki, S., Ikeda, Y., & Matsuzaki, M. (2005). Sorcin interacts with sarcoplasmic reticulum Ca^{2+}-ATPase and modulates excitation-contraction coupling in the heart. *Basic Res.Cardiol.* **100**, 250-262.

Matsuoka, S., Nicoll, D. A., He, Z., & Philipson, K. D. (1997). Regulation of cardiac Na^{+}-Ca^{2+} exchanger by the endogenous XIP region. *J.Gen.Physiol* **109**, 273-286.

McIntosh, M. A., Cobbe, S. M., & Smith, G. L. (2000). Heterogeneous changes in action potential and intracellular Ca^{2+} in left ventricular myocyte sub-types from rabbits with heart failure. *Cardiovasc.Res.* **45**, 397-409.

Meder, D. & Simons, K. (2006). Lipid Rafts, Caveolae, and membrane traffic., ed. Fielding, C. J. E., pp. 1-23. WILEY-VCH Verlag GmbH & Co. KGaA, Weinheim.

Mella, M., Colotti, G., Zamparelli, C., Verzili, D., Ilari, A., & Chiancone, E. (2003). Information transfer in the penta-EF-hand protein sorcin does not operate via the canonical structural/functional pairing. A study with site-specific mutants. *J.Biol.Chem.* **278**, 24921-24928.

Meyers, M. B. (1989). Protein phosphorylation in multidrug resistant Chinese hamster cells. *Cancer Commun.* **1**, 233-241.

Meyers, M. B., Fischer, A., Sun, Y. J., Lopes, C. M., Rohacs, T., Nakamura, T. Y., Zhou, Y. Y., Lee, P. C., Altschuld, R. A., McCune, S. A., Coetzee, W. A., & Fishman, G. I. (2003). Sorcin regulates excitation-contraction coupling in the heart. *J.Biol.Chem.* **278**, 28865-28871.

Meyers, M. B., Pickel, V. M., Sheu, S. S., Sharma, V. K., Scotto, K. W., & Fishman, G. I. (1995a). Association of sorcin with the cardiac ryanodine receptor. *J.Biol.Chem.* **270**, 26411-26418.

Meyers, M. B., Puri, T. S., Chien, A. J., Gao, T., Hsu, P. H., Hosey, M. M., & Fishman, G. I. (1998). Sorcin associates with the pore-forming subunit of voltage-dependent L-type Ca^{2+} channels. *J.Biol.Chem.* **273**, 18930-18935.

Meyers, M. B., Zamparelli, C., Verzili, D., Dicker, A. P., Blanck, T. J., & Chiancone, E. (1995b). Calcium-dependent translocation of sorcin to membranes: functional relevance in contractile tissue. *FEBS Lett.* **357**, 230-234.

Mirza, M. A., Zhang, X. Q., Ahlers, B. A., Qureshi, A., Carl, L. L., Song, J., Tucker, A. L., Mounsey, J. P., Moorman, J. R., Rothblum, L. I., Zhang, T. S., & Cheung, J. Y. (2004). Effects of phospholemman downregulation on contractility and $[Ca^{2+}]_i$ transients in adult rat cardiac myocytes. *Am.J.Physiol Heart Circ.Physiol* **286**, H1322-H1330.

Mitcheson, J. S., Hancox, J. C., & Levi, A. J. (1996). Action potentials, ion channel currents and transverse tubule density in adult rabbit ventricular myocytes maintained for 6 days in cell culture. *Pflugers Arch.* **431**, 814-827.

Mohiddin, S. A., Antaramian, A., Farrell, E. F., Gomez, A. M., Lin, J. P., Yu, Z. X., Valdivia, H. H., & Fananapazir, L. A naturally occurring sorcin missense mutation (F112L) is associated with hypertrophic cardiomyopathy, hypertension and impaired modulation of cardiac ryanodine receptor. American Heart Association . 2002.
Ref Type: Abstract

Monterrubio, J., Ortiz, G., Orkand, P. M., & Zuazaga, C. (2002). Tubular localization of silent calcium channels in crustacean skeletal muscle fibers. *Journal of Muscle Research and Cell Motility* **23**, 167-174.

Moorman, J. R., Ackerman, S. J., Kowdley, G. C., Griffin, M. P., Mounsey, J. P., Chen, Z., Cala, S. E., O'Brian, J. J., Szabo, G., & Jones, L. R. (1995). Unitary anion currents through phospholemman channel molecules. *Nature* **377**, 737-740.

Moorman, J. R., Palmer, C. J., John, J. E., III, Durieux, M. E., & Jones, L. R. (1992). Phospholemman expression induces a hyperpolarization-activated chloride current in Xenopus oocytes. *J.Biol.Chem.* **267**, 14551-14554.

Narang, R., Cleland, J. G. F., Erhardt, L., Ball, S. G., Coats, A. J. S., Cowley, A. J., Dargie, H. J., Hall, A. S., Hampton, J. R., & PooleWilson, P. A. (1996). Mode of death in chronic heart failure - A request and proposition for more accurate classification. *European Heart Journal* **17**, 1390-1403.

Neary, P., Cobbe, S. M., & Smith, G. L. (1998). Reduced sarcoplasmic reticulum Ca^{2+} release in rabbits with left ventricular dysfunction. *Ann.N.Y.Acad.Sci.* **853**, 338-340.

Neumann, J., Maas, R., Boknik, P., Jones, L. R., Zimmermann, N., & Scholz, H. (1999). Pharmacological characterization of protein phosphatase activities in preparations from failing human hearts. *J.Pharmacol.Exp.Ther.* **289**, 188-193.

Ng, G. A., Cobbe, S. M., & Smith, G. L. (1998). Non-uniform prolongation of intracellular Ca^{2+} transients recorded from the epicardial surface of isolated hearts from rabbits with heart failure. *Cardiovasc.Res.* **37**, 489-502.

Nicoll, D. A., Longoni, S., & Philipson, K. D. (1990). Molecular cloning and functional expression of the cardiac sarcolemmal Na^{+}-Ca^{2+} exchanger. *Science* **250**, 562-565.

Nicoll, D. A., Ottolia, M., Lu, L., Lu, Y., & Philipson, K. D. (1999). A new topological model of the cardiac sarcolemmal Na^{+}-Ca^{2+} exchanger. *J.Biol.Chem.* **274**, 910-917.

Ogata, T. & Yamasaki, Y. (1990). High-resolution scanning electron microscopic studies on the three-dimensional structure of the transverse-axial tubular system, sarcoplasmic reticulum and intercalated disc of the rat myocardium. *Anat.Rec.* **228**, 277-287.

Ohler, A., Houser, S. R., Tomaselli, G. F., & Rourke, B. Transverse tubules are unchanged in myocytes from failing human heart. Biophys.J. 82. 2002.
Ref Type: Abstract

Olivetti, G., Capasso, J. M., Meggs, L. G., Sonnenblick, E. H., & Anversa, P. (1991). Cellular basis of chronic ventricular remodeling after myocardial infarction in rats. *Circ.Res.* **68**, 856-869.

Page, E. (1978). Quantitative ultrastructural analysis in cardiac membrane physiology. *Am.J.Physiol* **235**, C147-C158.

Page, E. & McCallister, L. P. (1973). Quantitative electron microscopic description of heart muscle cells. Application to normal, hypertrophied and thyroxin-stimulated hearts. *Am.J.Cardiol.* **31**, 172-181.

Palmer, C. J., Scott, B. T., & Jones, L. R. (1991). Purification and complete sequence determination of the major plasma membrane substrate for cAMP-dependent protein kinase and protein kinase C in myocardium. *J.Biol.Chem.* **266**, 11126-11130.

Parton, R. G., Way, M., Zorzi, N., & Stang, E. (1997). Caveolin-3 associates with developing T-tubules during muscle differentiation. *J.Cell Biol.* **136**, 137-154.

Perchenet, L., Hinde, A. K., Patel, K. C., Hancox, J. C., & Levi, A. J. (2000). Stimulation of Na/Ca exchange by the beta-adrenergic/protein kinase A pathway in guinea-pig ventricular myocytes at 37 degrees C. *Pflugers Arch.* **439**, 822-828.

Perez-Reyes, E., Kim, H. S., Lacerda, A. E., Horne, W., Wei, X. Y., Rampe, D., Campbell, K. P., Brown, A. M., & Birnbaumer, L. (1989). Induction of calcium currents by the expression of the alpha 1-subunit of the dihydropyridine receptor from skeletal muscle. *Nature* **340**, 233-236.

Peterson, B. Z., DeMaria, C. D., Adelman, J. P., & Yue, D. T. (1999). Calmodulin is the Ca^{2+} sensor for Ca^{2+} -dependent inactivation of L-type calcium channels. *Neuron* **22**, 549-558.

Philipson, K. D. & Nicoll, D. A. (2000). Sodium-calcium exchange: a molecular perspective. *Annu.Rev.Physiol* **62**, 111-133.

Pogwizd, S. M., Qi, M., Yuan, W., Samarel, A. M., & Bers, D. M. (1999). Upregulation of Na^+/Ca^{2+} exchanger expression and function in an arrhythmogenic rabbit model of heart failure. *Circ.Res.* **85**, 1009-1019.

Poindexter, B. J., Smith, J. R., Buja, L. M., & Bick, R. J. (2001). Calcium signaling mechanisms in dedifferentiated cardiac myocytes: comparison with neonatal and adult cardiomyocytes. *Cell Calcium* **30**, 373-382.

Prescott, L. & Brightman, M. W. (1976). The sarcolemma of Aplysia smooth muscle in freeze-fracture preparations. *Tissue Cell* **8**, 248-258.

Presti, C. F., Jones, L. R., & Lindemann, J. P. (1985). Isoproterenol-induced phosphorylation of a 15-kilodalton sarcolemmal protein in intact myocardium. *J.Biol.Chem.* **260**, 3860-3867.

Prestle, J., Dieterich, S., Preuss, M., Bieligk, U., & Hasenfuss, G. (1999). Heterogeneous transmural gene expression of calcium-handling proteins and natriuretic peptides in the failing human heart. *Cardiovasc.Res.* **43**, 323-331.

Prestle, J., Janssen, P. M., Janssen, A. P., Zeitz, O., Lehnart, S. E., Bruce, L., Smith, G. L., & Hasenfuss, G. (2001). Overexpression of FK506-binding protein FKBP12.6 in cardiomyocytes reduces ryanodine receptor-mediated Ca^{2+} leak from the sarcoplasmic reticulum and increases contractility. *Circ.Res.* **88**, 188-194.

Puglisi, J. L., Yuan, W., Bassani, J. W., & Bers, D. M. (1999). Ca^{2+} influx through Ca^{2+} channels in rabbit ventricular myocytes during action potential clamp: influence of temperature. *Circ.Res.* **85**, e7-e16.

Putnam, R. W. (1996). Intracellular pH regulation in detubulated frog skeletal muscle fibers. *Am.J.Physiol* **271**, C1358-C1366.

Pye, M. P. & Cobbe, S. M. (1996). Arrhythmogenesis in experimental models of heart failure: the role of increased load. *Cardiovasc.Res.* **32**, 248-257.

Qin, D., Zhang, Z. H., Caref, E. B., Boutjdir, M., Jain, P., & el Sherif, N. (1996). Cellular and ionic basis of arrhythmias in postinfarction remodeled ventricular myocardium. *Circ.Res.* **79**, 461-473.

Quinn, F. R., Currie, S., Duncan, A. M., Miller, S., Sayeed, R., Cobbe, S. M., & Smith, G. L. (2003). Myocardial infarction causes increased expression but decreased activity of the myocardial Na^{+}-Ca^{2+} exchanger in the rabbit. *J.Physiol* **553**, 229-242.

Reeves, J. P. & Hale, C. C. (1984). The stoichiometry of the cardiac sodium-calcium exchange system. *J.Biol.Chem.* **259**, 7733-7739.

Reinecke, H., Studer, R., Vetter, R., Holtz, J., & Drexler, H. (1996). Cardiac Na^{+}/Ca^{2+} exchange activity in patients with end-stage heart failure. *Cardiovasc.Res.* **31**, 48-54.

Rembold, C. M., Ripley, M. L., Meeks, M. K., Geddis, L. M., Kutchai, H. C., Marassi, F. M., Cheung, J. Y., & Moorman, J. R. (2005). Serine 68 phospholemman phosphorylation during forskolin-induced swine carotid artery relaxation. *J.Vasc.Res.* **42**, 483-491.

Rosemblatt, M., Hidalgo, C., Vergara, C., & Ikemoto, N. (1981). Immunological and biochemical properties of transverse tubule membranes isolated from rabbit skeletal muscle. *J.Biol.Chem.* **256**, 8140-8148.

Ruknudin, A., He, S., Lederer, W. J., & Schulze, D. H. (2000). Functional differences between cardiac and renal isoforms of the rat Na^{+}-Ca^{2+} exchanger NCX1 expressed in Xenopus oocytes. *J.Physiol* **529 Pt 3**, 599-610.

Schaper, J., Froede, R., Hein, S., Buck, A., Hashizume, H., Speiser, B., Friedl, A., & Bleese, N. (1991). Impairment of the myocardial ultrastructure and changes of the cytoskeleton in dilated cardiomyopathy. *Circulation* **83**, 504-514.

Schlotthauer, K. & Bers, D. M. (2000). Sarcoplasmic reticulum Ca^{2+} release causes myocyte depolarization. Underlying mechanism and threshold for triggered action potentials. *Circ.Res.* **87**, 774-780.

Schulze, D. H., Muqhal, M., Lederer, W. J., & Ruknudin, A. M. (2003). Sodium/calcium exchanger (NCX1) macromolecular complex. *J.Biol.Chem.* **278**, 28849-28855.

Schwinger, R. H., Wang, J., Frank, K., Muller-Ehmsen, J., Brixius, K., McDonough, A. A., & Erdmann, E. (1999). Reduced sodium pump alpha1, alpha3, and beta1-isoform protein levels and Na^+,K^+-ATPase activity but unchanged Na^+-Ca^{2+} exchanger protein levels in human heart failure. *Circulation* **99**, 2105-2112.

Scriven, D. R., Dan, P., & Moore, E. D. (2000). Distribution of proteins implicated in excitation-contraction coupling in rat ventricular myocytes. *Biophys.J.* **79**, 2682-2691.

Sedarat, F., Xu, L., Moore, E. D., & Tibbits, G. F. (2000). Colocalization of dihydropyridine and ryanodine receptors in neonate rabbit heart using confocal microscopy. *Am.J.Physiol Heart Circ.Physiol* **279**, H202-H209.

Sehl, P. D., Tai, J. T., Hillan, K. J., Brown, L. A., Goddard, A., Yang, R., Jin, H., & Lowe, D. G. (2000). Application of cDNA microarrays in determining molecular phenotype in cardiac growth, development, and response to injury. *Circulation* **101**, 1990-1999.

Seidler, T., Miller, S. L., Loughrey, C. M., Kania, A., Burow, A., Kettlewell, S., Teucher, N., Wagner, S., Kogler, H., Meyers, M. B., Hasenfuss, G., & Smith, G. L. (2003). Effects of adenovirus-mediated sorcin overexpression on excitation-contraction coupling in isolated rabbit cardiomyocytes. *Circ.Res.* **93**, 132-139.

Seki, S., Nagashima, M., Yamada, Y., Tsutsuura, M., Kobayashi, T., Namiki, A., & Tohse, N. (2003). Fetal and postnatal development of Ca^{2+} transients and Ca^{2+} sparks in rat cardiomyocytes. *Cardiovasc.Res.* **58**, 535-548.

Selbert, S., Fischer, P., Pongratz, D., Stewart, M., & Noegel, A. A. (1995). Expression and localization of annexin VII (synexin) in muscle cells. *J.Cell Sci.* **108 (Pt 1)**, 85-95.

Shacklock, P. S., Wier, W. G., & Balke, C. W. (1995). Local Ca^{2+} transients (Ca^{2+} sparks) originate at transverse tubules in rat heart cells. *J.Physiol* **487 (Pt 3)**, 601-608.

Sheikh, S. M., Skepper, J. N., Chawla, S., Vandenberg, J. I., Elneil, S., & Huang, C. L. (2001). Normal conduction of surface action potentials in detubulated amphibian skeletal muscle fibres. *J.Physiol* **535**, 579-590.

Shepherd, N. & McDonough, H. B. (1998). Ionic diffusion in transverse tubules of cardiac ventricular myocytes. *Am.J.Physiol* **275**, H852-H860.

Shuba, Y. M., Iwata, T., Naidenov, V. G., Oz, M., Sandberg, K., Kraev, A., Carafoli, E., & Morad, M. (1998). A novel molecular determinant for cAMP-dependent regulation of the frog heart Na+-Ca2+ exchanger. *J.Biol.Chem.* **273**, 18819-18825.

Silverman, B. Z., Fuller, W., Eaton, P., Deng, J., Moorman, J. R., Cheung, J. Y., James, A. F., & Shattock, M. J. (2005). Serine 68 phosphorylation of phospholemman: acute isoform-specific activation of cardiac Na/K ATPase. *Cardiovasc.Res.* **65**, 93-103.

Sipido, K. R., Volders, P. G., Vos, M. A., & Verdonck, F. (2002). Altered Na/Ca exchange activity in cardiac hypertrophy and heart failure: a new target for therapy? *Cardiovasc.Res.* **53**, 782-805.

Smith, C. J., Sun, D., Hoegler, C., Roth, B. S., Zhang, X., Zhao, G., Xu, X. B., Kobari, Y., Pritchard, K., Jr., Sessa, W. C., & Hintze, T. H. (1996). Reduced gene expression of vascular endothelial NO synthase and cyclooxygenase-1 in heart failure. *Circ.Res.* **78**, 58-64.

Smith, G. L., Elliott, E. E., Kettlewell, S., Currie, S., & Quinn, F. R. (2006). Na^+/Ca^{2+} exchanger expression and function in a rabbit model of myocardial infarction. *J.Cardiovasc.Electrophysiol.* **17 Suppl 1**, S57-S63.

Smith, G. L., Loughrey, C. M., Currie, S., Miller, S. L. W., Seidler, T., Verzili, D., & Chiancone, E. Sorcin directly influences cardiac Na/Ca exchanger and and ryanodine receptor activity via the sorcin C-terminal domain. Biophys.J. 2348-Pos/B459. 2005a.
Ref Type: Abstract

Smith, G. L., Loughrey, C. M., Currie, S., Miller, S. L. W., Seidler, T., Verzili, D., & Chiancone, E. Sorcin Directly Influences Cardiac Na/Ca Exchanger And Ryanodine Receptor Activity Via The Sorcin C-Terminal Domain. Biophys.J. 2005b.
Ref Type: Abstract

Sobie, E. A., Dilly, K. W., dos Santos, C. J., Lederer, W. J., & Jafri, M. S. (2002). Termination of cardiac Ca^{2+} sparks: an investigative mathematical model of calcium-induced calcium release. *Biophys.J.* **83**, 59-78.

Soeller, C. & Cannell, M. B. (1999). Examination of the transverse tubular system in living cardiac rat myocytes by 2-photon microscopy and digital image-processing techniques. *Circulation Research* **84**, 266-275.

Song, J., Zhang, X. Q., Ahlers, B. A., Carl, L. L., Wang, J., Rothblum, L. I., Stahl, R. C., Mounsey, J. P., Tucker, A. L., Moorman, J. R., & Cheung, J. Y. (2005). Serine 68 of phospholemman is critical in modulation of contractility, $[Ca^{2+}]_i$ transients, and Na^+/Ca^{2+} exchange in adult rat cardiac myocytes. *Am.J.Physiol Heart Circ.Physiol* **288**, H2342-H2354.

Song, J., Zhang, X. Q., Carl, L. L., Qureshi, A., Rothblum, L. I., & Cheung, J. Y. (2002). Overexpression of phospholemman alters contractility and $[Ca^{2+}]_i$ transients in adult rat myocytes. *Am.J.Physiol Heart Circ.Physiol* **283**, H576-H583.

Song, L. S., Sham, J. S., Stern, M. D., Lakatta, E. G., & Cheng, H. (1998). Direct measurement of SR release flux by tracking 'Ca^{2+} spikes' in rat cardiac myocytes. *J.Physiol* **512 (Pt 3)**, 677-691.

Song, L. S., Sobie, E. A., McCulle, S., Lederer, W. J., Balke, C. W., & Cheng, H. (2006). Orphaned ryanodine receptors in the failing heart. *Proc.Natl.Acad.Sci.U.S.A* **103**, 4305-4310.

Srivastava, M., Atwater, I., Glasman, M., Leighton, X., Goping, G., Caohuy, H., Miller, G., Pichel, J., Westphal, H., Mears, D., Rojas, E., & Pollard, H. B. (1999). Defects in inositol 1,4,5-trisphosphate receptor expression, Ca^{2+} signaling, and insulin secretion in the anx7(+/-) knockout mouse. *Proc.Natl.Acad.Sci.U.S.A* **96**, 13783-13788.

Stengl, M., Mubagwa, K., Carmeliet, E., & Flameng, W. (1998). Phenylephrine-induced stimulation of Na^+/Ca^{2+} exchange in rat ventricular myocytes. *Cardiovasc.Res.* **38**, 703-710.

Suarez, J., Belke, D. D., Gloss, B., Dieterle, T., McDonough, P. M., Kim, Y. K., Brunton, L. L., & Dillmann, W. H. (2004). In vivo adenoviral transfer of sorcin reverses cardiac contractile abnormalities of diabetic cardiomyopathy. *Am.J.Physiol Heart Circ.Physiol* **286**, H68-H75.

Tada, M. & Katz, A. M. (1982). Phosphorylation of the sarcoplasmic reticulum and sarcolemma. *Annu.Rev.Physiol* **44**, 401-423.

Tada, M., Kirchberger, M. A., & Katz, A. M. (1975). Phosphorylation of a 22,000-dalton component of the cardiac sarcoplasmic reticulum by adenosine 3':5'-monophosphate-dependent protein kinase. *J.Biol.Chem.* **250**, 2640-2647.

Takeshima, H., Nishimura, S., Matsumoto, T., Ishida, H., Kangawa, K., Minamino, N., Matsuo, H., Ueda, M., Hanaoka, M., Hirose, T., & . (1989). Primary structure and expression from complementary DNA of skeletal muscle ryanodine receptor. *Nature* **339**, 439-445.

Tanaka, H., Sekine, T., Kawanishi, T., Nakamura, R., & Shigenobu, K. (1998). Intrasarcomere [Ca2+] gradients and their spatio-temporal relation to Ca^{2+} sparks in rat cardiomyocytes. *J.Physiol* **508 (Pt 1)**, 145-152.

Thomas, M. J., Sjaastad, I., Andersen, K., Helm, P. J., Wasserstrom, J. A., Sejersted, O. M., & Ottersen, O. P. (2003). Localization and function of the Na^{+}/Ca^{2+}-exchanger in normal and detubulated rat cardiomyocytes. *J.Mol.Cell Cardiol.* **35**, 1325-1337.

Tidball, J. G., Cederdahl, J. E., & Bers, D. M. (1991). Quantitative analysis of regional variability in the distribution of transverse tubules in rabbit myocardium. *Cell Tissue Res.* **264**, 293-298.

Trafford, A. W., Diaz, M. E., O'Neill, S. C., & Eisner, D. A. (1995). Comparison of subsarcolemmal and bulk calcium concentration during spontaneous calcium release in rat ventricular myocytes. *J.Physiol* **488 (Pt 3)**, 577-586.

Tucker, A. L., Song, J., Zhang, X. Q., Wang, J., Ahlers, B. A., Carl, L. L., Mounsey, J. P., Moorman, J. R., Rothblum, L. I., & Cheung, J. Y. (2006). Altered contractility and $[Ca^{2+}]_i$ homeostasis in phospholemman-deficient murine myocytes: Role of Na+/Ca2+ exchange. *Am.J.Physiol Heart Circ.Physiol.*

Tufty, R. M. & Kretsinger, R. H. (1975). Troponin and parvalbumin calcium binding regions predicted in myosin light chain and T4 lysozyme. *Science* **187**, 167-169.

Valdivia, H. H., Farrell, E. F., Antaramian, A., Benkusky, N., Zhu, X., Rueda, A., & Gomez, A. M. Sorcin and ryanodine recptors in heart failure. Journal of Muscle Research and Cell Motility 25[8], 605-607. 2004.
Ref Type: Abstract

Van der Bliek, A. M., Meyers, M. B., Biedler, J. L., Hes, E., & Borst, P. (1986). A 22-kd protein (sorcin/V19) encoded by an amplified gene in multidrug-resistant cells, is homologous to the calcium-binding light chain of calpain. *EMBO J.* **5**, 3201-3208.

Verzili, D., Zamparelli, C., Mattei, B., Noegel, A. A., & Chiancone, E. (2000). The sorcin-annexin VII calcium-dependent interaction requires the sorcin N-terminal domain. *FEBS Lett.* **471**, 197-200.

Volders, P. G., Vos, M. A., Szabo, B., Sipido, K. R., De Groot, S. H., Gorgels, A. P., Wellens, H. J., & Lazzara, R. (2000). Progress in the understanding of cardiac early afterdepolarizations and torsades de pointes: time to revise current concepts. *Cardiovasc.Res.* **46**, 376-392.

Vornanen, M., Shepherd, N., & Isenberg, G. (1994). Tension-voltage relations of single myocytes reflect Ca release triggered by Na/Ca exchange at 35 degrees C but not 23 degrees C. *Am.J.Physiol* **267**, C623-C632.

Walaas, S. I., Czernik, A. J., Olstad, O. K., Sletten, K., & Walaas, O. (1994). Protein kinase C and cyclic AMP-dependent protein kinase phosphorylate phospholemman, an insulin and adrenaline-regulated membrane phosphoprotein, at specific sites in the carboxy terminal domain. *Biochem.J.* **304 (Pt 2)**, 635-640.

Wang, S. Q., Song, L. S., Lakatta, E. G., & Cheng, H. (2001a). Ca^{2+} signalling between single L-type Ca^{2+} channels and ryanodine receptors in heart cells. *Nature* **410**, 592-596.

Wang, Z., Nolan, B., Kutschke, W., & Hill, J. A. (2001b). Na^{+}-Ca^{2+} exchanger remodeling in pressure overload cardiac hypertrophy. *J.Biol.Chem.* **276**, 17706-17711.

Wei, S. K., Ruknudin, A., Hanlon, S. U., McCurley, J. M., Schulze, D. H., & Haigney, M. C. (2003). Protein kinase A hyperphosphorylation increases basal current but decreases beta-adrenergic responsiveness of the sarcolemmal Na^{+}-Ca^{2+} exchanger in failing pig myocytes. *Circ.Res.* **92**, 897-903.

Wong, C., Soeller, C., Burton L, & Cannell, M. B. Changes in transverse tubular system architecture in myocytes from diseased human ventricles. Biophys.J. 82. 2002.
Ref Type: Abstract

Xie, X., Dwyer, M. D., Swenson, L., Parker, M. H., & Botfield, M. C. (2001). Crystal structure of calcium-free human sorcin: a member of the penta-EF-hand protein family. *Protein Sci.* **10**, 2419-2425.

Yang, Z., Pascarel, C., Steele, D. S., Komukai, K., Brette, F., & Orchard, C. H. (2002). Na^{+}-Ca^{2+} exchange activity is localized in the T-tubules of rat ventricular myocytes. *Circ.Res.* **91**, 315-322.

Yao, A., Su, Z., Nonaka, A., Zubair, I., Spitzer, K. W., Bridge, J. H., Muelheims, G., Ross, J., Jr., & Barry, W. H. (1998). Abnormal myocyte Ca^{2+} homeostasis in rabbits with pacing-induced heart failure. *Am.J.Physiol* **275**, H1441-H1448.

Yuan, S. H., Arnold, W., & Jorgensen, A. O. (1991). Biogenesis of transverse tubules and triads: immunolocalization of the 1,4-dihydropyridine receptor, TS28, and the ryanodine receptor in rabbit skeletal muscle developing in situ. *J.Cell Biol.* **112**, 289-301.

Yuan, W., Ginsburg, K. S., & Bers, D. M. (1996). Comparison of sarcolemmal calcium channel current in rabbit and rat ventricular myocytes. *J.Physiol* **493 (Pt 3)**, 733-746.

Zamparelli, C., Ilari, A., Verzili, D., Giangiacomo, L., Colotti, G., Pascarella, S., & Chiancone, E. (2000). Structure-function relationships in sorcin, a member of the penta EF-hand family. Interaction of sorcin fragments with the ryanodine receptor and an Escherichia coli model system. *Biochemistry* **39**, 658-666.

Zamparelli, C., Ilari, A., Verzili, D., Vecchini, P., & Chiancone, E. (1997). Calcium- and pH-linked oligomerization of sorcin causing translocation from cytosol to membranes. *FEBS Lett.* **409**, 1-6.

Zhang, X. Q., Ahlers, B. A., Tucker, A. L., Song, J., Wang, J., Moorman, J. R., Mounsey, J. P., Carl, L. L., Rothblum, L. I., & Cheung, J. Y. (2006a). Phospholemman inhibition of the cardiac Na^+/Ca^{2+} exchanger. Role of phosphorylation. *J.Biol.Chem.* **281**, 7784-7792.

Zhang, X. Q., Moorman, J. R., Ahlers, B. A., Carl, L. L., Lake, D. E., Song, J., Mounsey, J. P., Tucker, A. L., Chan, Y. M., Rothblum, L. I., Stahl, R. C., Carey, D. J., & Cheung, J. Y. (2006b). Phospholemman overexpression inhibits Na^+-K^+-ATPase in adult rat cardiac myocytes: relevance to decreased Na+ pump activity in postinfarction myocytes. *J.Appl.Physiol* **100**, 212-220.

Zhang, X. Q., Qureshi, A., Song, J., Carl, L. L., Tian, Q., Stahl, R. C., Carey, D. J., Rothblum, L. I., & Cheung, J. Y. (2003). Phospholemman modulates Na^+/Ca^{2+} exchange in adult rat cardiac myocytes. *Am.J.Physiol Heart Circ.Physiol* **284**, H225-H233.

Zhang, Y. H., Hinde, A. K., & Hancox, J. C. (2001). Anti-adrenergic effect of adenosine on Na^+-Ca^{2+} exchange current recorded from guinea-pig ventricular myocytes. *Cell Calcium* **29**, 347-358.

Zhu, X., Farrell, E. F., Robu, V., Schmidt, U., Hajjar, R. J., Allen, P. D., & Valdivia, H. H. Over-expression of sorcin improves cardiac excitation-contraction coupling in normal and failing ventricular myocytes. Journal of cardiac failure Supplement 1[9(5)]. 2003.
Ref Type: Abstract